VOLUME 77 DECEMBER 20, 1973 NUMBER 26

JPCHAx

THE JOURNAL OF PHYSICAL CHEMISTRY

PUBLISHED BIWEEKLY BY THE AMERICAN CHEMICAL SOCIETY

You don't have to search the archives for data . . .

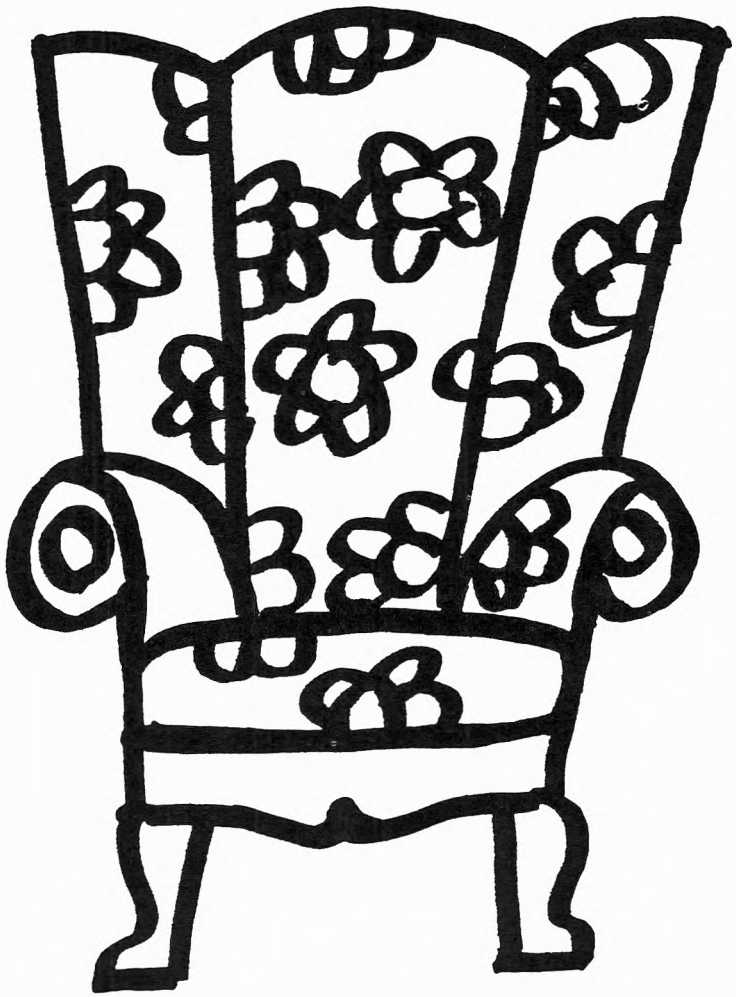

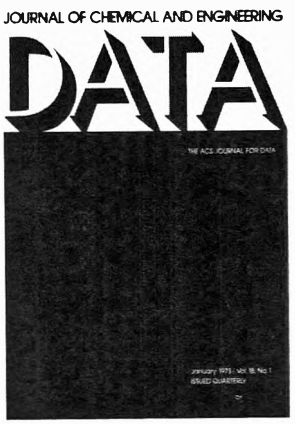

. . . because THE JOURNAL OF CHEMICAL AND ENGINEERING DATA will bring precise, reliable, useful technical information right to your fingertips quarterly! With a year's subscription, you'll receive a total of over 500 pages of valuable science and engineering data that are especially relevant now in light of today's new instrumentation. The information in JCED includes:

- experimental data relating to pure compounds or mixtures covering a range of states;
- manuscripts based on published experimental information which make tangible contributions through their presentation or which set forth a sound method of prediction of properties as a function of state;
- experimental data which aid in identifying or utilizing new organic or inorganic compounds; and
- papers relating primarily to newly developed or novel synthesis of organic compounds and their properties.

Start to benefit now from this "arm-chair" source of pertinent technical data—with your own personal subscription to JCED . . . just complete and return the form below . . . get your data without the dust.

. . . *another ACS service*

Journal of Chemical & Engineering Data

Journal of Chemical & Engineering Data
American Chemical Society
1155 Sixteenth Street, N.W.
Washington, D.C. 20036

Yes, I would like to receive the JOURNAL OF CHEMICAL & ENGINEERING DATA at the one-year rate checked below:

	U.S.	*Canada*	*Latin America*	*Other Nations*
ACS Member Personal-Use One-Year Rate	☐ $15.00	☐ $18.00	☐ $18.00	☐ $18.50
Nonmember	☐ $45.00	☐ $48.00	☐ $48.00	☐ $48.50

Bill me ☐ Bill company ☐ Payment enclosed ☐

Name _____

Street _____ Home ☐ Business ☐

City _____ State _____ *Zip* _____

T-73

THE JOURNAL OF

PHYSICAL CHEMISTRY

AMERICAN CHEMICAL SOCIETY, *1155 Sixteenth St., N.W., Washington, D. C. 20036*

Books and Journals Division

JOHN K CRUM *Director*
RUTH REYNARD *Assistant to the Director*

CHARLES R. BERTSCH *Head, Editorial Processing Department*
D. H. MICHAEL BOWEN *Head, Journals Department*
BACIL GUILEY *Head, Graphics and Production Department*
SELDON W. TERRANT *Head, Research and Development Department*

 Published biweekly by the American Chemical Society at 20th and Northampton Sts., Easton, Pa. 18042. Second-class postage paid at Washington, D. C., and at additional mailing offices.

All manuscripts should be sent to *The Journal of Physical Chemistry*, Department of Chemistry, University of Minnesota, Minneapolis, Minn. 55455.

Additions and Corrections are published once yearly in the final issue. See Volume 76, Number 26 for the proper form.

Extensive or unusual alterations in an article after it has been set in type are made at the author's expense, and it is understood that by requesting such alterations the author agrees to defray the cost thereof.

The American Chemical Society and the Editor of *The Journal of Physical Chemistry* assume no responsibility for the statements and opinions advanced by contributors.

Correspondence regarding accepted copy, proofs, and reprints should be directed to Editorial Processing Department, American Chemical Society, 20th and Northampton Sts., Easton, Pa. 18042. Head: CHARLES R. BERTSCH. Assistant Editor: EDWARD A. BORGER. Editorial Assistant: JOSEPH E. YURVATI.

Advertising Office: Centcom, Ltd., 142 East Avenue, Norwalk, Conn. 06851.

Business and Subscription Information

Send all new and renewal subscriptions *with payment* to: Office of the Controller, 1155 16th Street, N.W., Washington, D. C. 20036. Subscriptions should be renewed promptly to avoid a break in your series. All correspondence and telephone calls regarding changes of address, claims for missing issues, subscription service, the status of records, and accounts should be directed to Manager, Membership and Subscription Services, American Chemical Society, P.O. Box 3337, Columbus, Ohio 43210. Telephone (614) 421-7230.

On changes of address, include both old and new addresses with ZIP code numbers, accompanied by mailing label from a recent issue. Allow four weeks for change to become effective.

Claims for missing numbers will not be allowed (1) if loss was due to failure of notice of change in address to be received before the date specified, (2) if received more than sixty days from date of issue plus time normally required for postal delivery of journal and claim, or (3) if the reason for the claim is "issue missing from files."

Subscription rates (1973): members of the American Chemical Society, $20.00 for 1 year; to nonmembers, $60.00 for 1 year. Those interested in becoming members should write to the Admissions Department, American Chemical Society, 1155 Sixteenth St., N.W., Washington, D. C. 20036. Postage to Canada and countries in the Pan-American Union, $5.00; all other countries, $6.00. Single copies for current year: $3.00. Rates for back issues from Volume 56 to date are available from the Special Issues Sales Department, 1155 Sixteenth St., N.W., Washington, D. C. 20036.

Subscriptions to this and the other ACS periodical publications are available on microfilm. Supplementary material not printed in this journal is now available in microfiche form on a current subscription basis. For information on microfilm or microfiche subscriptions, write Special Issues Sales Department at the address above.

Notice to Authors last printed in the issue of December 6, 1973

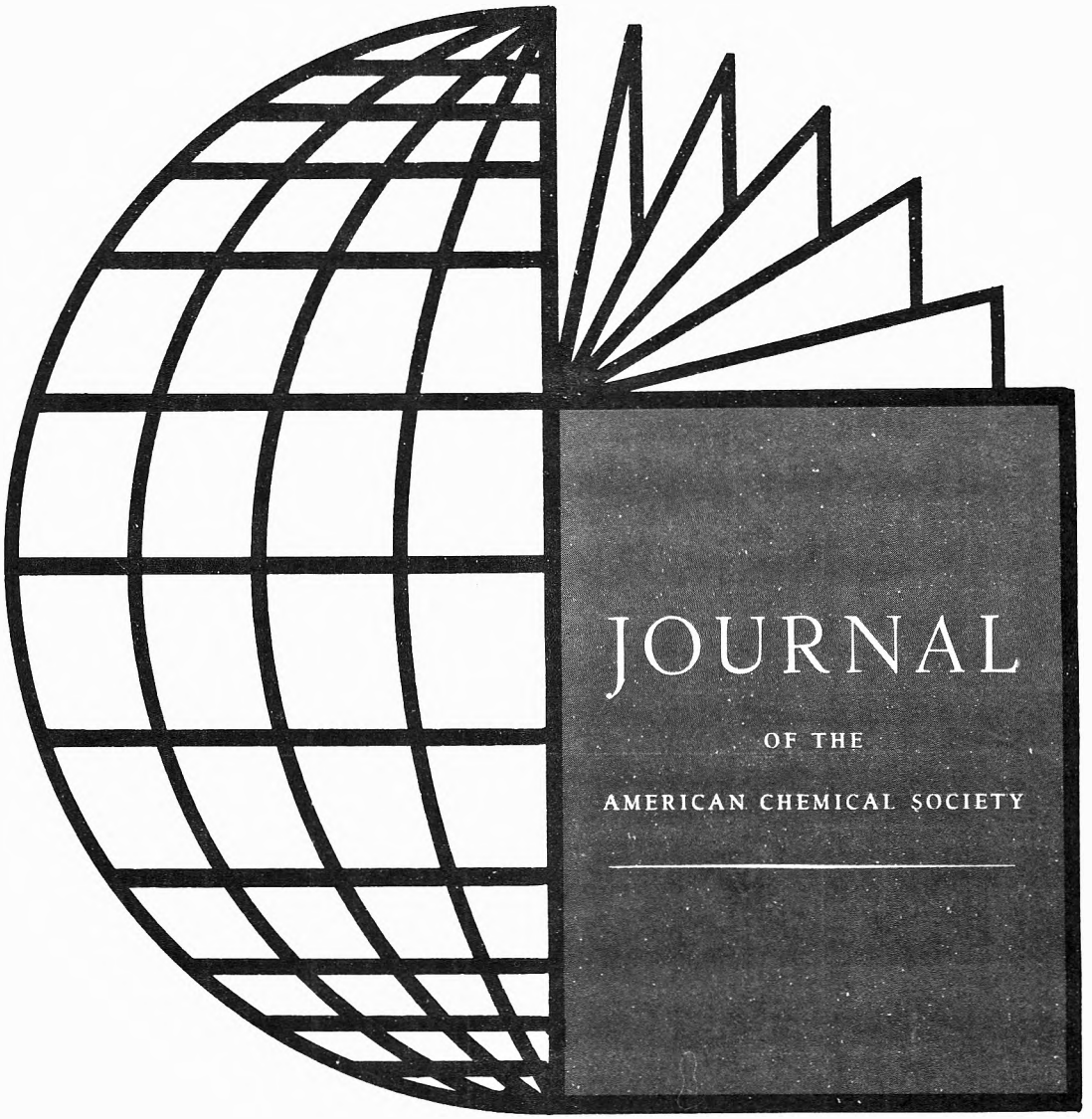

Most cited chemical journal in the entire world

. . . and one of publishing's best subscription values! That's right! You pay less per page for JACS—the most widely cited journal in chemistry—than for any other major scientific journal in the world.

But don't subscribe to this internationally respected journal because it's inexpensive. Subscribe because you will receive biweekly original research articles that cover ALL chemical research areas . . . together with many concise, up-to-the-minute Communications. Regardless of your major field of interest in chemistry, you'll find an abundance of authoritative and definitive data in each issue that cuts across ALL chemical research areas and is valuable and relevant to *your* work as well.

Order your own personal subscription to the number one chemical journal now. Complete and return the form.

. . . *another ACS service*

Journal of the American Chemical Society
American Chemical Society
1155 Sixteenth Street, N.W.
Washington, D.C. 20036

Yes, I would like to receive the JOURNAL OF THE AMERICAN CHEMICAL SOCIETY at the one-year rate checked below:

	U.S.	*Canada*	*Latin America*	*Other Nations*
ACS Member Personal-Use One-Year Rate	☐ $22.00	☐ $27.00	☐ $27.00	☐ $28.00
Nonmember	☐ $66.00	☐ $71.00	☐ $71.00	☐ $72.00

Bill me ☐ Bill company ☐ Payment enclosed ☐

Name _____

Street _____ Home ☐ Business ☐

City _____ State _____ Zip _____

J-73

THE JOURNAL OF

PHYSICAL CHEMISTRY

Volume 77, Number 26 December 20, 1973

JPCHAx 77(26) 3037-3124 (1973)
ISSN 0022-3654

COMMUNICATIONS TO THE EDITOR

■ Supplementary material for this paper is available separately, in photocopy or microfiche form. Ordering information is given in the paper.

* In papers with more than one author, the asterisk indicates the name of the author to whom inquiries about the paper should be addressed.

AUTHOR INDEX

THE JOURNAL OF

PHYSICAL CHEMISTRY

Volume 77

JANUARY—JUNE 1973

PAGES 1–1724

THE JOURNAL OF PHYSICAL CHEMISTRY

Volume 77

JULY—DECEMBER 1973

PAGES 1725–3124

INDEXES TO VOLUME 77

THE JOURNAL OF
PHYSICAL CHEMISTRY

VOLUME 77, NUMBER 26 DECEMBER 20, 1973

Cyclopropane Structural Isomerization in Shock Waves

Peter Jeffers,*

Department of Chemistry, State University College, Cortland, New York 13045

David Lewis, and Michael Sarr

Department of Chemistry, Colgate University, Hamilton, New York 13346 *(Received October 10, 1972)*

Publication costs assisted by Colgate University

The homogeneous unimolecular isomerization of cyclopropane has been studied in two independent sets of single-pulse shock tube relative rate experiments. Concentration of cyclopropane in argon ranged from 0.25 to 10%, total final pressures were 0.5–7 atm, and temperatures were 970–1265°K, with residence times of 180–900 μsec. The results, corrected by RRK theory for falloff, are in excellent agreement with conventional, lower temperature investigations and are consistent with a rate constant $k_\infty = 10^{15.2} \times \exp(-65{,}000/RT)\ \mathrm{sec}^{-1}$.

Introduction

The structural isomerization of cyclopropane to form propylene has been investigated extensively in static systems at temperatures of about 700–800°K.[1-3] A first attempt to extend this temperature range upward by use of shock tubes was reported by Miyama and Takeyama,[4] but their results were marked by extensive pyrolysis and thus were not precise enough for comparison with the earlier studies by conventional methods. Reports of two other shock tube investigations by Dorko, *et al.*,[5] and Bradley and Frend[6] appeared while this work was in progress. The former indicated reasonable agreement with the accepted Arrhenius parameters with low (0.1–1%) concentrations of cyclopropane in helium–argon diluent, (E_a = 65 kcal, log A = 14.5) but substantially different parameters with a mixture containing 5% cyclopropane (E_a = 33 kcal, log A = 8.2). The latter study indicated substantial disagreement with the accepted parameters and with Dorko, *et al.*, at all concentrations tested and also showed a curious change in the activation energy at 1300°K (low T: E_a = 55 kcal, log A = 11.9; high T: E_a = 11.6 kcal, log A = 4.75).[7] Barnard and Seebohm[8] also studied cyclopropane pyrolysis in a single-pulse shock tube and reported rate constants which agree fairly well with extrapolation of the low temperature work (E_a = 60.5 kcal/mol, log A = 14.2), but they also observed a noticable drop in activation energy for decomposition above 1250°K.

The present paper reports two studies of cyclopropane structural isomerization using the single-pulse shock tube relative rate technique developed by Tsang.[9] Two different size shock tubes were used, one at S.U.N.Y. Cortland and one at Colgate University, and different reactions served as the reference standards. We find that the results of the two relative rate studies are in good agreement with each other and with extrapolations of results from lower temperature static systems, over a considerable range of concentrations and pressures.

Experimental Section

Apparatus. The Cortland shock tube is constructed of ¾-in. i.d. Pyrex tubing and has been previously described.[10] It has been modified to allow a sample to be taken directly from the shock tube with a gas-tight syringe. The 10-cm i.d. stainless steel shock tube used at Colgate is also described elsewhere.[11]

Materials. Mixtures shocked at Cortland were prepared with cyclopropane (Matheson), *cis*-2-butene (Phillips Research Grade) and argon (Linde High Purity). Reactant concentrations were 1% each in argon or 10% cyclopropane–1% *cis*-2-butene in argon. Mixtures shocked at Colgate contained either 0.25 or 5.0% cyclopropane (Matheson) and 0.25% *tert*-butyl alcohol (Brothers Chemical Research Grade) in argon (Matheson Ultra-High Purity). The *cis*-2-butene and *tert*-butyl alcohol were included

TABLE I: Shock Conditions

A. Experiments Run at SUNY Cortland

Set	Δ/*cis*-2-butane	Initial sample pressure range, Torr	Driver gas pressure range, psia	Reflected shock conditions		
				T range, °K	*P*, atm	Reaction time, μsec
1 (7/30/71) 2 (12/28/71)	1%/1%	180–280	100–105	975–1265	6–7	180–240
3 (10/7/71) 4 (12/30/71)	10%/1%	100–200	100–105	970–1220	6–7	180–240

B. Experiments Run at Colgate

Set	Δ/*tert*-butyl alcohol	Initial sample pressure range, Torr	Driver gas pressure range, psia	Reflected shock conditions		
				T range, °K	*P*, atm	Reaction time, μsec
A	0.25%/0.25%	16–27	≈5	1010–1235	0.5–0.7	800–900
B	0.25%/0.25%	60–94	≈20	1025–1165	1.9–2.1	800–900
C	5.0%/0.25	17–27	≈5	1040–1195	0.5–0.7	800–900

in the reactant mixtures as standards for the relative rate measurements.

Analyses. Gas chromatographic analysis of the cyclopropane–*cis*-2-butene mixtures were performed on a Hewlett-Packard 5750 chromatograph with hydrogen flame detector, using a ¼ in. × 6-ft $AgNO_3$ saturated diethylene glycol column in series with a ⅛ in. × 12-ft silicone gum rubber column. Peak areas were measured by triangulation and calibrations indicated that the relative sensitivity of cyclopropane–propylene was 1.18 and *trans*-2-butene–*cis*-2-butene was 1.00.

Analysis of the cyclopropane–*tert*-butyl alcohol mixtures was performed on a Varian Aerograph 1440-20 chromatograph with hydrogen flame detector, using the above column. Peak areas were determined by the cut-and-weight method. Calibration samples were run before and after each day's runs.

Shock Conditions. Experimental conditions are summarized in Table I. Temperatures behind reflected shocks were calculated for measured extents of *cis*-2-butene isomerization or *tert*-butyl alcohol decomposition. Residence times were determined from oscilloscope records of $BaTiO_3$ gauge pressure histories on both shock tubes. As the relative rate method was used, no corrections to measured residence times were made for the finite cooling process. Mylar and aluminum diaphragms were used at Cortland and Colgate, respectively.

Calculations. Rate constants for cyclopropane and *tert*-butyl alcohol were calculated from the measured residence times and gas chromatographic analyses using the integrated form of a nonreversible first-order rate equation. The 2-butene rate constant calculation used the integrated form of a reversible first-order rate equation.[10] All first-order rate constants are in units of sec^{-1}.

Results

The relative rate plots of log k(cyclopropane) *vs.* log k(2-butene) or log k(*tert*-butyl alcohol) are presented in Figures 1 and 2, respectively. The slopes, intercepts and deduced values for log k(cyclopropane) are entered in Table II. These deduced values for log k(cyclopropane) are based on the following values for the rate constants of the standard reactions: log k(*cis*-2-butene → *trans*-2-butene) = $14.62 - 66{,}200/4.58T$°K (see Discussion section for justification of this value) and log k(*tert*-butyl alcohol → isobutene) = $14.6 - 66{,}200/4.58T$°K.[11] In Figure 1, the uncertainty limits log $A = \pm 0.5$, $E_a = \pm 3000$ reflect one standard deviation plus the uncertainty in the reference reaction. An earlier report on this type of study[10] listed uncertainties in log A of about ±0.2, but this did not include the uncertainty in the standard reaction parameters.

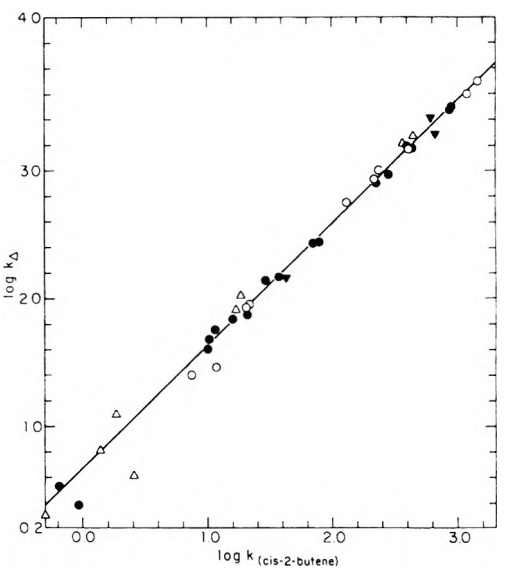

Figure 1. Relative rate plot of Cortland experiments: O, 1% cyclopropane, 1% *cis*-2-butene, 7/30/71; ●, 1% cyclopropane, 1% *cis*-2-butene, 12/28/71; ▼, 10% cyclopropane, 1% *cis*-2-butene, 10/7/71; Δ, 10% cyclopropane, 1% *cis*-2-butene, 12/30/71.

In Figure 2 the least-squares reductions indicate maximum standard deviations of log A and E_a of about 0.20 and 1000 cal, respectively, for the three lines. However, since the uncertainty associated with the standard reaction is on the order of log $A = \pm 0.4$, $E_a = \pm 1800$ cal, overall uncertainties for the cyclopropane isomerization parameters are estimated at log $A = \pm 0.5$, $E_a = \pm 2500$ cal. There was a slight overlapping of cyclopropane–pro-

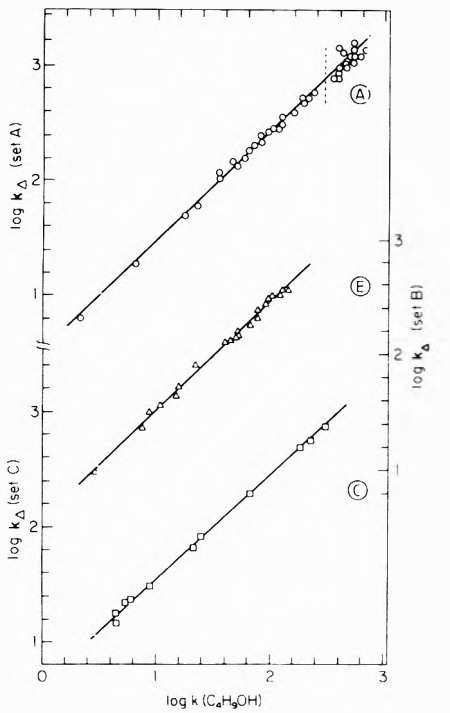

Figure 2. Relative rate plot of Colgate experiments: set A, ¼% cyclopropane, ¼% *tert*-butyl alcohol, ≈20 Torr; set B, ¼% cyclopropane, ¼% *tert*-butyl alcohol, ≈80 Torr; set C, 5% cyclopropane, ¼% *tert*-butyl alcohol, ≈20 Torr.

TABLE II: Rate Constants for Cyclopropane Isomerization Derived from Figures 1 and 2

Figure	Slope	Intercept	log *k* (cyclopropane → propylene)[a]
1	0.968	0.66	$14.8 - (64.1 \times 10^3)/4.58T$°K
2 (A)	0.958_3	0.52_2	$14.51 - (63.4 \times 10^3)/4.58T$°K
2 (B)	0.953_3	0.56_5	$14.48 - (63.1 \times 10^3)/4.58T$°K
2 (C)	0.928_0	0.59_8	$14.15 - (61.5 \times 10^3)/4.58T$°K

[a] See text for uncertainties.

pylene and propylene–isobutene peaks, with possibly a systematic high measurement of propylene or low measurement of isobutene concentrations which would be most significant for the low-T region of set C. For this reason, the Arrhenius parameters deduced from sets A and B are preferred from the Colgate data. However, it should be noted that the low-temperature disagreement of set C is slight, and the three sets are in complete agreement at high temperatures.

In Figure 2A, there are a number of data points to the right of the dotted vertical line. These represent temperatures above 1200°K, where substantial amounts of allene and propylene (which had the same retention time on this column) are formed as side products from the *tert*-butyl alcohol decomposition.[11] In calculating extents of cyclopropane isomerization for these points, the amounts of allene and propylene produced from *tert*-butyl alcohol, as estimated from a separate series of experiments on a mixture containing 0.25% *tert*-butyl alcohol in argon, were subtracted from the apparent concentrations of propylene. Because of the extensive formation of side products and relatively higher scatter of these runs, they were not included in the least-squares reduction of set A. However, they are included in Figure 2 to show that there is no apparent deviation from linearity in the relative rate plot at these higher temperatures.

Discussion

The description just given of side products found at the highest temperatures of these studies implies free radical processes. The active species involved here could lead to chain reactions which might seriously confuse the kind of relative measurements which we report. However, our studies employed different standards reacting by considerably different types of mechanism; our concentration ranges were usually wide for shock tube work; and pressures and residence times varied widely. The absence of any serious divergence of any of our results strongly suggests that interaction of the cyclopropane decomposition and the internal standard reaction was negligible, and relative rate results may be considered valid. The accuracy of any relative method obviously depends on the accuracy with which the standard reaction parameters are known. The Cortland standard was *cis*-2-butene which had previously been evaluated in the same relative way using *tert*-butyl alcohol,[10] thus making the *cis*-2-butene a secondary standard. The value $k(cis\text{-2-butene}) = 10^{14.62}(-66{,}200/RT)$ used in this study differs from the value reported earlier[10] of $k(cis\text{-2-butene}) = 10^{13.38}\exp(-61{,}600/RT)$ and reflects the revised value[11] for *tert*-butyl alcohol decomposition; $k(tert\text{-butyl alcohol}) = 10^{14.6}\exp(-66{,}200/RT)$ sec^{-1}. Since the Colgate measurements employed *tert*-butyl alcohol as standard, all the results reported are really relative to *tert*-butyl alcohol. In fact, Lewis'[11] value for *tert*-butyl alcohol decomposition was obtained in a similar relative rate experiment with cyclohexene decomposition to $C_2H_4 + C_4H_6$ as the standard, so that the real primary standard is cyclohexene. Tsang has found values for cyclohexene decomposition of $k = 10^{15.02}\exp(-66{,}700/RT)$[12a] and $k = 10^{15.30}\exp(-66{,}940/RT)$,[12b] over a temperature range of 950–1150°K. Uchiyama, Tomioka, and Amano[13] report $k = 10^{15.18}\exp(-66{,}200/RT)$ for 814–902°K. Extrapolation of the Arrhenius plot for these three studies passes through the rate constants found by Smith and Gordon[14] from 698 to 808°K, although they report quite different Arrhenius parameters. The consistency of all these studies covering a 700–1150°K temperature span appears to fix the activation energy to ±0.3 kcal/mol and log A to ±0.2 for our primary standard reaction of cyclohexene decomposition.

A comparison of the relevant low- and high-temperature work is displayed in Figure 3. Benson and O'Neal's[15] preferred value for cyclopropane isomerization is also included over the entire temperature range of the graph for reference. The Arrhenius parameters derived from Figure 3 are listed in Table III. All the low-temperature results shown have been corrected for unimolecular fall-off, as have the results of Dorko, *et al.*[5] However, the graph shows directly the experimental rate constants from this study and from Bradley and Frend.[6] Figure 3 indicates no serious discrepancy between the conventional studies and the shock tube findings of Dorko, *et al.*,[5] and of this study, even without consideration of falloff corrections. Barnard and Seebohm's results, not shown in Figure 3, cut across the "Colgate" line. Below 1250°K they are in reasonable agreement with the present results and with Dorko's[5] data. Bradley and Frend's[6] results appear slightly low and may reflect the kind of systematic uncertainty often associated with absolute shock tube measurements. These systematic uncertainties are clearly absent from

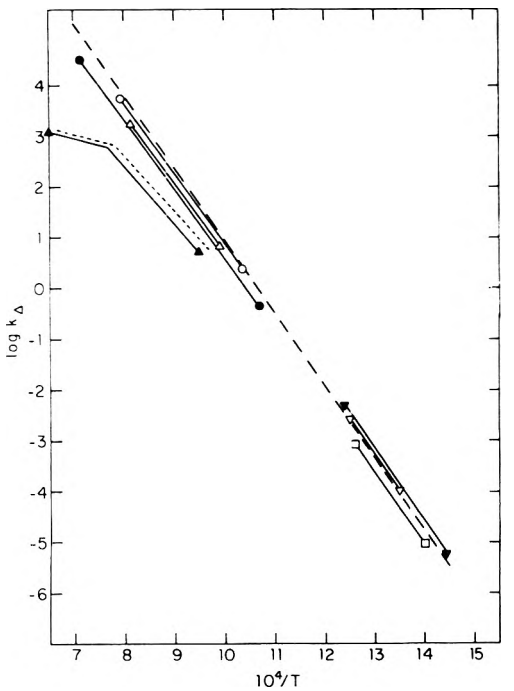

Figure 3. Arrhenius plot for cyclopropane isomerization: O, Cortland results, this study;* Δ, Colgate results, this study;* ●, Dorko, *et al.*;[5] ▲, Bradley and Frend;[6]*† ▼, Falconer, *et al.*;[3] ∇, Chambers and Kistiakowsky;[1] □, Corner and Pease;[2] dashed line, Benson and O'Neal,[15] preferred value. (* Not corrected for unimolecular falloff. See text for amount of correction to be added. † Dotted line is the correction mentioned in footnote 7.)

TABLE III: Cyclopropane Isomerization Parameters

Source	*T* range, °K	Log *A*	E_a
Chambers and Kistiskowsky[1]	743–801	15.17	65.0
Corner and Pease[2]	713–793	14.89	65.2
Falconer, *et al.*[3]	693–807	15.45	65.6
Benson and O'Neal[15]		15.2	65.5
Barnard and Seebohm[a]	860–1220	14.2	60.5
Bradley and Frend[6 a]	1060–1300	11.9	55
Dorko, *et al.*[5]	935–1397	14.5	65.1
This study (Colgate)[b]	1010–1235	14.5	63.3
This study (Cortland)[b]	1000–1300	14.8	64.1

[a] Not corrected for unimolecular falloff. [b] Not corrected for unimolecular falloff. RRK correction gives exact agreement with Benson and O'Neal's value.

relative shock tube studies where the major uncertainty is in the values assumed for the reference reaction Arrhenius parameters.

The importance of unimolecular falloff effects was evaluated from RRK theory following Golden, Solly, and Benson's[16] findings that the RRK and RRKM results are comparable, with considerably less labor involved in the RRK calculations. Details of the calculations are given in Table IV. The effective number of oscillators, *S*, was taken as C_{vib}/R again following the suggestion of Golden, Solly, and Benson.[16] For $B = E_\infty/RT$, a value of 65.5 kcal was used, and $A_\infty = 10^{15.2}$ was included in the parameter *D*. Collision efficiencies of 1.0, 0.07, and 1.0 were assumed for cyclopropane, argon, and 2-butene, respectively.[3] Table IV indicates that the Cortland results on Figure 3 should be raised about 0.1 log unit at the low-temperature end and about 0.2 log unit at the upper temperature

TABLE IV: RRK Falloff Calculations

	Temp, °K			
	1000	1100	1200	1300
B^a	32.8	29.8	27.3	25.2
S^b	13.8	14.5	15.2	15.8
D^c	5.93	5.88	5.89	5.90
$I(B,S,D)^d$	0.75	0.68	0.66	0.63
$1/T$	1.33	1.47	1.51	1.59
Log $(1/I)$	0.12	0.17	0.18	0.20
$10^4/T$	10.0	9.1	8.3	7.7

[a] $B \equiv E_\infty/RT = 65{,}500/RT$. [b] $S = C_{vib}/R$. Note that for cyclopropane, $3n - 6 = 21$ total oscillators. $S \equiv$ effective oscillators. [c] $D \equiv \log (A_\infty/k_1M)$, k_1 = collision frequency, M = effective total concentration. $A_\infty = 10^{15.2}$ sec^{-1}. Concentrations are for the Cortland experiments. [d] $I(B,S,D) = k/k_\infty$. Values taken from Emanuel's table.[17]

limit. These corrections give nearly exact coincidence with the line representing Benson and O'Neal's preferred value. The total effective density in the Colgate experiments was almost a factor of 10 lower than in the Cortland system, so that the calculated falloff correction amounts to 0.45 log unit at the high-temperature end, and Figure 3 shows that this correction leads to excellent agreement with Benson and O'Neal's value as well as with the Cortland results. Note that the line of Dorko, *et al.*,[5] is slightly low in comparison, but the disagreement hardly seems serious. The same can be said of Barnard and Seebohm's data.[8]

Evaluation of the falloff correction for the 2-butene and *tert*-butyl alcohol used as standards indicated that these reactions were essentially within the high-pressure region, since the effective number of oscillators is considerably larger than with cyclopropane.

One other relative rate measurement can be mentioned. In a direct relative rate comparison of cyclopropane and cyclohexene,[18] the rate constant found for cyclopropane was $k = 10^{15.26} \exp(-66{,}900/RT)$, in excellent agreement with the relative rate results of this study.

There remain several observations which are not completely explained. The first is the reported Arrhenius parameters of Dorko, *et al.*,[5] for 5% cyclopropane which were $E_a \pm 33$ kcal and log $A = 8.2$. The second is the decrease in activation energy above about 1300° which both Bradley and Frend[6] and Barnard and Seebohm[8] found.

The relative rate experiments of this study were specifically designed to check the effects of high cyclopropane concentration. However, both the Colgate 5% cyclopropane and the Cortland 10% cyclopropane experiments agree reasonably with the lower concentration findings. We suspect that high concentration of reactant may cause perturbation of the shock wave leading to the kind of difficulty mentioned by Dorko, *et al.*,[5] with their 5% mixture, particularly with a reaction as exothermic as this one. The relative rate results are apparently much less sensitive to such deviations from ideality, as one would expect for systems closely matched in activation energy. This insensitivity to nonideal conditions is certainly a most attractive feature of the relative techinque.

We can only speculate about the isomerization of cyclopropane above 1300°K. However, several points to consider are based on the very large per cents of conversion to products at these temperatures. With conversions above 90% the effects of boundary layer cooling could become significant.[19] In addition, as conversion approaches 99%, rate constants should be evaluated with consideration of

the reverse reaction, since K_{eq} falls to about 1000 by 1300°K.[20]

Dorko and coworkers[21] have recently published results of their efforts to find experimental evidence for an intermediate species involved in cyclopropane isomerization, and have suggested a five-step mechanism. We have already stated that we feel their parameters are in reasonably good agreement with the extrapolation of low-temperature studies. Further, we can see no clear proof that a five-step mechanism is a better explanation of cyclopropane isomerization than the accepted unimolecular mechanism. In fact, some of the proposed parameters are quite inconsistent with the physical model which they represent—for example, the activation energy value of 32 kcal/mol for k_5 (rearrangement of excited intermediate to form product. Rearrangement should involve only a lifetime or time lag for energy redistribution; there can be no activation energy.)

In conclusion, the shock tube relative rate measurements reported here are in good agreement with each other and with lower temperature studies of cyclopropane structural isomerization by conventional methods. It appears from this study that if any unexpected perturbations are occurring, both the cyclopropane and the two different references standards used must have been affected to exactly the same extent. There appears to be no strong evidence to support a questioning of currently accepted unimolecular reaction rate theory or its application to the cyclopropane system below 1300°K.

However, some additional experimental work at temperatures above 1300°K is probably warranted. We would suggest especially a single-pulse shock tube study in which both the incident and reflected shock temperatures would be measured which should allow a check on the ideality of shock structure. Perhaps even more useful information could be gained from a study employing the laser schlieren interferometry technique which would measure directly the heat release as the isomerization proceeds.

Acknowledgments. The authors thank the Sloan Foundation, the Colgate University Research Council, and the State University of New York Research Foundation for financial support. Thanks are also due to the Cabot Corporation which contributed the shock tube used at Colgate. This work was presented at the 164th National Meeting of the American Chemical Society, New York, N. Y., Aug 1972.

References and Notes

(1) T. S. Chambers and G. B. Kistiakowsky, *J. Amer. Chem. Soc.*, **56**, 399 (1934).
(2) E. S. Corner and R. N. Pease, *J. Amer. Chem. Soc.*, **67**, 2067 (1945).
(3) W. E. Falconer, T. F. Hunter, and A. F. Trotman-Dickinson, *J. Chem. Soc.*, 609 (1961).
(4) H. Miyama and T. Takeyama, *Bull. Chem. Soc. Jap.*, **38**, 2189 (1965).
(5) E. A. Dorko, D. B. McGhee, C. E. Panter, A. J. Caponecchi, and R. W. Crossley, *J. Phys. Chem.*, **75**, 2526 (1971).
(6) J. N. Bradley and M. A. Frend, *Trans. Faraday Soc.*, **67**, 72 (1971).
(7) In a private communication, Professor Bradley informed us that a computer program error had been discovered which made all calculated temperatures high by about 30°K. The corrected results are in much better agreement with other findings below 1300°K.
(8) J. A. Barnard and R. P. Seebohm, Symposium on Gas Kinetics, Szeged, Hungary, July 1969.
(9) W. Tsang, *J. Chem. Phys.*, **40**, 1171 (1964); **41**, 2487 (1964); **42**, 1805 (1965); **43**, 352 (1965); **44**, 4283 (1966).
(10) P. M. Jeffers and W. Shaub *J. Amer. Chem. Soc.*, **91**, 7706 (1969).
(11) D. Lewis, M. Keil, and M. Sarr, submitted for publication in *J. Amer. Chem. Soc.*
(12) (a) W. Tsang, *J. Chem. Phys.*, **42**, 1805 (1965); (b) W. Tsang, *Int. J. Chem. Kin.*, **II**, 311 (1970).
(13) M. Uchiyama, T. Tomioka, and A. Amano, *J. Phys. Chem.*, **68**, 1878 (1964).
(14) S. R. Smith and A. S. Gordon, *J. Phys. Chem.*, **65**, 1124 (1961).
(15) S. W. Benson and H. E. O'Neal, "Kinetic Data on Gas Phase Unimolecular Reactions," NSRDS-NBS 21 (1970).
(16) D. M. Golden, R. K. Solly, and S. W. Benson, *J. Phys. Chem.*, **75**, 1333 (1971).
(17) G. Emanuel, "Table of Kassel Integral," National Technical Information Service, A.D685157, 1969.
(18) P. M. Jeffers, C. Dasch, and S. H. Bauer, *Int. J. Chem. Kinet.*, **5**, 545 (1973).
(19) T. A. Brabbs and F. E. Belles, Fifth International Shock Tube Symposium, Silver Spring, Md., 1965. Also, private communication from F. E. Belles.
(20) R. E. Duff and S. H. Bauer, *J. Chem. Phys.*, **36**, 1754 (1962).
(21) E. A. Dorko, R. W. Crossley, V. W. Grimm, G. W. Mueller, and K. Scheller, *J. Phys. Chem.*, **77**, 143 (1973).

Quenching of the Luminescent State of Tris(2,2′-bipyridine)ruthenium(II) by Electronic Energy Transfer

Mark Wrighton* and Janet Markham

Department of Chemistry, Massachusetts Institute of Technology, Cambridge, Massachusetts 02139
(Received July 23, 1973)

Publication costs assisted by Undergraduate Research Opportunities Program of M.I.T.

The quenching of $Ru(bipy)_3^{2+}$ luminescence by anthracene, *trans*-2-styrylpyridine, *trans*-4-styrylpyridine, *trans*-stilbene, and *cis*-1,3-pentadiene has been studied in deoxygenated fluid solutions. Both the changes in quenching activity with triplet energy (E_T) of the quencher and data for the $Ru(bipy)_3^{2+}$ sensitized olefin cis-trans isomerization support efficient triplet-triplet electronic energy transfer from the $Ru(bipy)_3^{2+}$ excited state to anthracene, the styrylpyridines, and stilbene. Electronic energy transfer to *cis*-1,3-pentadiene is energetically unfavorable and little quenching activity could be detected using this quencher.

Discussion surrounding the deactivation of the excited state of $Ru(bipy)_3^{2+}$ either by *electron transfer*[1] or by *electronic energy transfer*[2,3] to quenchers has not included consideration of experiments involving quenchers having a known behavior in a role as an acceptor of triplet excitation from a well-characterized donor. Adamson[1] correlates the Stern-Volmer constants for quenching of the $Ru(bipy)_3^{2+}$ triplet state by $Co(NH_3)_5(X)^{2+}$ (X = F^-, Cl^-, Br^-, NH_3) with the ease of reduction of the Co(III) complex, but the results could be rationalized as well by correlating quenching rates with the energy of the lowest spin-allowed d-d absorption. The sensitized Co(III) → Co(II) reduction,[1,3a,b] the sensitized aquation of $PtCl_4^{2-}$,[2a] and the sensitized reactions of oxalato complexes[3c] are not judicious choices to characterize the electronic energy transfer ability of a new triplet donor since the excited states responsible for these reactions are not well established. The qualitative observation[2b] of $Ru(bipy)_3^{2+}$ sensitized $Cr(CN)_6^{3-}$ emission provides unequivocal spectroscopic evidence to invoke electronic energy transfer as at least one component of a quenching mechanism. It is known[4] that certain organic quenchers can be used to characterize the donor properties of triplet sensitizers, and we now report some results of $Ru(bipy)_3^{2+}$ luminescence quenching by organic quenchers.

Results

Quenching of the luminescence of $Ru(bipy)_3^{2+}$ was investigated using anthracene (E_T = 42 kcal/mol),[4] *trans*-stilbene (E_T = 49 kcal/mol),[5] *trans*-2-styrylpyridine ($E_T \approx$ 50 kcal/mol),[6] *trans*-4-styrylpyridine ($E_T \approx$ 50 kcal/mol),[6] and *cis*-1,3-pentadiene (E_T = 57 kcal/mol).[5] Typical Stern-Volmer plots for quenching are shown in Figures 1 and 2 and the data are summarized in Table I. From the two figures it is seen that the slope of the Stern-Volmer plot changes by a factor of about 3.5 in aerated compared to deoxygenated solutions consistent with competitive quenching of the $Ru(bipy)_3^{2+}$ state by O_2. Little or no quenching activity could be ascribed to *cis*-1,3-pentadiene.

In Figure 3 the quantum yield for the $Ru(bipy)_3^{2+}$ sensitized *trans* → *cis*-stilbene isomerization as a function of *trans*-stilbene concentration is given and the limiting $\phi_{t\rightarrow c}$ is 0.44 ± 10%. The limiting $\phi_{t\rightarrow c}$ was determined by repeated determinations of the observed quantum yield at a given stilbene concentration followed by correction for incomplete quenching of the $Ru(bipy)_3^{2+}$ triplets. The amount of quenching was measured by comparing the relative luminescence intensities of $Ru(bipy)_3^{2+}$ with and without added *trans*-stilbene. As can be seen in Figure 3 the inverse of the limiting $\phi_{t\rightarrow c}$ falls in a position consistent with an extrapolated value from the concentration data. This latter result is taken as verification of the internal consistency of the results. An equivalent check of internal consistency for different stilbene concentrations is found in the comparison of the information in Figures 2 and 3. For example, consider the data at 0.02 *M* and 0.05 *M* *trans*-stilbene; the $\phi_{t\rightarrow c}$ values are 0.12 and 0.21, respectively, while the fractions of $Ru(bipy)_3^{2+}$ triplets quenched are 0.225 and 0.422, respectively. Adjusting the $\phi_{t\rightarrow c}$ values for the fact that 100% of the triplets were not intercepted gives 0.53 and 0.50 in good agreement with each other and the limiting $\phi_{t\rightarrow c}$ value. Initial limiting $Ru(bipy)_3^{2+}$ sensitized trans → cis isomerization quantum yields for 4-styrylpyridine and 2-styrylpyridine were found to be 0.4 ± 0.05. Finally, large amounts of the cis isomer are found at the photostationary state achieved by $Ru(bipy)_3^{2+}$ sensitization: stilbene (95.0 ± 1.0%), 2-styrylpyridine (91.5 ± 2.0%), and 4-styrylpyridine (96.5 ± 1.0%).

Discussion

The results outlined above are consistent with the conclusion that the $Ru(bipy)_3^{2+}$ behaves as a normal triplet donor (sensitizer) with respect to the acceptors studied. Both energetics and the isomerization data support this conclusion. The energetic dependence of the acceptor triplet level relative to the donor triplet level is as expected: the *cis*-1,3-pentadiene triplet at ~57 kcal/mol is apparently inaccessible with the ~49 kcal/mol available from the $Ru(bipy)_3^{2+}$; having a nearly isoenergetic triplet level *trans*-stilbene, *trans*-4-styrylpyridine, and *trans*-2-styrylpyridine ($E_T \approx$ 49 kcal/mol) quench but not as effectively as anthracene ($E_T \approx$ 42 kcal/mol) where the energy transfer is clearly exothermic. None of the quench-

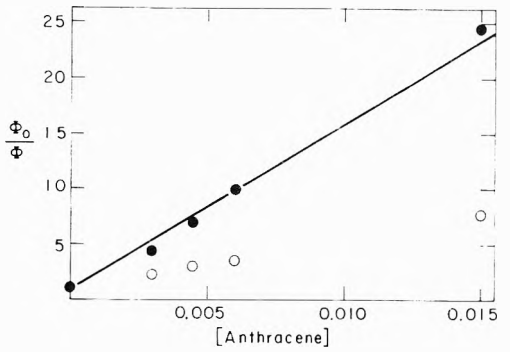

Figure 1. Stern–Volmer plot for quenching of $Ru(bipy)_3^{2+}$ luminescence by anthracene in aerated (○) and degassed (●) solutions at 25°.

TABLE I: Quenching of $Ru(bipy)_3^{2+}$ Luminescence

Quencher	E_T, kcal/mol	$k_q\tau^a$	k_q^b
Anthracene	42	1500	2.2×10^9
trans-2-Styrylpyridine	~50	30.9	4.5×10^6
trans-4-Styrylpyridine	~50	29.2	4.3×10^6
trans-Stilbene	49	14.7	2.1×10^6
cis-1,3-Pentadiene	57	~0	~0

[a] Slope of Stern–Volmer plot, *cf.* Figure 1.2; k_q is the quenching constant and τ is the lifetime of the $Ru(bipy)_3^{2+}$ excited state in the absence of quenchers. [b] Assuming $\tau = 0.685 \times 10^{-6}$ sec, ref 2.

ers studied have an energetically available singlet excited state to account for the quenching activity.

The fact that an electronically excited state of *trans*-stilbene is produced upon deactivation of the $Ru(bipy)_3^{2+}$ excited state is evidenced by the production of *cis*-stilbene from the trans isomer. This isomerization represents movement away from the thermodynamic ratio[7] of this isomeric pair. Similar reasoning can be used to invoke excited state formation for the *trans*-styrylpyridines. Further, the limiting $\phi_{t\to c}$ is near that for the benzophenone triplet sensitized reaction[6] for all three olefins implicating very efficient electronic energy transfer from the $Ru(bipy)_3^{2+}$ excited state resulting in information of the olefin triplet which decays in a characteristic way. Further, the large fraction of the cis isomers present at the photostationary states is consistent with electronic energy transfer from a donor of substantially lower E_T than the ≈57 kcal/mol[5] associated with cis olefin.

Finally, we note that both the efficient quenchers, anthracene and *trans*-stilbene, are substantially more difficult to reduce ($E_{1/2}$ *vs.* sce ≈ −2.2 and −1.94 V. respectively)[8] than the poor quenchers[1] $Co(NH_3)_6^{3+}$ and $Co(NH_3)_5F^{2+}$ ($E_{1/2}$ *vs.* sce = −0.44 and −0.33 V. respectively).[9] In this regard our results, at the very least, show that ease of reduction is not a necessity to deactivate the $Ru(bipy)_3^{2+}$ excited state with high quenching constants.

Experimental Section

Materials. The $Ru(bipy)_3Cl_2$ was a gift from G. S. Patterson. The quenchers used are commercially available: *cis*-1,3-pentadiene (Chemical Samples Co.) *trans*-stilbene and 4-styrylpyridine (Eastman Chemical Co.), 2-styrylpyridine (Chemical Procurement Labs. Inc.) and anthracene (Baker Chemical Co.). The same solvent system (ethanol: benzene 2:30 by volume) was used in all experiments.

Quenching Experiments. Luminescence spectra were obtained using an Aminco-Bowman emission spectrophotometer. Typically 3.0-ml solutions of ~10^{-3} *M* $Ru(bipy)_3^{2+}$ with variable quencher concentrations were placed in 13 × 100 mm test tubes with constrictions and degassed by several freeze–pump–thaw cycles. The samples were hermetically sealed and relative luminescence emission quantum yields measured.

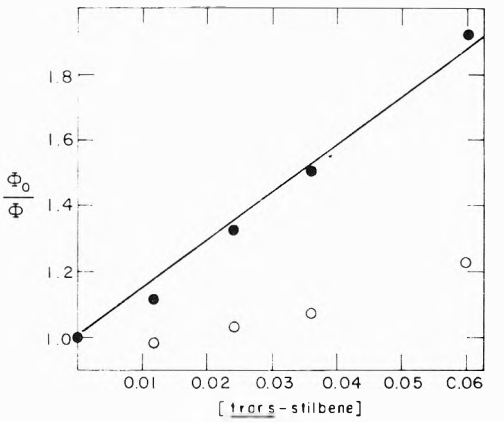

Figure 2. Stern–Volmer plot for quenching of $Ru(bipy)_3^{2+}$ luminescence by *trans*-stilbene in aerated (○) and degassed (●) solutions at 25°.

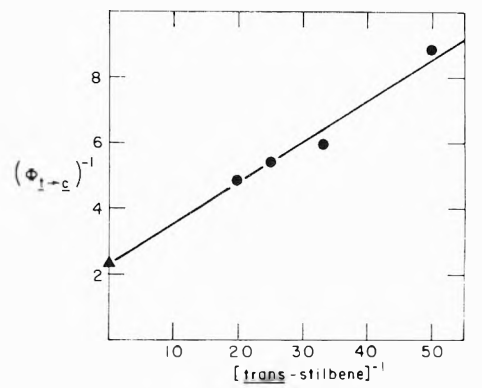

Figure 3. Quantum yield determination for $Ru(bipy)_3^{2+}$ sensitized *trans* → *cis*-stilbene conversion as a function of *trans*-stilbene concentration (●). The imiting quantum yield (▲) was determined by compensating for lack of 100% quenching of the $Ru(bipy)_2^{2+}$ excited states in separate measurements.

Isomerization of Olefins. Quantum yields for the $Ru(bipy)_3^{2+}$ sensitized trans → cis olefin conversion were measured using a merry-go-round[10] apparatus equipped with a 550-W Hanovia Hg lamp and Corning glass filters to isolate the 436-nm Hg line. Light intensity was measured using ferrioxalate actinometry.[11] Analysis for olefin isomerization was carried out using a Varian 1400 flame ionization gas chromatograph equipped with a 6 ft × ⅛ in. 5% DEGS or a 6 ft × ⅛ in. 3% SE-30 column operated at ≈160°. Prolonged irradiation at 436 nm was required to achieve a photostationary state and darkening of the solutions was observed, but approach to the photostationary state was monotonic.

Acknowledgment. We thank the Undergraduate Research Opportunities Program of M.I.T., the Uniroyal Foundation, and the National Science Foundation for support of this research.

References and Notes

(1) H. D. Gafney and A. W. Adamson, *J. Amer. Chem. Soc.*, **94**, 8238 (1972).

(2) (a) J. N. Demas and A. W. Adamson, *J. Amer. Chem. Soc.*, **93**, 1800 (1971); (b) N. Sabbatini and V. Balzani, *ibid.*, **94**, 7587 (1972).
(3) (a) P. Natarajan and J. F. Endicott, *J. Amer. Chem. Soc.*, **94**, 3635 (1972); **95**, 2470 (1973); (b) P. Natarajan and J. F. Endicott, *J. Phys. Chem.*, **77**, 971 (1973); (c) J. N. Demas and A. W. Adamson, *J. Amer. Chem. Soc.*, **95**, 5159 (1973).
(4) N. J. Turro, "Molecular Photochemistry," W. A. Benjamin, New York, N. Y., 1965, p 132.
(5) J. Saltiel, J. D'Agostino, E. D. Megarity, L. Metts, K. R. Neuberger, M. Wrighton, and O. C. Zafiriou, *Org. Photochem.*, **3**, 1 (1973).
(6) D. G. Whitten and M. T. McCall, *J. Amer. Chem. Soc.*, **91**, 5097 (1969).
(7) G. Fischer, K. A. Muszkat, and E. Fischer, *J. Chem. Soc. B*, 156 (1968).
(8) L. Meites, "Polarographic Techniques," 2nd ed, Interscience, New York, N. Y., 1965, pp 671–711.
(9) A. A. Vlček, *Discuss. Faraday Soc.*, **26**, 164 (1958).
(10) F. G. Moses, R. S. H. Liu, and B. M. Monroe, *Mol. Photochem.*, **1**, 245 (1969).
(11) C. G. Hatchard and C. A. Parker, *Proc. Roy. Soc., Ser. A*, **235**, 518 (1956).

Photodissociation of Iodoaromatics in Solution

A. Levy,* D. Meyerstein,

Nuclear Research Centre—Negev, Beer-Sheva 84190, Israel

and M. Ottolenghi

Department of Physical Chemistry, The Hebrew University, Jerusalem, Israel *(Received June 4, 1973)*

Publication costs assisted by the Nuclear Research Centre–Negev

Deiodination and isotopic-exchange processes are employed for determining the photodissociation yields of various iodoaromatic molecules in solution as a function of temperature and excitation wavelength. In the case of 1-iodonaphthalene the direct-excitation yields are compared with those obtained by photosensitization with benzophenone. The data indicate that dissociation takes place after thermal relaxation from either singlet or lowest triplet states. Photodissociation of these two excited states exhibits a different temperature dependence. Rate constants for the reaction of phenyl radicals with aromatic scavengers are determined and discussed along with the possibility of H-atom migration within the radical ring.

Introduction

In previous publications[1] we proposed a mechanism consisting of reactions 1–3 to account for the competition between the photoinduced exchange and deiodination in iodobenzene (PhI) solutions in the presence of radioactive iodine ($I^{131}I$).

$$PhI + h\nu \xrightarrow{k_1} Ph\cdot + I\cdot \quad (1)$$

$$Ph\cdot + O_2 \xrightarrow{k_2} \text{oxidation products} \quad (2)$$

$$2I\cdot \longrightarrow I_2 \text{ (deiodination)}$$

$$Ph\cdot + I^{131}I \xrightarrow{k_3} PhI^{131} + I\cdot \text{ (exchange)} \quad (3)$$

The final consequences of light absorption by the system are thus determined by the competition between dissolved oxygen and iodine on the phenyl radicals produced by photodissociation of iodobenzene. Alternative mechanisms, such as exchange induced by photodissociation of I_2, or *via* excitation of the $PhI\cdot I^{131}I$ charge-transfer complex, were ruled out. The observation that the photocleavage of iodobenzene (1) is wavelength dependent in the uv range, where part of the absorbed light leads directly to the triplet state of the molecule, raised questions relevant to the nature of the primary photodissociation step of iodoaromatics in solution. In the present work we have carried out photochemical experiments bearing principally on the following points. (a) The applicability of the proposed mechanism to other iodoaromatic molecules. (b) The details of the primary photodissociation step, such as the exact roles of the excited, thermalized, or nonthermalized singlet and triplet states. (c) Properties of the aryl radical, related to its reactivity with added solutes and to the possibility of H atom migration along its ring.

The results lead to a new insight into the photodissociation of iodoaromatics in solution for which only qualitative information was available.

Experimental Section

(*a*) *Materials.* All details concerning iodobenzene, iodine, iodine-131 and methylcyclohexane have been previously described.[1] o- and *m*-iodotoluenes (BDH) were purified by vacuum distillation in a dry nitrogen atmosphere. In the case of the para isomer a preparative gas-chromatographic procedure was employed. The purity of all isomers was checked by glc analysis and by uv spectroscopy. Benzene, chlorobenzene, toluene, benzonitrile, and benzophenone (all Merck, analytical grade) as well as 1-iodonaphthalene (Fluka purum) were used without further purification.

(*b*) *Procedure.* Deiodination and exchange measurements at various excitation wavelengths were carried out as previously described.[1] Iodotoluene isomers were separated gas chromatographically using a diethylene glycol adipate column (Analabs GP 35A ⅛ in. diameter, 6.5 m long). The retention times obtained at 100°, with a 35 cc/min rate of gas flow, for the ortho, para, and meta isomers, were 37.08, 38.83, and 39.33 min, respectively. Under the above conditions, ortho–para and ortho–meta mixtures were readily separable with a 5% sensitivity. However, due to the close values of the corresponding re-

TABLE I: Maximum Quantum Yield Values (ϕ_{DE}° and ϕ_{EX}°)[a] and Rate Constant Ratios Measured by 5×10^{-2} *M* Solutions of Iodotoluenes in Methylcyclohexane, Irradiated at 313 nm, in the Presence of $\sim 5.3 \times 10^{-4}$ *M* Iodine

Isomer	ϕ_{DE}°	ϕ_{EX}°	k_3/k_2 b	k_3/k_2 c
Ortho	0.41 ± 0.02	0.41 ± 0.02	1.95 ± 0.2	2.30 ± 0.2
Meta	0.41 ± 0.02	0.41 ± 0.02	1.70 ± 0.2	1.93 ± 0.2
Para	0.39 ± 0.02	0.38 ± 0.02	1.96 ± 0.2	1.96 ± 0.2

[a] ϕ_{DE}° and ϕ_{EX}° are the deiodination and exchange quantum yields measured correspondingly when $k_2[O_2] \gg k_3[I_2]$ and when $k_3[I_2] \gg k_2[O_2]$. According to the mechanism of reactions 1-3 they should be equal, representing the net photodissociation yield of iodobenzene. [b] Obtained from slopes of $1/R_{DE}$ *vs.* $1/[O_2]$ plots. [c] Obtained from slopes of $1/R_{EX}$ *vs.* $[O_2]$ plots.

tention times, we have not been able to separate mixtures of para and meta isomers.

Temperature effects were measured using a metal cell mount, thermostated (±0.2°) by alcohol or water circulation.

Results

(*a*) *Photoinduced Exchange and Deiodination in Solutions of Iodotoluenes.* Photochemical experiments were carried out in methylcyclohexane solutions of the three iodotoluene isomers, measuring the rates of deiodination and exchange (R_{DE} and R_{EX}) as a function of the oxygen concentration. The mechanism of reactions 1-3 predicts linear relationships between $1/R_{DE}$ and $1/[O_2]$, as well as between $1/R_{EX}$ and $[O_2]$.[1] Both relations are found to be accurately fulfilled in the above iodotoluenes system. The ratio k_3/k_2, obtained from the slopes of such plots using 313-nm excitation, as well as the maximum yields, ϕ_{DE}° and ϕ_{EX}°, are presented in Table I. Similar experiments were also carried out at 365 nm leading, in all cases, to the appreciably lower value of 0.23 ± 0.02 for both ϕ_{DE}° and ϕ_{EX}°. This wavelength effect on the yields is similar to that previously observed for iodobenzene.[1]

The feasibility of a photoinduced interchange between the isomers was investigated by exciting deaerated 0.1 *M* solutions at 313 nm, varying the iodine concentration in the range between 2×10^{-6} and 2×10^{-4} *M*. In all cases the total amount of aryl radicals produced by irradiation (determined from the product of the absorbed light intensity, the irradiation time, and the photodissociation quantum yield) was above 20% of the iodotoluene concentration. Under such conditions no photoinduced isomerization could be detected.

(*b*) *Temperature Effects on the Photochemistry of Iodobenzene.* Temperature effects on the deiodination of iodobenzene were studied by exciting air-saturated methylcyclohexane solutions at 254, 313, and 365 nm. The formation of I_2 was followed by measuring the absorbance at 520 nm as a function of the irradiation time. Figure 1 presents the values of ϕ_{DE}° obtained from the slopes of such initially linear curves, where $k_2[O_2] \gg k_3[I_2]$ and consequently $\phi_{DE} = \phi_{DE}^{\circ}$. In the same figure we present values of ϕ_{EX}° measured in evacuated, or N_2 saturated, PhI solutions where $k_2[O_2] \ll k_3[I_2]$ and $\phi_{EX} = \phi_{EX}^{\circ}$. In all cases we confirmed that the increase of the PhI absorption with temperature could be neglected. The excellent agreement, at all temperatures, between the values of ϕ_{EX}° and ϕ_{DE}° indicates that genuine temperature effects on the net yield of photodissociation are actually observed.

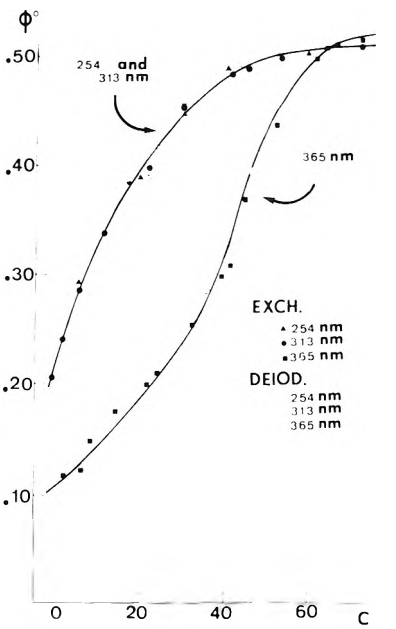

Figure 1. Temperature effects on the yield of iodobenzene photodissociation (ϕ°) in methylcyclohexane. (a) Yield determinations by deiodination were performed at 254 ([PhI] = 0.001 *M*), 313 ([PhI] = 0.03 *M*), and 365 nm ([PhI] = 0.5 *M*). (b) Yield determinations by isotope exchange were performed at 254 ([PhI] = 10^{-3} *M* and $[I_2] = 2 \times 10^{-4}$ *M*), 313 ([PhI] = 3×10^{-2} *M* and $[I_2] = 2 \times 10^{-4}$ *M*), and 365 nm ([PhI] = 0.5 *M* and $[I_2] = 2\text{-}6 \times 10^{-4}$ *M*).

As clearly demonstrated in Figure 1 an identical temperature effect is observed at 254 and 313 nm, differing from that observed at 365 nm.

(*c*) *Photosensitized Exchange and Deiodination of 1-Iodonaphthalene.* In order to clarify the role of the triplet state in the photodissociation of iodoaromatics, we have carried out photochemical experiments attempting to obtain selective triplet population *via* triplet-triplet energy transfer using benzophenone as sensitizer.

Irradiation of deaerated benzophenone solutions in the presence of I_2 resulted in an efficient iodine consumption, ultimately leading to total bleaching of the solution. This process, suppressed by molecular oxygen, was attributed to the triplet reaction

$$^3(\text{Ph CO Ph})^* + I_2 \xrightarrow{k_4} \text{iodo-organic products} \quad (4)$$

Energy transfer from the triplet state of benzophenone to an iodoaromatic (ArI) acceptor can thus occur only if reaction 5

$$^3(\text{Ph CO Ph})^* + \text{ArI} \xrightarrow{k_5} \text{Ph CO Ph} + {}^3(\text{ArI})^* \quad (5)$$

competes efficiently with reaction 4. In view of the relative inefficiency of reaction 5, in the case of iodobenzene, this requirement could not be fulfilled even at low $[I_2]$ and high [PhI] values. However, the addition of 1-iodonaphthalene was found to inhibit bleaching process 4 leading to its complete suppression when $[\text{ArI}]/[I_2] \geq 10^2$. Thus, under such conditions, any organic radioiodine originating in reaction 4 could be neglected.

An additional factor in choosing the exact concentrations in the photosensitization experiments is associated with the observation that relatively high benzophenone concentrations lead to deiodination of ArI even in deaerated solutions. The effect which, as shown below, is observed for several aromatic compounds is attributed to the Ar· radical scavenging reaction

$$Ar\cdot + Ph\ CO\ Ph \xrightarrow{k_6} \text{addition products} \qquad (6)$$

followed by

$$I\cdot + I\cdot \longrightarrow I_2 \text{ (deiodination)}$$

where I· and Ar· are formed from the dissociation of $^3(ArI)^*$ [2]

$$^3(ArI)^* \longrightarrow Ar\cdot + I\cdot \qquad (7)$$

Reaction 6 competes with

$$Ar\cdot + I^{131}I \xrightarrow{k_8} ArI^{131} + I\cdot \text{ (exchange)} \qquad (8)$$

To suppress reaction 6 we have carried out all experiments at $[Ph\ CO\ Ph]/[I_2] \leq 20$, where no deiodination is observed. The exchange rates induced at various temperatures by benzophenone photosensitization *via* reactions 5, 7, and 8 are presented in Figure 2. The temperature effect is compared with those observed in the case of direct excitation of 1-iodonaphthalene at 365 and 313 nm.

(*d*) *Iodobenzene Deiodination and Exchange in Aromatic Solvents.* Solutions of iodobenzene and iodine in deaerated aromatic solvents undergo an iodine exchange process which is accompanied by deiodination as in the case of aerated methylcyclohexane solutions. The dependence of the exchange yields on the iodine concentration in the cases of benzene, toluene, and chlorobenzene are shown in Figure 3a. The irradiation time at 313 nm was always short so as to minimize the change in $[I_2]$ during the exposure. We have also carried out experiments in methylcyclohexane as solvent to which varying amounts of aromatic compounds were added. The relevant data obtained with 365-nm excitation for iodobenzene and cyanobenzene are presented in Figure 3b.

In all cases the exciting light was exclusively absorbed by iodobenzene, thus avoiding possible complications due to the photolysis of other aromatics.

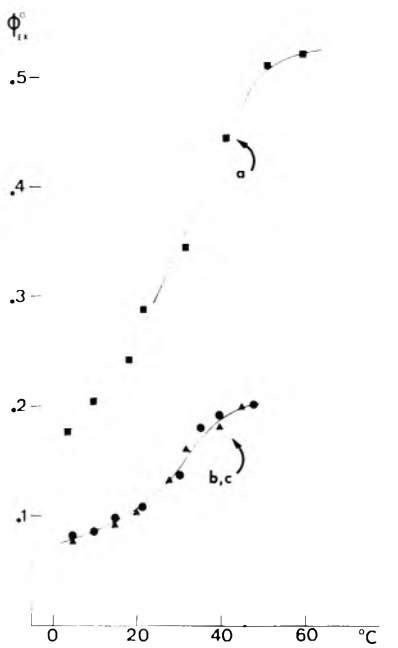

Figure 2. Temperature effects on the exchange quantum yield of 1-iodonaphthalene (ArI) in deaerated methylcyclohexane. (a, ■) Exchange induced by direct excitation of 1-iodonaphthalene (at 313 nm) leading to S_1:$[ArI] = 10^{-3}$ *M*; $[I_2] = 10^{-4}$ *M*. (b, ▲) Exchange induced by direct excitation (at 365 nm) of 1-iodonaphthalene to the triplet state: $[ArI] = 10^{-1}$ *M*; $[I_2] = 2 \times 10^{-4}$ *M*. (The data have been obtained after subtracting the contribution of excitation to S_1). (c, ●) Exchange induced by benzophenone photosensitization at 365 nm: $[ArI] = 10^{-1}$ *M*; $[I_2] = 2 \times 10^{-4}$ *M*; $[PhCOPh] = 2.5 \times 10^{-2}$ *M*. The data have been corrected for a small (~20%) contribution of direct excitation of 1-iodonaphthalene at this wavelength. The correction was carried out by measuring the exchange when 1-iodonaphthalene was directly excited at 365 nm, taking into account the light fraction absorbed by 1-iodonaphthalene in the presence of benzophenone.

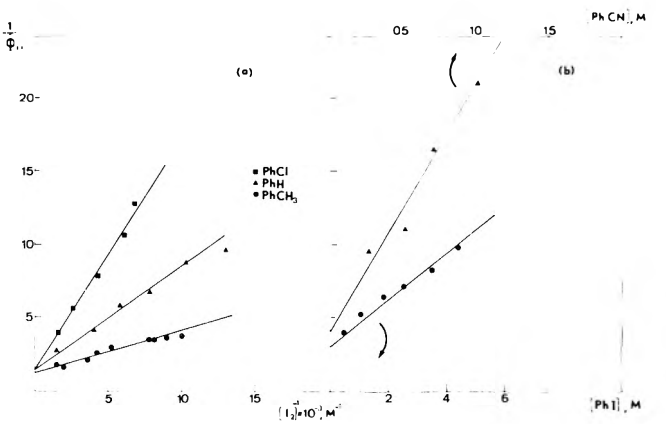

Figure 3. Kinetic plots showing the competition between I_2 and aromatic molecules on the scavenging of phenyl radicals: (a) excitation at 313 nm, $[PhI] = 0.03$ *M* in all three aromatic solvents; (b) (●) excitation at 365 nm in methylcyclohexane, $[I_2] = 2 \times 10^{-4}$ *M*; (▲) excitation at 365 nm in methylcyclohexane, $[I_2] = 5.2 \times 10^{-5}$ *M*, $[PhI] = 0.1$ *M*.

Discussion

(*a*) *Primary Dissociation Process.* The results presented above show that the basic deiodination and exchange mechanism of reactions 1–3 previously proposed for iodobenzene[1] is also valid for the iodotoluene isomers as well as for 1-iodonaphthalene. The question arises as to the details of photodissociation process 1. In all cases, excitation at 254 and 313 nm leads directly to the lowest excited singlet state of the molecule (S_1). Figure 1 shows that within the 0–65° range the quantum yield for photodissociation at 254 nm is identical with that at 313 nm. This lack of a wavelength effect indicates that photodissociation in the S_1 state occurs after complete thermal relaxation. Figure 1 shows, however, that the quantum yields measured with 365-nm excitation are usually lower, exhibiting a different temperature behavior, than those at 254 and 313 nm. This apparent discrepancy can be readily rationalized by the fact that excitation at 365 nm is within the tail of the $S_0 \rightarrow S_1$ band where the superimposed direct transition to the lowest triplet state ($S_0 \rightarrow T_1$) contributes substantially (~50%) to the extinction coefficient.[1,3] Thus, the difference observed between excitation at 254 or 313 nm and that at 365 nm can be attributed to differences in the photodissociation efficiencies of S_1 and T_1.

Direct evidence for photodissociation of the triplet state of iodoaromatics is derived by comparing the photosensitized dissociation yields in the 1-iodonaphthalene system with those obtained by direct excitation to T_1 at 365 nm. Figure 2 shows that absolute quantum yields of the two processes, as well as their dependence on temperature, are exactly identical. The data not only prove that dissociation may occur *via* triplet energy transfer from benzophenone but also that, in respect to dissociation, the triplet populated by direct $S_0 \rightarrow T_1$ excitation is indistinguishable from that obtained by photosensitization. The same data also suggest that, as in the case of S_1, dissociation occurs from T_1 after thermalization. The conclusion that

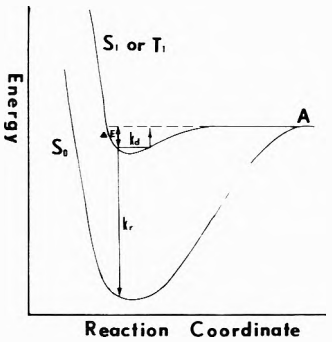

Figure 4. Schematic energy level diagram showing the thermally activated dissociation of S_1 and T_1 of iodoaromatics.

the optically populated T_1 state is photochemically active is in variance with the suggestion that direct excitation to T_1 leads to negligible photodissociation.[2] The early deiodination experiments were carried out in deaerated solutions where reaction 2 does not occur and reaction 1 is followed by the recombination of Ar· and I·. In these photosensitization experiments benzophenone not only acted as a triplet sensitizer but also replaced O_2 in reaction 2. This explains why in the presence of benzophenone the photosensitized deiodination yields in deaerated solutions[2] are essentially identical with the present exchange quantum yields, both representing the yield of triplet photodissociation.

When attempting to understand the temperature effects on the thermal dissociation of either S_1 or T_1 as shown in Figures 1 and 2, the complex nature of photodissociation in solution should be considered. Temperature may affect the primary yield of radicals initially formed in a photochemical cage as well as the net yield of pairs which escaped secondary geminate recombination.[4] A tentative expression for the photodissociation yield is

$$\phi = [k_d/(k_d + k_r)]K\theta \qquad (9)$$

where k_d and k_r are competitive rate constants as shown in Figure 4. If $k_d = k_d^\circ e^{-\Delta E/RT}$ with ΔE, k_d (and k_r) being different for S_1 and T_1, the factor $k_d/(k_d + k_r)$ will exhibit a different temperature dependence for the two corresponding states. θ is the probability of escaping secondary recombination *via* a random walk process, and depends on the initial radical separation determined by the solvent viscosity[5] and will thus increase with the temperature. Our data (Figure 1 and 2) indicate that ϕ° approaches a plateau at high temperatures suggesting that $k_d\theta/(k_d + k_r)$ approaches unity. Since our limiting value is (for iodobenzene) $\phi^\circ = 0.51 < 1$, an additional transmission factor K determining the fraction escaping deactivation to S_0 at point A (see Figure 4) should be introduced. This interpretation is consistent with data obtained using isopentane as solvent, in experiments similar to those described for methylcyclohexane in Figure 1.[1c] Higher ϕ° values are obtained at low temperatures, fitting the characteristic S-shaped curve which levels off at the same plateau around 0.51. In view of the lower viscosity of isopentane these results may be rationalized by higher $\theta(T)$ and k_d values, as well as by solvent-independent K. According to this general picture T_1 and S_1 exhibit similar K value for iodobenzene but different ones in the case of 1-iodonaphthalene. A quantitative analysis of eq 9 requires a knowledge of the temperature effect on θ. When assuming that θ is temperature independent and plotting log $[(\phi^\circ_{max}/\phi^\circ) - 1]$ against $1/T$ we obtained apparent ΔE values in the range between 6 and 12 kcal/mol. These values are unreasonable since, in view of the time scale in which the photodissociation takes place, they predict unacceptably high frequency factors (k_d°). Lower values for ΔE and k_d are obtained when assuming a temperature effect on θ. However in the absence of suitable models describing quantitatively the function $\theta(T)$ no reliable values could be obtained.

TABLE II: Relative Rate Constants for the Reaction between Phenyl Radicals and Some Aromatic Compounds

PhX	k_{I_2}/k_{PhX} [a]	k_{PhX}/k_{PhH} Present measurements	k_{PhX}/k_{PhH} Ref 7 and 8
PhH	2.0×10^4	1.0	1.0
PhCN	5.1×10^3	3.9	3.7
PhI	0.9×10^4	2.2	1.8
PhCl	1.3×10^4	1.5	1.4
$PhCH_3$	4.0×10^4	0.5	1.7

[a] Calculated from data in Figure 3.

(*b*) *Reactivity of the Phenyl Radicals.* The failure to observe a photoinduced isomerization between iodotoluene isomers indicates that, in agreement with previous suggestions,[6] no H atom migration around the aromatic ring takes place within the lifetime of the radicals. Assuming the value of $\sim 10^{10}\ M^{-1}\ sec^{-1}$ for the scavenging rate constant of Ar· by I_2 (which is an upper limit), one obtains (with $[I_2] = 2 \times 10^{-6}\ M$) a value of $\tau_{1/2} = 0.693/k[I_2] = 0.035$ msec for the half-life of the aromatic radical. In view of the sensitivity of our analytical methods this implies a lower limit of 0.1 msec for the half-life of the hydrogen migration process.

The relative rate constants for the reaction of the phenyl radical with aromatic scavengers, as calculated from the data of Figure 3, are presented in Table II. With the exception of toluene the table shows a fair agreement with previous data obtained from thermal decomposition experiments at elevated temperatures.[7,8] According to the present room-temperature data, it appears that the reaction of Ph· with aromatics is nucleophilic in nature as compared to electrophilic reaction of aromatics with iodine atoms.[9] This may be consistent with a charge-transfer intermediate $[ArX^-Ph^+]$ analogous to the species $[ArX^+ \cdot I^-]$ which has been observed spectroscopically at room temperature.[10]

Acknowledgment. The authors wish to thank Professor A. Treinin for valuable discussions. They are indebted to Mr. S. Shrem for his help in carrying out photochemical experiments and to Mr. Ch. Klein for the gas-chromatographical determinations.

References and Notes

(1) (a) A. Levy, D. Meyerstein, and M. Ottolenghi, *J. Phys. Chem.*, **75**, 3350 (1971); (b) *J. Appl. Radiat. Isotopes*, in press; (c) A. Levy, Ph D. Thesis, Hebrew University, Jerusalem, 1973.
(2) F. Wilkinson, *J. Phys. Chem.*, **66**, 2569 (1962).
(3) E. Olaerts and J. C. Jungers, *Discuss. Faraday Soc.*, **2**, 222 (1947).
(4) R. M. Noyes, *Progr. React. Kinet.* **1**, 129 (1961).
(5) D. Booth and R. M. Noyes, *J. Amer. Chem. Soc.*, **82**, 1868 (1960).
(6) R. K. Sharma and N. Kharasch, *Angew. Chem., Int. Ed. Engl.*, 7, 36 (1968).
(7) C. Walling, "Free Radicals in Solution," Wiley, London, England, 1957, p 484.
(8) G. H. Williams, "Homolytic Aromatic Substitution," Pergamon Press, London, England, 1960.
(9) M. Nakashima, C. Y. Mok, and R. M. Noyes, *J. Amer. Chem. Soc.*, **91**, 7635 (1969).
(10) S. J. Rand and R. L. Strong, *J. Amer. Chem. Soc.*, **82**, 5 (1960).

Study of Alcohol–Silica Surface Reactions *via* Infrared Spectroscopy

Raymond G. Azrak and C. L. Angell*

Union Carbide Corporation, Research and Development Laboratories, Bound Brook, New Jersey 08805, and Tarrytown Technical Center, Tarrytown, New York 10591 *(Received July 23, 1973)*

Publication costs assisted by the Union Carbide Corporation

Infrared spectroscopy was employed to follow the reactions of various alcohols with the surface groups of amorphous silica. Alcohols were observed to undergo condensation reactions with the free silanol groups on the silica surface and this reaction was seen to be markedly enhanced by the presence of Lewis bases such as ammonia and organic amines. A primary alcohol was found to react to a somewhat greater extent than a secondary alcohol. Unsaturation in the 2 position modified reactivity while unsaturation beyond the 2 position appeared to have little effect. Polar substituents on the alcohol affected reactivity. Several of the surface-bound alcohols exhibited good hydrolytic and thermal stability.

Introduction

Amorphous silica (SiO_2) and its surface reactions are of interest for a variety of reasons. Silica is employed as a filler for elastomers and thermoplastics, and as a thixotrope for waxes, polishes, and numerous other systems. It often serves as a catalyst support, and its surface silanol groups are analogous to those which exist in reinforcing siliceous glass fibers. The high surface-to-volume ratio of silica (50–300 m^2/g) allows analysis of surface reactions by such techniques as infrared spectroscopy. The reactions of organosilanes with silica have been extensively studied[1-3] and reactions of alcohols with silica have been suggested by Iler.[4] His work indicated that alcohols should undergo surface condensation reactions with silica. Iler treated amorphous silica with alcohols at elevated temperatures (about 200°) to prepare a hydrophobic silica. He proposed that he had prepared an organic-coated silica *via* condensation of the alcohol with surface silanols to give an SiOC bond. Although such a bond is hydrolytically unstable, the organic portion of the alcohol could act as a barrier to prevent the corroding H_2O from reaching the bond; thus hydrophobicity could be maintained. Very little direct evidence has been reported to confirm these propositions of surface reactivity.

Here we report first infrared spectroscopic investigation of uncatalyzed reactions of various alcohols with the surface of amorphous silica. Second, we report that this surface reaction can be markedly enhanced by Lewis bases.

Experimental Section

The silica employed in this investigation was Cab-O-Sil MS-5 amorphous fumed silica (particle size ~0.012 μ surface area ~200 m^2/g) from Cabot Corp.

The silica powder was pressed into a thin (0.5-in. diameter, ~0.2 mm thick, 12–20 mg weight) self-supporting wafer. This was placed in a specially designed vacuum cell,[5] where it could be treated at any temperature *in vacuo* or in the presence of some gas, and could be examined at room temperature with or without some gas present. The spectra were obtained in transmission on a Perkin-Elmer Model 225 grating spectrophotometer.

The silica wafer was activated by room temperature evacuation to $<10^{-4}$ Torr. Samples were treated by freeze–thaw degassed reagents in the vapor phase at pressures indicated below: 1-butanol (3 Torr), 2-butanol (10 Torr), 3-buten-1-ol (6 Torr), 2-buten-1-ol (5 Torr), 2-mercaptoethanol (2 Torr), 3-amino-1-propanol (room temperature vapor pressure), furfuryl alcohol (room temperature vapor pressure), *n*-propylamine (100 Torr), *n*-propylamine/1-butanol 1/1 mixture (12 Torr), NH_3/1-butanol 1/1 mixture (12 Torr). All spectra bearing the same figure number were run on the same wafer treated sequentially with additional doses of alcohol added at each treating temperature. When evacuated, samples were at pressures $<10^{-4}$ Torr. Hydrolysis tests were performed in a flow stream of water vapor in nitrogen at the indicated relative humidity and temperature.

Origin of Reagents. 1-Butanol, MCB; 2-buten-1-ol, Aldrich; aminopropanol, Aldrich; *n*-propylamine, Eastman; 2-butanol, Aldrich; 3-buten-1-ol, Aldrich; furfuryl alcohol, MCB; mercaptoethanol, Wateree Chemical Co., vacuum distilled.

Results and Discussion

Silica. The surface silanol groups (Si–OH) on silica are principally of two types:[6] free silanols which have a sharp infrared absorption band (3750 cm^{-1}) and adjacent silanols which hydrogen bond with each other; these adjacent silanols absorb in a broad region centered at 3600 cm^{-1}. When exposed to the atmosphere surface silanols adsorb water; this adsorption shifts the ir absorption to a very broad region between 3600 and 3000 cm^{-1}. As shown below, when heated under vacuum the silica surface first loses physisorbed water and then loses additional water *via* condensation of adjacent hydroxyls. This condensation reaction is reversible up to about 400°.

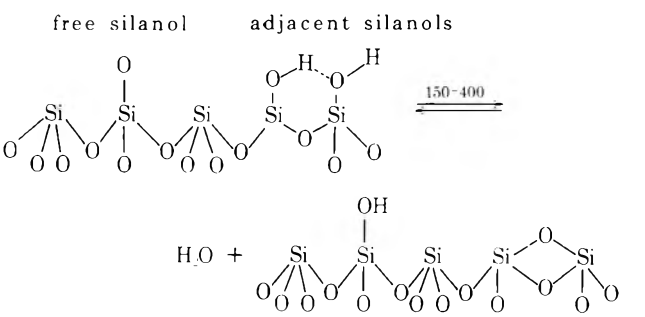

Figure 1 of ref 7 illustrates the ir spectra of the changes that take place upon thermal treatment for a typical

fumed, amorphous silica: Cab-O-Sil MS-5. The loss of water is shown by an increase in the intensity of the free silanol absorption and by the reduced intensity and narrowing of the low-frequency band. Further heating results in the loss of adjacent hydroxyls *via* the condensation reaction. The intensity of the free silanol band is not diminished below 700°.

Saturated Alcohols. Figures 1 and 2 (Figure 2 is available on microfilm, see paragraph at end of paper regarding supplementary material) show the effect of treating Cab-O-Sil MS-5 with 1-butanol (from the vapor phase) at various temperatures. Note the broadening of the OH band due to hydrogen bonding with the alcohol. Evacuation removes most of this hydrogen bonded material. Little, if any, reaction has occurred on room temperature treatment but significant organic material is bound to the silica after treatment at 250° and above; this correlates with a partial reduction in the intensity of the free silanol band. Extended exposure to 100% relative humidity at 100° does not remove a significant amount of alcohol; this is consistent with the hydrophobic nature of the treated silica.

We have investigated the effect of the nature of the alcohol (primary, secondary, or tertiary) on surface reactivity and stability. Figure 3 (available on microfilm) shows that *sec*-butyl alcohol is somewhat less reactive and the reaction products are less stable than primary butyl alcohol. Note the decomposition occurring at 500° and compare with Figure 2. Nonspectral studies[4] had indicated that secondary alcohols were less reactive than primary and that tertiary alcohols were far less reactive than either. These observations are consistent with the assumption that the condensation reaction between silanol and alcohol proceeds through loss of a proton from the alcohol rather than through formation of a carbonium ion.

Unsaturated Alcohols. Figures 4 and 5 (available on microfilm) illustrate that the interaction and reaction of unsaturated alcohols with the surface of silica is dependent upon the location of the double bond. It was anticipated that a molecule unsaturated in the 3 position would have a reactivity comparable to a saturated alcohol. Unsaturation in the 2 position was expected to increase the stability of the carbonium ion and thus to reduce the alcohol reactivity closer to that of a tertiary alcohol than to that of a primary alcohol. In addition to indicating that this is roughly true, the spectra reveal additional interesting features.

3-Buten-1-ol (Figure 4) behaved very much like its saturated counterpart 1-butanol in that it showed reversible adsorption at room temperature and increased reactivity as the treating temperature was increased to 250 and to 500°. Although the spectrum is not included here, it could be observed that the double bond remained intact (3130 cm^{-1}) even at 500° (under vacuum). Thus, a thermally stable double bond could be bound to a silica surface *via* this alcohol route.

2-Buten-1-ol (Figure 5) unlike 3-butene-1-ol and 1-butanol apparently *interacts* strongly with the silica surface at room temperature; it could not be pumped off at this temperature. This may indicate that the π system is involved in the surface interaction. Heating at 250° caused no increase in the amount of adsorbed alcohol. Unlike 3-buten-1-ol, heating 2-buten-1-ol/silica at 500° (spectrum not shown) caused the double bond to disappear without any significant reduction in the amount of adsorbed organic material. This, in addition to reflecting the generally lower thermal stability of this alcohol, may again point to some unusual interaction involving the π system and silica.

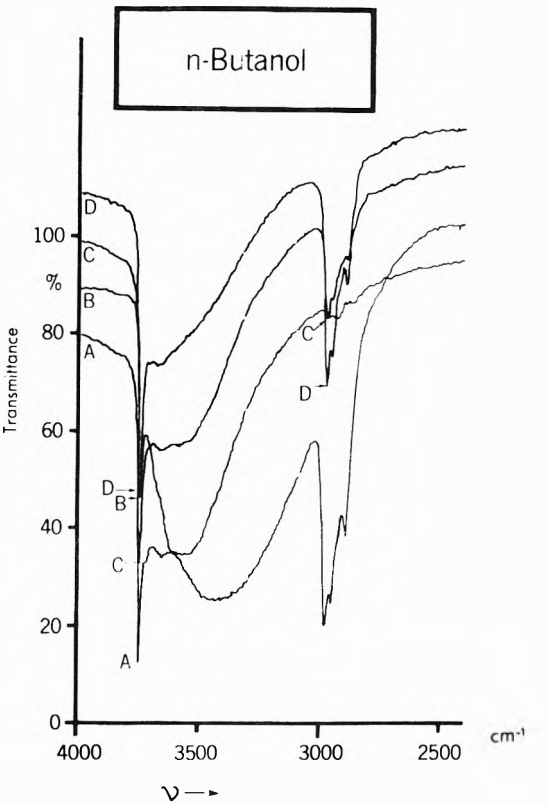

Figure 1. Reaction of 1-butanol with MS-5 silica: (A) silica alone; (B) exposed to 3 Torr of butanol at room temperature; (C) evacuated at room temperature; (D) heated with butanol at 250°, evacuated at room temperature.

Substituted Alcohols. When a room temperature activated sample of Cab-O-Sil MS-5 was exposed to 2 Torr of 2-mercaptoethanol, strong hydrogen bonding occurred with the free OH group giving rise to a broad OH band at 3500 cm^{-1}. Some of the adsorbed species could be removed by evacuation at room temperature. Heating the silica sample with mercaptoethanol at 100 and 250° further decreased the free OH band; the continued presence of bands of the mercaptoethanol even after heating under vacuum at 250° definitely indicates a chemical reaction of the alcohol with the silica. The band of the SH group at 2580 cm^{-1} was present throughout these experiments. Heating the sample at 400° resulted in considerable increase of the free OH band, decrease of the CH bands, and disappearance of the SH band, indicating decomposition of the surface compound. The reaction product formed at 250° was stable on treatment with water-saturated N_2 stream of 100° for 1 hr. These experiments indicate that it is possible, by allowing the silica to react with mercaptoethanol, to chemically bond to the silica a molecule that has an active grouping, the SH group, still present after the reaction; and that the reaction product is stable to heating at 250° and to hydrolysis at 100°.

In following the reaction of substituted alcohols with surface silanols we noted that furfuryl alcohol

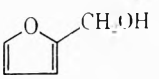

and especially 3-aminopropanol reacted to a much greater extent and at a lower temperature than did 1-butanol and

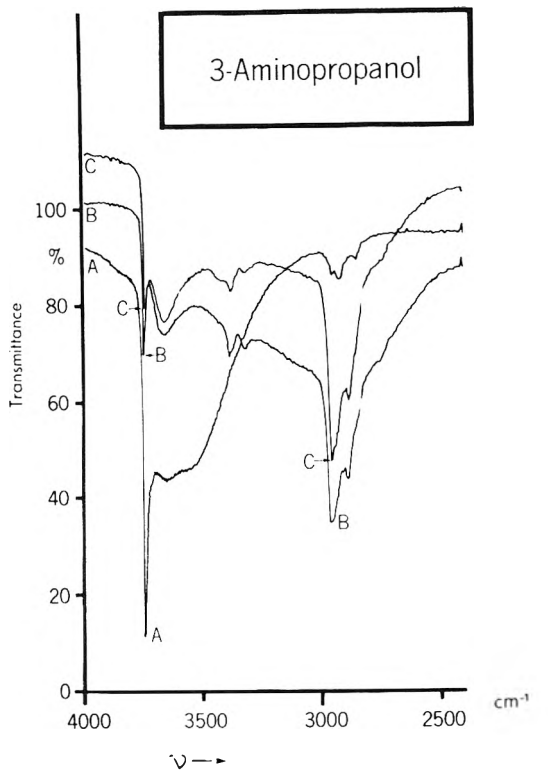

Figure 7. Reaction of 3-aminopropanol with MS-5 silica: (A) silica alone; (B) heated with aminopropanol at 250°; (C) evacuated at 250°.

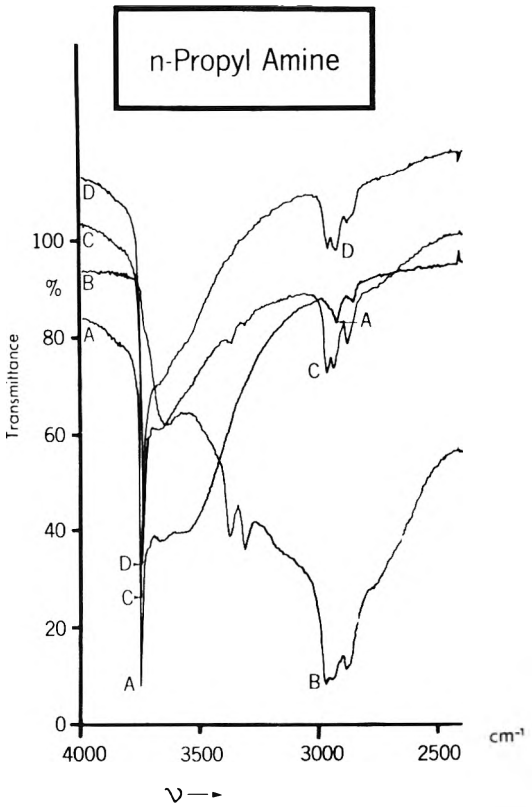

Figure 8. Reaction of *n*-propylamine with MS-5 silica: (A) silica alone; (B) exposed to 100 Torr propylamine at room temperature; (C) evacuated at room temperature; (D) heated with propylamine at 100°, evacuated at 100°.

the other alcohols discussed. The furfuryl alcohol results are shown in Figure 6 (available on microfilm) and the amino alcohol results are illustrated in Figure 7. For the amino alcohol a large amount of organic material, the presence of the amino group (3330–3390 cm^{-1}), and nearly complete absence of the free silanol could be observed after evacuation. This has been interpreted as almost complete reaction of the free silanols with alcohol hydroxyl groups. It might, however, be attributed in part to a low-frequency shift of the SiOH absorption band due to hydrogen bonding with the amine groups bound to the surface through SiOC linkages, *i.e.*

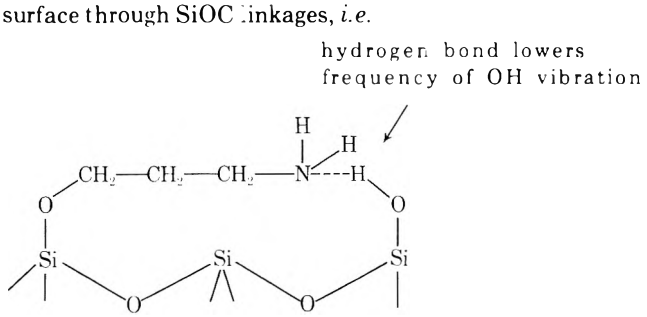

This association, however, cannot fully explain the free silanol disappearance, since significant bonding of this type should lead to a markedly increased intensity and broadening of the 3400–3700-cm^{-1} band, which should be removed on pumping (such a broadening and its removal on pumping can be observed in the case of *n*-propylamine, see Figure 8). Such a marked effect is not observed after evacuation. Thus, hydrogen bonding to the surface cannot be the full explanation for the observed effects; chemical bonding must be the primary reaction.

The reaction is so complete at room temperature that no further reaction could be observed on heating at 250°. The amino group was still present after the 250° evacuation indicating fairly high thermal stability.

Effect of Lewis Bases on Reactivity. It seemed unlikely that the enhanced surface reactivity of the amino and furfuryl alcohols could be caused by an inductive effect of the functional group. In order to better understand this phenomenon the two functional parts of the amino alcohol were separated. That is, we investigated the effect on silica of *n*-propylamine alone, of 1-butanol alone, and of mixtures of the two. Figures 1, 8, 9, and 10 illustrate a dramatic enhancing effect of the amino compound on the alcohol–silica surface reactions. We have seen in Figure 1 that butanol does not react significantly with silica at room temperature; Figure 8 shows that *n*-propylamine is not significantly reacted at room temperature. However, Figures 9 and 10 show that the combination of these (~1/1 mole ratio) yields a marked effect on the silica surface; after evacuation significant organic material is present and the free silanol band is completely removed. Note that the product of the reaction is only slightly effected by exposure to 100% relative humidity at 100°.

The same enhancing effect is also observed when a tertiary amine (triethylamine) or ammonia (Figure 11) is employed in place of *n*-propylamine. When ammonia alone is adsorbed on Cab-O-Sil, it can be completely desorbed and the silica spectrum restored by room temperature pumping.[8] Similarly, butanol is removed by evacuation at room temperature (Figure 1). However, when a 1:1 mixture of the two is applied to a silica sample (Figure 11) the free OH band at 3750 cm^{-1} is completely missing and the CH bands are very strong even after room temperature evacuation.

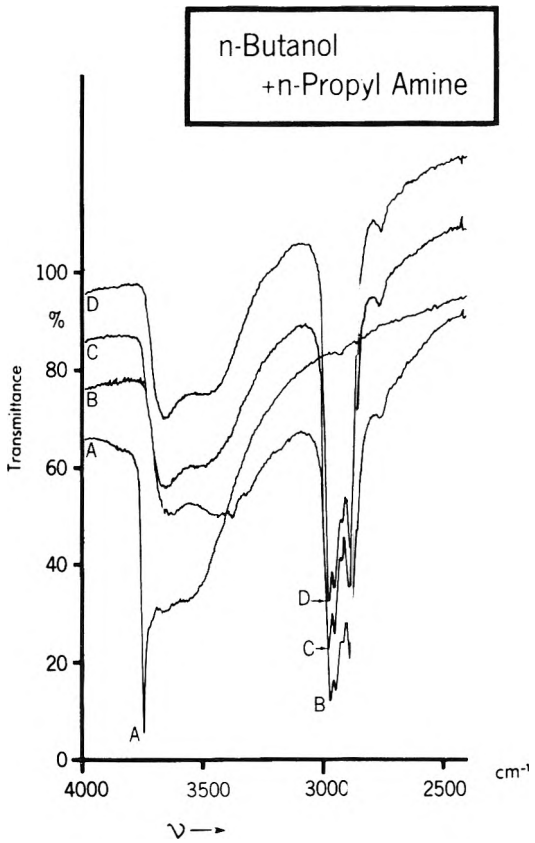

Figure 9. Reaction of 1-butanol/*n*-propylamine mixture with MS-5 silica: (A) silica alone; (B) exposed to 12 Torr (butanol/propylamine 1/1) at room temperature; (C) evacuated at room temperature; (D) heated with mixture at 100°; evacuated at 100°.

Clearly, these Lewis bases are enhancing the alcohol reactivity. One possible mechanism for this enhanced reactivity is illustrated in the following reaction scheme where the amine is shown to function as a catalyst *via* acceptance of a proton.

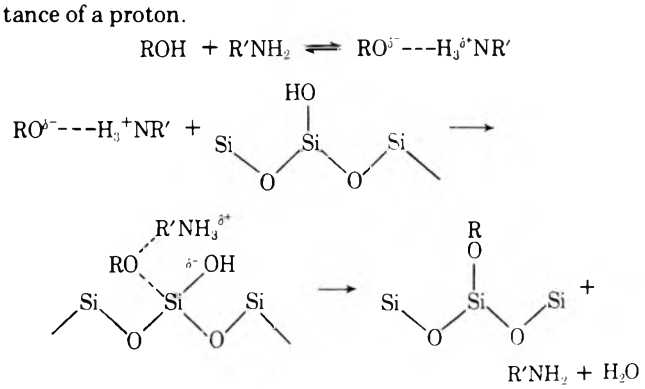

If the true mechanism is of this type, the acidic mercapto group in a mercapto alcohol might be expected to interfere with the action of the Lewis base by transfer of its proton. Spectra reveal that the effect of the amine is indeed reduced when 6-mercaptohexanol is employed in place of 1-butanol; nevertheless, there still appears to be some enhancement of reactivity when the amine is present.

Free vs. Adjacent Silanol Group Reactivity. It was of interest to determine whether alcohol silica reactions were occurring with free or adjacent silanol groups on the silica surface. To this end the surface was first prereacted with

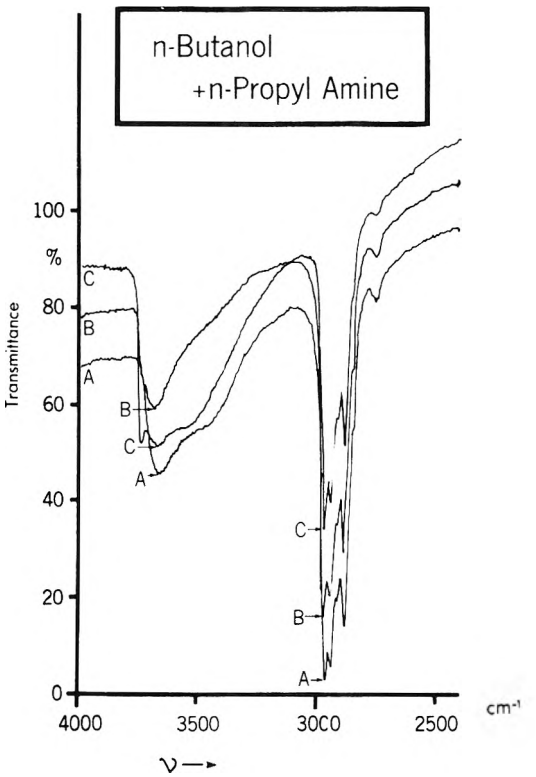

Figure 10. Reaction of 1-butanol/*n*-propylamine-mixture with MS-5 silica: (A) heated with mixture at 250°, evacuated at 250°; (B) heated with mixture at 400°, evacuated at 400°; (C) exposed to 100% relative humidity at room temperature for 2 hr, evacuated at room temperature.

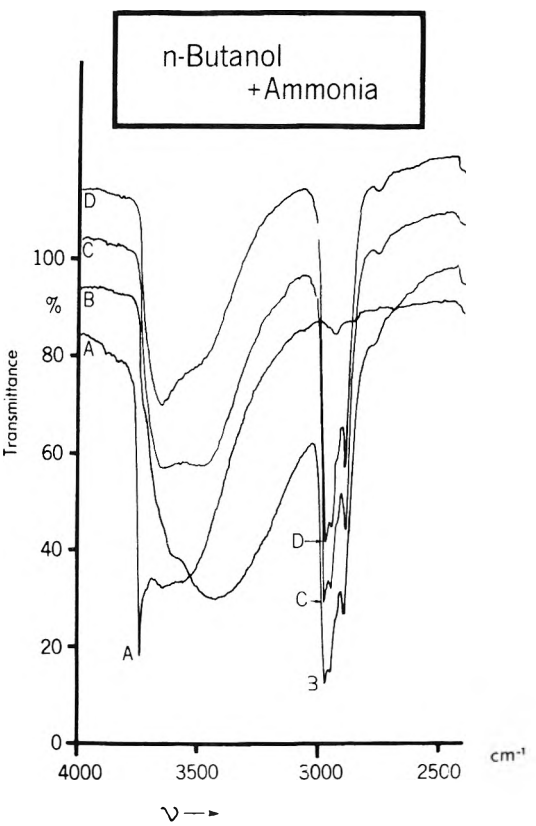

Figure 11. Reaction of 1-butanol/ammonia mixture with MS-5 silica: (A) silica alone; (B) exposed to 12 Torr (butanol/ammonia 1/1) at room temperature; (C) evacuated at room temperature; (D) evacuated at 250°.

a silane (trimethylsilyldimethylamine, TMSA) to block the free silanols. The silica sample was vacuum activated at room temperature and then treated with TMSA and evacuated. The resulting spectrum showed complete removal of free surface OH's and very strong CH bands. The sample was then exposed to either furfuryl alcohol or 3-aminopropanol at room temperature and at 250°. In each case there were no visible changes in the spectrum indicating that no reaction of the alcohols occurred when the free silanols were blocked. This indicates that the alcohols react with the free surface silanols.

Conclusions

Alcohols have been shown to undergo condensation reactions with the free silanol groups on the surface of silica. The extent of this reaction is dependent upon several factors. Primary alcohols were found to react to a somewhat greater extent than secondary alcohols and the product to be thermally more stable. Unsaturation in the 2 position modifies reactivity while unsaturation beyond the 2 position appears to have little effect. Most notably, Lewis bases (both as alcohol substituents and as separate molecules) markedly enhance (catalyze) these condensation reactions and allow them to occur at room temperature. A similar enhancing effect of Lewis bases has been reported for silane–silica reactions.[7] Several of these surface reaction products exhibit good hydrolytic and thermal stabilities.

Acknowledgment. We wish to acknowledge the excellent assistance of Messers. R. W. Larson and M. J. O'Hara.

Supplementary Material Available. Figures 2-6 will appear following these pages in the microfilm edition of this volume of the journal. Photocopies of the supplementary material from this paper only or microfiche (105 × 148 mm, 20× reduction, negatives) containing all of the supplementary material for the papers in this issue may be obtained from the Journals Department, American Chemical Society, 1155 16th St., N.W., Washington, D. C. 20036. Remit check or money order for $3.00 for photocopy or $2.00 for microfiche, referring to code number JPC-73-3048.

References and Notes

(1) T. E. White, 20th Annual SPI Reprints, Chicago, Feb 1965, Section 3B.
(2) M. L. Hair and W. Hertl, *J. Phys. Chem.*, **73**, 2372 (1969).
(3) E. V. Broun, *et. al.*, *Russ. J. Phys. Chem.*, **44**, 443 (1970).
(4) R. K. Iler, U. S. Patent 2,657,149 (1953).
(5) C. L. Angell and P. C. Schaffer, *J. Phys. Chem.*, **69**, 3463 (1965).
(6) M. L. Hair, "Infrared Spectroscopy in Surface Chemistry," Marcel Dekker, New York, N. Y., 1967.
(7) R. L. Kaas and J. L. Kardos, *Polym. Repr.*, **11**, 258 (1970).
(8) N. W. Cant and L. H. Little, *Can. J. Chem.*, **43**, 1252 (1965).

Infrared Studies of the Formation of Hydroxyl Groups during Hydrogen–Oxygen Reactions on Noble Metal Catalysts

B. A. Morrow* and P. Ramamurthy

Department of Chemistry, University of Ottawa, Ottawa, Canada K1N 6N5 *(Received May 11, 1973)*

Publication costs assisted by the National Research Council of Canada

Infrared spectroscopy has been used to investigate the conditions under which surface metal–hydroxyl groups can be formed on some silica-supported group VIII metals. When O_2 reacts with hydrogen-covered metals, ν(OH) bands of MOH species are observed in the infrared for Pt(3497 cm^{-1}), Ir(3585 cm^{-1}), Rh(3538 cm^{-1}), Ni(3672 cm^{-1}), Co(3660 cm^{-1}), and Fe(3685 cm^{-1}) but not for Ru and Os. In addition, a second PtOH band is observed at 3544 cm^{-1} when H_2O reacts with a partially reduced PtO surface. In agreement with other work, MOH species are not formed when H_2O reacts with bare metal, nor when H_2 reacts with metal oxide. The experimental evidence suggests that the ratio of PtOH/PtO is approximately 1/2 when O_2 reacts with hydrogen covered Pt, and using existing literature data for the H_2–O_2 titration reactions on Pt, a new reaction mechanism is proposed which is based on this ratio.

In a previous communication[1] we reported the first infrared spectroscopic evidence for the formation of PtOH groups on the surface of silica-supported platinum. Although the existence of such species have for many years been evoked by electrochemists,[2,3] such species have not been widely recognized by those whose major interest is concerned with chemisorption at the gas-solid interface.[4-8] In some recent reports.[9,10] the possible existence of PtOH is discussed. and in view of the importance of this species when discussing mechanisms of the H_2–O_2 reaction on platinum, it is important to establish the conditions under which surface hydroxyl species are formed. In the present paper, we have investigated whether metal hydroxyl species can be formed on other group VIII metals.

Experimental Section

Silica-supported metal samples were prepared by mixing about 2 g of Cab-O-Sil (H5) with 1 g of a suitable salt (Table I) dissolved in about 20 ml of anhydrous acetone. The solvent was removed by evacuation at room temperature and 200 mg sample disks of each material were pressed in a die at about 1000 lb/

TABLE I: Experimental Details for Silica-Supported Metal Samples

Metal	Salt used	Wt % of metal after reduction
Pt	H_2PtCl_6	15.8
Ir	H_2IrCl_6	15.7
Rh	$Rh(NO_3)_2 \cdot 2H_2O$	13.5
Ru	$RuCl_3$	13.7
Os	H_2OsCl_6	12.6
Pd	$PdCl_2$	10.7
Ni	$Ni(NO_3)_2 \cdot 6H_2O$	9.2
Co	$Co(NO_3)_2 \cdot 6H_2O$	9.2
Fe	$Fe(NO_3)_3 \cdot 9H_2O$	6.5

in.[2] for a few seconds. The silica-supported salts were reduced to metal by heating in hydrogen in a standard all glass infrared cell at 400° (500° for Fe). Prior to impregnation, the silica had been heated in an oven at 700° for about 12 hr in order to drive off all of the physically adsorbed water. This treatment removed most of the hydrogen-bonded surface silanol groups and rendered the support relatively hydrophobic so that the hydroxyl groups did not re-form after exposure to ambient atmosphere.[11,12] Anhydrous acetone was used for the impregnation to minimize the rehydration of the support. Since we expected that metal–hydroxyl species would absorb in the infrared between 3750 and 3400 cm^{-1}, it was extremely important to take these precautions so as to remove all possible interference due to infrared absorption by the support itself in this spectral region. A pure silica prepared by heating at 700° as described shows a single sharp absorption band at 3750 cm^{-1} due to isolated surface silanol groups,[11-13] whereas a fully hydrated silica has a very broad and intense absorption between 3750 and 3400 cm^{-1}. A typical background spectrum of a silica-supported metal sample showing the silanol band is given in Figure 3A.

Oxygen-18 enriched H_2O (98.8% ^{18}O) and O_2 (99.4% ^{18}O) were obtained from Oak Ridge National Laboratory, and ^{13}C ethylene (60% ^{13}C) was obtained from Isomet Corporation. High-purity hydrogen was prepared by passage of cylinder H_2 through a palladium hydrogen purifier and oxygen was prepared by the decomposition of $KMnO_4$ or was Matheson Extra Dry Grade. Starting materials and final metal loadings of the various silica-supported metals are listed in Table I

Because the validity of our earlier communication has been challenged,[14] the details of our reaction cell are shown in Figure 1. The sample (1 in. diameter) was placed in a forked quartz holder and was held in place by the pressure on the fork. This holder could be raised with an external magnet to a heating area which is about 20 cm from the cell windows and it was in this area where all thermal treatments were carried out. About six cells have been used in this work, and the windows were of either CaF_2 or NaCl (both types used at least once in all experiments), and all samples could be used repeatedly after the initial reduction by regenerating the sample in H_2 at 400° as described previously.[15] All of the spectral features noted in this work could be reproduced with samples which were either new, or which were up to 1 year old and had been subjected to many (10 to 100) "regeneration" cycles, or samples which had been used in a variety of other adsorption experiments. No infrared absorptions attributable to species on the cell windows have ever been noted.

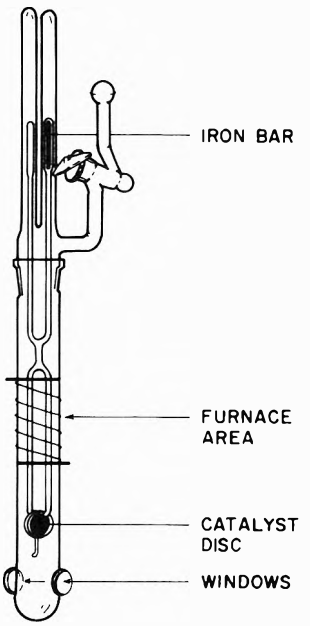

Figure 1. Infrared cell. The lower section and the sample holder are made of quartz; the upper section, including stopcock, is constructed of Pyrex. The distance from the windows to the heating area is about 20 cm.

All spectra were recorded on a modified Perkin-Elmer Model 13G infrared spectrometer, employing spectral slit widths of about 2–4 cm^{-1}. Spectra were calibrated against atmospheric water bands, but because of the breadth and variability in position of some absorptions, observed wave numbers are believed to be accurate to about ± 3 cm^{-1}.

Results

When gaseous water was added to any new or regenerated silica-supported metal sample, no new absorptions were detected except the broad feature between 3600 and 3400 cm^{-1} and at 1600 cm^{-1} due to physically adsorbed water (*e.g.*, see Figure 3C), and (near 3600 cm^{-1}) to the re-formation of a small number of hydrogen-bonded silanol groups.[11,12] However, when oxygen was added to hydrogen-covered platinum, iridium, rhodium, and nickel, the spectra shown in Figure 2A, 2C, 3B, and 4B, respectively, were obtained; in each case an additional new feature to low wave number of the 3750-cm^{-1} band is observed. Hydrogen-covered samples were prepared by cooling the disks from 400 to 25° in hydrogen after reduction or regeneration followed by evacuation for about 5 min.[15] The wave number shift for oxygen-18 (from $^{18}O_2$) or deuterium (from D_2O) substitution indicated that the new features are all associated with the formation of a new OH containing species.[13] The wave number of the observed bands for all isotopic species are listed in Table II. The same absorption for nickel could also be produced by degassing silica-supported nickel nitrate at 400° under vacuum (Figure 4C). None of these features was produced with silica alone and in view of the differing wave number for each band, and of the absence of any absorption in the 1600-cm^{-1} spectral region (corresponding to the angle deformation mode of water) the new features are all assigned to surface metal–hydroxyl groups; these will be referred to as type I hydroxyl groups. Further evidence in support of this assignment is presented below. Some additional experiments are described for each metal.

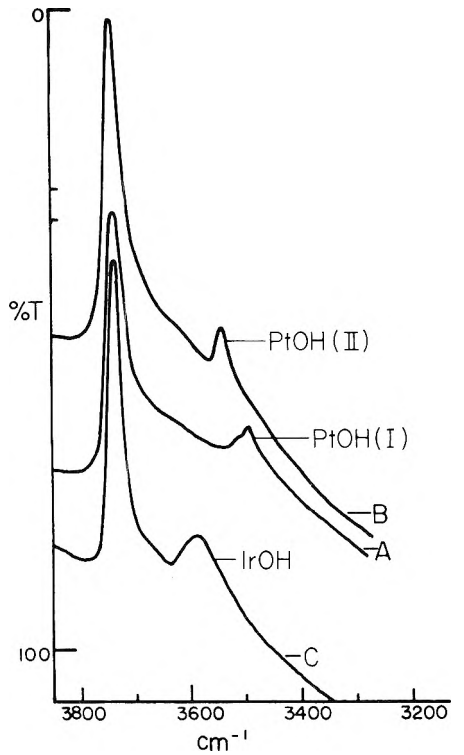

Figure 2. (A) Spectrum obtained after adding O_2 to hydrogen covered Pt. The strong band at 3750 cm^{-1} is due to SiOH groups of the support and the weak band at 3497 cm^{-1} is the type I PtOH band. (B) Type II PtOH band after adding H_2O to a sample which had been degassed at 400° after formation of the type I PtOH band. (C) IrOH band after adding O_2 to hydrogen covered Ir. The transmittance scale (large horizontal dashes) refers to the top-most spectrum (B), whereas the small dashes give the zero transmittance points for the remaining spectra. A typical background spectrum for all the noble metals is shown in Figure 3A.

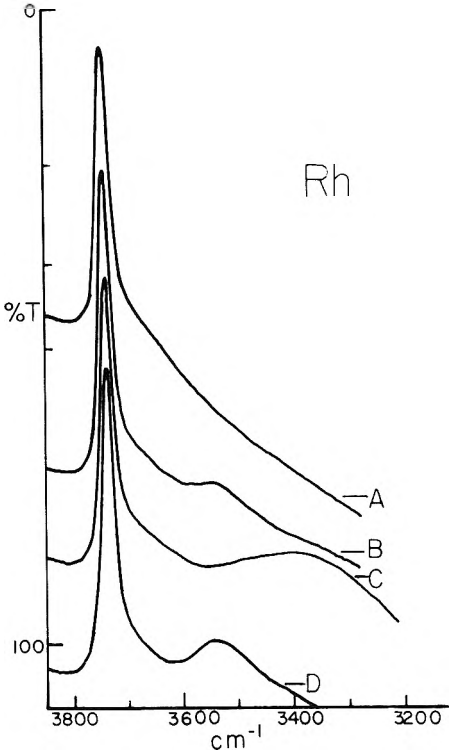

Figure 3. (A) Background spectrum of H-covered silica-supported Rh. (B) Spectrum obtained after adding O_2 to A. (C) After adding H_2 to B. The broad band is due to physically adsorbed water. (D) After adding O_2 to C and heating at 100° for 30 min, followed by degassing.

TABLE II: Observed Wave Numbers for Metal–Hydroxyl Species (cm^{-1})

Metal	^{16}OH	^{18}OH	^{16}OD
Pt	3497 (I)	3487	2580
	3544 (II)	3534	2609
Ir	3585	3575	2635
Rh	3538		2607
Ni	3672	3662	2715
Co	3660		2690
Fe	3685		

Platinum. For platinum, when O_2 was added to a sample which was covered with both H_2 and H_2O (*i.e.*, after adding about 40 Torr of H_2 and evacuating, then adding 10 Torr of H_2O and evacuating), an additional weak feature at 3544 cm^{-1} was observed (type II hydroxyl, see ref 1 for spectra). Neither band (nor the 3497-cm^{-1} band alone) diminished in intensity after prolonged evacuation at 25°, but they did slowly diminish after heating for 2 hr at 400°. When water was added (at 25°) to a sample which had been briefly heated to 400° so as to remove the hydroxyl groups, both bands were regenerated. However, after longer periods of evacuation at 400° only the 3544-cm^{-1} band was regenerated (Figure 2B) when H_2O was added at 25°, and this could be converted to a weak type I hydroxyl band by adding O_2 at room temperature. The 3497-cm^{-1} band also appeared in some spectra as a doublet, as seen in the spectrum in Figure 2A.

Both types of hydroxyl band immediately disappeared when ethylene or ethylene-^{13}C was added, and a band near 2050 or 2000 cm^{-1}, respectively, appeared which is attributed to adsorbed PtCO species.[16] This behavior was also found with a variety of other organic molecules and with CO and CO_2, and such behavior does not occur with the support alone.

Iridium. The 3585-cm^{-1} band was stable to evacuation up to 200°, but at higher temperatures it eventually disappeared. However, the band reached its maximum intensity if the sample was heated in O_2 to 100°; with Pt, the 3497-cm^{-1} band always decreased in intensity when heated under vacuum or in O_2. When ethylene was added, the IrOH band disappeared and a spectrum of IrCO groups was observed near 2050 cm^{-1}. After adding water to a sample which had been degassed at 400° (using the same conditions which were used to produce the type II PtOH band) a very weak type I IrOH band at 3585 cm^{-1} was regenerated and adsorbed CO was produced after the subsequent addition of ethylene.

Rhodium. The single RhOH band was thermally stable up to 300° and disappeared completely if heated at higher temperatures. After this dehydroxylation was carried out at 400°, the same RhOH band was regenerated when water was added, but it was of greatly diminished intensity. When hydrogen was added to the original RhOH containing sample, the hydroxyl band disappeared and water was formed (Figure 3C), but when O_2 was subsequently added the RhOH band was immediately regenerated. Like irridium, the hydroxyl band intensified after heating in oxygen at 100° (Figure 3D). Unlike Pt and Ir, the RhOH band did not disappear when ethylene was added, at room temperature, nor was a spectrum of adsorbed CO ob-

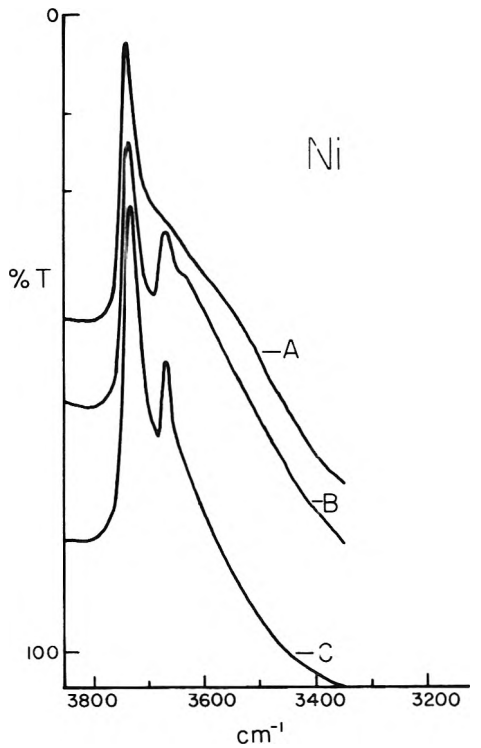

Figure 4. (A) Backgraound spectrum of H-covered silica-supported Ni. (B) After adding O_2 to A. (C) Spectrum obtained after degassing silica-supported $Ni(NO_3)_2$ at 400° for 2 hr.

served; however, the reverse happened when CO was added.

Nickel. The NiOH band at 3672 cm^{-1} disappeared only after heating under vacuum at 600°, and the hydroxyl band could be regenerated by adding water at room temperature. The hydroxyl band could not be removed by adsorption of ethylene, CO, or H_2 at room temperature, but it could be removed by reduction with H_2 at 300°. In the presence of gaseous NH_3, or pyridine, the sharp band disappeared or decreased in intensity depending on the pressure as hydrogen bonds were formed between the NiOH groups and the reactant species, but the sharp band was restored when the gas was pumped off. This showed that all of the NiOH groups were at the surface, an important finding, since Peri[17] had observed a similar band at 3620 cm^{-1} on partially reduced nickel–silica aerogels and had assigned this band to SiOH groups perturbed by the presence of nickel ions.

Cobalt. When oxygen was added to a hydrogen-covered silica-supported cobalt sample, only a broad shoulder was observed to the low wave number side of the SiOH band. However, on degassing for 2 hr at 200°, a distinct but weak band due to CoOH groups was observed at 3660 cm^{-1}. This band was only removed by evacuation at 500° or heating in H_2 at 400°.

Iron. It was not possible to prepare a "clean" sample (*i.e.*, free of many spurious infrared absorption bands) with the techniques described above and no new bands formed when O_2 was added to a hydrogen-covered sample. However, if a silica-supported $Fe(NO_3)_3$ sample was reduced in H_2 at 500° for 13 hr then a "clean" sample resulted. When O_2 was added to this hydrogen-covered sample, no new bands were observed in the first instance, but a weak band slowly developed near 3685 cm^{-1} after 13-hr contact with gaseous O_2 which we have assumed is due to the presence of surface FeOH groups. No further investigations of this system were carried out as we were mainly interested in the noble metal systems.

Other Metals. No spectroscopic evidence for the formation of surface hydroxyl groups on palladium, osmium, or ruthenium was found after allowing either water or oxygen to react with hydrogen-covered or hydrogen-free supported metals. In the case of Pd, since only water could be used as a solvent for $PdCl_2$, extensive rehydration of the silica support occurred resulting in a broad band near 3500 cm^{-1} which could obscure a weak PdOH band if one formed.

Discussion

The present work, and our previous communication,[1] represents the first infrared spectroscopic evidence for the existence of surface hydroxyl species on Pt, Rh, and Ir, whereas the spectroscopic observation of surface nickel hydroxyl groups has been reported by others.[18,19] One of the most important questions concerns the relative proportion of oxide and hydroxide at the surface; we will discuss this and other questions below.

Platinum. The OH stretching mode of the surface PtOH species in the present work is close in frequency to that of some known PtOH containing compounds; $(CH_3)_3PtOH$,[20] 3559 cm^{-1}; $Ag_2(PtCl_5OH)$,[1] 3512 cm^{-1}; $Pt(OH)_2(CN)_2(NH_3)_2$,[21] 3438 cm^{-1}.

Surface hydroxyl species on platinum have always played an important mechanistic role in electrochemical processes[3,4,22] in aqueous media, but their existence has largely been ignored in gas–solid work, particularly in considerations of the H_2–O_2 titration reaction.[4,5,7,8] Of particular interest in the present work are the conditions under which PtOH species are generated. That they are not formed when H_2O reacts with a fresh Pt surface, or when H_2 is added to an oxygen-covered Pt surface, is in agreement with the findings of Darensbourg and Eischens.[6] Further, this work would also support the widely held notion that water is the sole reaction product when adsorbed oxygen is titrated with H_2.[4,5,7,8]

A quantitative study of the oxidation of ethylene to CO when surface oxide or hydroxyl groups are present can provide some idea of the surface coverage by these species. Since relatively large dead volumes and small samples were employed in this work it has not been possible to carry out a quantitative analysis of the reaction products from this reaction. Furthermore, the mechanistic details of the oxidation when excess O_2 is present are not known and H_2O and CO_2 are virtually the sole gaseous products.[23] Therefore, we cannot comment on how the present oxidation proceeds, nor can we speculate about the fate of the ethylenic hydrogens except to note that small quantities of water were formed during the reaction and this remained physically adsorbed on the catalyst. Within these limitations, we have assumed that the PtCO band intensity near 2050 cm^{-1} (and the results below were identical using either peak adsorbances or band areas) will be proportional to the total original "oxygen" content of the surface (either as oxide or hydroxide) in order to obtain a very crude estimate of this parameter. We have also assumed that the areas of the PtOH bands will be related to the proportions of type I to type II hydroxyl species. By following the spectral changes after "titrating" our samples with small doses of ethylene, the following results and conclusions were reached.

(1) The intensity of either the type I or II hydroxyl band decreased in direct proportion to the increase in intensity

TABLE III: CO Band Intensities after Saturation of Oxygen-Treated Pt with C_2H_4

Condition	Treatment	CO band intensity (arbitrary units)	No. of surface oxygen atoms	No. of surface OH groups	No. of surface oxide atoms
a	Only type I OH present	12	12*n*	4*n*	8*n*
b	Type I OH formed, sample heated to 400°, cooled to 25°; no PtOH present	1	1*n*	0	1*n*
c	Only type II OH present [condition b + H_2O added and evacuated]	2	2*n*	2*n*	0

TABLE IV: Data of Akhtar and Tompkins[a] for O_2-H_2 Reactions on Evaporated Pt Films

Film A			Film B		
O_2 uptake, mol × 10^{-8}	H_2 uptake, mol × 10^{-8}	*n*th H_2 uptake/ (*n* + 1)th O_2 uptake	O_2 uptake, mol × 10^{-8}	H_2 uptake, mol × 10^{-8}	*n*th H_2 uptake/ (*n* + 1)th O_2 uptake
45.4	132.0	2.28	59.0	166.8	2.29
58.0	115.5	2.16	72.9	134.0	1.96
53.5	113.0	2.08	68.5	143.0	2.03
54.4[b]	110.0	1.95	70.4	142.6	2.07
56.3	108.0	2.01	69.0	134.8	1.97
53.8	106.0	1.92	68.5		
55.2					
Mean 55.2	110.5		69.3	138.6	

[a] Reference 9. [b] Incorrectly listed as 45.4 by Akhtar and Tompkins (private communication).

of the PtCO band. At the same time, a weak spectrum due to chemisorbed ethylene was observed,[15] and this reached its maximum intensity at approximately the same point in the titration as did the PtCO spectrum. Therefore, there is no preferential oxidation of ethylene by PtOH or PtO.

(2) When the type I hydroxyl band was observed alone, its intensity was twice as great as that observed when only the type II hydroxyl was present. Therefore, at maximum coverage for each type of hydroxyl, the ratio of PtOH(I)/PtOH(II) equals 2.

(3) The data for the final relative PtCO band intensities measured after saturating a sample with ethylene at various stages of treatment are given in Table III. By assuming that this intensity is proportional to the number of "oxygen" atoms originally present, the latter has been arbitrarily designated as *n* times this intensity factor since it is only the relative proportions of surface oxygen resulting from these treatments that will be of further interest.

The addition of H_2O is a necessary condition to generate the type II hydroxyls after treatment b in Table III, and since treatment c simply doubles the total oxygen content relative to b, the stoichiometry of the reaction during treatment c must be of the type

$$Pt_2O + H_2O \longrightarrow 2PtOH$$

where the Pt represents surface atoms. We can presume that after treatment b there would be many other surface Pt atoms which do not have oxygen atoms associated with them and which are unreactive with H_2O, as has been found on a freshly prepared nonoxygen treated Pt surface. It follows from the above argument that the 2*n* "oxygen" sites after treatment c must all be in the form of type II PtOH groups, and therefore, in view of item 2 above, there must be 4*n* type I hydroxyl groups after treatment a.

The number of oxide and hydroxide sites for each treatment has been entered in the last two columns of Table III since the sum of these must equal the total number of "oxygen" atoms as determined by the CO intensity measurements. From the table it can be seen that when only the type I hydroxyl groups are present, the ratio of PtOH/PtO sites is 1/2.

Akhtar and Tompkins[9] have recently investigated the stoichiometry of the following reactions on platinum films at 195°K

$$Pt + \tfrac{1}{2}O_2 \longrightarrow PtO \quad (1)$$

$$PtO + \tfrac{3}{2}H_2 \longrightarrow PtH + H_2O \quad (2)$$

$$PtH + \tfrac{3}{4}O_2 \longrightarrow PtO + \tfrac{1}{2}H_2O \quad (3)$$

By measuring the initial oxygen uptake, and the subsequent uptake of both H_2 and O_2 during the sequence of titration reactions depicted by eq 2 and 3, they found that the ratio of the second to first uptake of O_2 [reaction 3/reaction 1] was about 1.27 instead of 1.50, thus suggesting that some of the oxygen initially chemisorbed is inactive with respect to hydrogen titration. On the basis of the oxygen uptake, they then went on to show that if about 15–17% of the oxygen sites were "inactive" in reaction 2, perhaps forming PtOH groups or a $PtOH_2$ complex, then they could account for their findings.

Akhtar and Tompkins also state that the ratio of H_2 uptake/O_2 uptake during titration is very close to 2.00. In fact, their values differ widely, and only average to 2.00 (ignoring the first uptake of O_2 and H_2). It is more revealing to consider the ratio of the *n*th uptake of H_2/(*n* + 1)th

uptake of O_2, $n = 1,2 \ldots$, since this is the order in which the successive titrations were carried out after the initial O_2 chemisorption (reaction 1). Akhtar and Tompkins' data for two Pt films and the above ratios are given in Table IV. From this table it can be seen that the ratio of the first uptake of H_2/second uptake of O_2 (2.28 and 2.29) is considerably greater than this ratio for successive titrations ($n > 1$), the values tending to decrease to a mean of 2.00 as the number of titrations increases.

Akhtar and Tompkins have attributed the anomalously high value for the first H_2 uptake, and the previously mentioned anomalously low ratio of the second O_2 uptake/first O_2 uptake (1.28 instead of 1.50 theoretical) to the formation of "inactive" oxygen centers which form during the first O_2 chemisorption and first H_2 titration and which yield PtOH and $PtOH_2$ species. Our work has indicated that such species are not apparently formed *via* reaction 2, but PtOH species can be formed *via* reaction 3. If we assume that one of every three oxygen atoms as a result of reaction 3 is a hydroxyl group, the following sequence of reactions might occur during the Akhtar and Tompkins reaction cycle

$$Pt + \tfrac{1}{2}O_2 \longrightarrow PtO \quad (1)$$

$$PtO + \tfrac{3}{2}H_2 \longrightarrow PtH + H_2O \quad (2)$$

$$PtH + \tfrac{2}{3}O_2 \longrightarrow \tfrac{1}{3}PtOH + \tfrac{2}{3}PtO + \tfrac{1}{3}H_2O \quad (4)$$

$$\tfrac{1}{3}PtOH + \tfrac{2}{3}PtO + \tfrac{4}{3}H_2 \longrightarrow PtH + H_2O \quad (5)$$

where (1) and (2) correspond to the first uptake of O_2 and H_2, respectively, and reactions 4 and 5 correspond to successive titrations. From this scheme, the ratio of the first uptake of H_2/second uptake of O_2 [(2)/(4)] would be 2.25 (experiment 2.28–2.29), and the ratio of the nth uptake of H_2/(n + 1)th uptake of O_2 [(5)/(4)] would be 2.00 for $n >$ 1 (experimental mean 2.02 for film A and 2.01 for film B). Further, the ratio of the second uptake of O_2/first uptake of O_2 [(4)/(1)] would be 1.33 as compared with experimental values of 1.28 and 1.24, values which are more reasonable than the value of 1.50 predicted by the scheme of Akhtar and Tompkins.

Hence it is not necessary to postulate that "inactive" oxide centers exist on Pt in order to account for the results of Akhtar and Tompkins, and the calculations above can be considered independently from our experimental work. We have stressed that our own value of 1/2 for the hydroxyl/oxide ratio is at best a crude approximation and in the absence of a careful parallel gravimetric study is to be treated as a guide only.

The explanation of the existence of two types of surface hydroxyl groups on Pt is almost certainly connected with the average oxidation state of the individual Pt atoms. Thus, when the surface oxygen content is high, the type I hydroxyl groups may correspond to a situation in which the Pt atom is bonded to other oxygen atoms, whereas the type II hydroxyls exist only when the oxygen content is low and in view of the CO results, these may correspond to isolated PtOH species where the Pt is bonded only to other Pt atoms. Support for this comes from the observation that the type II hydroxyl band can be converted to a type I hydroxyl after addition of O_2.

Iridium and Rhodium. Unlike Pt, we were unable to find any examples in the literature of Ir or Rh compounds which have nonhydrogen bonded OH groups; therefore, a comparison of our metal–OH frequencies with those for model compounds is not possible. However, the fact that only type I hydroxyls are formed and that the reactivity of the oxides toward CO and ethylene differs from that of Pt does illustrate that these surfaces have quite different properties.

The only characterized anhydrous oxides of Pt, Ir, and Rh are PtO, PtO_2, IrO_2, and Rh_2O_3, and the stability with respect to disproportionation into oxygen and metal is in the order Pt < Ir < Rh.[24,25] The fact that O_2 treated Rh–H is not capable of oxidizing ethylene is probably just a reflection of the greater stability of the Rh surface oxide. Also, the fact that both Rh and Ir are unreactive with H_2O after degassing at 400° (*i.e.*, type II hydroxyls are not formed) is probably again a reflection of their stability with respect to Pt. This increased stability might well be related to the fact that many partial oxidation products are produced when Ir and Rh are used as catalysts for the oxidation of O_2/hydrocarbon mixtures, whereas CO_2 and H_2O are almost the sole products when Pt is used.[23]

Nickel. The NiOH band in the present work (3672 cm^{-1}) is close to the single band reported by Kober[18] (3650 cm^{-1}) for pure $Ni(OH)_2$ prepared at room temperature. Tretyakov and Filimonov[19] report three bands at 3735, 3690, and 3630 cm^{-1} (no spectrum or relative intensities given) after heating NiO in air at 500°. The band reported at 3620 cm^{-1} by Peri[17] for a nickel–silica aerogel system appears at first to be quite different from ours (apart from the frequency shift) since it could not be removed by heating in hydrogen at 400°. Peri[17] suggests that this band is due to SiOH groups perturbed by the presence of nickel ions; however, Mathieu[26] suggests that it is due to NiOH species since he has observed such a band from pure $Ni(OH)_2$ near the same wave number. Mathieu[26] and Webb[27] have pointed out that Peri's aerogel support is somewhat unusual and might introduce features not encountered in the conventional supported systems as used in this work. We would be inclined to assign Peri's band to perturbed NiOH and not to perturbed SiOH.

Since nickel oxide is much more stable than the oxides of Pt, Ir, and Rh, the lack of reactivity with CO or ethylene is not surprising.

Osmium and Ruthenium. The failure to detect OsOH species (near 3200 cm^{-1}) was a disappointment, since many OsOH containing compounds are known. However, in view of the well-known volatility of OsO_4 and RuO_4, it is possible that the oxygen treatment simply resulted in the formation of these volatile oxides which subsequently left the surface.

Acknowledgment. We are very grateful to Atomic Energy of Canada Ltd. for a contract which provided the major financial support for this work. Partial assistance was also provided by the National Research Council of Canada. We wish to thank Dr. B. E. Conway and Dr. A. D. Westland for many helpful discussions.

References and Notes

(1) B. A. Morrow and P. Ramamurthy, *Can. J. Chem.*, **49**, 3409 (1971).
(2) H. Angerstein-Kozlowska, B. E. Conway, and W. B. A. Sharp, *J. Electroanal. Chem.*, **43**, 9 (1973).
(3) S. Gottesfeld and B. E. Conway, *J. Chem. Soc., Faraday Trans. 1*, **69**, 1090 (1973).
(4) G. R. Wilson and W. K. Hall, *J. Catal.*, **24**, 306 (1972).
(5) R. A. Dalla Betta and M. Boudart, paper no. 100, 5th International Congress on Catalysis, Palm Beach, Aug 1972.
(6) D. J. Darensbourg and R. P. Eischens, paper no. 2[illegible], 5th International Congress on Catalysis, Palm Beach, Aug 1972.
(7) G. R. Wilson and W. K. Hall, *J. Catal.*, **17**, 190 (1970).
(8) Y. Barbaux, B. Roger, J.-P. Beaufils, and J. E. Germain, *J. Chim. Phys.*, **67**, 1035 (1970).

(9) M. Akhtar and F. C. Tompkins, *Trans. Faraday Soc.*, **67**, 2454 (1971).
(10) C. W. Jowett, P. J. Cobson, and B. J. Hopkins, *Surface Sci.*, **17**, 474 (1969).
(11) C. G. Armistead and J. A. Hockey, *Trans. Faraday Soc.*, **63**, 2549 (1967).
(12) C. G. Armistead, A. J. Tyler, F. H. Hambleton, S. A. Mitchell, and J. A. Hockey, *J. Phys. Chem.*, **73**, 3947 (1969).
(13) B. A. Morrow and A. Devi, *J. Chem. Soc., Faraday Trans. 1*, **68**, 403 (1972).
(14) M. Primet and M-V. Mathieu, *Can. J. Chem.*, **51**, 2255 (1973).
(15) B. A. Morrow and N. Sheppard, *Proc. Roy. Soc., Ser. A*, **311**, 391 (1969).
(16) R. M. Hammaker, S. A. Francis, and R. P. Eischens, *Spectrochim. Acta*, **21**, 1295 (1965).
(17) J. B. Peri, *Discuss. Faraday Soc.*, **41**, 121 (1966).
(18) F. P. Kober, *J. Electrochem. Soc.*, **112**, 1064 (1965); **114**, 215 (1967).
(19) N. E. Tretyakov and U. N. Filimonov, *Kinet. Katal.*, **13**, 815 (1972).
(20) M. N. Hoechstetter, *J. Mol. Spectrosc.*, **13**, 407 (1964).
(21) Yu Ya. Kharitonov, O. N. Evstafeva, I. B. Baranovskii, and G. Ya. Mazo, *Russ. J. Inorg. Chem.*, **14**, 248 (1969).
(22) A. K. Vijh, *Can. J. Chem.*, **49**, 78 (1971).
(23) N. W. Cant and W. K. Hall, *J. Catal.*, **16**, 220 (1970).
(24) W. P. Griffith, "The Chemistry of the Rarer Platinum Metals," Interscience, London, 1967.
(25) N. V. Sidgwick, "The Chemical Elements and Their Compounds," Clarendon Press, Oxford, 1950.
(26) M. V. Mathieu, *Discuss. Faraday Soc.*, **41**, 177 (1966).
(27) A. N. Webb, *Discuss. Faraday Soc.*, **41**, 178 (1966).

Temperature-Dependent Electron Spin Resonance Spectrum of Chlorine Trioxide Radicals Trapped in Magnesium Perchlorate

Kazuo Shimokoshi* and Yuji Mori

Department of Chemistry, Tokyo Institute of Technology, Meguro-ku, Tokyo, Japan *(Received July 24, 1973)*

The esr spectrum of the ClO_3, produced by the γ-irradiation of $Mg(ClO_4)_2$ at room temperature, and its dependence on temperature were studied. It was found that at temperatures lower than $-80°$ the spectra of ClO_3 showed the presence of two ClO_3 radicals, while the spectra obtained at higher temperatures consisted of a single component. From the experimental results and the CNDO molecular orbital calculations of the radical, an inversion, together with a lattice vibration, is proposed for the molecular motion, which is operative in the system of ClO_3 trapped in $Mg(ClO_4)_2$ lattice, to interpret the observed temperature dependence of the spectrum. A CNDO treatment for the electronic energy of ClO_3 showed a reasonable trends as a function of the bond angle ($\angle OClO$), in particular, for the spin densities and hyperfine splittings of ClO_3.

Introduction

A number of paramagnetic centers have been observed in irradiated chlorates[1] and perchlorates.[2] Among these the presence of ClO_3 is now well established. Vinther[1b] has recently found that in the X-ray irradiated $NaClO_3$ crystal at low temperatures ClO_3 is formed in two modifications with different g and A tensors. The explanations for these two species have been proposed by the same author through his results of thermal and optical transformation of one modification to another, though the observed transformation was not reversible.

Recently we have observed the temperature-dependent esr spectra of ClO_3 formed by the irradiation of $Mg(ClO_4)_2$ powder at room temperature. The spectrum change with temperature, which was observed in the present experiments, was strictly reversible. The spectra observed at temperatures lower than $-80°$ have shown the presence of two types of radicals, while the spectra obtained at higher temperatures were the same as those reported by Atkins, *et al.*,[2] where they have observed the spectra of ClO_3 produced by the irradiation of $Mg(ClO_4)_2$ powder and recorded at $-78°$.

This paper describes the results of our esr study of ClO_3 radicals and the dependence of esr spectra upon the temperature, together with the CNDO molecular orbital calculation for the radical.

Experimental Section

$Mg(ClO_4)_2$ obtained from Wako Pure Chemicals Ltd. was dried at 200° *in vacuo* for several days. The samples in a sealed quartz tube (4 mm o.d.) were irradiated by ^{60}Co γ-rays (2.4×10^7 R) at room temperature. The esr measurements were made by a JES-3BSX X-band spectrometer with 100-kHz modulation. The spectra were recorded at various temperatures. The temperature of the sample was controlled by a conventional thermocontrol unit.

Esr Results

In Figures 1 and 2 are shown the spectra observed at room temperature and $-196°$, respectively, after the irradiation of $Mg(ClO_4)_2$ powder at room temperature. Spectrum R in Figure 1 is almost identical with that obtained by Atkins, *et al.*[2] Peaks and shoulders in the spectra are evident for ^{35}Cl and ^{37}Cl. As has been done by Atkins, *et al.*, the spectra can be identified with that of ClO_3. The signals appearing in the central part of the spectrum may be due to other radical species, such as O^- and O_3^-, and/or to the forbidden transitions of ClO_3.[3] Therefore, for the present purposes, these signals in the central part were neglected. In Figure 2 a series of new signals (spectrum B) is clearly identified as indicated in the figure. Spectrum A in Figure 2 is almost identical with spectrum R in Figure

TABLE I: Magnetic Parameters for ClO_3

Species	Temp, °C	A(iso), G	$A_\perp$, G[a]	$A_\parallel$, G	$g_\perp$	$g_\parallel$
ClO_3(R)	20	132.9	−17.2	34.3	2.007 ± 0.001	2.009 ± 0.001
ClO_3(A)	−196	132.2	−16.8	33.6	2.007 ± 0.001	2.009 ± 0.001
ClO_3(B)	−196	144.4	−22.2	44.3		

[a] The sign of $A_\perp$ and $A_\parallel$ could not be determined from the observed spectra. They, however, should be of opposite sign.[2]

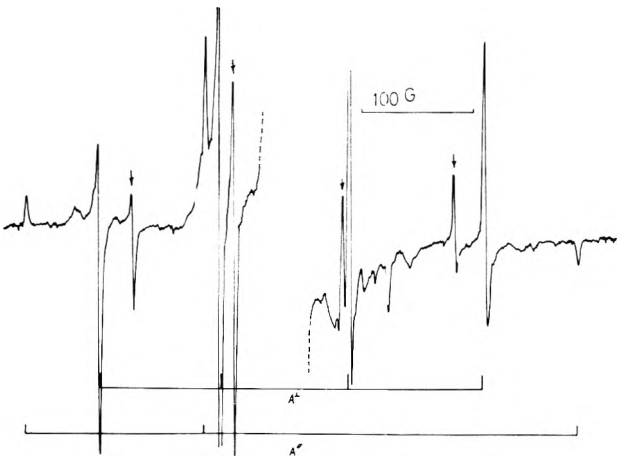

Figure 1. Esr spectrum (R) of ClO_3 recorded at room temperature (20°). Arrows show the hyperfine components of ^{37}Cl. The stick diagram indicates assignment of the hyperfine splitting for ^{35}Cl in each direction. For clarity the central part of the spectrum is omitted.

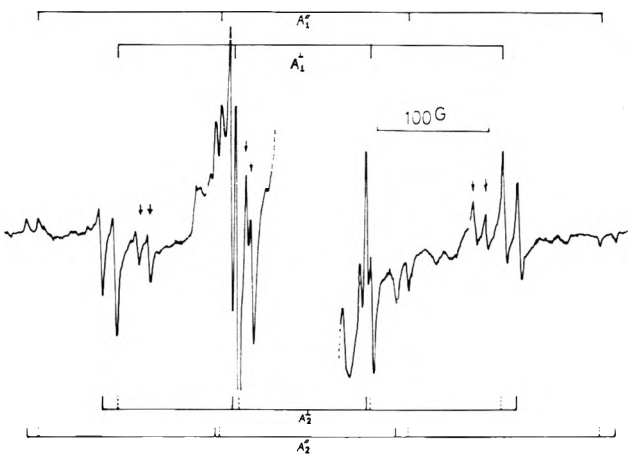

Figure 2. Esr spectra of ClO_3 recorded at −196°. The stick diagram indicates assignment of the hyperfine splitting for ^{35}Cl in each direction. The suffices 1 and 2 of the hyperfine splittings A correspond to the spectra A and B, respectively. Arrows show the hyperfine components of ^{37}Cl.

1. From a comparison of the spectra in Figures 1 and 2, it was found that both spectra A and B have similar features in spite of the appreciable difference in the hyperfine splittings.

In our estimation of magnetic parameters, A and g tensors were assumed to be axial, though the splittings and intensities of each component may deviate from the simple axial symmetry because of the second-order effect and possibly the nuclear quadrupole interaction from the chlorine nucleus. The parameters estimated from the present experiments are listed in Table I. The spectra in Figure 2 and the values in Table I clearly indicate the presence of two types of spectra at −196°, one of which is considered to be quite similar to that observed at room temperature (Figure 1).

Figure 3. Variation of the spectra with temperature on the hyperfine component of $M_I = -1/2$.

The spectra were also measured at various temperatures in order to follow the spectrum change. The spectra in Figure 2 did not show any change up to −110°. If the temperature was elevated above −110°, the intensity of signal B decreased accompanying the increase in that of A. On cooling the samples the spectra in Figure 1 changed, showing a new spectrum at about −80°, which was the same as B in Figure 2. These variations of the spectra with temperatures were reversible, and are shown in Figure 3 on the hyperfine components of $M_I(^{35}Cl) = -1/2$, and $M_I(^{37}Cl) = -1/2$. If the samples were kept in a sealed tube, the radicals were stable more than a month at room temperature and the effect of the temperature on the spectral feature was the same as that observed in the fresh samples. By heating the samples to 50° for a few hours, the intensities of the spectra were gradually decreased. However, both spectra A and B could still be detected as observed before the annealing.

Discussion

It is, of course, observed that there is good agreement between our esr parameters of spectrum R and those reported previously.[2] It may, therefore, not be necessary to discuss further the spectra obtained at higher temperatures. In the interpretation of spectra A and B observed at low temperatures, the difference may not be attributed to the species placed in the equivalent positions of the crystalline lattice and in the different orientations with respect to the applied field, since the spectra were obtained from powdered samples. In any events, since the spectra were dependent upon temperature, the dynamical processes may be taken into consideration to interpret the dependence. Therefore, the possible explanation of the data in Table I should be as follows: (a) the two species are connected by inversion, which gives rise to different crystalline environmental effects for the radicals, and are interchanging between both states; (b) the radicals interacts with crystalline atoms or other radiation-induced de-

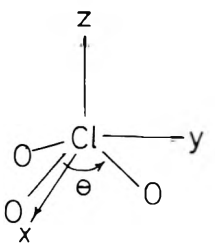

Figure 4. Coordinate system of ClO_3.

fects in the lattice; and (c) the radicals have the electronic isomers with the slightly different geometries, energies, and, therefore, the spin densities on Cl.

CNDO Calculations. It may be essential to have knowledge of the electronic states of the radicals in order to provide an assessment of the possibilities mentioned above. Though Walsh[4] has made a systematic discussion on AB_2 and AB_3 molecules, it may be useful to have results of a detailed calculation, particularly a semiquantitative estimation of the spin densities, to compare with experimental values. There have been several CNDO calculations on radicals containing the phosphorus atom.[5] However, there seems to have been no CNDO calculation of ClO_3 reported thus far. Therefore, we have made some calculations with the open-shell CNDO molecular orbital method.[6] The basis set chosen for the present calculation involves Slater-type 2s and 2p orbitals on each oxygen atom, and 3s, 3p, and 3d orbitals at the chlorine atom. The orbital exponents for the atomic orbitals of the chlorine and oxygen atoms have been selected according to Slater's rule. Calculations have been made for various bond angles ($\angle$OClO) of ClO_3, where the molecule has C_{3v} symmetry, with the Cl–O bond length fixed at 1.5 Å.[7] The choice of the coordinate system for ClO_3 is shown in Figure 4.

Variations of molecular energy and valence shell s and p_z orbital spin densities on the chlorine atom are shown in Figure 5 as a function of bond angle θ for the ground electronic state. When θ is smaller than 111.5°, the singly occupied molecular orbital with a_2 symmetry consists of $2p_x$ and $2p_y$ orbitals at the oxygen atoms. As θ increases the energy of the a_2 orbital decreases and for θ larger than 112°, the singly occupied orbital is changed to that with a_1 symmetry involving 3s, $3p_z$, and $3d_z2$ at the chlorine atom. As might be expected,[4] therefore, CNDO calculation predicts a sudden change in the ground electronic state from $^2A_2$ to $^2A_1$, as θ increases through 112°, and this accounts for the discontinuities as seen in Figure 5.

In the static approach to the configuration of ClO_3 it is possible to estimate the molecular geometry of ClO_3 from the observed hyperfine splitting. Variation of the calculated molecular energy with bond angle shows the double minima at 110.5 and 116°. These minima arise from the different electronic configurations. Since the a_2 orbital does not involve chlorine orbitals and the 3s spin density at the chlorine atom is extremely small at bond angles (θ) smaller than 111.5°, the A_2 state can not be attributed to any of the observed species A and B, both of which have large isotropic hyperfine coupling constants.

In an optimized geometry with respect to molecular energy, which is found at θ = 116° and a bond length of 1.5 Å, 3s spin density is 0.0466. Taking the free atom value of $a_{Cl}(3s)$ as 1685 G[8] for ^{35}Cl, the experimental s orbital spin densities for Cl in ClO_3 are 0.0785 and 0.0859 from spectra A and B, respectively. The anisotropic coupling estimated from the calculated 3p density on Cl is 35.22 G, taking the value of $B(3P)$ as 50 G[8] for ^{35}Cl. This value for the anisotropy may be compared with the experimental values of 33.6 (A) and 44.3 G (B) in Table I.

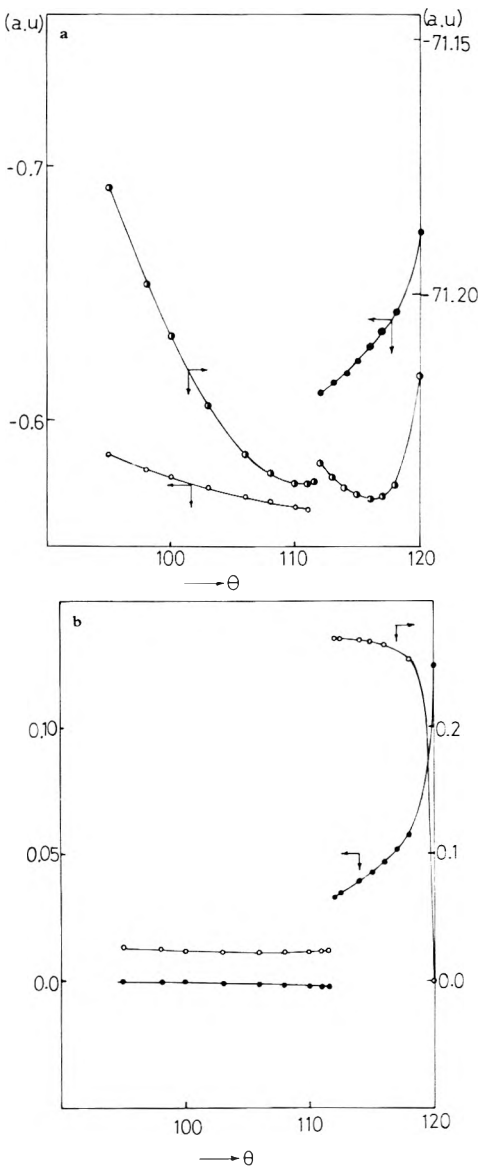

Figure 5. Plot of molecular energies and spin densities of ClO_3 calculated by the CNDO method as a function of the bond angle ($\angle$OCLO): (a) ◑, total energies; O, energies of singly occupied orbital (a_2); ●, energies of singly occupied orbital (a_1); (b) ●, Cl(3s) spin densities; O, Cl($3p_z$) spin densities.

Contrary to the results expected from Walsh's rule,[4] the 3s spin density decreases as the angle θ decreases as shown in Figure 5. This is, possibly, a result of the inclusion of d orbitals, as has appeared in CNDO calculations of radicals containing phosphorus atoms by Kilcast and Thomson.[5] Further it may be pointed out[9] that, since in the present calculation we used the common exponent for 3d, 3s, and 3p orbitals, the effects of 3d involvement is overemphasized. Therefore, agreement between the calculated and measured spin densities would be satisfactory, even though the calculation is not sufficient to give quantitative estimates of the hyperfine couplings for the spectra A and B, and the effects of the crystal field on the molecular state may be by no means negligible.

From the experimental results that the species A and B are interchangeable with rather a low potential barrier, we

have investigated the possible dynamic processes. Since both spectra were anisotropic even at higher temperatures, it is expected that the dynamic process can be restricted to two interchangeable states. The CNDO calculation does not show the double minimum potential within A_1 symmetry, and also suggests that the ground state of ClO_3 may have A_1 symmetry because the experimental large hyperfine splittings can not be explained by the A_2 ground state. It is conceivable, as has been suggested by Vinther,[1b] that the two species are related by inversion, where the molecule passes through a D_{3h} configuration, since in the perfect lattice the environmental effects are not symmetric with respect to inversion of ClO_3. According to the CNDO calculations the potential barrier for this geometrical distortion is 15.1 kcal/mol. This calculated barrier seems to be a little high to interpret the observed temperature dependency. However, the environmental perturbation on the molecular states, inevitably, more or less limits the usefulness of the free-molecule calculations. In the present case of the ClO_3 radical formed in $Mg(ClO_4)_2$ lattice it was found that the observed isotropic hyperfine splitting was larger than that calculated for the optimized molecular configuration with respect to bond angle, and that the calculated spin density on Cl(3s) increased with θ. It is, therefore, suggested that the geometry of ClO_3 stabilized in the crystalline lattice is different and possibly has an angle larger than that obtained from the free-molecule calculation. The distortion of the geometry in the stabilized form toward a planar conformation may reduce the energy barrier for the inversion to make this feasible.

In view of the above discussion and the experimental results that the change of the spectrum occurred over a relatively narrow range of temperature, we have made an investigation of the type of motion governing the temperature dependence of the spectrum. If the motion of the radical is independent of the lattice vibration throughout the experimental temperatures, the observed temperature dependence would be interpreted by a jumping type of motion. The studies by Davidson and Miyagawa,[10] and Clough, *et al.*,[11] show that magnetic resonance spectra of the $RR'C-CH_3$ radical are affected by the interchange of the methyl protons during tunneling motions. According to this model, however, it may be expected, contrary to the present results, that the spectrum observed at higher temperatures is the intermediate of low-temperature spectra A and B, and the actual spectrum observed around $-90°$ in our experiments is affected by the jumping motion to show a complex pattern.[11] Therefore, it is likely that the lattice vibration also contributes to the spectrum change.

The following scheme may be conceivable for the interpretation of the spectrum change in the present system, though the tunnelling motion can be operative simultaneously. At higher temperatures the inversion is rapid enough to average spectra A and B. However, the hyperfine splittings of the spectra obtained at higher temperatures are not necessarily equal to the average splittings of A and B, because the increased vibration of atoms surrounding the radical may produce a different environment at higher temperatures. The difference in environmental effects can give a similar splitting constant of spectrum R to that of A in Figure 2, as shown in Table I. At lower temperatures the radicals are stabilized with the two modifications related by inversion.

There may be other modes of interaction of the radicals with the crystalline atoms or other radiation-induced centers. It is possible that the fragment ions formed from ClO_4^-, such as O^-, are trapped nearby sites of the radicals, and influence the electronic states of the radicals through its polarizability. Therefore, if the radicals are influenced by those centers and experiencing the interchange between the equilibrium positions, the spectra obtained in the present experiments can be expected. However, there seems to be no evidence of such trapping sites of fragment ions.

Consequently, though there may be a possibility for the presence of electronic isomers with slightly different geometries, it may be concluded that the observed spectra can be explained more reasonably by the inversion of radicals than the other modes of motion. This model could be better explained by the CNDO calculation of ClO_3.

Acknowledgments. The authors would like to thank Professor H. Chihara of Osaka University for bringing the present results to his attention and for his kindly supplying the data of the thermal differential analysis of $Mg(ClO_4)_2$.

References and Notes

(1) (a) P. F. Patrick and F. P. Sargent, *Can. J. Chem.*, **46**, 1818 (1968); (b) O. Vinther, *J. Chem. Phys.*, **57**, 183 (1972).
(2) P. W. Atkins, J. A. Brivati, N. Keen, M. C. R. Symons, and P. A. Trevalion, *J. Chem. Soc.*, 4785 (1962).
(3) F. G. Herring, C. A. McDowell, and J. C. Tait, *J. Chem. Phys.*, **57**, 4567 (1972).
(4) A. D. Walsh, *J. Chem. Soc.*, 2296, 2301 (1953).
(5) D. Kilcast and C. Thomson, *J. Chem. Soc., Faraday Trans. 2*, **68**, 435 (1972).
(6) J. A. Pople and D. L. Beveridge, "Approximate Molecular Orbital Theory," McGraw-Hill, New York, N. Y., 1970.
(7) "Tables of Interatomic Distances and Configurations in Molecules and Ions," Chemical Society, London, 1958.
(8) P. W. Atkins and M. C. R. Symons, "The Structure of Inorganic Free Radicals," Elsevier Publishing Co., Amsterdam, 1967, p 21.
(9) D. P. Santry and G. A. Segel, *J. Chem. Phys.*, **47**, 158 (1967).
(10) R. B. Davidson and I. Miyagawa, *J. Chem. Phys.*, **52**, 1727 (1970).
(11) S. Clough, M. Starr, and N. D. McMillan, *Phys. Rev. Lett.*, **25**, 839 (1970).

Argon Matrix Raman Spectra of Cl_2O and Its Photolysis Products ClO and ClClO. Infrared Matrix Spectra of ClO and $(ClO)_2$

Frank K. Chi and Lester Andrews*

Chemistry Department, University of Virginia, Charlottesville, Virginia 22903 *(Received July 5, 1973)*

The Raman spectrum of argon matrix-isolated Cl_2O exhibited bands at 638, 298, and 678 cm^{-1}, in agreement with the infrared spectrum. Laser photolysis (4880 Å) of the sample was evidenced by intense Raman bands at 962, 373, and 241 cm^{-1} due to the Cl-ClO photoisomerism product and a weak Raman band at 850 cm^{-1} due to the ClO photolysis product; infrared studies confirmed these assignments. The mercury arc photolysis of Cl_2O, O_3 matrix samples produced an intense doublet at 995 and 986 cm^{-1} which is assigned to Cl=O-Cl=O, another form of ClO dimer.

Introduction

The Raman spectrum of argon matrix-isolated OF_2 has been recently reported by Andrews using argon ion laser excitation.[1] During laser illumination for Raman scattering, the Raman fundamental of the OF radical appeared in the spectrum; the OF signal increased as a function of laser irradiation time on the sample. Accordingly, the Raman spectra of Cl_2O and the ClO free radical were sought using the same techniques.

Infrared spectra of matrix-isolated Cl_2O and its mercury arc photolysis products ClClO and $(ClO)_2$ have been reported by Rochkind and Pimentel (hereafter called RP).[2,3] Gardiner[4] has recently reported Raman spectra of liquid and solid Cl_2O and confirmed the RP vibrational assignments.

In a study of alkali metal atom matrix reactions with Cl_2O, Andrews and Raymond[5] observed two new infrared bands at 995 and 850 cm^{-1} which showed proper oxygen-18 shifts for the ClO free radical. Following the rationale that the ClO fundamental should be higher than the ClO frequency in Cl-ClO (which occurs at 962 cm^{-1}) these workers assigned 995 cm^{-1} to ClO and 850 cm^{-1} to a perturbed ClO species, although the reverse possibility could not be excluded.

The electronic spectrum of the ClO free radical has been investigated extensively.[6,7] In a very recent study of the vacuum ultraviolet absorption spectrum of ClO by Basco and Morse,[8] six electronic band systems were assigned to ClO; hot bands in three of these systems provided the ground state vibrational frequency of 845 ± 4 cm^{-1}.

The major aim of this study was to observe the Raman fundamental of ClO and to identify the ClO species absorbing at 995 and 850 cm^{-1}. Infrared spectra of the mercury arc photolysis products of Cl_2O and O_3 mixtures in solid argon and laser-Raman studies of argon matrix-isolated Cl_2O are described in a subsequent article.

Experimental Section

The cryogenic apparatus, vacuum vessel, experimental technique, and instrumentation for the laser-Raman matrix isolation experiments have been described earlier.[1,9] Dichlorine monoxide and $Cl_2{}^{18}O$ were synthesized using the apparatus and methods described elsewhere.[5] The Cl_2O samples were diluted in argon (Ar/Cl_2O = 50, 100) and deposited from a stainless steel vacuum line for 6 hr at the rate of 2 mmol/hr onto a tilted copper block maintained at 16°K. The 4880- and 5145-Å argon ion laser lines were used as sources for Raman excitation. Typical spectra were recorded at 20 cm^{-1}/min using a 3-sec rise time and the 0.3 × 10^{-9} Å range. The spectra were calibrated against argon ion emission lines superimposed on the actual scan; frequency accuracy was ±2 cm^{-1}.

The refrigeration system, vacuum vessel, and infrared matrix techniques have been described in earlier papers.[10] Ozone was synthesized by tesla coil discharge of O_2 gas in a Pyrex finger immersed in liquid nitrogen.[11] O_3 and Cl_2O samples were deposited from separate manifolds in one experiment and these reagents were mixed in and deposited from the same stainless steel can in several experiments.

Infrared spectra were recorded during and after deposition and also after each photolysis on a Beckman IR-12 filter-grating infrared spectrophotometer in the 200–2000-cm^{-1} spectral region. Deposition time and rate for infrared experiments were approximately 20 hr and 1.5 mmol/hr, respectively. High-resolution spectra were taken using 8 cm^{-1}/min scan speed and 20 cm^{-1}/in scale expansion; wave number accuracy was ±0.5 cm^{-1} with better than 1-cm^{-1} resolution.

Sample irradiations were made using a high-pressure mercury arc (General Electric BH6). A saturated aqueous $NiSO_4$ + $CoSO_4$ solution filter (transmits 90% at 2200–3600 Å and 10% at 5600–6300 Å), a water filter, and a water filter plus a Pyrex glass plate were used separately for different experiments.

Results and Discussion

Raman Spectra. Dichlorine Monoxide, Cl_2O. Eight new bands were observed in the Raman spectrum of argon matrix-isolated dichlorine monoxide; these are illustrated in Figure 1a. Three of these Raman bands, designated a at 638, 298, and 678 cm^{-1} are respectively due to ν_1, ν_2, and ν_3 of Cl_2O. The stretching modes were observed as split bands at 639.8 and 637.0 cm^{-1} and 677.2 and 675.2 cm^{-1} due to chlorine isotopes in the infrared matrix spectrum. The Raman argon matrix bands are in good agreement with the Raman bands of liquid Cl_2O: 634, 293, and 673 cm^{-1}.[4]

The remaining five Raman bands designated by b, c, and d are due to laser photolysis products of Cl_2O formed during the recording of Raman spectra. The intense

Raman bands at 962 and 373 cm^{-1} labeled b agree well with the RP[3] infrared assignments of 962 and 374 cm^{-1} to ClClO following mercury arc photolysis of Cl_2O in solid argon. The very intense b band at 241 cm^{-1} is associated with the 962- and 373-cm^{-1} bands by their parallel growth and disappearance behavior during laser photolysis. The new 241-cm^{-1} Raman band, which is assigned to the Cl-Cl-O bending mode, ν_3, completes the vibrational spectrum for ClClO.

The weak Raman band labeled c at 850 cm^{-1} is most interesting since this frequency is in good agreement with the 850-cm^{-1} infrared band from alkali metal-Cl_2O matrix reactions and the 845 ± 4 cm^{-1} frequency for ClO deduced from the electronic spectrum.[8] In the best of 15 runs, the 850-cm^{-1} band was observed with enough intensity to partially resolve a splitting at 845 cm^{-1} which may be contributed by natural Cl-37; this band is shown in the inset block of Figure 1. In the oxygen-18 experiment discussed below, the 850-cm^{-1} band shifted to 818 cm^{-1}. The isotopic frequencies are appropriate for a diatomic harmonic oscillator. Noteworthy is the absence of Raman signal at 995 cm^{-1}, the frequency of the earlier infrared assignment[5] to ClO. The Raman observation of 850 cm^{-1} and *not* 995 cm^{-1} suggests the reassignment of 850 cm^{-1} to ClO and 995 cm^{-1} to a perturbed ClO species.

The shoulder labeled d at 944 cm^{-1} in the Raman spectrum has an infrared counterpart at 947 cm^{-1} in argon and a nitrogen matrix absorption at 945 cm^{-1}. The frequency has been assigned to $(ClO)_2$ by Alcock and Pimentel.[12]

All of the eight labeled bands in Figure 1a were observed in the same spectrum scanning a fresh spot of sample with minimum exposure to the laser. However, the intensity behavior of the eight bands under laser irradiation was quite different. During the course of repeating scans of the 200–1000-cm^{-1} region bands b and d increased in intensity as the intensity of a decreased; then the intensity of d began to decrease while b was still growing. This indicates that $(ClO)_2$ is not a stable species, but is subject to further photolysis, perhaps to Cl_2 and O_2. Due to the lack of appreciable intensity for the 850-cm^{-1} band, the photolytic behavior of ClO relative to ClClO is not quite clear. However, the 850-cm^{-1} ClO band is one of the photolysis products of Cl_2O. In the 400–600-cm^{-1} spectral region omitted from Figure 1a, a single strong band at 534 cm^{-1} due to Cl_2 was observed; the Cl_2 Raman band increased in intensity as a function of laser illumination time. This indicates that Cl_2 is also a photolysis product of Cl_2O. As expected the other photolysis product, O_2, was observed at 1552 cm^{-1}. After 1 hr of exposure to 300 mW of 4880-Å radiation all signal intensities were reduced; the reddish-brown sample appeared to be bleached by the laser beam. 5145-Å excitation produced comparable Raman signals to 4880-Å excitation although 4880 Å produced a slightly better yield of photolysis products. The 5682-Å line of a krypton plasma laser produced weak signals for ν_1 and ν_3 of Cl_2O, a weak band at 940 cm^{-1}, and no detectable Cl-ClO or ClO photolysis products.

Oxygen-18 Dichlorine Monoxide, $Cl_2{}^{18}O$. The Raman spectrum of an equimolar $Cl_2{}^{16}O$-$Cl_2{}^{18}O$ argon matrix sample was examined in three experiments; Figure 1b presents the best spectrum obtained. New oxygen-18 species are labeled with a prime corresponding to the oxygen-18 counter-part of a band observed previously: a-$Cl_2{}^{16}O$ and a′-$Cl_2{}^{18}O$. The ν_1 and ν_3 Raman bands of $Cl_2{}^{18}O$ labeled a′ were observed at 612 and 647 cm^{-1} in good agreement with chlorine isotopic infrared bands[5] at 615.8, 613.0 cm^{-1} and 649.3, 647.5 cm^{-1}. The bending mode band near 298 cm^{-1} was not resolved into oxygen isotopic components. The b′ band at 927 cm^{-1} corresponds to the oxygen-18 counterpart of the 962-cm^{-1} ClClO ν_1 band. The intense bands at 373 and 238 cm^{-1} labeled b + b′ contain both $ClCl^{-6}O$ and $ClCl^{18}O$ isotopic bands for ν_2 and ν_3 of Cl-ClO. A weak band at 818 cm^{-1} labeled c′ is the oxygen-18 counterpart of the 850-cm^{-1} Raman ClO band. The weak d′ shoulder at 908 cm^{-1} corresponds to $(Cl^{18}O)_2$ observed in the infrared at 909 cm^{-1} in solid N_2[3] and at 910 cm^{-1} in solid argon.

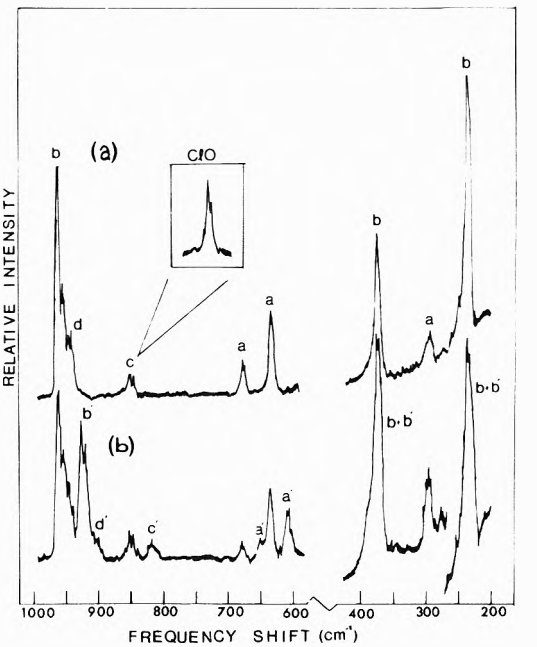

Figure 1. Raman spectra of argon matrix-isolated Cl_2O and its laser photolysis products at 15°K. Approximately 300 mW of 4880-Å excitation at the sample: (spectrum a) Ar/Cl_2O = 100, inset box contains best Raman spectrum of 850-cm^{-1} band; (spectrum b) Ar/Cl_2O = 100, $Cl_2{}^{16}O/Cl_2{}^{18}O \approx 3/2$.

Infrared Spectra. In order to correctly identify the 995-cm^{-1} band assigned earlier[5] (and now we believe incorrectly) to ClO, it was desired to produce as large a yield of the 995-cm^{-1} band as possible. Arkell and Schwager have shown that *in situ* photolysis of Cl_2O-O_3 argon matrix samples produced an extraordinarily good yield of the 995-cm^{-1} band.[13] Accordingly the photolysis of Cl_2O-O_3 matrix samples was investigated. First, the photolysis of Cl_2O in argon was studied to seek the infrared counterpart of the 241-cm^{-1} Raman band assigned above to ν_3 of ClClO. Second, the photolysis of ozone-dichlorine monoxide mixtures will be discussed. Lastly, two new experimental techniques for producing ClO species, microwave discharge and proton beam irradiation, will be briefly reported.

Dichlorine Monoxide Photolysis. Figure 2 contrasts the spectral regions of interest; trace a illustrates the 200–260-, 340–420-, and 900–1000-cm^{-1} spectral regions for an Ar/Cl_2O = 100 sample deposited for 20 hr; trace b shows the effect of mercury arc photolysis through a saturated $NiSO_4$-$CoSO_4$ filter for 10 min. The intense doublet at 961.8 and 953.7 cm^{-1} is in excellent agreement with the RP[3] result for ν_1 of ClClO, the Cl-O stretch. Note the well-resolved chlorine isotopic splitting. Arkell and Schwager[13] have also observed this intense doublet at 961.0 and 952.7 cm^{-1} after mercury arc photolysis of Cl_2,

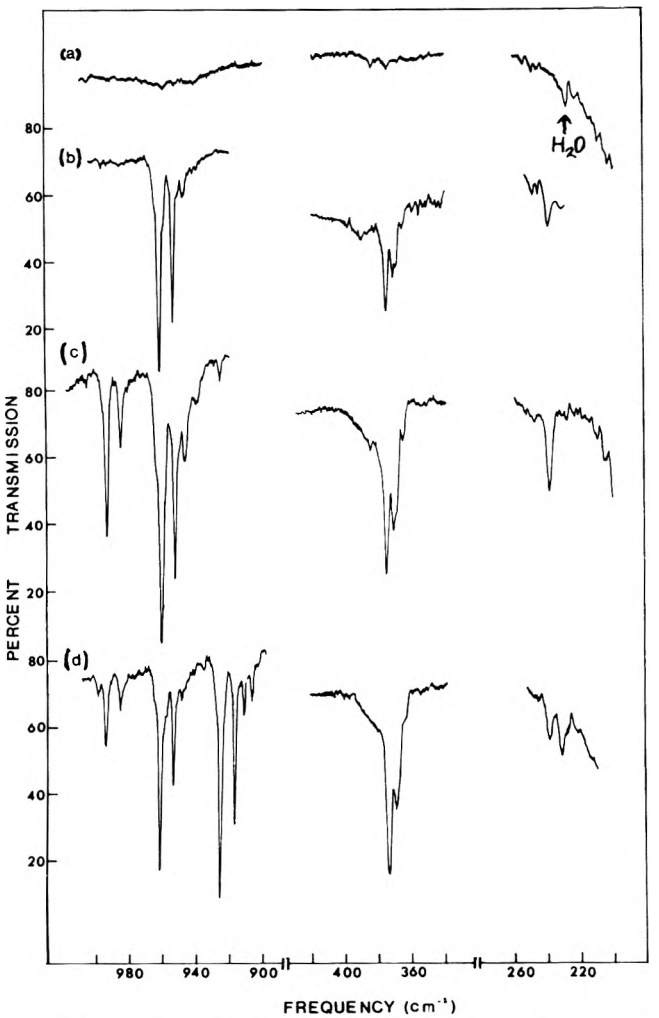

Figure 2. Infrared spectra of *in situ* mercury arc photolysis of Cl_2O and Cl_2O–O_3 mixtures in solid argon at 15°K: (a) Ar/Cl_2O = 100 sample before photolysis; (b) after photolysis for 10 min using ultraviolet radiation (saturated $CoSO_4$–$NiSO_4$ filter); (c) $Ar/Cl_2O/O_3$ = 100/1/1 sample after 33-min ultraviolet and 3-min ultraviolet and visible (water bath filter) photolysis; (d) Ar/Cl_2O + $Cl_2{}^{18}O/{}^{16}O_3$ = 120/1/1, $Cl_2{}^{16}O/Cl_2{}^{18}O \approx 2/3$ sample after 15-min ultraviolet photolysis.

O_3 argon matrix samples. The partially resolved quartet at 375.1, 371.2, 369.3, and 365.7 cm^{-1} in Figure 2b agrees with the RP finding;[3] the chlorine isotopic structure is appropriate for a Cl–Cl stretch of two nonequivalent chlorine atoms. The new band at 239.4 cm^{-1} parallels the other two bands in photolysis growth behavior; this feature was not observed by RP due to the 250-cm^{-1} low-frequency limit of their spectrophotometer. The weak 239.4-cm^{-1} infrared band is associated with the intense 241-cm^{-1} Raman band.

Dichlorine Monoxide–Ozone Photolysis. An $Ar/Cl_2O/O_3$ = 100/1/1 sample was subjected to a detailed mercury arc photolysis study. First, a saturated $NiSO_4$–$CoSO_4$ filter was used (transmits 2200 Å < λ < 3600 Å) for ultraviolet photolysis without appreciable visible light; four spectra were recorded at regular intervals during a 33-min photolysis period. The 995-, 986-cm^{-1} doublet and the 962-, 954-cm^{-1} doublet uniformly appeared during photolysis reaching intensities of 0.16 OD for the 995-cm^{-1} band and 0.09 OD for the 962-cm^{-1} band after 33 min of uv photolysis. Clearly, uv photolysis favored the production of the 995-, 986-cm^{-1} doublet relative to the 962-, 954-cm^{-1} doublet. Second, a water filter only was used (transmits 2200 Å < λ < 10,000 Å) for an additional 3 min of photolysis; this spectrum is shown in Figure 2c. The 995-cm^{-1} band increased to 0.38 OD while the 962-cm^{-1} feature markedly grew to 1.3 OD; no band was observed at 850 cm^{-1}. Note the parallel intensity behavior of the 962-, 375-, and 240-cm^{-1} Cl–ClO bands. An additional 20 min of full uv and visible photolysis further increased the 962-cm^{-1} band but the 995-cm^{-1} band *decreased* to 0.14 OD. The 986-cm^{-1} band maintained a constant one-third intensity relative to the 995-cm^{-1} band during photolysis studies; the 986-cm^{-1} band is clearly the Cl-37 counterpart of the 995-cm^{-1} Cl-35 band. This was verified by a harmonic diatomic calculation with the two frequencies measured at 994.3 and 985.6 cm^{-1} on expanded scale.

The 994.3-, 985.6-cm^{-1} photolysis doublet agrees well with the 994.8-, 985.8-cm^{-1} doublet observed by Andrews and Raymond[5] following lithium atom–Cl_2O matrix reactions. These workers also observed the oxygen-18 isotopic species at 957.3 cm^{-1}. Clearly these isotopic shifts are appropriate for a harmonic isolated Cl–O vibration. The observation of the greatest yield of the 995-, 986-cm^{-1} doublet with O_3 and Cl_2O photolysis and no detectable quantity with Cl_2O photolysis indicates that these bands are a photolytic reaction product of Cl_2O and O_3. Furthermore, these bands were favored by ultraviolet photolysis which dissociates ozone to O_2 and an oxygen atom which is free to diffuse through the argon matrix and react with a suitable molecule. This evidence strongly points to the identification of the 995-, 986-cm^{-1} doublet as Cl═O–Cl═O, another structural isomeric $(ClO)_2$ species. In the lithium –Cl_2O matrix reaction work,[5] this species was produced by dimerization of ClO radicals, evidenced by the 850-cm^{-1} absorption, now correctly assigned as isolated ClO monomer.

The ultraviolet photolysis of a $Cl_2{}^{16}O/Cl_2{}^{18}O \approx 2/3$ sample with $^{16}O_3$ using the $CoSO_4$–$NiSO_4$ filter is shown in Figure 2d. Oxygen-18 counterparts for the Cl–ClO bands are immediately obvious. The intense doublet at 925.5 and 916.8 cm^{-1} is the Cl–O stretch for the $Cl^{35}Cl^{18}O$ and $Cl^{37}Cl^{18}O$ isotopic species. Again, the isotopic structure of the 374-cm^{-1} band was not completely resolved; components at 374.1, 370.1, 368.8, and 364.5 cm^{-1} were observed under high resolution. The oxygen-18 shift for the Cl–Cl mode of Cl–ClO is on the order of 1 cm^{-1}. In the low-frequency region, the oxygen-18 counterpart of the 239.4-cm^{-1} band was resolved at 231.8 cm^{-1}. This doublet confirms the bending mode assignment of Cl–ClO.

Microwave Discharge of Ar–Cl_2–O_2 Mixtures. It was desired to produce the 995- and 850-cm^{-1} infrared bands with as many physical techniques as possible. Three experiments were conducted passing argon, chlorine, oxygen mixtures through a microwave discharge and condensing the effusing gases at 15°K; the apparatus has been described by Smith and Andrews.[14] Best results were obtained using $Ar/Cl_2/O_2$ = 100/2/1. In one particularly productive experiment, discharged sample was deposited for 28 hr and a number of familiar new bands were observed. The most intense feature was a doublet 1039 and 1033 cm^{-1} due to ozone; ClO_2 bands were observed at 1100 and 952 cm^{-1}. ClClO was evidenced by an intense doublet at 962 and 954 cm^{-1} and a single feature at 375 cm^{-1} with low-frequency shoulders. Of most interest were sharp reproducible bands at 849.5 (0.025 OD) and 994.6

cm^{-1} (0.015 OD). These features are assigned here to the ClO radical and a ClO dimer, respectively.

Proton Beam Irradiation of Ar-Cl_2O Mixtures. An apparatus has been developed in this laboratory[15] to deposit a 2-keV proton beam into matrix samples. The gross effect is the production of bombarding electrons through the matrix from ionizing argon atoms as the proton kinetic energy is absorbed. Sample deposition of $Ar/Cl_2O = 100$ with simultaneous proton beam irradiation was conducted for 24 hr. The ozone band at 1039, 1033 cm^{-1} and the ClO_2 band at 1100 cm^{-1} were observed. Interestingly ClClO was produced in large yields as evidenced by bands at 962 and 954, 375, and 240 cm^{-1}. Also observed was the 696-cm^{-1} feature assigned by Noble and Pimentel[16] to HCl_2, and a doublet at 984, 975 cm^{-1} which was assigned by RP[3] to another $(ClO)_2$ dimer. Lastly, a good yield of the 994.8-cm^{-1} feature (0.09 OD) and a typical yield of the 849.3-cm^{-1} band (0.02 OD) were recorded.[16b] Sample warming to approximately 38°K and recooling to 15°K essentially eliminated the weak 850-cm^{-1} band and reduced the 995-cm^{-1} band to 75% of its original intensity while the 984-, 975-cm^{-1} doublet increased to 180% of its original intensity. This diffusion experiment reduced the ClClO features by 30%.

Normal Coordinate Analysis. With a complete set of Cl-ClO fundamental frequencies in hand, a normal coordinate analysis was done using the Wilson *FG* matrix method[17] and the Schachtschneider[18] programs GMAT and FADJ. Since no structural data are available for the Cl-ClO intermediate species, preliminary force constant estimates and Badger's rule[19] were used to estimate the Cl-O bond length of 1.587 Å and the Cl-Cl bond length of 2.263 Å for Cl-ClO. Valence angles of 180, 120, and 90° were used; 120° gave the best correlation between calculated and observed frequencies; thus, we estimate the Cl-ClO bond angle is in the 120° vicinity, near the 110° bond angle for the isoelectronic Cl_2O molecule.[2]

Twenty-four frequencies (fourteen of them were independent) for the isotopes $^{35}Cl^{35}Cl^{16}O$, $^{35}Cl^{37}Cl^{16}O$, $^{37}Cl^{35}Cl^{16}O$, $^{37}Cl^{37}Cl^{16}O$, $^{35}Cl^{35}Cl^{18}O$, $^{35}Cl^{37}Cl^{18}O$, $^{37}Cl^{35}Cl^{18}O$, and $^{37}Cl^{37}Cl^{18}O$ were used as input data for the force constant calculations. Three calculations were done for the 120° geometry: first, the best diagonal force constants were determined holding the off-diagonal constants at zero; second, the diagonal and Cl-Cl stretch-bend interaction force constants were calculated; third, the diagonal and three off-diagonal potential constants were determined. All three of these calculations produced an excellent frequency fit (average error 0.4 cm^{-1}). More importantly, the diagonal force constants changed by only ±0.06 units when one or three off-diagonal potential constants were determined. The interaction constants were small with errors of the same magnitude, but the principal constants were well defined with very small errors. The diagonal potential function listed in Table II together with the potential energy distribution for the $^{35}Cl^{35}Cl^{16}O$ isotopic frequencies adequately defines the vibrational frequencies of Cl-ClO which are listed in Table I. The excellent frequency fit without interaction force constants and the lack of appreciable potential energy distribution to interaction force constants when calculated show that the normal modes of Cl-ClO are well described, respectively, by the internal coordinates Cl-O and Cl-Cl bond stretching and Cl-Cl-O valence angle bending.

The Cl-O force constant of Cl-ClO, 5.94 mdyn/Å, is lower than this constant for ClO_2 (7.02 mdyn/Å)[20] but it is higher than the ClO force constants for ClO radical (850 cm^{-1}, 4.66 mdyn/Å), HOCl (3.9 mdyn/Å),[21] and Cl_2O (2.75 mdyn/Å).[2] The Cl-Cl force constant for Cl-ClO, 1.37 mdyn/Å, is lower than the diatomic chlorine force constant (554 cm^{-1}, 3.16 mdyn/Å).[22] The Cl-Cl-O valence angle bending force constant, 0.78 mdyn Å/rad^2, is near the bending force constant for Cl_2O (1.32 mdyn Å/rad^2)[2] which has a slightly higher frequency.

Bonding in ClO Species. The observation of the ClO free radical at a frequency (850 cm^{-1}) lower than its chlorine bonded counterpart Cl-ClO (962 cm^{-1}) in marked contrast to the second row species NO (1875 cm^{-1})[23] and Cl-NO (1799 cm^{-1})[24] invites further consideration of the bonding to third row diatomics as compared to second row diatomics. Notice the parallel frequency behavior for the X-SN and X-ClO species in Table III which differ from the X-NO and X-OO molecules. Furthermore, the $(ClO)_2$ frequencies (995, 982, and 945 cm^{-1}, antisymmetric modes, symmetric frequencies are not known), which are probably due to three different isomeric structures, are above ClO monomer whereas the $(NO)_2$ frequencies (1776, 1866 cm^{-1})[23] fall below the monomer (1875 cm^{-1}). It appears, therefore, that the bonding to third row diatomics does not follow the Spratley-Pimentel arguments for second row diatomics.[25]

TABLE I: Observed and Calculated Frequencies[a] from Normal Coordinate Analysis of Cl-ClO[b]

	Isotopic frequencies, cm^{-1}			Isotopic frequencies, cm^{-1}	
	obsd	calcd		obsd	calcd
$^{35}Cl^{35}Cl^{16}O$			$^{35}Cl^{35}Cl^{18}O$		
ν_1	961.8	962.1	ν_1	925.5	925.4
ν_2	375.1	375.1	ν_2	374.1	374.1
ν_3	239.4	240.8	ν_3	231.8	233.5
$^{35}Cl^{37}Cl^{16}O$			$^{35}Cl^{37}Cl^{18}O$		
ν_1	953.7	953.7	ν_1	916.8	916.6
ν_2	369.3	369.7	ν_2	368.8	368.6
ν_3	239.4	239.6	ν_3	231.8	232.3
$^{37}Cl^{35}Cl^{16}O$			$^{37}Cl^{35}Cl^{18}O$		
ν_1	961.8	962.1	ν_1	925.5	925.4
ν_2	371.2	371.2	ν_2	370.1	370.0
ν_3	239.4	238.9	ν_3	231.8	231.5
$^{37}Cl^{37}Cl^{16}O$			$^{37}C\ ^{37}Cl^{18}O$		
ν_1	953.7	953.6	ν_1	916.8	916.6
ν_2	365.7	365.6	ν_2	364.5	364.4
ν_3	239.4	237.7	ν_3	231.8	230.4

[a] Average difference between calculated and observed frequencies, $\Delta\nu = 0.4$ cm^{-1}. [b] Geometry: Cl-O distance 1.587 Å, Cl-Cl distance 2.263 Å, Cl-Cl-O angle 120°.

TABLE II: Potential Constants and Potential Energy Distribution from Normal Coordinate Analysis of Cl-ClO[a]

		F_{11}[b]	F_{22}	F_{33}
Force constants		5.94	1.37	0.78
Error		0.05	0.03	0.03
Potential energy	ν_1	99.1	0.7	0.2
distribution	ν_2	0.4	83.1	16.5
for $^{35}Cl^{35}Cl^{16}O$	ν_3	0.6	16.1	83.3

[a] Interaction force constants fixed at zero. [b] F_{11} and F_{22} are Cl-O and Cl-Cl stretching force constants, respectively, in mdyn/Å units. F_{33} is the Cl-Cl-O bending force constant in mdyn Å/rad^2 units.

TABLE III: Frequencies for Second and Third Row Diatomics Bonded to Halogen Atoms

Molecule	ν_{N-O} or ν_{O-O}	F_{N-O} or F_{O-O}	Ref (ν, F)
	Second Row		
NO	1875	15.5	*a*
F-NO	1844	14.7	*b, c*
Cl-NO	1799	14.1	*d, c*
O_2	1552	11.4	*e*
F-OO	1500	10.5	*f*
Cl-OO	1441	9.7	*g*
Molecule	ν_{S-N} or ν_{Cl-O}	F_{S-N} or F_{Cl-O}	Ref (ν, F)
	Third Row		
SN	1204	8.30	*h*
F-SN	1372	10.71	*i, j*
Cl-SN	1325	10.03	*k*
ClO	850	4.66	*e*
F-ClO	1038	6.85	*l*
Cl-ClO	962	5.94	*e*

[a] Reference 23. [b] R. J. H. Woltz, E. A. Jones, and A. H. Nielsen, *J. Chem. Phys.*, **20**, 378 (1952). [c] J. P. Devlin and I. C. Hisatsune, *Spectrochim. Acta*, **17**, 206 (1961). [d] Reference 24. [e] This work. [f] P. N. Noble and G. C. Pimentel, *J. Chem. Phys.*, **44**, 3641 (1966). [g] A. Arkell and I. Schwager, *J. Amer. Chem. Soc.*, **89**, 5999 (1967). [h] P. B. Zeeman, *Can. J. Phys.*, **29**, 174 (1951). [i] H. Richert and O. Glemser, *Z. Anorg. Allg. Chem.*, **307**, 328 (1961). [j] W. Sawodny, A. Fadini, and K. Ballein, *Spectrochim. Acta*, **21**, 995 (1965). [k] A. Muller, G. Nagarajan, O. Glemser, S. F. Cyrin, and J. Wegener, *ibid.*, **23**, 2683 (1967). [l] L. Andrews, F. K. Chi, and A. Arkell, to be submitted for publication.

Here we seek a difference between O and N on the one hand and S and Cl on the other. The possible use of 3d orbitals[26] on S and Cl to form additional π bonding between Cl-O or S-N is a controversial issue. Certainly, the 3d orbitals are very high in energy for the atom itself, but the bonding of an electronegative X atom may make the 3d orbitals more accessible for π bond formation. The amount of d orbital participation is not insignificant in ClO itself.[27] The data in Table III tempts one to suggest that the Cl-O bond in Cl-ClO has additional π character due to Cl_{3d}-O_{2p} π bond formation enhanced by the Cl atom bonded to ClO. However, this is a relatively weak Cl-Cl bond; the weak Cl interaction with the ClO is evidenced by the diatomic like character of the ClO part of Cl-ClO. The case for $(ClO)_2$ is complicated by the observation of antisymmetric (out-of-phase) Cl-O frequencies only, but presumably the symmetric counterparts are not very different. Again the intermolecular ClO-ClO bonding is weak and the diatomic-like character of these modes is retained. The relatively weak interaction between Cl and ClO in Cl-ClO and the two ClO parts of $(ClO)_2$ is probably insufficient to involve the Cl 3d orbital as a possible means of strengthening the ClO bonds in Cl-ClO and $(ClO)_2$.

Returning to the Spratley-Pimentel (p-π^*) picture,[25] one possible explanation of the data for third row diatomics requires that electron density be withdrawn from the ClO (p-p) π^* orbitals. In the case of $(ClO)_2$, this could be accomplished in forming a bond between the two ClO species, Cl=O-Cl=O. For the F-ClO and Cl-ClO species, the electronegativity of fluorine and chlorine atoms may be sufficiently greater than the electronegativity of ClO to remove antibonding electron density from ClO leaving a stronger ClO bond. Table III shows that a fluorine atom produces a greater frequency shift for the third row diatomics than for the second row diatomics. This interpretation suggests that ClO and SN are less electronegative than O_2 and NO, which is, of course, the relationship between the electronegativities of second and third row atoms.

Conclusions

The Raman spectrum of matrix-isolated Cl_2O agrees well with the infrared matrix spectrum. Laser illumination photolyses some of the Cl_2O to ClClO as observed by intense Raman bands at 962, 373, and 241 cm^{-1} in excellent agreement with infrared spectra following mercury-arc photolysis.

The observation of a Raman band at 850 cm^{-1} with an oxygen-18 counterpart at 818 cm^{-1} confirms the ultraviolet assignment of the ground-state ClO fundamental. The vibrational fundamental of ClO at 850 cm^{-1} has been directly observed in three different systems by infrared matrix techniques and in the Raman spectrum of matrix-isolated Cl_2O as produced by laser photodissociation of Cl_2O. Infrared studies have been impeded by the apparent very low infrared extinction coefficient of ClO; *in situ* photolysis studies have been hindered by the competing photolytic rearrangement of Cl_2O to Cl-ClO. The cage effect inhibits the photolytic yield of ClO by trapping the Cl atom adjacent to ClO leading to the formation of Cl-ClO.

The 995-, 986-cm^{-1} doublet observed in infrared matrix studies is reassigned to another $(ClO)_2$ species, perhaps Cl-O-Cl-O, based on the production of extraordinarily high yields by ultraviolet photolysis of O_3, Cl_2O matrix samples.

Unlike the second row diatomics whose fundamentals are lowered upon bonding to a halogen atom, the ClO fundamental is increased upon dimerization or bonding to a halogen atom. It is suggested that this may be due to the removal of antibonding electron density by the more electronegative halogen atom or in forming the intermolecular dimer bond.

Acknowledgments. The authors gratefully acknowledge financial support for this research by the National Science Foundation under Grant No. GP-28582 and partial support for the laser-Raman instrument under Grant No. GP-18251. We also acknowledge helpful discussions with Dr. Alfred Arkell on his unpublished work.

References and Notes

(1) L. Andrews, *J. Chem. Phys.*, **57**, 51 (1972).
(2) M. M. Rochkind and G. C. Pimentel, *J. Chem. Phys.*, **42**, 1361 (1965).
(3) M. M. Rochkind and G. C. Pimentel, *J. Chem. Phys.*, **46**, 4481 (1967).
(4) D. J. Gardiner, *J. Mol. Spectrosc.*, **38**, 476 (1971).
(5) L. Andrews and J. Raymond, *J. Chem. Phys.*, **55**, 3087 (1971).
(6) G. Porter, *Discuss. Faraday Soc.*, **9**, 60 (1950).
(7) R. A. Durie and D. A. Ramsey, *Can. J. Phys.*, **36**, 25 (1958).
(8) N. Basco and R. D. Morse, *J. Mol. Spectrosc.*, **45**, 35 (1973).
(9) D. A. Hatzenbuhler and L. Andrews, *J. Chem. Phys.*, **56**, 3398 (1972).
(10) L. Andrews, *J. Chem. Phys.*, **48**, 972 (1968); **54**, 4935 (1971).
(11) L. Andrews and R. C. Spiker, Jr., *J. Phys. Chem.*, **76**, 3208 (1972).
(12) (a) W. G. Alcock and G. C. Pimentel, *J. Chem. Phys.*, **48**, 2373 (1968). (b) Depolarization ratio (ρ) measurements for the ν_1 Raman band of Cl_2O yielded 0.85 ± 0.07. Clearly this high value does not represent the true depolarization ratio for the molecule. Presumably the high matrix ρ is due to scrambling of the scattered light by the polycrystalline matrix. Similar high ρ values were determined for the three Raman bands of Cl-ClO.
(13) A. Arkell and I. Schwager, unpublished results.

(14) D. W. Smith and L. Andrews, *J. Chem. Phys.*, in press.
(15) R. O. Allen, L. Andrews, and J. M. Grzybowski, to be submitted for publication.
(16) (a) P. N. Noble and G. C. Pimentel, *J. Chem. Phys.*, **49**, 3165 (1968). (b) A similar proton beam experiment using ClO_2 produced the 849.6-cm^{-1} band (0.05 OD) and the 995.0-cm^{-1} band (0.10 OD).
(17) E. B. Wilson, Jr., J. C. Decius, and P. C. Cross, "Molecular Vibrations," McGraw-Hill, New York, N. Y., 1955.
(18) J. H. Schachtschneider, Shell Development Co. Technical Report No. 57-65.
(19) D. R. Herschbach and V. W. Laurie, *J. Chem. Phys.*, **35**, 458 (1961).
(20) M. G. K. Pillai and R. F. Curl, Jr., *J. Chem. Phys.*, **37**, 2921 (1962).
(21) I. Schwager and A. Arkell, *J. Amer. Chem. Soc.*, **89**, 6006 (1967).
(22) W. Holzer, W. F. Murphy, and H. J. Bernstein, *J. Chem. Phys.*, **52**, 399 (1970).
(23) W. G. Fateley, H. A. Bent, and B. Crawford, Jr., *J. Chem. Phys.*, **31**, 204 (1959).
(24) W. G. Burns and H. J. Bernstein, *J. Chem. Phys.*, **18**, 1669 (1950).
(25) R. D. Spratley and G. C. Pimentel, *J. Amer. Chem. Soc.*, **88** 2394 (1966).
(26) See, for example, E. L. Wagner, *J. Chem. Phys.*, **37**, 751 (1962).
(27) P. A. G. O'Hare and A. C. Wahl, *J. Chem. Phys.*, **54**, 3770 (1971).

Matrix Isolated $M^+NO_3^-$ Ion Pairs in Argon, Glassy Water, and Ammonia

Norman Smyrl and J. Paul Devlin*

Department of Chemistry, Oklahoma State University, Stillwater, Oklahoma 74074 *(Received August 9, 1973)*

Publication costs assisted by the National Science Foundation

The infrared spectrum of lithium nitrate and potassium nitrate ion pairs ($M^+NO_3^-$) matrix isolated in argon, glassy water, and glassy ammonia at 12°K have been measured. These spectra show a drastic reduction in the splitting of the ν_3(e) nitrate asymmetric stretch mode in the H_2O and NH_3 matrices when compared to the argon case. This effect apparently results from solvation of the cation of the contact ion pairs with the solvent-cation interaction through the oxygen and nitrogen lone pair electrons. This result is consistent with the place exchange mechanism for aqueous nitrate solutions. The new data, when combined with published dilute solution spectra, complete the spectra for the two nitrate environments required by the place exchange view and are used here to argue for the importance of cooperative effects in the spectra of molten nitrates and their concentrated aqueous solutions.

Introduction

The relatively recent recognition that alkali metal nitrate salts volatilize *in vacuo* near their melting points without dissociation[1,2] has made possible a number of informative studies. In particular, the spectra of the metal nitrate monomers (ion pairs), $M^+NO_3^-$, isolated in inert matrices, such as argon, have been reported with the emphasis placed on the splitting of the degenerate ν_3 asymmetric stretching mode as a useful measure of the extent of cation distortion of the anion. More recently it has also been shown that the salt volatility enables the study of pure simple nitrate glasses for the first time.[3] Since a glass structure is believed to be essentially the same as that of the corresponding melt, preparation of the vapor-deposited films has greatly simplified the infrared spectroscopic study of such structures as well as the measurement of the glass transition temperatures.[4]

It seems, however, that possibly the chemically most informative study to be facilitated by nitrate volatility has been overlooked. It is now possible to deliberately place a metal nitrate ion pair in a particular environment for comparison with the abundance of published spectra which have been interpreted by invoking the presence of such ion pairs. The most obvious medium for a comparison is that of aqueous solutions for which contact ion pairs have been invoked and place exchange equilibrium constants have been evaluated.[5,6] If it is assumed that the ion pair environment in glassy water resembles that for the aqueous solution,[7] then the matrix isolation of the ion pair in a glassy water deposit permits a rather direct test of the assumptions made in interpreting the aqueous solution spectra and should help establish the degree of importance of contact ion pairs in such systems.

This paper reports the results of a study of the lithium and potassium nitrate ion pairs in glassy water and glassy ammonia matrice prepared by deposition at 12°K. New spectra have also been obtained for crystalline argon matrices with the metal-oxygen stretch for the ($M^+NO_3^-$) species now observed. The argon matrix spectra are presented here in detail for comparison with the glassy-matrix spectra.

Experimental Section

The volatilization of the metal nitrates was from the melts in Pyrex glass Knudsen cells as described earlier.[3] The matrix gases (argon, water, and ammonia) were metered through a Fisher-Porter 1/16-in. glass flow meter and co-condensed with the nitrate molecular beam within a standard low-temperature infrared cell fitted to an Air Products CS202 closed-cycle helium refrigerator. Since precise control of the nitrate beam density is not possible, optimum matrix ratios were established by trial and error. In the case of water and ammonia, the useful ratio is limited by the absorption spectrum of the matrix. The substrate deposition temperature was 12°K, guaranteeing that, for the deposition rates used, the water condenses as an amorphous (glassy) solid.[8]

The infrared spectra were recorded using a Beckman IR-7 infrared spectrometer. A CsI interchange is available for the 200–600-cm^{-1} range but this wave number range was not useful for study of the water or ammonia systems because of strong absorption by the matrices. Deuterated water, D_2O, was used in preference to H_2O for several experiments since the 1400-cm^{-1} range, encompassing the ν_3 nitrate doublet, is more nearly transparent for D_2O. The recently reported ion-pair studies for aqueous solutions of metal nitrates have also made use of this property of D_2O.[6]

Results

(*A*) *Argon Matrix.* The results presented here for the $Li^+NO_3^-$ ion pair in the argon matrix represent a refinement of the previously reported results obtained for this ion pair in CO_2 and CCl_4 matrices.[2] The results for an argon matrix are presented in Table I and Figure 1 for comparison with the H_2O and NH_3 matrix data. The anion ν_3(e) splitting (260 cm^{-1}) from cation distortion is slightly greater than in CO_2, as has previously been noted for $Na^+NO_3^-$ and $K^+NO_3^-$, and the ν_1 (1011 cm^{-1}) symmetric stretching frequency as well as the ν_2 (817 cm^{-1}) out-of-plane bending frequency are each 6 cm^{-1} lower than for a CO_2 matrix.

However, the most noteworthy aspect of the argon matrix spectrum is the observation of the metal–anion stretching mode at 528 cm^{-1} and the detection of the components of ν_4, the degenerate planar bending mode of the undistorted D_{3h} anion. The interion mode appears with an intensity greater than ν_2, but much less than that observed for either component of ν_3. The observation of the split ν_4(e) components is of interest since the doubling of the ν_4 band has been used as a criterion of contact ion-pair formation in aqueous solution studies.[6] One ν_4 component appears with reasonable intensity ($\sim\frac{1}{3}$ that of ν_2) at 765 cm^{-1} and is assigned with little chance for error. Examination of Figure 1 reveals the difficulty of identifying the second ν_4 component. Weak features appear regularly at 692, 736, 747, and 783 cm^{-1}. The 747-cm^{-1} feature is known to result from aggregates, $(LiNO_3)_n$, while the 783-cm^{-1} value is outside the range normally expected for a nitrate ν_4 mode. The choice is thus narrowed to the bands at 692 and 736 cm^{-1}. The 736-cm^{-1} feature is sharp, like the 765-cm^{-1} component, but assuming that ν_4 splits uniformly about the solid state value (735 cm^{-1}) as is the practice of ν_3, which splits uniformly about 1390 cm^{-1}, then the 692-cm^{-1} band is the preferred choice. Nevertheless, we prefer the 736-cm^{-1} assignment, and thus a ν_4 splitting of 29 cm^{-1}, because of the recent observation that, for isolated metal chlorate ion pairs, the splitting of ν_4 appears as an increase in the high-frequency component while the low-frequency component is nearly invariant at approximately the solid state value ($\sim$480 cm^{-1}).[9]

It is noteworthy that the 765-cm^{-1} ν_4 component is an order of magnitude more intense than the 736 cm^{-1} (or 692) feature. A similar intensity behavior of the two ν_4 components has been found in this study for amorphous (glassy) $LiNO_3$, from spectra obtained as described in ref 3, *i.e.*, a feature appears at 749 cm^{-1} much more intensely than a very weak component near 715 cm^{-1}. These intensities are reversed in the Raman spectrum of the melt[10] for which the tendency has been to relate the two components to anions in two types of environments within the melt.[5] However, it is unlikely that ν_4 for the anion in one type of site would have a transition dipole an order of magnitude greater than for the second type of environment.

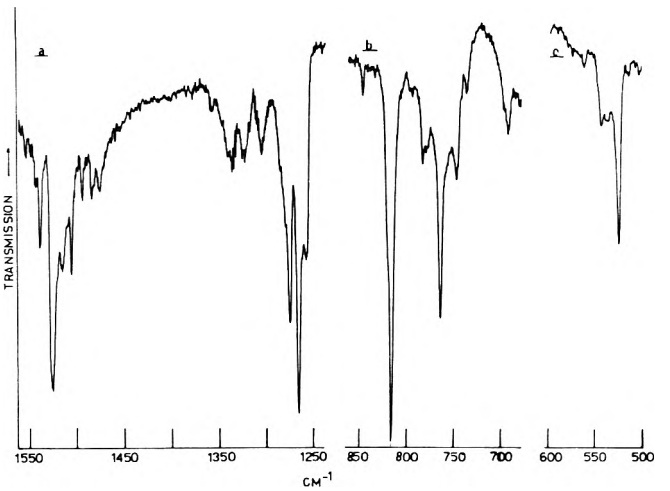

Figure 1. Infrared spectrum for $LiNO_3$ vapors matrix isolated in argon at 12°K. Curve b is for a sample five times as thick as the one used to obtain curves a and c.

TABLE I: Infrared Band Frequencies (cm^{-1}) for Monomeric $LiNO_3$ and KNO_3 Matrix Isolated in Argon, Water, and Ammonia

	$LiNO_3$			KNO_3		
	Argon	H_2O	NH_3	Argon[a]	H_2O	NH_3
ν_1	1011			1031		
ν_2	817	827	828	830		830
ν_{3a}	1264	1347	1345	1291	1348	1348
ν_{3b}	1524	1412	1392	1462	1398	1368
ν_{4a}	736					
ν_{4b}	765					
ν_{M-O}	528					

[a] From ref 2.

(*B*) *Water and Ammonia Matrices.* The infrared windows for thick films of H_2O and NH_3 are such that this study has been limited to observations of ν_2 and the two components of the ν_3 mode of the ion pair. In the regions of these bands the matrix materials contribute only to a slowly changing background and, therefore, it is unnecessary to reproduce the pure matrix spectra here. In other regions, such as the O–H stretching region and the torsional frequency range, the samples were totally opaque.

The ν_3 components for the $Li^+NO_3^-$ ion pair are presented in Figure 2a. These features were largely unchanged throughout a series of runs wherein the matrix ratio and sample thickness were varied. Since the splitting observed was only 65 cm^{-1}, compared to the 260 cm^{-1} for an argon matrix (Figure 1), we were very hesitant to accept this as the ν_3 band system for the isolated contact ion pair. However, there are basically only two other possibilities: (1) the nitrate ion pairs aggregate in the water matrix so that the Figure 2a curve is the aggregated (glassy) nitrate spectrum and (2) the water, even at 12°K, completely solvates the cation (and/or the anion) so that the spectrum is that for solvent-separated ion pairs.

The spectrum for glassy $Li^+NO_3^-$ aggregates in a CO_2 matrix has been published,[3] and shows a ν_3 splitting of 120 cm^{-1}, twice that of Figure 2a. The improbability of

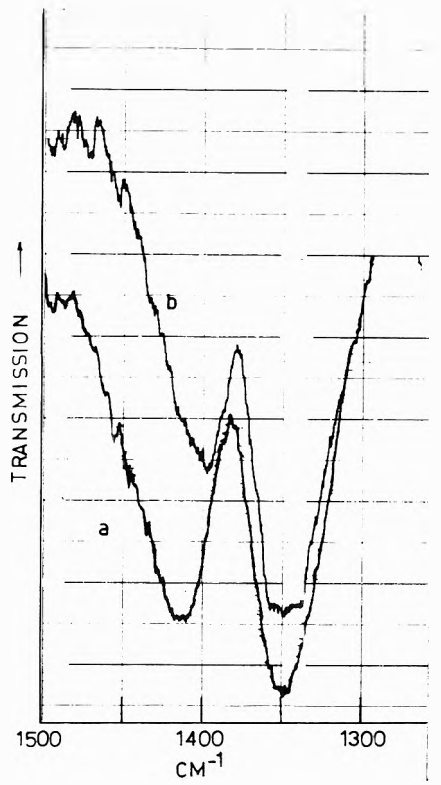

Figure 2. Infrared spectrum of the vapors of $LiNO_3$ (a) and KNO_3 (b) matrix isolated in glassy H_2O at 12°K.

possibility (1) is further emphasized by the spectrum in Figure 3a, obtained under essentially identical conditions except using NH_3 as a matrix. The splitting in the NH_3 matrix is reduced even further, to only 47 cm^{-1}, reflecting a sensitivity to matrix environment not likely for glassy aggregates.

The second possibility is most easily discounted by testing the spectral sensitivity to a change of cation. Thus, Figures 2 (curve b) and 3 (curve b) contain the ν_3 band complex curve for $K^+NO_3^-$ in H_2O and NH_3 matrices, respectively. The splittings for the $K^+NO_3^-$ cases are sharply reduced from values observed for the lithium nitrate samples. In water the splitting drops from 65 to 50 cm^{-1} while the splitting in NH_3 is reduced roughly by half (from 47 to 20 cm^{-1}). The sensitivity, measured in terms of per cent change in the ν_3 splitting ($\Delta\nu_3$), is comparable to the 34% decrease for cation change in an argon matrix (260 cm^{-1} for $LiNO_3$ and 171 cm^{-1} for KNO_3). The influence of cation change on $\Delta\nu_3$ seems much too great to be consistent with solvent-separated ion pairs.

Thus, it is concluded that the spectrum observed for $M^+NO_3^-$ codeposited with water and ammonia is for the contact ion pairs interacting very strongly with the matrix. The data for such ion pairs are summarized in Table I.

Discussion

The contact ion pair spectra for $Li^+NO_3^-$ and $K^+NO_3^-$ in the H_2O and NH_3 matrices are informative in several respects. Most obviously, they indicate that the polarizing power of the cation is sharply reduced *via* interaction with the matrix molecules. The interaction apparently involves the lone pair oxygen and nitrogen electrons which, by participating in a partial electron transfer to the M^+ ion, reduce the positive charge density in the cation. The other

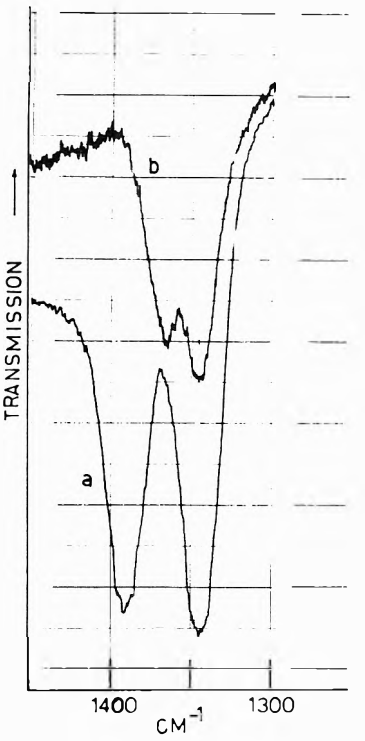

Figure 3. Infrared spectrum of the vapors of $LiNO_3$ (a) and KNO_3 (b) matrix isolated in glassy NH_3 at 12°K.

possibility is ion-dipole interaction but this is not consistent with the observation that the interaction is stronger with NH_3 than H_2O. A study is in process using an HCl matrix to check this conclusion.

A second related point is that the cation in the contact ion pair is strongly solvated. As a result, one cannot use matrix isolation data for inert matrices to draw any direct conclusions about ion pairing in water or ammonia systems since the solvation is undoubtedly equally prevalent in liquid solutions. This view of the ion pair is consistent with the place-exchange equilibrium model of Irish, *et al.*, for aqueous solutions.[5,6]

The results are particularly revealing regarding data for concentrated and moderately concentrated aqueous salt solutions. It has been pointed out that the splitting of ν_3 ($\sim$110 cm^{-1}) in molten and concentrated aqueous solutions of $LiNO_3$ is too great to be a direct result of anion distortion,[2,5] and the present result confirms this view since the 65 cm^{-1} ion-pair splitting value must approach the maximum possible for an aqueous solution. The present result also shows, somewhat surprisingly, that the distortion splitting and ν_3 band positions are the same for the solvated contact ion pair of $K^+NO_3^-$ as for the aquated anion alone (50 cm^{-1}) as measured for dilute aqueous solutions.[11]

The question remaining is what types of interactions are responsible for the increase in the ν_3 splitting with increasing concentration in the aqueous phase.[12] The two anion environments, as described by the place exchange view, have now been shown to have splittings of 50 and 65 cm^{-1} for $LiNO_3$ with all features maximizing in the 1345-1420-cm^{-1} range. The possibility of different anion environments other than these two has been raised but, to explain the maximum near 1470 cm^{-1}, requires either a much greater splitting for these other environments or a shift of the entire ν_3 complex to much higher frequencies. The latter possibility is ruled out by the observation that

the ν_3 band center for $LiNO_3$ samples regardless of phase, and including the monomer in an argon matrix, never varies outside the 1370–1400-cm^{-1} range. Further, the nature of a species capable of giving a splitting greater than the contact ion pair is not clear, although, conceivably, in concentrated systems the incomplete solvation of the cation of the ion pair could leave a center of greater positive charge density which, in turn, could permit a slightly greater anion distortion within the ion pair.

We prefer to interpret the increased splitting with increased salt concentration in the same terms used to explain the increase in ν_3 splitting from 70 to 110 cm^{-1} for a 5% $LiNO_3$ in $LiClO_3$ mixture going to the pure $LiNO_3$ melt.[13] That is, in the dilute and moderately concentrated $LiNO_3$ aqueous cases, the anion is distorted giving rise to two internal normal modes, ν_{3a} and ν_{3b}, most likely of different symmetry and split 50–65 cm^{-1} depending on the anion position without or within the first coordination sphere. Each of these modes has an intense dipole oscillation associated with it and, in the moderated concentration range, dipole–dipole coupling between nitrate ions becomes important. When this occurs the symmetry of a mode is no longer an individual molecule affair, but must be viewed in terms of many molecules. Since in the liquid any many molecule domain has no symmetry this implies that the two original components now must have the same symmetry. Two energy states of the same symmetry and closely spaced will repell one another provided there is a coupling mechanism. Since both ν_{3a} and ν_{3b} have associated large oscillating dipoles, there is a strong coupling mechanism and the two components of ν_3 are forced apart by a resonance interaction through the dipole coupling. This coupling increases with increasing concentration of nitrate entities and in the case of $LiNO_3$ culminates in the 110-cm^{-1} splitting of the melt. The magnitude of the resonance splitting, like the solid state transverse–longitudinal splitting, which is 120 cm^{-1} for $LiNO_3$, depends on the magnitude of the molecular vibrational transition moments and the density of the nitrate ions, and, thus, is greater in the $LiNO_3$ case than for KNO_3, for comparable solution molarities.

Acknowledgment. This research has been supported by the National Science Foundation through Grant No. GP-32341.

References and Notes

(1) J. P. Nalta, N. W. Schubring, and R. A. Dark in "Thin Film Dielectrics Symposium," the Electrochemical Society, New York, N. Y., 1969, p 236.
(2) D. Smith, D. W. James, and J. P. Devlin, *J. Chem. Phys.*, **54**, 4437 (1971).
(3) G. Pollard, N. Smyrl, and J. P. Devlin, *J. Phys. Chem.*, **76**, 1826 (1972).
(4) N. Smyrl and J. P. Devlin, *J. Phys. Chem.*, **76**, 3093 (1972).
(5) D. E. Irish, D. L. Nelson, and M. H. Brooker, *J. Chem. Phys.*, **54**, 654 (1971).
(6) J. D. Riddell, D. J. Lockwood, and D. E. Irish, *Can. J. Chem.*, **50**, 2951 (1972).
(7) This assumption is supported by the observation that glassy salt vibrational spectra very closely resemble the spectra of the corresponding molten salts but not necessarily the crystalline spectra (ref 3). Such a similarity of structure has been suggested by Angell (C. A. Angell, J. Wong, and W. F. Edgell, *J. Chem. Phys.*, **51**, 4519 (1969)) for salt systems. It is also interesting that the presence of dangling OH groups in the vapor-deposited glassy water at 12°K, as for liquid H_2O, is made evident in the present study by distinct absorption features at ~3690 cm^{-1}.
(8) D. S. Olander and S. A. Rice, *Proc. Nat. Acad. Sci. U. S.*, **69**, 98 (1972).
(9) N. Smyrl and J. P. Devlin, Symposium on Molecular Structure and Spectroscopy, The Ohio State University, Columbus, Ohio, June 1973, Paper H5.
(10) D. W. James and W. H. Leong, *J. Chem. Phys.* **51**, 640 (1969).
(11) D. E. Irish and A. R. Davis, *Can. J. Chem.*, **46**, 943 (1968).
(12) This discussion could equally well be made in terms of ammonia matrix data and ammonia solution data. D. J. Gardiner, R. E. Hester, and W. E. L. Grossman (*J. Chem. Phys.*, **59**, 175 (1973)), have very recently reported a thorough study for a large concentration range for $LiNO_3$ in liquid ammonia. They find three stages in the evolution of the ν_3 spectrum with increasing concentration: (1) no splitting, (2) ~ 50-cm^{-1} splitting, and (3) 113-cm^{-1} splitting. Comparison with our data would suggest that the 51-cm^{-1} splitting, which occurs for a salt/NH_3 ratio of 1/4.1, may be attributed to the solvated *contact* ion pair.
(13) J. P. Devlin, G. Ritzhaupt, and T. Hudson, *J. Chem. Phys.*, **58**, 817 (1973).

Near-Infrared Study of the State of Water in Aqueous Solutions of Tetraalkylammonium and -Phosphonium Bromides and Alkali Halides at 10, 25, and 40° [1]

P. R. Philip and C. Jolicoeur*

Department of Chemistry, Université de Sherbrooke, Sherbrooke, Québec, Canada *(Received August 9, 1973)*

The near-infrared spectrum of water in the region 0.8 → 1.2 μ has been investigated over the temperature range 5–50° and in the presence of various ionic solutes at 10, 25, and 40°. As in previous work, the spectra were recorded differentially using cells with adjustable pathlengths which allow correction for thermal expansion and solute volume. The differential spectra were further corrected for solute absorption, if required (*e.g.*, R_4N^+), and resolved into their Gaussian components. The differential spectra obtained for pure water at various temperatures are interpreted in terms of an equilibrium between two states for the -OH oscillators of the water molecules: nonbonded (species I) and bonded (species II). At 25°, an enthalpy change of 1.87 ± 0.05 kcal mol^{-1} is associated with this bond-breaking process. From spectral changes which are very similar to those produced by lowering the temperature of pure water, the R_4N^+ (R = Me to *n*Bu) and nBu_4P^+ ions all appear to shift the hydrogen-bonding equilibrium in favor of species II. The magnitude of these structural shifts (ΔT_{str}) decreases as the solution temperature is increased. With alkali halides, the ΔT_{str} show that Li^+ and F^- decrease the concentration of species I, while the opposite is found for the other alkali metal and halide ions. The relative order for the structure-breaking abilities of these ions is $F^- < Cl^- < Br^- < I^-$ and $Li^+ < Cs^+ < Na^+ \simeq Rb^+ < K^+$, with no noticeable temperature dependence in the range 10–40°.

1. Introduction

Since the hydrogen-bonding equilibrium has been recognized as an important factor in determining the physicochemical properties of liquid water, numerous models have been proposed to describe the various species possibly involved in such equilibrium. Statistical-mechanical treatments of some of these models[2] have been successful in reproducing many of the physical and thermodynamic properties of water, but the factual characterization of the equilibrium species remains very elusive.[3]

It is only recently that different spectral evidences have been reconciled to indicate that indeed water should be regarded as a two-state liquid, at least in the sense that two types of -OH oscillators are distinguishable.[3-9] This concept now receives much support from infrared and Raman studies of the stretching modes of the water molecule, and from near-infrared investigations of overtones and combinations bands. In the fundamental stretching region, the two-state behavior of liquid water is usually evidenced by the appearance of an isosbestic point on an assymetric band contour.[4-6] The band contour is analyzed to resolve the underlying components which are then assigned to distinct equilibrium species, namely, bonded and free -OH groups. Similar analyses have also been carried out on overtone and combination bands in the near-infrared spectrum of liquid water.[10-15] The shapes of the latter have been shown to be very sensitive to temperature, and the spectral changes have been assigned to shifts in equilibrium concentrations of different -OH groups, rather than to other effects such as Fermi resonance.[16]

The ir and Raman spectra of water in various aqueous solutions have also been investigated to determine the influence of the solutes on the hydrogen-bonding equilibrium in water.[14,15,17-24] Of special interest is the category of hydrophobic solutes which are believed to stabilize some hydrogen-bonded structure in solution. The near-ir spectrum of water in the region 0.8 → 1.2 μ has been shown particularly useful in studying the structural changes produced by various large hydrophobic ions, namely, Bu_4NBr, Ph_4AsCl, and $NaBPh_4$.[25] The method described previously[25] has now been extended to investigate the temperature dependence of the structural effects of different quaternary ammonium and phosphonium ions, as well as those produced by alkali halides. Also, the temperature dependence of the $(2\nu_1 + \nu_3)$ combination band has been reexamined to calculate the enthalpy change associated with hydrogen bond breakage in liquid water.

2. Experimental Section

The details of the experimental methods used in this study, as well as the justification for the choice of the second overtone region, can be found in a previous report.[25] Essentially the technique consists in recording a differential spectrum in the region 0.8 → 1.2 μ, with water in the reference cell (10 cm) and a solution (or water at a different temperature) in the working cell. The length of the latter is adjusted so that it contains the same number of moles of water as the reference cell. In studying the relative effects of alkali halides on the water spectrum, an aqueous NaCl solution (1.00 *m*) was used in the reference cell.

All spectra were recorded on a Cary-14 spectrophotometer; the temperature of the cells was regulated within ±0.01° by water jackets. The solutions were prepared gravimetrically at a concentration of 1.00 *m* and the solution densities required for adjusting the length of the working cell were taken from the literature[26a] or measured using a recently developed digital flow densimeter.[26b] All solutions were filtered immediately before use.

For solutes which have intrinsic absorption in the spectral region of interest, (*e.g.*, R_4N^- ions) we recorded the

solute absorbance in D_2O solutions. In preparing the latter, we assumed that the partial molal volume of the salt is the same in both H_2O and D_2O, which is usually the case within less than 1%.[27]

The water used in this work was doubly distilled over alkaline permanganate; D_2O 99.8% was purchased from Stohler Isotope Chemicals. Tetraalkylammonium bromides were purchased from Eastman Kodak; tetrabutylphosphonium bromide was purchased from Alfa Inorganics; all were purified by standard methods. Alkali halides were Fisher Reagents (LiCl, NaCl, NaBr, NaI), Baker reagents (NaF, KCl), Alfa Inorganics Ultrapure (RbCl), and EM Reagent (CsCl); these were used without further purification. All salts were dried under vacuum at temperatures ranging between 50 and 100°, and to the extent possible, manipulations were carried out under a dry nitrogen atmosphere.

3. Analysis of the Spectra

The differential spectra recorded with water in the reference cell (temperature T_0) having in the working cell either an aqueous solution of a nonabsorbing solute or pure water at $T \neq T_0$, usually exhibit an S shape (*e.g.*, Figure 1 of ref 25 and Figure 1 herein). For example, if $T < T_0$ (cell length corrected for density differences), negative absorbance is observed in the 0.9 → 1.0 μ region and positive absorbance from 1.0 → 1.1 μ, with isosbestic points at 1.0 and 1.1 μ. If, as previously,[25] we associate these two regions of absorbance respectively to unbonded -OH oscillators (weakly interacting, species I) and bonded -OH oscillators (strongly interacting, species II,) we can then analyze the temperature dependence of the spectrum in terms of shifts in the concentrations of these two species.[28] Furthermore, since addition of ionic solutes often produces spectral changes similar to changes in temperature,[25] we can define a "structural temperature" of the solution by quantitative comparison of the two effects; this procedure is analogous to that used by several other investigators.[14,22]

The two components contributing to the S-shape differential spectra observed in these studies can be resolved using computer simulation techniques. In Figure 1, we illustrate the results of band contour decomposition into two Gaussian lines, each given by

$$A = A_i \exp[-\lambda^2/2\sigma^2] \quad (1)$$

where A_i is the maximum (or minimum) absorbance, λ the wavelength, and σ the half-width of the band at its point of maximum slope. The Gaussian line shape was judged satisfactory since, in the first half of the differential spectrum (see below), the standard deviation between calculated and experimental curves is within the experimental error. Over the whole spectrum, however, an improved fit could be obtained using a mixture of Lorentzian and Gaussian line shapes.[30]

Since reliable line width studies of the individual components did not appear feasible in the present case, we choose to simply integrate the absorbance component in the short wavelength region (free -OH groups, species I). In fact, only the first half of this band was integrated ($S_I^{1/2}$) to avoid the region of overlap with the bonded -OH component. For the latter, quantitative treatment is further complicated by overlap with the strong absorption band at 1.2 μ. In addition, there may be several types of bonded -OH oscillators each with different absorption

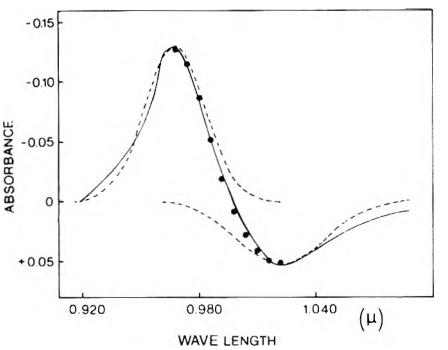

Figure 1. Typical differential spectrum obtained from two water samples at different temperatures or from a R_4NBr solution *vs.* pure water after subtraction of solute absorbance and effect of Br^- ion. The spectrum shown is from a 1 *m* solution Pr_4NBr *vs.* H_2O at 25°. Dashed curves are calculated Gaussian components; the bold dots show the sum of these components.

frequencies and extinction coefficients, particularly in the presence of strongly interacting solutes. The absorption region assigned to the free -OH groups thus seemed more convenient for studying changes in the hydrogen-bonding equilibrium in water.

With solutions of alkyl-substituted ions, the spectra were analyzed according to the procedure described earlier.[25] The absorption spectrum of the solute was first subtracted from the differential spectrum of a solution of $R_4M^+Br^-$ (M = N, P) *vs.* water. From the resultant spectrum, we further subtract the differential spectrum of a solution of NaBr *vs.* water, so that there remains only the effect of the quaternary ion, relative to that of Na^+, on the water spectrum. The spectrum illustrated in Figure 1 was obtained in this manner. As noted before,[25] these corrected differential spectra are very similar to those observed for water at two different temperatures. We thus followed the integration procedure given above to obtain $S_I^{1/2}$, and by comparison with the results obtained from the temperature dependence of the pure water spectrum, we evaluated a molal ΔT_{str} for each of the quaternary ions. For the differential spectra of the various alkali halide solutions obtained against a solution of NaCl, we also calculated $S_I^{1/2}$ and ΔT_{str} as above, though in these cases, the absorption extrema were shifted slightly to longer wavelengths.

4. Results and Discussion

(*a*) *Temperature Dependence of the Pure Water Spectrum.* The data collected from the spectra of pure water at various temperatures are reported in Table I. The integrated intensities $S_I^{1/2}$ from the differential spectra are plotted against temperature in Figure 2, for three temperatures of the reference cell. These curves will be used to evaluate ΔT_{str} of aqueous solutions as described in section 3.

The absorbances A_I^0 and A_{II}^0 of 10 cm of water measured at the wavelengths of the extrema in the differential spectra (respectively 0.970 and 1.080 μ) were used to evaluate $\Delta H°(OH\cdots O)$ for the breaking of 1 mol of hydrogen bonds, according to the present operational definition of this process. From the Van't Hoff plot of log (A_I^0/A_{II}^0), shown in Figure 3, we find $\Delta H°(OH\cdots O) = 1.87 \pm 0.05$ kcal mol^{-1}. Other estimates of the enthalpy of hydrogen bond breakage reported in various infrared studies are collected in Table II. The values quoted range between 2.2 and 3.2 kcal mol^{-1}; it is interesting to note, however, that

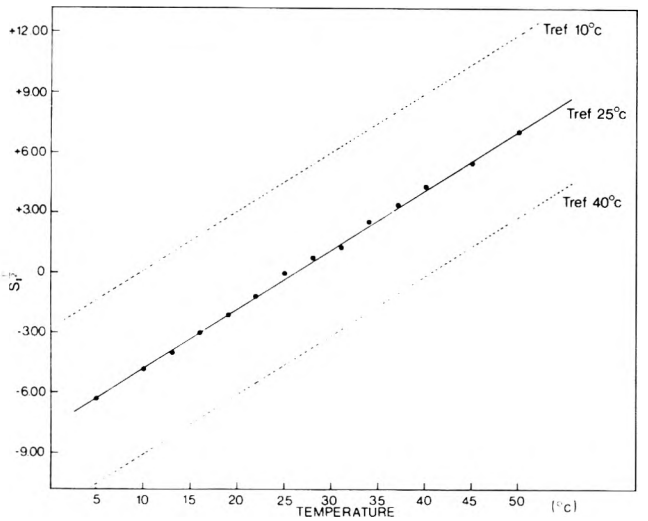

Figure 2. Area of the first half of the short wavelength component of the experimental differential spectrum of water at various temperatures against water at 25°. (- - -) $S_I^{1/2}$ calculated for reference temperatures of 10 and 40°.

TABLE I: Absorbance and Intensity Data from the Spectrum of Water at Various Temperatures[a]

			T_{ref} = 25°	
T, °C	A_I^0	A_{II}^0	A_I	$S_I^{1/2}$
5	1.631	1.067	−0.277	−6.276
10	1.695	1.052	−0.213	−4.824
13	1.733	1.041	−0.175	−3.966
16	1.775	1.031	−0.133	−2.988
19	1.815	1.020	−0.093	−2.100
22	1.854	1.010	−0.054	−1.200
25	1.908	1.000	0.000	0.000
28	1.939	0.992	0.031	1.356
31	1.978	0.977	0.070	1.326
34	2.025	0.974	0.117	2.604
37	2.058	0.960	0.150	3.360
40	2.100	0.951	0.192	4.338
45	2.166	0.932	0.258	5.532
50	2.233	0.916	0.325	7.104

[a] A_I^0 and A_{II}^0 are the absorbance of 10 cm of water measured respectively at 0.970 and 1.080 ± 0.003 μ. A_I is the differential absorbance measured at the first extremum on the differential spectra (0.970 μ). $S_I^{1/2}$ is the integrated intensity of the differential absorption measured from 0.8 μ to the first extremum of the differential spectra. The integration was carried out with the trapezium method using a unit step of 0.006 μ.

all the results from the near-ir investigations agree rather well, although the data were obtained from different combination and overtone bands.

Another remarkable feature of the Van't Hoff plot is the linearity observed over the temperature range studied. This has been observed in other studies[10,14,15] and, in the present case, yields a $\Delta H°$(OH···O) value which is constant within a few per cent, between 5 and 50°. For a given temperature increment, the fractional change in the concentrations of species I and II thus appear much larger than the fractional change in the heat of formation of the hydrogen bond in water. This observation is highly relevant to the interpretation of thermodynamic quantities such as the partial molal heat capacities of aqueous solutes, to which solvent structural changes are believed to contribute significantly.

The temperature dependence of the mole fraction of species I, dX_I/dT, can also be computed from the data in

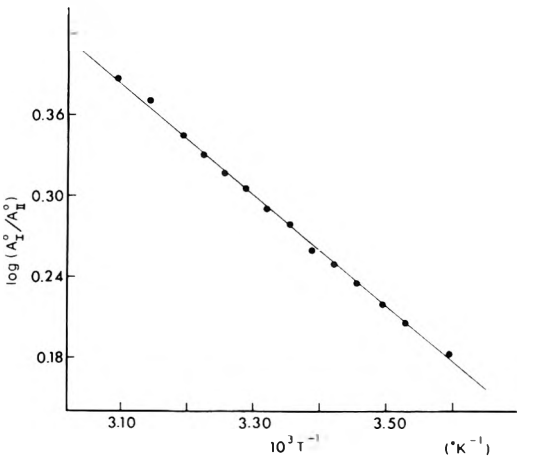

Figure 3. Absorbance of 10 cm of water measured at 0.970 and 1.080 μ *vs.* temperature; the chosen wavelengths correspond to the minimum and maximum observed on the differential spectra (Figures 1 and 2).

TABLE II: $\Delta H°$ (OH···O) from Several Spectroscopic Studies

Authors	Method and spectral region	$\Delta H°$(OH···H), kcal mol^{-1}
Stevenson[31]	Uv, 1800 Å	3.17 ± 0.33[a]
Clarke and Glew[6]	Ir, 3400 cm^{-1}	2.9 ± 0.5[b]
Walrafen[4a,b]	Raman, 2500 cm^{-1}	2.5_5 ± 0.6[c]
Bonner and Woolsey[15a]	Near-ir, 1.0 μ	2.67
Senior and Verrall[5]	Ir, 2500 cm^{-1}	2.3 ± 0.4
Worley and Klotz[14]	Near-ir, 1.5 μ	2.37
McCabe, *et al.*[10]	Near-ir, 1.5 μ	2.18
Present work	Near-ir, 1.0 μ	1.87 ± 0.05

[a] Result given as 6.34 kcal mol^{-1} for the formation of the water monomer. [b] A value of 6.8 ± 1.1 kcal mol^{-1} is obtained if a second-order bond-forming process is assumed. [c] Refer to 1 mol of O-D···O bonds.

Table I and eq 1 of ref 25. At 25°, we find $dX_I/dT = 0.0022_8$ K^{-1}, somewhat larger than the values given by Luck and Ditter[9a] and Bonner and Woolsey,[15a] *i.e.*, 0.0009_5 and 0.0011_4 K^{-1}, respectively.

(*b*) *Aqueous Solutions of R_4NBr and Bu_4PBr.* The differential spectra recorded with solutions of R_4NBr and Bu_4PBr against pure water have been corrected as described in section 3. The resultant spectra, which are believed to illustrate mainly the spectral changes produced on the solvent by the cations, are shown in Figure 4. An example of the temperature dependence of these corrected differential spectra is given in Figure 5 for Bu_4N^+. The data obtained from the spectra of R_4NBr and Bu_4PBr solutions at three temperatures are collected in Table III. In Table IV, we report the molal ΔT_{str} evaluated from $S_I^{1/2}$ (Table III) and the curves shown in Figure 2.

As found in an earlier study of Bu_4NBr solutions,[25] the influence of all R_4N^+ ions on the water spectrum is very similar to the effect observed upon lowering the temperature of pure water. In terms of the assumed equilibrium between species I and II, the differential spectra shown in Figure 4 suggest that relative to Na^+ *all* of the alkyl-substituted ions studied here shift the equilibrium in favor of species II (structure-promoting effect). The magnitude of these shifts, as given by ΔT_{str} (Table IV), is correlated with the size of the quaternary ions, Bu_4P^+ having a larger effect than Bu_4N^+. The corrected spectrum obtained for Bu_4P^+ is remarkably different from that found earlier[25] with Ph_4P^+, which again emphasizes the differences

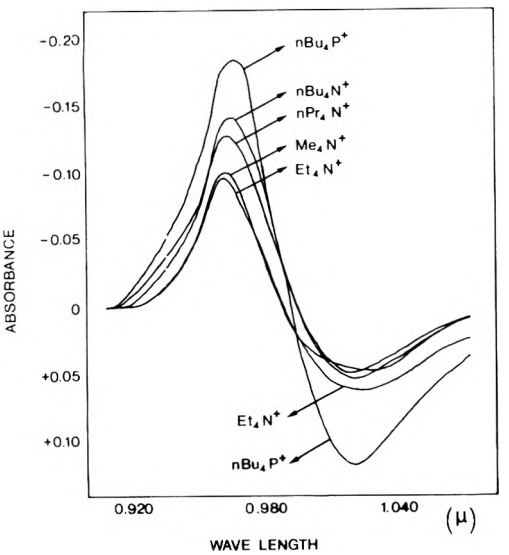

Figure 4. Corrected differential spectra of 1 *m* solutions of R_4NBr and Bu_4PBr at 25°.

TABLE III: Data from Corrected Differential Absorption Spectra of Aqueous Solutions of Tetraalkylammonium and -Phosphonium Bromides at Various Temperatures[a]

	T_{ref}, °C	λ_1, μ	A_1	$S_1^{1/2}$	σ, mμ	Std dev
Me_4N^+	10	0.969	−0.128	−2.406	13	0.008
Et_4N^+		0.969	−0.143	−2.346	11	0.009
nPr_4N^+		0.969	−0.180	−3.318	12	0.014
nBu_4N^+		0.969	−0.201	−4.236	14	0.023
nBu_4P^+		0.970	−0.142	−3.126	14	0.012
Me_4N^+	25	0.972	−0.100	−1.692	13	0.004
Et_4N^+		0.970	−0.098	−1.638	12	0.005
nPr_4N^+		0.972	−0.128	−2.346	14	0.010
nBu_4N^+		0.975	−0.141	−3.510	18	0.015
nBu_4P^+		0.976	−0.095	−2.502	20	0.007
Me_4N^+	40	0.974	−0.064	−1.512	19	0.003
Et_4N^+		0.972	−0.077	−1.668	17	0.005
nPr_4N^+		0.976	−0.105	−2.196	14	0.011
nBu_4N^+		0.977	−0.106	−2.412	13	0.014
nBu_4P^+		0.976	−0.077	−1.908	18	0.006

[a] λ_1 represents wavelength of first extremum on corrected differential spectra (±0.003 μ); σ, the half-width of first (short wavelength) Gaussian component of corrected spectrum; the standard deviation is given for the first half of this component.

in the solvation and structural effects of aromatic and aliphatic substituents.[25,32]

Within the series of R_4N^+ ions, the order of ΔT_{str} found here is consistent with that found in other spectroscopic investigations[18,22] and various thermodynamic[33] and kinetic[34] measurements. In the latter two types of studies, however, Bu_4N^+ and Pr_4N^+ usually appear as having an overall solvent structure-promoting effect, while Me_4N^+ mainly exhibits a structure-breaking character; Et_4N^+ shows neither tendency to any definite extent. The discrepancy between these results and the negative ΔT_{str} found here for all R_4N^+ ions might arise from an electrostatic perturbation of the –OH oscillators, or from overlap of the hydration cosphere of the various ions. From the data on alkali halide solutions given below, it seems clear that the influence of cations on the water spectrum is

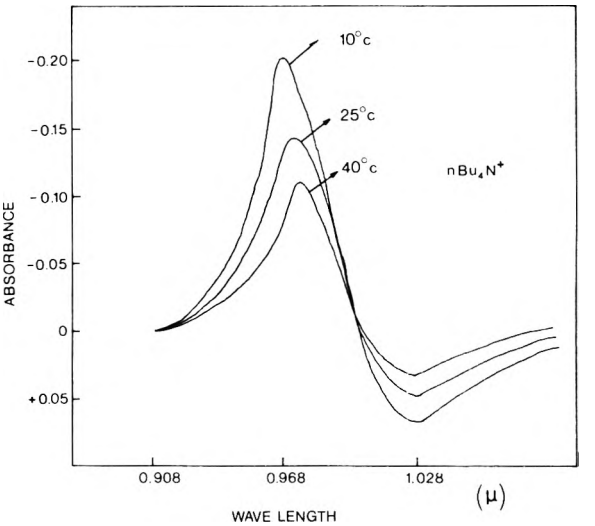

Figure 5. Corrected differential spectra of a 1 *m* Bu_4NBr solution at 10, 25, and 40°.

TABLE IV: Molal ΔT_{str} of Various Quaternary Ions (Relative to Na^+) at 10, 25, and 40°[a]

	ΔT_{str}, °C				
Ion	10°		25°		40°
Me_4N^+	−8	(0.20)	−5	(0)	−5
Et_4N^+	−8	(0.23)	−4.5	(0)	−5
nPr_4N^+	−11	(0.26)	−7	(0)	−7
nBu_4N^+	−14	(0.20)	−11	(0.20)	−8
nBu_4P^+	−18	(0.20)	−15	(0.20)	−12

[a] Values quoted are within ±1°; numbers in parentheses are $d\Delta T_{str}/dT$. Experimental data for Bu_4P^+ were obtained at 0.5 *m* and the resultant ΔT_{str} multiplied by 2 for comparison with other 1 *m* solutions.

small, even for ions having rather large surface charge densities (*e.g.*, Na^+, K^+). A contribution resulting from overlap of the hydration cospheres of the ions seems, on the other hand, more plausible. At 1 *m*, the solvent cospheres of the various ions overlap significantly, particularly for (+,−) pairs, and this can result in additional structure-breaking or structure-promoting effects. It thus appears from our data that the structural effect resulting from Me_4N^+–Br^- overlap interactions is structure promotion (or less water structure disruption). This is in agreement with a previous qualitative explanation of excess thermodynamic functions[35] in terms of cosphere overlap effects. Recent model computations of several excess thermodynamic functions[36] of the tetraalkylammonium halides and alkali halides have also shown a large negative contribution to TS^{ex} from the overlap of the solvation cosphere of the (+,−) pairs.[37]

The temperature dependence of the molal ΔT_{str} obtained for the various quaternary ions (Table IV) indicates that the structure-promoting character of these ions decreases with increasing temperature. This also is in qualitative agreement with thermodynamic[33] and kinetic[34] data. If we assume a constant $d\Delta T_{str}/dT$ (Table IV), we would predict that Bu_4N^+ loses its structure-making ability near 80°.[39] With the smaller tetraalkylammonium ions, $d\Delta T_{str}/dT$ apparently decreases above 25°. Whether this is again related to the cosphere overlap effect might be understood through a systematic study involving other anions at various concentrations and temperatures.

TABLE V: Estimated Thickness of the Hydration Cosphere of Quaternary Ions in Layers of Water Molecules (2.76 Å)[a]

Cations	r_i, Å	10°		25°		40°	
		n_1	n_2	n_1	n_2	n_1	n_2
Me_4N^+	2.85	1.4_9	1.0_2	0.6_4	0.5_9	0.4_7	0.4_9
Et_4N^+	3.48	1.3_0	0.8_6	0.4_5	0.4_1	0.3_6	0.3_8
nPr_4N^+	3.98	1.4_3	0.9_4	0.6_0	0.5_5	0.4_1	0.4_5
nBu_4N^+	4.37	1.5_6	1.0_1	0.7_2	0.6_7	0.3_9	0.4_3
nBu_4P^+	4.42	1.7_7	1.1_8	0.8_9	0.8_2	0.5_4	0.5_8

[a] r_i represents ionic radii calculated from apparent molal volumes.[41] n_1 is calculated from dX_I/dT given above (0.0022_8 K^{-1}) and assuming that water in the cosphere is identical with water at 0°, *i.e.*, $X_I(c) = X_I(0°)$. n_2 is calculated using literature values of $X_I(T)$ and dX_I/dT, taking $X_I(c) = 0$; ref 9a $X_I(25°) \simeq 0.12$; $dX_I/dT = 0.0009_5$; ref 15a $X_I(25°) \simeq 0.12$; $dX_I/dT = 0.0011_4$. Both sets of data yield n values which are not significantly different.

With the larger quaternary ions Bu_4N^+ and Bu_4P^+ the molal ΔT_{str} found at 10° imply that the solvent is below its freezing point. However, we observed no distinct modification of the spectra that could be attributed to ice clusters, which seems a good indication that the solvent structure promotion by these ions does not lead to regular ice I structures.[40] The molal ΔT_{str} discussed here can be used, as previously,[25] to picture the extent of solvent structural changes around the quaternary ions. The ΔT_{str} are first converted to dn_I/dm, the change in the number of moles of species I per mole of solute, using the following simple relationships

$$\frac{dn_I}{dm} = 111\frac{dX_I}{dm} = 111\frac{dX_I}{dT}\Delta T_{str}$$

where 111 is the number of moles of OH groups per kg of solvent. Taking the dX_I/dT given above (0.0022_8 K^{-1}) as constant in the temperature range investigated, we find

$$dn_I/dm = 0.25_3\Delta T_{str}$$

From these results, the thickness of the modified solvent cospheres is readily estimated[25] knowing the ionic radii, the mole fraction of species I in water $X_I(T)$, and in the solvation cosphere, $X_I(c)$. Such estimates, obtained following two methods of calculations, are reported in Table V.

In the first method, we choose as previously[25] $X_I(c) = X_I(0°)$ using the dX_I/dT value found here. In the second calculation, we use values of $X_I(T)$ and dX_I/dT given by Luck and Ditter[9a] and Bonner and Woolsey,[15a] assuming $X_I(c) = 0$; *i.e.*, in the cosphere, all of species I are converted to species II. Both methods yield a physically reasonable cosphere thickness with remarkable agreement for $T > 25°$, in spite of different data and assumptions for $X_I(T)$, $X_I(c)$, and dX_I/dT.

(c) *Aqueous Solutions of Alkali Halides.* The differential spectrum of aqueous NaCl (1.0 *m*) *vs.* water at 25° is shown in Figure 6a. Differential spectra for other alkali halides (metal chlorides and sodium halides) were recorded using this 1 *m* NaCl solution as reference, and are shown in Figure 6b and 6c. This procedure seemed appropriate for obtaining directly the influence of cations relative to Na^+, and of anions relative to Cl^-, on the water spectrum. Though it is obvious from Figure 6b and 6c that anions perturb the water spectrum much more than cations do, there is little ground for assigning ionic contributions to the spectrum obtained with NaCl (Figure 6a), and only relative influences can be given. The relative

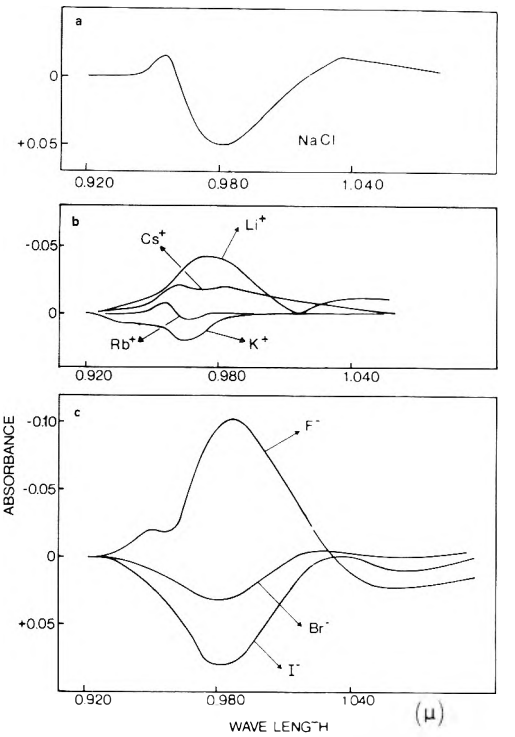

Figure 6. (a) Differential spectrum of a 1 *m* NaCl solution *vs.* pure water at 25°. (b) Differential spectra of 1 *m* alkali metal chlorides solutions *vs.* a 1 *m* NaCl solution at 25°. (c) Differential spectra of 1 *m* sodium halides solutions *vs.* a 1 *m* NaCl solution at 25°.

TABLE VI: Molal ΔT_{str} of Alkali Halides Relative to NaCl[a]

M^+/Na^+	ΔT_{str}, °C	X^-/Cl^-	ΔT_{str}, °C
Li^+	−3	F^-	−7.5
K^+	+1	Br^-	+2.5
Rb^+	0	I^-	+7
Cs^+	−2		

[a] ΔT_{str} for NaCl: +3°; for these salts $d\Delta T_{str}/dT$ is zero within experimental error in the range 10–40°.

ΔT_{str} obtained from the spectra in Figure 6b,c, are reported in Table VI; within experimental error, these were found independent of temperature over the range 10–40°.

It may be useful to recall that according to the present assignments of the observed spectral changes, we monitor variations in the concentration of species I, the –OH oscillators which are not involved in strong interactions with either water molecules or solute species. It has been found[42] that the M^+–OH_2 interaction does not strongly perturb the O–H stretching mode, and thus the differential spectra should reflect mostly the influence of the cations on the hydrogen-bonding equilibrium, *i.e.*, the structural effect. With anions, on the other hand, the $X^-\cdots HOH$ interaction will lead to a decrease in the concentration of species I, in addition to the structure-breaking effects that might occur in the outer solvation sphere (structure broken region[34,43]). From these considerations and the spectra in Figure 6a, NaCl exhibits an overall structure-breaking character. Relative to Cl^-, F^- decreases the concentration of species I, confirming the predominance of strong $F^-\cdots HO$ interactions, found in other studies.[42,44,45] By the same criteria, Br^- and I^- act

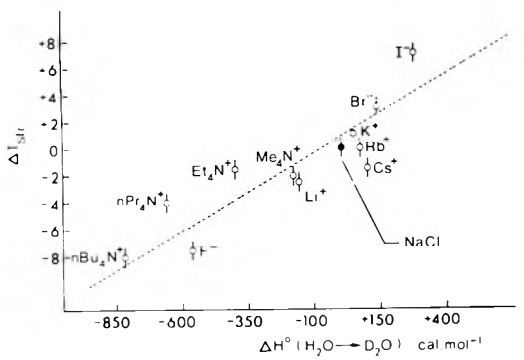

Figure 7. Correlation of the molal ΔT_{str} with $\Delta H^\circ(H_2O \rightarrow D_2O)$ the heat of transfer from H_2O to D_2O for alkali halides and tetraalkylammonium bromides at 25°. On both scales the contributions of Na^+ and Cl^- are taken as zero.

as net structure breakers, also in good agreement with earlier work.[42,44,46]

The behavior of alkali metal ions offers a more puzzling situation. From the ΔT_{str} quoted in Table VI, the increasing order of structure-breaking ability is $Li^+ < Cs^+ < Na^+ \simeq Rb^+ < K^+$. This lack of correlation between the observed spectral changes and the radii of the cations has been reported in several other near-ir studies[14,21,24] involving either frequency shifts or intensity measurements. This is also found in the more recent studies of Bonner and Woolsey[15a] and McCabe and Fisher,[20a] in which the given sequences of structure-breaking character differ mainly with respect to the Cs^+ ion, *i.e.*, ref[15a], $Na^+ < K^+ \simeq Rb^+ < Cs^+$; ref 20a, $Li^+ < Cs^+ < Na^+ \simeq K^+$. The poor agreement between various results raises doubts about the applicability of the near-ir methods to the study of ionic hydration. It is interesting however that our results agree closely with those of McCabe and Fisher;[20a] the methods used are similar, but, in the two studies, different combination bands were investigated. In view of this agreement, it seems worthy to attempt further interpretation of the present data.

From its thermodynamic properties of hydration,[47] Li^+ is known to induce ordering in the surrounding water dipoles. Following our interpretation of the differential spectra, Li^+ (relative to Na^+) decreases the amount of "free" -OH groups in the solution. If, as quoted, $M^+ \cdots OH_2$ interactions do not significantly perturb the -OH oscillator (nor its absorption intensity), we may then suggest that there is more than one hydration layer; the -OH of the water molecules in the first layer are strongly interacting with the molecules in other layers further out. Adopting this view, the smaller ΔT_{str} observed with Na^+ and K^+ are readily understood.

The upturn of Cs^+, which shows a order-producing character (relative to Na^+), is difficult to explain since, as Me_4N^+ discussed above, Cs^+ is usually inferred to be a more efficient structure breaker than Na^+. Possibly, overlap effects suggested in the case of Me_4NBr apply to CsCl also. The spectral changes produced by the latter (relative to NaCl) is so small, however, that a concentration dependence is unlikely to help solve the case.

Correlation with Thermodynamic Data

Since the differential spectra examined here reflect, to a large extent, the influence of solutes on the hydrogen-bonding equilibrium in water, we might anticipate a correlation between ΔT_{str} and thermodynamic quantities which are believed sensitive toward solvent structural changes. The thermodynamic properties of transfer from H_2O to D_2O are often used as a measure of the structural influence of solutes;[38,47-49] they seem particularly appropriate to attempt a correlation with the spectral data, since the solvent isotope effect on the thermodynamic properties will have contributions from all interactions involving the -OH oscillators, much the same as the spectral changes discussed above.

In Figure 7, we report a correlation plot of the standard enthalpy of transfer from H_2O to D_2O *vs.* ΔT_{str} for the various solutes studied here. The relationship between these quantities is quite remarkable in that it holds for both hydrophilic and hydrophobic ions. This can be taken as an indirect confirmation of the validity of the ir method used here, at least to the extent that solute-solvent interactions, including structural changes, are understood from solvent isotope effects.

References and Notes

(1) Financial support of this research by the National Research Council of Canada is gratefully acknowledged.
(2) G. Nemethy and H. A. Scheraga, *J. Chem. Phys.*, **36**, 382, 3401 (1962); V. Vand and W. A. Senior, *ibid.*, **43**, 1869 (1965); M. S. Jhon, J. Gorsh, T. Ree, and H. Eyring, *ibid.*, **44**, 1465 (1966); A. Ben-Naim, *ibid.*, **52**, 5531 (1970); **57**, 3605 (1972); K. Arakawa and K. Sasaki, *Bull. Chem. Soc. Jap.*, **43**, 3048 (1970); J. W. Perram, *Advan. Mol. Relax. Process.*, **3**, 51 (1972); A. Rahman and F. H. Stillinger, *J. Chem. Phys.*, **55**, 3336 (1971)
(3) H. S. Frank, *Science*, **169**, 635 (1970).
(4) (a) G. E. Walrafen, *J. Chem. Phys.*, **47**, 114 (1967); (b) *ibid.*, **48**, 244 (1968); (c) *Advan. Mol. Relax. Process.*, **3**, 43 (1972).
(5) W. A. Senior and R. E. Verrall, *J. Phys. Chem.*, **73**, 4242 (1969).
(6) E. C. W. Clarke and D. N. Glew, *Can. J. Chem.*, **50**, 1655 (1972).
(7) L. M. Kleiss, H. A. Strobel, and M. C. R. Symons, *Spectrochim. Acta, Part A*, **29**, 829 (1973).
(8) W. F. Murphy and H. J. Bernstein, *J. Phys. Chem.*, **76**, 1147 (1972).
(9) (a) W. A. P. Luck and W. Ditter, *Advan. Mol. Relax. Process.*, **3**, 321 (1972); (b) E. U. Franck and K. Roth, *Discuss. Faraday Soc.*, **43**, 108 (1967).
(10) W. C. McCabe, S. Subramanian, and H. F. Fisher, *J. Phys. Chem.*, **74**, 4360 (1970).
(11) K. Buijs and G. R. Choppin, *J. Chem. Phys.*, **39**, 2035 (1963).
(12) M. R. Thomas, H. A. Scheraga, and E. E. Schrier, *J. Phys. Chem.*, **69**, 3722 (1965).
(13) J. J. Péron, C. Bourdéron, and C. Sandorfy, *Can. J. Chem.*, **49**, 3901 (1971).
(14) J. D. Worley and I. M. Klotz, *J. Chem. Phys.*, **45**, 2868 (1966).
(15) (a) O. D. Bonner and G. B. Woolsey, *J. Phys. Chem.*, **72**, 899 (1968); (b) O. D. Bonner, *ibid.*, **76**, 1228 (1972); (c) P. A. Giguère, *ibid.*, **76**, 3675 (1972).
(16) D. F. Hornig, *J. Chem. Phys.*, **40**, 3119 (1964); J. Schiffer, *ibid.*, **50**, 566 (1969); G. E. Walrafen, *ibid.*, **50**, 567 (1969).
(17) For discussion of the earlier data see J. E. Desnoyers and C. Jolicoeur in "Modern Aspects of Electrochemistry," J. O'M. Bockris and B. E. Conway, Ed., Plenum Press, New York, N. Y., 1969, p 43-48.
(18) G. E. Walrafen, *J. Chem. Phys.*, **55**, 768 (1971).
(19) A. de Trobriand, M. Ceccaldi, M. Henry, M. M. Marciaq-Rousselot, and M. Lucas, *C. R. Acad. Sci., Ser. C*, **274**, 919 (1972).
(20) (a) W. C. McCabe and H. F. Fisher, *J. Phys. Chem.*, **74**, 2990 (1970); (b) S. Subramanian and H. F. Fisher, *ibid.*, **76**, 84 (1972).
(21) K. Buijs and G. R. Choppin, *J. Chem. Phys.*, **39**, 2042 (1963).
(22) K. W. Bunzl, *J. Phys. Chem.*, **71**, 1358 (1967).
(23) O. D. Bonner, *J. Phys. Chem.*, **72**, 2512 (1968); *J. Amer. Chem. Soc.*, **92**, 4197 (1970).
(24) H. Yamatera, B. Fitzpatrick, and G. Gordon, *J. Mol. Spectrosc.*, **14**, 268 (1964).
(25) C. Jolicoeur, N. D. The, and A. Cabana, *Can. J. Chem.*, **49**, 2008 (1971).
(26) (a) Me_4NBr, Et_4NBr, Pr_4NBr, and Bu_4NBr: A. Lo Surdo and H. E. Wirth, *J. Phys. Chem.*, **76**, 1333 (1972); NaCl: F. J. Millero, *ibid.*, **74**, 356 (1970); NaBr: A. F. Scott, *ibid.*, **35**, 2315 (1931); (b) P. Picker, E. Tremblay, and C. Jolicoeur, *J. Solution Chem.*, in press.
(27) B. E. Conway and L. H. Laliberté, *Trans. Faraday Soc.*, **66**, 1 (1970).
(28) A closer examination of the various possible hydrogen-bonded species suggests six types of different "free -OH" oscillators, depending on the states of the remaining -OH groups and oxygen lone pairs of the water molecule. As discussed elsewhere[29] and below for ion-water interaction, the ir absorption spectra do not show distinct bands for these various species.
(29) A. Cabana and C. Jolicoeur, *Can. J. Spectrosc.*, **12**, 1 (1967).

(30) This has also been reported by Clarke and Glew[6] and Murphy and Bernstein[8] in studies of the fundamental stretching modes.
(31) D. P. Stevenson, *J. Phys. Chem.*, **69**, 2145 (1965).
(32) C. Jolicoeur, P. R. Philip, G. Perron, F.-A. Lecuc, and J. E. Desnoyers, *Can. J. Chem.*, **50**, 3167 (1972).
(33) W. Y. Wen in "Water and Aqueous Solutions," R. A. Horne, Ed., Wiley, New York, N. Y., 1972, Chapter 15.
(34) R. L. Kay, *Advan. Chem. Ser.*, **No. 73**, 1 (1968).
(35) J. E. Desnoyers, M. Arel, G. Perron, and C. Jolicoeur, *J. Phys. Chem.*, **73**, 3346 (1969).
(36) P. S. Ramanathan, C. V. Krishnan, and H. L. Friedman, *J. Solution Chem.*, **1**, 237 (1972).
(37) In these model calculations, no clear distinction could be established between the effects of (+,−) cosphere overlap occuring in Me_4NX and Bu_4NX solutions (except, of course, in magnitude). This, together with the present results and other thermodynamic excess functions,[33,38] suggests that perhaps the classification among the R_4N^+ ions, in terms of their structural effects, is not as definite as is often assumed.
(38) P. R. Philip and J. E. Desnoyers, *J. Solution Chem.*, **1**, 353 (1972).
(39) This result differs from that obtained recently by de Trobriand, *et al.*,[9] from a study of the frequency shifts of the 2135-cm^{-1} mode. As discussed earlier,[17] measurements of frequency shifts and absorption intensities, such as done here, have often led to conflicting results, especially with respect to the tetraalkylammonium ions.
(40) In the region of interest, the absorption line shape of ice I is drastically different from that of water at 0°.
(41) B. E. Conway, R. E. Verrall, and J. E. Desnoyers, *Trans. Faraday Soc.*, **62**, 2738 (1966).
(42) R. E. Weston, *Spectrochim. Acta*, **18**, 1257 (1962).
(43) H. S. Frank and W. Y. Wen, *Discuss. Faraday Soc.*, **24**, 133 (1957).
(44) J. W. Shultz and D. F. Hornig, *J. Phys. Chem.*, **65**, 2131 (1961).
(45) G. E. Walrafen, *J. Chem. Phys.*, **36**, 1035 (1962).
(46) R. D. Waldron, *J. Chem. Phys.*, **26**, 809 (1957).
(47) J.-L. Fortier, P. R. Philip, and J. E. Desnoyers, *J. Solution Chem.*, submitted for publication.
(48) E. M. Arnett and D. R. McKelvey in "Solute-Solvent Interactions," J. F. Coetzee and C. D. Ritchie, Ed., Marcel Dekker, New York, N. Y., 1969, Chapter 6.
(49) C. V. Krishnan and H. L. Friedman, *J. Phys. Chem.*, **74**, 2356 (1970).

Polarized Electronic Crystal Absorption Spectra of Dibromo(ethylenediamine)platinum(II)

Roy F. Kroening, L. D. Hunter, Rhonda M. Rush, Jon C. Clardy, and D. S. Martin, Jr.*

The Ames Laboratory of the USAEC and the Department of Chemistry, Iowa State University, Ames, Iowa 50010
(Received June 29, 1973)

Publication costs assisted by Ames Laboratory—USAEC

Dibromo(ethylenediamine)platinum(II) crystallizes in an orthorhombic lattice in which the planar molecules stack along the *c* direction. Absorption spectra have been recorded with light polarized in the *c* direction from 17,000 to 32,000 cm^{-1} and in the *b* direction from 17,000 to 38,000 cm^{-1} at 300 and 15°K. Molecular transitions in c polarization are excited vibronically and by ligand field perturbation and have enhanced intensity from the proximity of an allowed transition which has been shifted from 46,000 cm^{-1} in solution to 37,500 cm^{-1} by crystal interactions. In the *b* polarization there is a weak but dipole-allowed transition at 34,500 cm^{-1} which has been assigned as an excitation to a crystal bound ionic state in which an electron has been transfered from one molecule to its adjacent neighbor.

Introduction

The polarized absorption spectra for single crystals of $Pt(en)Cl_2$ have been reported recently.[1] In that compound the molecules stack along the c axis of an orthorhombic crystal with a separation of 3.39 Å. There were strong crystal effects in the absorption of light with some similarities to the absorption spectra of Magnus' green salt, $Pt(NH_3)_4PtCl_4$, (MGS). However, unlike MGS[2] there were weak but dipole-allowed transitions with polarization normal to the stacking axis which could be attributed to unusual ionic crystal (exciton) states. The present work was undertaken to seek additional systems in which the ionic exciton absorptions might be observed and to provide a comparison of the influence of a different halide ligand upon the molecular and the crystal spectra.

Experimental Section

The $Pt(en)Br_2$ was synthesized by the method of Watt and McCarley.[3] The product was purified by dissolution in *N,N*-dimethylformamide from which it was recrystallized by the addition of water. Very thin flat crystals with well-developed faces, which proved to be the 100, were grown by evaporating a water solution containing about 0.01 *M* KBr and saturated with $Pt(en)Br_2$. Somewhat thinner crystals were formed than were normally obtained for the $Pt(en)Cl_2$ system. The crystals for spectral measurements typically had faces of 1–2 mm^2 and they were mounted over pinholes which were 0.6–0.8 mm in diameter in platinum plates. A Cary Model 14 spectrophotometer was used to measure the spectra for solutions and crystals. The associated equipment and procedures for recording polarized spectra at room temperature, 77°K (liquid N_2), and with liquid He (nominally 15°K) have been discussed previously.[1,4] For the $Pt(en)Br_2$ no difficulty was encountered in taking the crystals to liquid helium temperature as was the case for $Pt(en)Cl_2$.

Since the crystals were found to be air stable, they were mounted on glass fibers for the X-ray diffraction. A crystal having the approximate dimension 0.04 × 0.10 × 0.13 mm along the *a*, *b*, and *c* axes, respectively, was used for

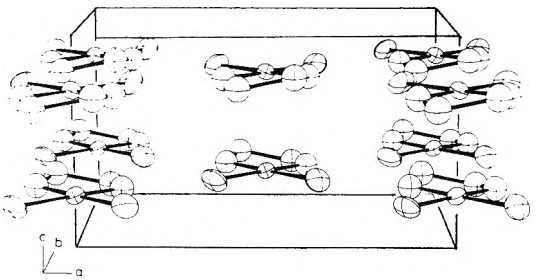

Figure 1. Arrangement of molecules in a unit cell.

TABLE I: Bond Distances (Å) and Angles (degrees) for Pt(en)Br_2

Pt-N	1.99(4)	N-Pt-N	95.7(12)
Pt-Br	2.450(5)	N-Pt-Br	84.7(12)
N-C	1.51(12)	Pt-N-C	117(5)
C-C	1.20(18)	N-C-C	96(12)

data collection. The crystal was mounted with the c axis along the spindle axis for data collection. Data were recorded at room temperature with a Hilger-Watts X-ray diffractometer equipped with scintillation counter and employing Zr-filtered Mo Kα radiation. All unique data were recorded within a 2θ sphere of 60°. A total of 950 reflections were measured using the θ-2θ scan technique. Three standard reflections were measured periodically, and these observations indicated that no crystal decomposition occurred during the data collection.

Dibromo(ethylenediamine)platinum(II), molecular weight 415.01, crystallizes in the orthorhombic system with the space group $C222_1$ and a Z of 4: a = 12.89(1), b = 8.27(1), c = 6.990(4) Å, temperature ~24°, d_{calcd} = 3.70 g/cm^3. Under examination of thin plates with 100 faces by means of a polarizing microscope, the crystals exhibited a distinct dichroism, appearing yellow for light polarized in the c direction and nearly colorless for light with b polarization.

A Patterson map was computed from the diffraction data. Analysis of the heavy atom vectors in this map indicated an acentric symmetry. Consistent with the systematic extinctions, $h + k = 2n + 1$, the space group was assumed to be $C222_1$. (Attempted refinement in space group $Cmm2_1$ revealed unusual coupling of thermal and positional parameters.) The platinum and bromine atom positions with isotropic temperature factors were refined by full-matrix least-squares techniques. Difference electron density maps were computed to locate the carbons and nitrogen. Refinement continued to a conventional discrepancy factor of $R = \Sigma||F_o| - |F||/\Sigma|F| = 0.093$ and a weighted R factor, $wR = 0.110$. Throughout the refinement the scattering factors, reported by Cromer and Waber,[5] for Pt, Br, C, and N were used.[3]

The arrangement of molecules in the unit cell, drawn by the ORTEP program, is shown in Figure 1. The interatomic distances, the bond angles, and standard deviations for a molecule are given in Table I, with the standard deviations indicated by the variance-covariance matrix from the final least-squares cycle. In the presence of the heavy Pt and Br atoms the locations of C and N could not be determined accurately. These uncertainties are evident from the values in Table I.

Results and Discussion

Solution Spectrum of Pt(en)Br_2. The spectrum of an aqueous solution of Pt(en)Br_2 is shown in Figure 2. The portion for $\bar{\nu} < 39{,}000$ cm^{-1} was recorded in the presence of 0.32 M KBr to suppress the aquation. However, for $\bar{\nu} > 40{,}000$ the spectrum was determined as rapidly as possible upon dissolving the compound to avoid absorption by free bromide ions. The components of this spectrum and proposed transition assignments are listed in Table II. For assignment of the transitions, the molecular x, y, and z axes are directed along the crystallographic a, b, and c directions. Thus the z axis is normal to the molecular plane, and the y axis is directed along the molecular symmetry axis. The molecular symmetry is only C_2, because of puckering of the chelate ring. However, the local symmetry of the atoms bonded to Pt is C_{2v} within the experimental error, and this symmetry probably is effective in establishing the selection rules.

With the choice of axes, the d orbital involved in the σ-bonding system is $5d_{xy}(b_2)$ and the lowest unfilled orbital is usually taken to be the antibonding orbital, σ^*, involving this d_{xy}. In the solution spectrum the absorption from 21,000 to 27,000 cm^{-1} apparently involves absorption by the spin-forbidden $\sigma^* \leftarrow$ d transitions. A spin-allowed transition, with the peak at 31,400 cm^{-1}, is attributed to $\sigma^*(b_2) \leftarrow d_{x^2-y^2}(a_1)$ from analogy with $PtCl_4^{2-}$ where this transition was identified from the polarized crystal spectrum.[7] A shoulder at *ca.* 35,000 cm^{-1} is assigned to the pair of transitions, $\sigma^*(b_2) \leftarrow d_{xz}(a_2)$, $d_{yz}(b_1)$. In the $PtCl_4^{2-}$ D_{4h} system these two excited states are degenerate, and the transitions to degenerate excited states have been identified by magnetic circular dichroism.[8,9]

The intense absorptions at high energy are due apparently to dipole-allowed transitions. The shoulders at 44,000 and 47,500 cm^{-1} may be attributed to $\sigma^* \leftarrow L\pi$. An absorption maximum was not reached before the 50,000 cm^{-1} limit for the instrumentation. It is possible, as well, that the allowed Pt $p_z \leftarrow$ d may occur in this region. Since the Pt(en)Br_2 possesses a dipole moment, the $\sigma^* \leftarrow$ d transitions are not strictly forbidden by symmetry because perturbation by the ligand fields can mix in asymmetric wave functions with the d orbitals. The selection rules for the ligand field excitations can be inferred from the symmetry of the ground and excited states. Since the ground state is $^1A_1$, spin-allowed excitations of $^1A_1$, $^1B_1$, and $^1B_2$ states may have nonzero transition moments for y, z, and x polarizations, respectively. The ligand field polarizations for the transitions assigned in the solution spectrum are included in Table II.

Crystal Spectra for Pt(en)Br_2. The technique for recording crystal spectra measures the difference of the absorbance at some wavelength from that of a standard wavelength. Since the absorbance at 600 nm in both b and c polarizations was very low, the absorbances at shorter wavelengths were measured with respect to those at 600 nm. For comparison of a crystal spectrum with that for a solution, it is desirable to determine a molar absorptivity, ϵ. Such a determination requires the crystal thickness L, for

$$\epsilon = A/LC \qquad (1)$$

where A is the absorbance and C is the molar concentration, 8.91, from the crystal density. Two techniques were utilized to determine a crystal thickness. In one, the weight of a crystal was determined to be 18.1 ± 1.0 μg by means of a Cahn electromicrobalance. Under a microscope with a calibrated scale, the somewhat irregular area was determined to be 0.404 mm^2. The thickness was therefore indicated to be 12.1 μ. The indicated molar absorptivity

TABLE II: Transitions in $Pt(en)Br_2$ from the Solution Spectrum

$\bar{\nu}$, cm^{-1}	Molar absorptivity, M^{-1} cm^{-1}	Oscillator strength $\times 10^3$	Transition assignment C_{2v} symmetry $\leftarrow A_1$	Predicted ligand field polarization
22,000–28,000	47	1.2	$^3B_2$, $^3A_2$, $^3B_1$	Spin forbidden
31,400	283	4.7	$^1B_2\ \sigma^*(d_{xy}) \leftarrow d_{x^2-y^2}$	x–a
35,000	172	3.9	$^1A_2\ \sigma^*(d_{xy}) \leftarrow d_{yz}$	Forbidden
			$^1B_1\ \sigma^*(d_{xy}) \leftarrow d_{xy}$	z–c
Not observed			$^1B_2\ \sigma^* d_{xy} \leftarrow d_{z^2}$	x–a
44,000	(3000)	36	$\sigma^* d_{xy} \leftarrow L\pi$	Dipole allowed
47,500	(7000)	120		

at the 410-nm peak in c polarization was 299 cm^{-1} M^{-1}. However, it was evident from observation of the crystal under crossed polarizers that the crystal was not uniform and the uncertainty in ϵ must be of the order of ±15%.

In the second technique the crystal, whose b polarized spectrum is shown in Figure 2, was utilized. It can be seen that in the region of low absorbance, $\bar{\nu} < 25{,}000$ cm^{-1}, there were weak periodic fluctuations in the recorded absorbance. These fluctuations are the result of the constructive and destructive interference by light which suffers two successive reflections from the crystal faces with the transmitted light beam. At an absorbance minimum the phase delay for the reflected light, δ_0, is $2\pi N$ where N is an integer. Such interference effects were utilized to provide both the thickness and indices of refraction for crystals of Magnus' green salt,[2] $Pt(NH_3)_4PtCl_4$. From the wavelengths of two minima, λ_1 and λ_2, the following equation applies[2]

$$N_1\lambda_1/n_1 = N_2\lambda_2/n_2 \qquad (2)$$

where $2\pi N_i$ is the phase delay at λ_i and n_i is the index of refraction at λ_i. Since $(N_2 - N_1)$ is available by counting the number of absorbance minima between λ_1 and λ_2, eq 2 can be used to find N_1 or N_2 provided the index of refraction is known as a function of wavelength. For a thinner crystal than the one shown in Figure 2, only four interference minima were recorded for b polarization, at 330.4, 375.4, 441.9, and 544.4 nm. An acceptable wavelength dependence for n_b was obtained only with an assignment of $N = 4$ to 544.4 nm. In that case, n_b decreased by 6% from 330.4 to 544.4 nm. When a value of 5 for N was assigned to 544.4 nm, there was a maximum in the index of refraction between 330.4 and 544.4 nm, and when a value of 3 was assigned to N for 544.4 nm the index of refraction decreased by 21% from 330.4 to 544.4 nm. The wavelength shift for λ_i was next determined for this crystal when it was rotated by 30° in the spectrophotometer beam about the c axis. From these wavelength shifts the indicated value of n_b at Na_D was determined to be 1.85 ± 0.1 with the assumption that $n_a = n_b$. Because the angle of refraction was not large in this experiment, a calculation showed that with a birefringence, $|n_b - n_a|$, of 0.2 the calculated value of n_b was shifted only by 0.03. This crystal proved to have a thickness of only 0.6 μ. This high value of the index of refraction was in agreement with the observation by the Becke line method that the index of refraction was greater than 1.74, the index of refraction of diiodomethane.

From the minima in the b spectrum in Figure 2, the value of N at the absorbance minimum for 20,300 cm^{-1} was calculated by the application of eq 2 to be 12 ± 1. The thickness for this crystal was found to be 1.6 ± 0.2 μ. This thickness provided a value of 261 cm^{-1} M^{-1} for ϵ at 410 nm, c polarization. Since the two determinations of ϵ appeared to have comparable accuracy of ±15%, the average of the two determinations, 280 cm^{-1} M^{-1}, was utilized in preparing the plots in Figures 2 and 3.

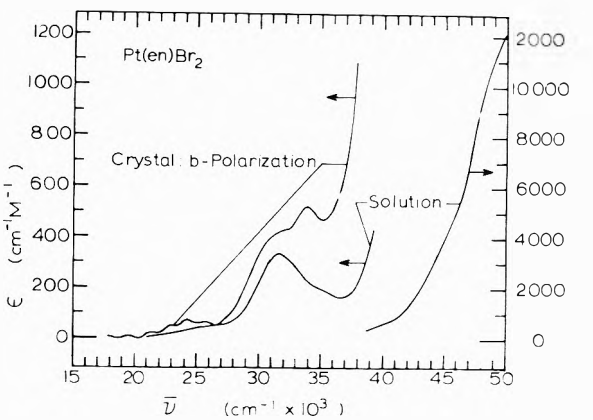

Figure 2. Absorption spectrum of an aqueous solution of $Pt(en)Br_2$ and for a crystal with b polarization at 300°K.

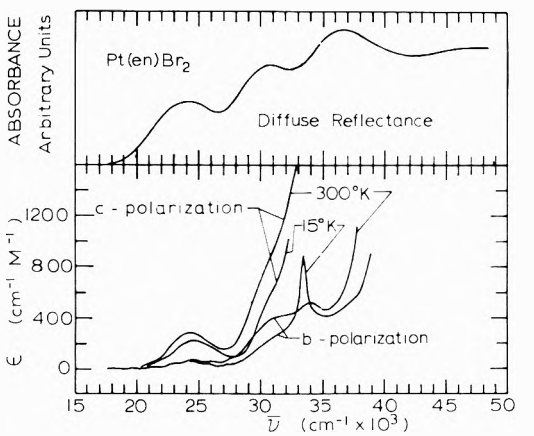

Figure 3. Crystal spectra, b, and c polarization, for a crystal of $Pt(en)Br_2$, 1.6 μ thick.

The polarized crystal spectra in b and c polarization at 300°, and with liquid He, nominally 15°K, are presented in Figure 3. In addition, a diffuse reflectance spectrum for the compound is included.

In c polarization the absorption is much stronger than in b polarization. The c intensity is about five times higher in the region of the maximum at 24,000 cm^{-1}. The c absorption becomes too intense to record for a single crystal beyond 33,000 cm^{-1} where the molar absorptivity is 1600 cm^{-1} M^{-1} and rising rapidly. At 15°K the peak maximum has shifted to 24,500 cm^{-1} and decreased in intensity so presumably the spin forbidden transitions are somewhat excited by the vibronic mechanism. A shoulder can be recognized at 20,500 cm^{-1} in the low-temperature

TABLE III: Transition Assignments for the Crystal Spectra of Pt(en)Br_2

$\tilde{\nu}$, cm^{-1}	Polarization	Oscillator strength at 15°K	Proposed assignment: excitation
20,000–27,000	c	4.6×10^{-3}	$\sigma^*(d_{xy}) \leftarrow$ d, spin forbidden: vibronic and ligand field
21,000–27,000	b	1.8×10^{-3}	$\sigma^*(d_{xy}) \leftarrow$ d, spin forbidden: vibronic and ligand field
31,000	b	2.9×10^{-3}	$\sigma^*(d_{xy}) \leftarrow d_{x^2-y^2}$, spin allowed: vibronic
33,500	b	1.4×10^{-3}	$\sigma^*(d_{xy}) \leftarrow d_{xz}$, ionized exciton; cipole allowed by overlap
36,700	c	(~0.1)	$\sigma^*(d_{xy}) \leftarrow L\pi a_2$, Frenkel exciton, dipole allowed

spectrum and at still lower energies the interference waves are apparent.

In the diffuse reflectance spectrum there is also a peak at *ca.* 24,000 cm^{-1}. The highest absorbance out to beyond 48,000 cm^{-1} appears at 36,700 cm^{-1}. It apparently belongs to an intense transition in c polarization which must have an energy higher than 44,000 cm^{-1} in the solution spectrum, and which therefore has been red shifted by 7000–12,000 cm^{-1}. It was shown in the discussion for Pt(en)Cl_2[1] that such a shift for a transition polarized in the stacking direction can be expected for excitation into Frenkel exciton states. Since the g ← g transitions at lower energy in *c* polarization borrow intensity from this transition, their intensity is enhanced in the crystal from its proximity.

For *b* polarization at room temperature, the molar absorptivity over much of the transition energy region is only moderately higher than for the solution spectrum, Figure 2. There is a distinct shoulder at *ca.* 31,000 cm^{-1} which is very close to the maximum for the solution spectrum. Evidence of a weak band at 34,000 cm^{-1} appears which does provide a total molar absorptivity of 530 cm^{-1} M^{-1}. The crystal spectrum then has a minimum at 35,200 cm^{-1} which is close to the shoulder assigned to the $^1B_1$ state in the solution. At 15°K, the intensity of the shoulder at 31,000 has fallen drastically, consistent with its assignment as a vibronic excitation to the $^1B_2$ state, $\sigma^* \leftarrow d_{x^2-y^2}$. However, the small hump at 34,000 cm^{-1} has narrowed and increased in height to more than 900 cm^{-1} M^{-1} with small a shift to 33,500 cm^{-1}. This is similar but even more definitive than the behavior of the band at 33,100 cm^{-1} in Pt(en)Cl_2. This band apparently corresponds to a weak transition which is dipole allowed in *b* polarization. The same assignment is proposed for this band, *viz.*, an excitation to a bound ionic state, in which an electron from d_{xz} orbital moves into the $\sigma^*(d_{xy}$ orbital) of an adjacent molecule, *i.e.*, $\sigma^*(d_{xy})_{j\pm1} \leftarrow (d_{xz})_j$, where the subscripts on the d orbitals designate the position in the stacking array of molecules. The energy of the transition is at slightly higher energy in Pt(en)Br_2 than in Pt(en)Cl_2, despite the usual red shift of most bands for bromide in accordance with the spectrochemical series.[10,11] Apparently, the higher energy for the Pt(en)Br_2 results from the slightly higher separation of the molecules along the stacking axis 3.50 Å *vs.* the 3.39 Å for Pt(en)Cl_2. The energies of transitions to the ionic states increase strongly with the molecular separations because of the greater separation of charge which occurs in the excited state. A second allowed transition was observed in Pt(en)Cl_2. However, because the ligand to metal transitions occur at lower energies in Pt(en)Br_2, the absorption becomes too intense to follow beyond 39,000 cm^{-1}.

The intermediate maximum in the diffuse reflectance spectrum at 31,000 cm^{-1} coincides with the shoulder in the solution spectrum which was assigned to the $^1B_2$ excited state, $[\sigma^*(d_{xy}) \leftarrow d_{x^2-y^2}]$. This transition is allowed by the vibronic mechanism in the *b* and c polarization but is dipole allowed by the ligand field perturbation in the *a* direction. Hence, it should be much stronger in *a* polarization than in *b* and presumably is strong enough to provide the peak in the reflectance spectrum.

The transition assignments from the crystal spectra have been summarized in Table III. The results have demonstrated a stacking of the molecules along the c axis of an orthorhombic crystal and the presence of a weak but dipole-allowed transition which can logically be assigned to an excited ionic crystal state.

Supplementary Material Available. Listings of structure factors, coordinates, and anisotropic temperature factors will appear following these pages in the microfilm edition of this volume of the journal. Photocopies of the supplementary material from this paper only or microfiche (105 × 148 mm, 20× reduction, negatives) containing all of the supplementary material for the papers in this issue may be obtained from Journals Department, American Chemical Society, 1155 16th St., N.W., Washington, D. C. 20036. Remit check or money order for $3.00 for photocopy or $2.00 for microfiche, referring to code number JPC-73-3077.

References and Notes

(1) D. S. Martin, Jr., L. D. Hunter, R. F. Kroening, and R. F. Coley, *J. Amer. Chem. Soc.*, **93**, 5433 (1971).
(2) D. S. Martin, Jr., R. M. Rush, R. F. Kroening, and P. F. Fanwick, *Inorg. Chem.*, **12**, 301 (1973).
(3) G. W. Watt and R. E. McCarley, *J. Amer. Chem. Soc.*, **79**, 3315 (1957).
(4) D. S. Martin, Jr., *Inorg. Chim. Acta Rev.*, **5**, 107 (1971).
(5) D. T. Cromer and J. T. Waber, *Acta Crystallogr.*, **18**, 104 (1965).
(6) See paragraph at end of paper regarding supplementary material.
(7) D. S. Martin, Jr., M. A. Tucker, and A. F. Kassman, *Inorg. Chem.*, **5**, 491 (1966).
(8) D. S. Martin, Jr., J. F. Foss, M. E. McCarville, M. A. Tucker, and A. J. Kassman, *Inorg. Chem.*, **5**, 491 (1966).
(9) A. F. McCaffery, P. N. Schatz, and P. J. Stephens, *J. Amer. Chem. Soc.*, **90**, 5730 (1968).
(10) R. Tschida, *Bull. Chem. Soc. Jap.*, **13**, 388, 436 (1938).
(11) K. Fajans, *Naturwissenshaften*, **11**, 165 (1923).

Monte Carlo Calculations of Reaction Rates and Energy Distributions among Reaction Products, F + HD → HF + D and F + HD → DF + H[1]

Roger L. Wilkins

The Aerospace Corporation, El Segundo, California 90009 *(Received July 13, 1973)*

Publication costs assisted by The Aerospace Corporation

Rate constants are calculated for the exothermic reactions F + HD(v, J) → HF(v') + D and F + HD(v, J) → DF(v') + H by analyzing the results of three-dimensional classical trajectories on an assumed London–Eyring–Polanyi–Sato (LEPS) potential energy surface. The Monte Carlo method is used to start each collision trajectory. An analysis is given of the dependences of the total reaction cross sections σ_r and specific reaction cross sections $\sigma(v, J, v', E_R)$ on the relative translational energy and the vibrational–rotational energy of the reagent molecule HD(v, J). Data are presented for the temperature dependences of (1) the overall rate constants, (2) the rate constants for the formation of HF and DF in specified vibrational states, and (3) the distribution of vibrational, rotational, and translational energies in the products of these exothermic reactions. The relative rate constants at room temperature for the formation of HF and DF in specific vibrational states are (1) for F + HD → HF(v') + D, $k(v' = 1) = 0.26$, [$k(v' = 2) = 1.00$], and $k(v' = 3) = 0.67$; and (2) for F + HD → DF(v') + H, $k(v' = 2) = 0.15$, [$k(v' = 3) = 1.00$], and $k(v' = 4) = 0.62$. Each reaction exhibits a high fractional conversion of available reaction energy into vibrational energy of the newly formed molecule. The mean fractions of available energy-entering vibration plus rotation are (1) for F + HD → HF(v') + D, $\bar{f}_{v'} + \bar{f}_{R'} = (0.77 + 0.12) = 0.89$, and (2) for F + HD → DF(v') + H, $\bar{f}_{v'} + \bar{f}_{R'} = (0.67 + 0.20) = 0.87$. The isotopic analogs of the reaction between atomic fluorine and H_2 all have similar energy distributions of the reaction products, but the relative rate constants for formation of product molecules in specified vibrational states are different. The overall rate constants at room temperature for the two reactions between F and HD indicate that the fluorine atom abstracts the hydrogen atom from HD about 1.5 times as fast as it abstracts the deuterium atom from HD.

I. Introduction

Relative rate constants for the formation of HF and DF in specific vibrational states from the reactions of F atoms with H_2 and D_2 have been determined experimentally by infrared chemiluminescence techniques,[2-5a] chemical laser techniques,[6,7] a molecular beam technique,[8,9] and theoretically[10-15] by classical trajectory calculations. Overall rate constants for the formation of HF or DF in the reactions

$$F + HD \xrightarrow{K_H} HF + D \quad (1)$$

and

$$F + HD \xrightarrow{K_D} DF + H \quad (2)$$

have not been determined experimentally. The temperature dependences of relative rate constants for the formation of HF and DF in specified vibrational states have *not* been reported for the reactions[5b]

$$F + HD \longrightarrow HF(v') + D \quad (3)$$

and

$$F + HD \longrightarrow DF(v') + H \quad (4)$$

Classical trajectory analysis[11-14] with a London–Eyring–Polanyi–Sato (LEPS) potential energy surface for the reactions F + H_2 → HF + H and F + D_2 → DF + D gave results that were in quantitative agreement with available experimental data. This same potential energy surface[14] was used to make a trajectory analysis[16] of the reactions of H atoms with vibrationally excited HF, and the results were in quantitative agreement with available experimental data. Since the potential energy function used in this analysis is independent of isotopic substitution, it is reasonable to expect that this surface will give results for the reaction F + HD that are in quantitative agreement with future experimental data. Rate constants for reactions 3 and 4, in which HF and DF are vibrationally excited, are required in the calculation of the performance of HF and DF chemical lasers.

The present paper reports the results of 8400 classical trajectories on a semiempirical LEPS potential energy surface for reactions of F atoms with HD. The purpose of this paper is to present the temperature dependences of the overall rate constants, the energy distributions of the reaction products, and the rate constants for the formation of HF and DF in specific vibrational states.

II. Classical Trajectory Calculations

The LEPS method was used to construct the F–HD potential energy surface. The potential energy parameters used in the present calculation are tabulated in a previous paper.[14]

The method of calculation is discussed in a previous paper[14] and the references cited therein. The reactant HD molecule was assigned quantum vibrational v and rotational J states. Calculations were made for $v = 0$ with $J = 0$, 1, 2, 3, and 4. A minimum of 200 trajectories were calculated for each (v, J) state of HD at each of the collision energies 1.0, 1.5, 2.0, 2.5, 3.0, 3.5, 4.0, and 4.5 kcal/mol. The value of the maximum impact parameter, b_{max}, at a given collision energy represents the smallest value of the impact parameter for which 50 randomly chosen trajec-

tories gave no reaction. The value of b_{max} increases with increasing collision energy. The values of b_{max} used in this calculation varied from 1.5 to 2.0 Å for the stated collision energies.

The equation used to evaluate the rate constants from the cross section is

$$k_{v,J,v',J'}(T) = \left(\frac{8k_BT}{\pi\mu}\right)^{1/2} \frac{1}{k_B^2T^2}\int_0^\infty \sigma(v,J,v',J',E_R)E_R \times \exp\left(-\frac{E_R}{k_BT}\right) dE_R \quad (5)$$

where k_B is the Boltzmann constant and μ is the reduced mass of the colliding species. v' and J' are the quantum vibrational and rotational states, respectively, of the product molecule HF or DF. In order to obtain the rate constants $k_{v',J'}(T)$, the rate constants $k_{v,J,v',J'}(T)$ were averaged over a Boltzmann distribution of v, J states of the initial reactant molecule. The rate constants $k_{v'}(T)$ were calculated from the rate constants $k_{v',J'}(T)$ by summation of $k_{v',J'}(T)$ over all J' states for a fixed value of v'.

An empirical fit for the rate constant data can be obtained from Arrhenius equation

$$k_{v'}(T) = A(v') \exp[-E_a(v')/RT] \quad (6)$$

The values of $A(v')$ and $E_a(v')$ are shown in Figures 4 and 5. The specific rate constants computed from eq 5 were fitted to the form given in eq 6 for the convenience of users of present available chemical kinetic programs.[17-19]

III. Results and Discussions

Figure 1a-e shows specific reaction cross sections $\sigma(v, J, v', E_R)$ and overall reaction cross sections $\sigma_r(v, J, E_R)$ for the reaction of F atoms with HD molecules.[20] The total reaction cross sections σ_r for formation of DF decreases as J increases, and σ_r for formation of HF increases with increasing J. This result is in agreement with the recent trajectory studies reported by Muckerman.[11-13] Previous trajectory studies[10-14] have shown that σ_r increases for the reaction F + H_2 as J increases from 0 to 1, and σ_r decreases as J increases from 1 to 5. Wilkins[21] found that σ_r increases for the reaction F + D_2 as J increases from 0 to 1, and σ_r decreases as J increases from 1 to 5. Muckerman[11] found, for F + D_2 at a single collision energy, that σ_r decreases as J increases from 0 to 5. Blais and Truhlar[15] found, for F + D_2 at a single collision energy (E_R = 4.5 kcal/mol), that σ_r decreases as J increases from 0 to 1, and then σ_r increases as J increases from 1 to 5. Our studies indicate that one should be extremely careful in reaching conclusions from results of trajectory calculations at a single collision energy. Examination of the trajectory calculations for F + D_2 over a wide range of collision energies indicates that σ_r increases as J increases from 0 to 1, and σ_r decreases as J increases from 1 to 5. Extrapolations of the σ_r *vs.* E_R data in Figure 1a-e for formation of HF give apparent threshold energies of 1.0 kcal/mol for J = 0; 1.1 kcal/mol for J = 1; 1.15 kcal/mol for J = 2; 1.2 kcal/mol for J = 3; and 1.25 kcal/mol for J = 4. The present study and previous theoretical studies[10-15,21] show that initial rotational energy of the reagent hinders reaction.

This work shows that the molecular products HF and DF are scattered in the backward direction ($\bar{\theta} > 90°$). The angular distribution $I(\theta)$ shifts toward the forward direction as V_R, the relative velocity of the reagents, increases. Muckerman,[11] Jaffe and Anderson,[10] Blais and Truhlar,[15] and Wilkins[14,16] found this result in their trajectory studies. Lee and coworkers[9] also found in their molecular beam experiments for the reaction F + H_2 that $I(\theta)$ shifts toward the forward direction as the relative velocity V_R is increased.

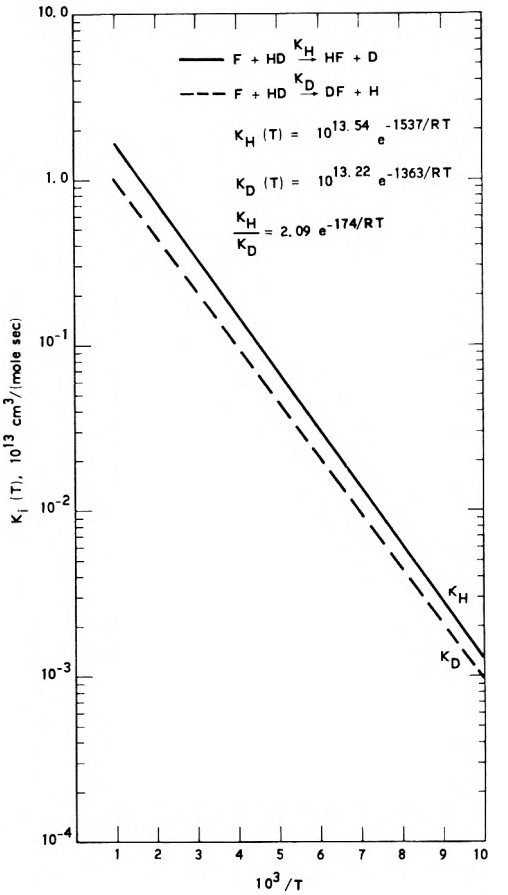

Figure 2. The overall rate constants $K_H(T)$ and $K_D(T)$ for reactions 1 and 2.

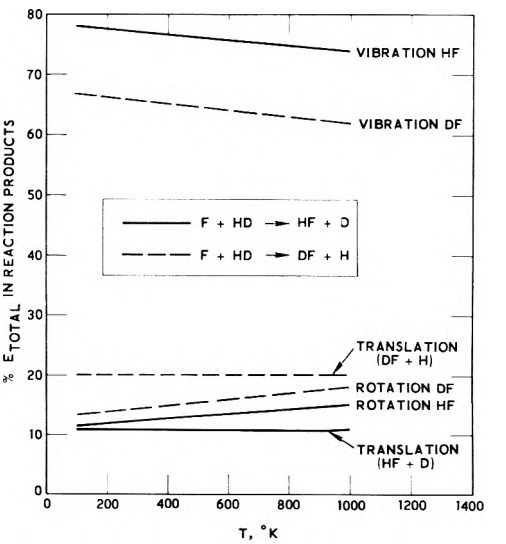

Figure 3. Partitioning of the heat of reactions for F + HD → HF + D and F + HD → DF + H into various degrees of freedom as a function of temperature.

Muckerman[11-13] has discussed the intramolecular isotope effect in the reaction F + HD. He found that the reaction F + HD is very strongly dependent on the rotational energy of the reagent HD. DF formation is favored for J = 0, and HF is formed preferentially for $J \geq 1$. At J > 4, HF is formed exclusively. The present study (Figure

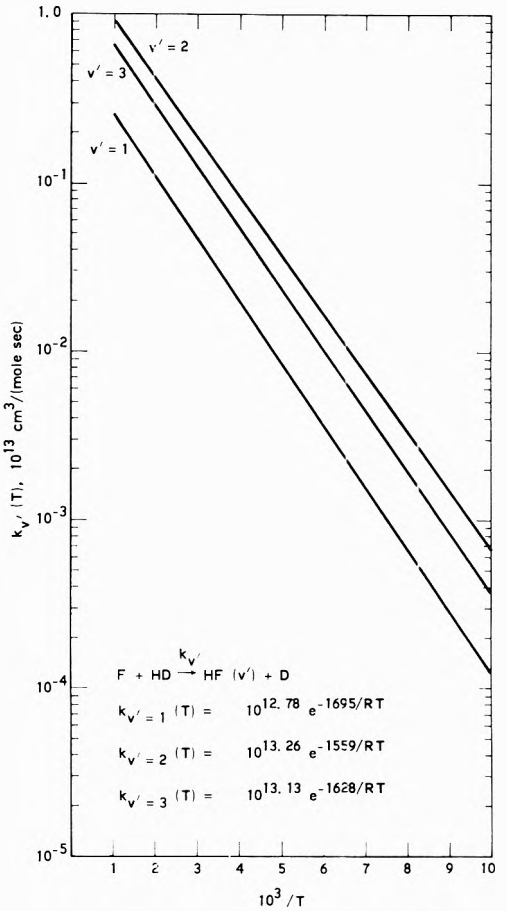

Figure 4. Rate constants for the formation of HF in specific vibrational states for the reaction F + HD → HF (v' + D ($k_{v'}$).

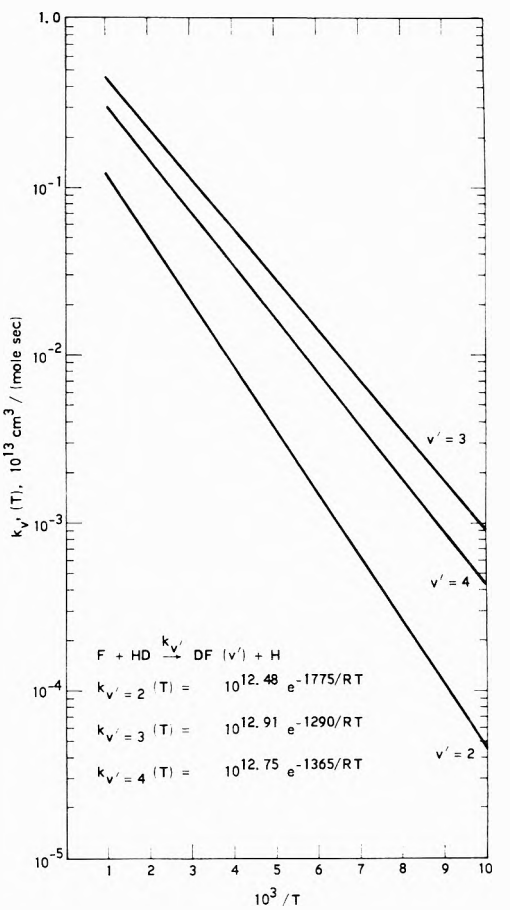

Figure 5. Rate constants for the formation of DF in specific vibrational states for the reaction F + HD → DF (v') + H ($k_{v'}$).

1a–e) also predicts this intramolecular isotope effect in the reaction F + HD. The reaction cross section σ_r increases (Figure 1a–e) with increased relative translational energy. This conclusion is in agreement with results reported by Jaffe and Anderson,[10] Muckerman,[11-13] Wilkins,[14,16,21-23] and Blais and Truhlar.[15]

The overall rate constants K_H and K_D for reactions 1 and 2 are shown in Figure 2. Kompa, *et al.*,[6] estimated a ratio of K_H/K_D = 2.5 at room temperature. This was based on their findings that a UF_6–HD mixture gave DF emission that was three-tenths as intense as that observed from the corresponding UF_6–D_2 mixture. This trajectory analysis predicts a ratio of K_H/K_D = 1.5 at room temperature. The curves for K_H and K_D show that F abstracts H from HD about 1.5 times as fast as it abstracts D from HD.

In Figure 3, it is shown that the energy distributions of the product molecules HF and DF are slowly varying linear functions of temperature. The present trajectory analysis predicts that 77% of the total available energy will become vibrational energy of HF when reaction 3 occurs and only 67% will become vibrational energy of DF when reaction 4 occurs. Previous trajectory calculations predicted the energy distributions of the reaction products for the reaction F + H_2 to be similar to those for the reaction F + D_2. The trajectory calculations for the reactions of F + HD predict that the energy distributions of the products will be sensitive to a change from reaction 3 to reaction 4. At present, there is no experimental evidence to substantiate this conclusion.

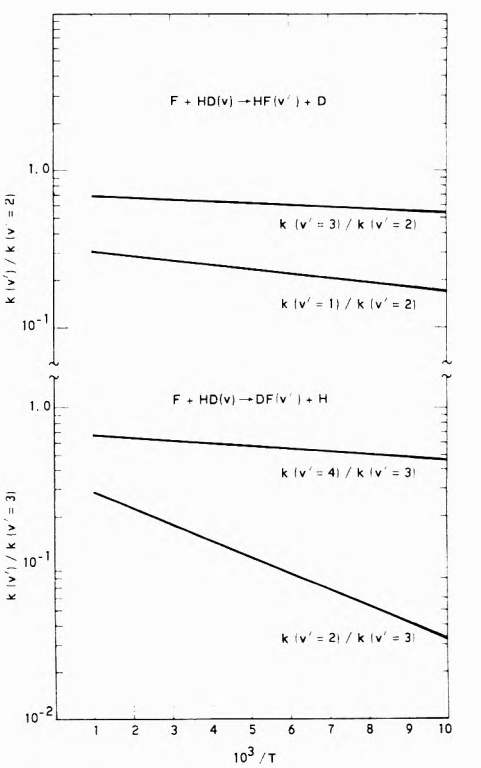

Figure 6. Relative rate constants for the formation of HF and DF in specific vibrational states.

Plots of $k_{v'}(T)$ are shown in Figures 4 and 5. The values of $k_{v'}(T)$ are the rate constants for the formation of HF and DF in specified vibrational states. The $v' = 2$ levels are the most highly populated vibrational levels for the reactions F + H_2 and F + HD when HF (v') molecules are formed. The $v' = 3$ levels are the most highly populated vibrational levels for the reactions F + D_2 and F + HD when DF (v') molecules are formed.

The temperature dependence of the relative rate constants for the formation of HF and DF in specific vibrational states for reactions 3 and 4 is shown in Figure 6. At room temperature, these relative rate constants are (1) for F + HD → HF(v') + D, $k(v' = 1) = 0.26$, [$k(v' = 2) = 1.0$], and $k(v' = 3) = 0.67$; and (2) for F + HD → DF(v') + H, $k(v' = 2) = 0.15$, [$k(v' = 3) = 1.0$], and $k(v' = 4) = 0.62$. A comparison of these theoretical data with experimental data is not possible because the latter have not yet been reported. It is expected that these results will be in quantitative agreement with future experimental data.

IV. Conclusions

Classical trajectory analysis of the reaction between F atoms and HD to form either HF or DF indicates, for both reactions 3 and 4, a very efficient conversion of reaction energy into product vibrational energy due to the repulsive energy released and the heavy attacking atom.[5a] The energy distributions of the reaction products are predicted to be sensitive to a change from reaction 3 to reaction 4. At present, there is no experimental evidence to substantiate this conclusion. The intramolecular isotope effect for the reaction F + HD(v, J) is very strongly dependent on the reactant rotational energy. The isotopic analogs of the reaction F + H_2 have quite similar energy distributions of the reaction products, but the relative rate constants for the formation of product molecules in specific vibrational states are quite different. The overall rate constants for reactions 1 and 2 at room temperature indicate that the fluorine atom abstracts the hydrogen atom from HD about 1.5 times as fast as it abstracts the deuterium atom from HD.

This paper gives theoretical predictions for the reaction attributes of the reaction F + HD. There is a need for experimental work on this system. Experimental data are not available for comparison with our theoretical results. It is expected that the theoretical results presented herein will be in quantitative agreement with future experimental data.

Supplementary Material Available. The cross-section data (Figure 1a–e) will appear following these pages in the microfilm edition of this volume of the journal. Photocopies of the supplementary material from this paper only or microfiche (105 × 148 mm, 20× reduction, negatives) containing all of the supplementary material for the papers in this issue may be obtained from the Journal Department, American Chemical Society, 1155 Sixteenth St., N.W., Washington, D. C. 20036. Remit check or money order for $3.00 for photocopy or $2.00 for microfiche, referring to code number JPC-73-3081.

References and Notes

(1) This work reflects research supported by the Air Force Weapons Laboratory under U. S. Air Force Space and Missile Systems Organization (SAMSO) Contract No. F04701-73-C-0074.
(2) (a) J. C. Polanyi and D. C. Tardy, *J. Chem. Phys.*, **51**, 5717 (1969); (b) K. G. Anlauf, P. E. Charters, D. S. Horne, R. G. MacDonald, D. H. Maylotte, J. C. Polanyi, W. J. Skrlac, D. C. Tardy, and K. B. Woodall, *ibid.*, **53**, 4091 (1970).
(3) N. Jonathan, C. M. Melliar-Smith, and D. H. Slater, *Mol. Phys.*, **20**, 93 (1971).
(4) N. Jonathan, C. M. Melliar-Smith, D. Timlir, and D. H. Slater, *Appl. Opt.*, **10**, 1821 (1971).
(5) (a) J. C. Polanyi and K. B. Woodall, *J. Chem. Phys.*, **57**, 1574 (1972). (b) Experiments are underway on this system according to ref 5.
(6) K. L. Kompa, J. H. Parker, and G. C. Pimental, *J. Chem. Phys.*, **49**, 4257 (1968).
(7) J. H. Parker and G. C. Pimentel, *J. Chem. Pnys.*, **51**, 91 (1969).
(8) T. P. Shafer, P. E. Siska, J. M. Parson, F. P. Tully, Y. C. Wong, and Y. T. Lee, *J. Chem. Phys.*, **53**, 3385 (1970).
(9) Y. T. Lee, Invited talk at the Proceedings of the 7th International Conference on the Physics of Electrons in Atomics Collisions, Amsterdam, 1961, unpublished.
(10) R. L. Jaffe and J. B. Anderson, *J. Chem. Phys.*, **54**, 2224 (1971).
(11) J. T. Muckerman, *J. Chem. Phys.*, **54**, 1155 (1971).
(12) J. T. Muckerman, *J. Chem. Phys.*, **56**, 2997 (1972).
(13) J. T. Muckerman, *J. Chem. Phys.*, **57**, 3388 (1972).
(14) R. L. Wilkins, *J. Chem. Phys.*, **57**, 912 (1972).
(15) N. C. Blais and D. G. Truhlar, *J. Chem. Phys.*, **58**, 1090 (1973).
(16) R. L. Wilkins, *J. Chem. Phys.*, **58**, 3038 (1973).
(17) S. N. Suchard, R. L. Kerber, G. Emanuel, and J. S. Whittier, *J. Chem. Phys.*, **57**, 5066 (1972).
(18) N. Cohen, TR-0172(2779)-2, The Aerospace Corporation, El Segundo, Calif., Sept 1972.
(19) E. B. Turner, G. Emanuel, and R. L. Wilkins, TR-0059(6240-20)-1, The Aerospace Corporation, El Segundo, Calif., July 1970.
(20) See paragraph at end of paper regarding supplementary material.
(21) R. L. Wilkins, to be submitted for publication.
(22) R. L. Wilkins, *J. Chem. Phys.*, **58**, 2326 (1973).
(23) R. L. Wilkins, *J. Chem. Phys.*, **59**, 698 (1973).

Bicentric Rescaling of CNDO/2 Theory. Applications to Inorganic Fluorides

A. L. Companion

Department of Chemistry, Illinois Institute of Technology, Chicago, Illinois 60616 *(Received August 15, 1973)*

Relative bicentric contributions to the total CNDO/2 molecular energy are examined for 41 molecules using energy partitioning concepts. External rescaling of bicentric contributions permits estimation of reliable bond and atomization energies but brings about no improvement in the potential of CNDO theory in predicting geometries. Specific results are discussed for the fluorides of oxygen and boron.

Introduction

In two recent molecular orbital studies of the fluorides of sulfur[1] and the fluorides of nitrogen and phosphorus[2] we have pointed out that the CNDO/2 theory with usual parameterization[3] incorrectly weights the relative contributions to the total molecular energy from chemically different atom pairs, for example, from P-P and P-F pairs in P_2F_4. We believe, as a result, that many published CNDO-based predictions of relative stabilities of molecular conformations or geometries may be unreliable. In this paper we demonstrate further the incorrect relative weighting in a study of a broader series of 41 small inorganic molecules, and attempt to localize the main source of error by an energy partitioning analysis of the CNDO total energy.

We have also shown previously[1,2] for a limited group of molecules that if the total molecular energy is partitioned into atomic and diatomic components

$$E_T = \Sigma E_{AB} + \Sigma E_A^* \quad (1)$$

as defined by Pople and Beveridge,[3] the bicentric components E_{AB} may be individually rescaled with known bond energies and summed to obtain molecular atomization energies in reasonably good agreement with experimental ones. Here we extend these ideas to a broader series of molecules and consider also rescaling of the bicentric CNDO resonance-exchange energies.

Thus far the proposed diatomic rescaling procedure has been applied to molecules *at their known equilibrium geometries*. Comments are offered here on the potential of the procedure in *predicting* molecular geometries.

Calculations and Results

In Table I we summarize known thermodynamic data and sources of structural data for the 41 calibrating or test molecules considered. Experimental heats of atomization, labeled HATX, include zero-point energies but do not include temperature corrections to 0°K.

For all these species *at known or estimated geometries*, binding energies were computed on the Univac 1108 with the Dobosh CNDO/2 program[4] and *unmodified* internal parameters. Binding energies are defined according to

$$BE = E_T - \Sigma E_A^0 \quad (2)$$

where E_T is the total energy and E_A^0 are ground-state energies of isolated atoms.

Figure 1, a plot of HATX *vs.* BE values, illustrates that for these complex molecules no simple linear relationship exists such as that proposed by Wiberg[5] for a series of simple organic molecules. The results of a linear least-squares analysis, shown in Figure 1, include a linear correlation coefficient between HATX and BE values of only 0.535.

Approximate straight lines *can* be drawn connecting members of a family of molecules with like bonds such as SF, SF_2, SF_4, SF_6 or PF, PF_2, PF_3, PF_5. However, the slopes of these family lines differ markedly from one another, and all molecules related to the family but with at least one different bond pair, *e.g.*, FSSF or P_2F_4, deviate considerably from the family line. These latter observations led us to an analysis of individual *diatomic* contributions to the total molecular energy

The Dobosh program was modified accordingly to permit collection of all bulk bicentric terms E_{AB} after the terminal SCF iteration, and furthermore to subdivide each E_{AB} as follows (for closed shell systems)

$$E_{AB} = E_{AB}^{RE} + E_{AB}^{C} + E_{AB}^{N} \quad (3)$$

where

$$E_{AB}^{RE} = \sum_{\mu \in A} \sum_{\nu \in B} P_{\mu\nu}[F_{\mu\nu} + H_{\mu\nu}] \quad (4)$$

$$E_{AB}^{C} = [P_{AA}P_{BB} - P_{AA}Z_B - P_{BB}Z_A]\gamma_{AB} \quad (5)$$

$$E_{AB}^{N} = Z_A Z_B / R_{AB} \quad (6)$$

E_{AB}^{RE} contains all interactions labeled "resonance" and "exchange" by Fischer and Kollmar[6] in their energy partitioning analysis, E_{AB}^{C} contains coulombic attractions and repulsions, and E_{AB}^{N} represents the repulsions of the nuclei and cores. E_{AB} quantities are related to the CNDO total molecular energy and the energies of promoted atoms E_A^* through eq 1. All other symbols are precisely those defined by Pople and Beveridge.[3] Analogous expressions were developed for open-shell systems.

Figure 2 illustrates that a marked improvement in linear correlation results when HATX values are plotted *vs.* sums of bicentric energies, ΣE_{AB}. Comparing eq 1 and 2 we see that the difference between ΣE_{AB} and BE is a sum over atomic *promotional energies*. Hence much of the scatter observed in Figure 1 and much of the error in the computed CNDO binding energies may be attributed to approximations involved in *one-center energies*.

Further improvement is noted in Figure 3, a plot of HATX values *vs.* sums of bicentric "resonance-exchange" energies, ΣE_{AB}^{RE}, defined according to eq 4. Association of bond energies with such computed quantities is not a new idea.[3] Here, removal of the influence of the approximations involved in evaluating core repulsions and coulomb interactions permits the linear correlation coefficient to increase to 0.931. The integrals γ_{AB} contribute to both

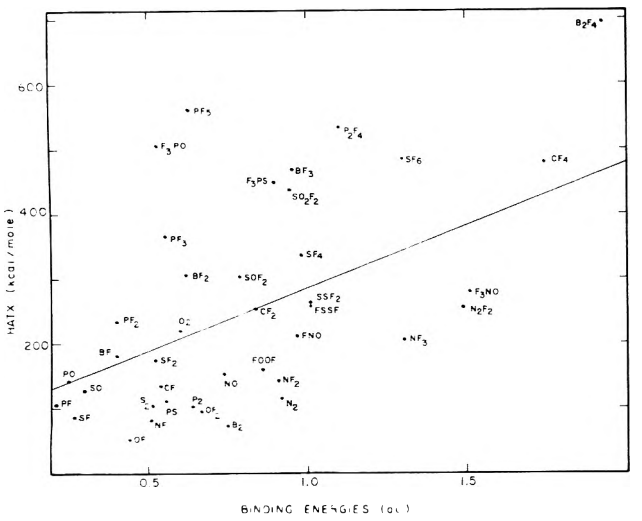

Figure 1. Experimental atomization energies (HATX) for the 41 molecules considered *vs.* CNDO binding energies. The least-squares straight line shown has the form $y = 193.3x + 93.2$ with standard deviation $\sigma_y = 99.0$ and linear correlation coefficient $r = 0.535$. x and y represent quantities plotted as abscissa and ordinate with units indicated.

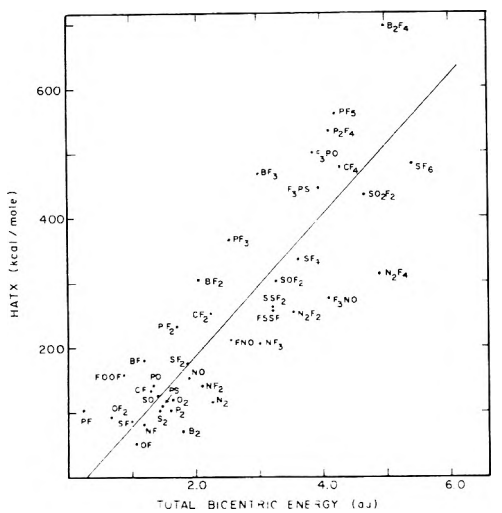

Figure 2. Experimental atomization energies (HATX) *vs.* sums of unrescaled bicentric energies, E_{AB}. The least-squares straight line has the form $y = 108.2x - 29.7$ with $\sigma_y = 78.2$ kcal/mol and linear correlation coefficient $r = 0.854$.

$F_{\mu\nu}$ and $E_{AB}{}^{C}$, while the one-center electron densities P_{AA} and P_{BB} appear only in $E_{AB}{}^{C}$; hence it is tempting to attribute the error in $E_{AB}{}^{C}$ again to one-center quantities. Despite the increase in correlation shown in Figure 3, the standard deviation in computed atomization energies, 44.2 kcal/mol, is too large to make the observed linear relation useful to chemists.

The world-wide availability and employment of CNDO-based programs appears to justify exploratory attempts to make them more useful. As an alternative to immediate internal reparameterization of the theory and as a guide to appropriate directions for reparameterization we considered *external* rescaling of bicentric energies with known bond energies. Within the limitations to be described, such rescaling of either $E_{AB}{}^{RE}$ or E_{AB} values permits the computation of meaningful bond and atomization energies with the CNDO programs. In the first of two procedures considered, the computed values of E_{AB} were rescaled by requiring for 16 molecules involving *only one bond type*, AB, that the sum over E_{AB} values, computed at equilibrium distances, must total the experimental heat of atomization. The 16 calibrating molecules are starred in Table I, while the rescaling factors obtained are listed in Table II. These latter are to be interpreted as, for example, one unit of CNDO computed bulk bicentric energy for a nitrogen–fluorine pair, E_{NF}, is equivalent to 70.19 kcal/mol in real life.

The rescaling factors thus obtained were tested by calculation of atomization energies for 25 additional molecules involving combinations of these atom pairs. These are of assorted experimental geometries, most much more complex than those of the calibrating systems, but with bond distances *generally* near those involved in calibra-

TABLE I: Thermodynamic Data and Sources of Structural Data for Molecules Considered

Molecule	HATX, kcal/mol	Structural data source
*B_2	72.2[a]	*a*
BF	181.4[a]	*b*
BF_2	304.9[a]	*c*
*BF_3	468.9[a]	*a*
B_2F_4	695.9[a]	*a, k*
*CF	133.6[a]	*a*
CF_2	253.0[a]	*a*
CF_4	479.1[a]	*a*
*N_2	229.4[a]	*d*
NF	82[d]	*d*
NF_2	142.1[d]	*d*
*NF_3	206.4[d]	*d*
N_2F_2 (cis)	254.9[d]	*d*
N_2F_4	314.2[d]	*d*
*O_2	120.2[a]	*a*
OF	54.0[a]	*j*
*OF_2	94.7[e]	*f*
FOOF	158.3[e]	*g*
*P_2	103.5[d]	*d*
PF	105[d]	*d*
PF_2	234[d]	*d*
*PF_3	366[d]	*d*
PF_5	562[d]	*d*
P_2F_4	534[d]	*d*
*S_2	103[h]	*h*
SF	87.1[h]	*h*
SF_2	174.8[h]	*h*
*SF_4	330.7[h]	*h*
*SF_6	484.5[h]	*h*
FSSF	257.4[h]	*h*
SSF_2	261.2[h]	*h*
*NO	153.7[a]	*a*
FNO	211.6[a]	*a*
F_3NO	277.6[a]	*i*
*PO	142.6[a]	*a*
F_3PO	500.7[a]	*a*
*SO	126.8[a]	*a*
F_2SO	303.8[a]	*a*
F_2SO_2	436.0[a]	*a*
*PS	110.2[a]	*a*
F_3PS	447.7[a]	*a*

[a] Reference 8. [b] F. J. Lovas and D. R. Johnson, *J. Chem. Phys.*, **55**, 41 (1971). [c] R_{BF} estimated as average of that for BF and BF_3. ∠FBF from W. Nelson and W. Gordy, *J. Chem. Phys.*, **51**, 4710 (1969). [d] From data summarized in ref 2. [e] Reference 9. [f] L. Pierce, N. DiCianni, and R. H. Jackson, *J. Chem. Phys.*, **38**, 730 (1963). [g] R. H. Jackson, *J. Chem. Soc.*, 4585 (1962). [h] From data summarized in ref 1. [i] V. Plato, W. D. Hartford, and K. Hedberg, *J. Chem. Phys.*, **53**, 3488 (1970). [j] Reference 7, theoretical value. [k] From data in ref 12.

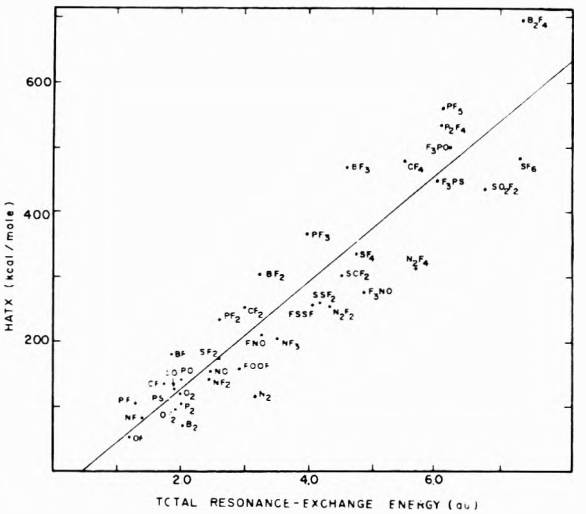

Figure 3. Experimental atomization energies (HATX) *vs.* sums of unrescaled "resonance-exchange" energies, E_{AB}^{RE}. The least-squares straight line has the form $y = 82.8x - 38.5$ with $\sigma_y = 44.2$ kcal/mol and linear correlation coefficient $r = 0.931$.

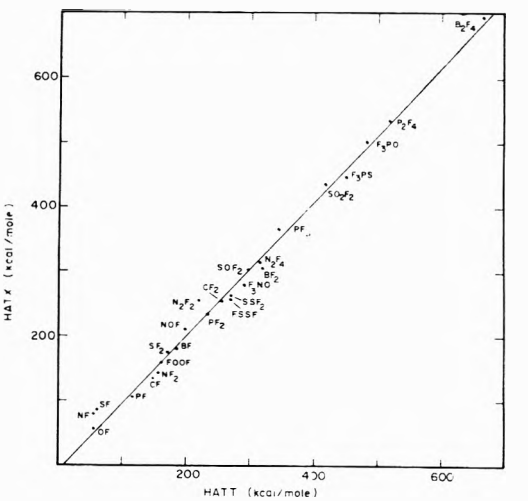

Figure 4. Experimental atomization energies (HATX) *vs.* theoretical ones (HATT), computed by rescaling bicentric energies E_{AB}. Calibrating molecules are excluded. The least-squares straight line has the form $y = 1.05x - 9.40$, with $\sigma_y = 7.8$ kcal/mol and linear correlation coefficient $r = 0.997$.

TABLE II: Rescaling Factors for CNDO Bicentric Energies

AB in E_{AB}	Energy equivalent to one E_{AB} unit, kcal/mol	AB in E_{AB}	Energy equivalent to one E_{AB} unit, kcal/mol
BB	[40.27][a]	PP	73.69
NN	101.3	SS	72.91
OO	73.49	PF	136.5
FF, OO (repulsion)	~200	SF	93.79
BF	158.1	PS	75.91
CF	114.6	NO	81.70
NF	70.19	PO	107.0
OF	54.35	SO	91.13

[a] See discussion of this quantity in section on boron fluorides.

TABLE III: Rescaling Factors for CNDO Resonance-Exchange Energies

AB in E_{AB}^{RE}	Energy equivalent to one E_{AB}^{RE} unit, kcal/mol	AB in E_{AB}^{RE}	Energy equivalent to one E_{AB}^{RE} unit, kcal/mol
BB	[35.50][a]	PP	51.64
NN	72.78	SS	59.26
OO	60.52	PF	88.70
OO, FF (repulsion)	~500	SF	72.17
BF	103.3	PS	61.24
CF	91.93	NO	62.17
NF	62.26	PO	71.34
OF	50.50	SO	66.98

[a] See footnote *a* to Table II.

tion. The results are illustrated in Figure 4, where relatively small deviations are observed from the ideal straight line relating experimental atomization energies (labeled HATX) and computed ones (HATT), and the linear correlation coefficient is 0.997. Calibrating molecules are excluded from this evaluation.

The variation shown in rescaling factors (Table II) reinforces our contention that CNDO/2 parameterization misweights relative energy contributions to the total energy, E_T, from different atom pairs, and accordingly that conclusions based upon optimization of E_T for a molecule may be in considerable error.

A similar external rescaling was performed on sums over E_{AB}^{RE} with the resultant energy equivalents listed in Table III. A least-squares analysis of HATX *vs.* HATT values yielded a standard deviation of 11.3 kcal/mol in computed atomization energies and a linear correlation coefficient of 0.995. Thus either rescaling method gives reasonable estimates of bond and atomization energies.

Improved sets of rescaling parameters may be obtained by optimizing the least-squares fit for a larger group of molecules. In the present calculations, for example, the bicentric energy between nonbonded fluorine atoms was estimated by simultaneously fitting E_{SF} and E_{FF} with the atomization energies of SF_4 and SF_6.[1] This same energy factor was used to correct repulsions between oxygen pairs and repulsions between oxygen–fluorine pairs, all very small. A better fit would be expected if these latter two pairs were rescaled explicitly.

With the above rescaling methods yielding atomization energies with less than an average 5% error, we hoped for improvement in the potential of CNDO calculations in the *prediction* of molecular geometries. However, in studies of several of the molecules considered in this paper optimization of HATT with respect to bond distances and bond angles occurred at geometries no closer to the true ones than those consistent with the optimum CNDO binding energy. For molecules of bond type such as NF_2 the CNDO bond distance, 1.23 Å, is largely determined by strongly varying NF interactions; F–F repulsions vary slowly and are too small to increase the NF bond distance to the experimental 1.36 Å. Rescaling with a constant factor does not of course change the variation of NF energies with distance, and even with the large E_{FF} rescaling factor F–F repulsions are insignificant in influencing geometry. For molecules with two bond types such as *cis*-N_2F_2, F–F repulsions are even smaller, E_{NN} varies very *slowly* with bond distance, and E_{NF} again very quickly. Although the rescaling factor for E_{NN} is larger than that of E_{NF}, variation in the latter dominates in determining optimum geometry.

Since rescaling procedures do not appear to correct improper variation of CNDO energies with bond distances, we may justifiably ask why the method appears to describe properly trends in atomization energies of a diverse series of molecules such as N_2, NF, NF_2, NF_3, N_2F_2, and N_2F_4. The NF bond distance in these species varies little; hence a E_{NF} rescaling factor computed with one molecule is applicable to others with reasonable safety. In contrast, the N–N bond distance varies from 1.09 Å in N_2 (a calibrating molecule) to a 1.49 Å in N_2F_4. As noted above E_{NN}, however, varies *slowly* with distance for a given molecule and it is dramatic changes in *bond order* in going from N_2 to N_2F_2 to N_2F_4 that are reflected in the strong corresponding changes in E_{NN}. It appears that the CNDO computed bicentric energies *do* properly reflect changes in bond order in a series of related molecules.

From this discussion we conclude that criteria for selecting calibrating molecules for a particular bond type AB must include (besides known geometry and thermochemistry) (1) an AB bond distance close to that of AB in all other molecules to be rescaled or (2) a slow variation in E_{AB} with bond distance.

Comments on Specific Molecules

Specific results for some of the species treated here statistically may be of interest in themselves.

Oxygen Fluorides. O'Hare and Wahl[7] have computed an *ab initio* Hartree–Fock dissociation energy for the OF radical, D_0 = 3.0 (+0.3, −0.8) eV. Our computed value is 2.35 eV (E_{AB} rescaling), within the range of the O'Hare and Wahl result and several other experimental values quoted in their paper. For the radical FOO (not included in our statistical study) we computed with JANAF[8] geometry an HATT = 133.8 kcal/mol, supporting the atomization energy favored by O'Hare,[9] 138.1 kcal/mol. Predicted and experimental atomization energies of FOOF differ by only 5 kcal/mol. Some observations on the comparative structures of FOOF *vs.* FSSF follow.

In calculations on FSSF[1] a S–S bond energy slightly *stronger* than that in diatomic sulfur was predicted, a result consistent with experimental indications that FSSF is in essence a $S_2^{\delta+}$ diatomic with $F^{\delta-}$ ions bonded sufficiently loosely that equilibrium interconversion between this and the $S{=}SF_2$ form occurs readily. The increased S–S bond strength was attributed to partial removal of the topmost antibonding electrons from diatomic sulfur. In the FOOF molecule, although the O–O distance is similar to that of diatomic O_2, more extensive mixing of atomic orbitals occurs over the molecule, perhaps since all involved are first-row atoms, and the charge distribution corresponds to a somewhat less ionic molecule. In contrast to FSSF, the overall orbital picture in FOOF seems less like that of a slightly perturbed diatomic. Furthermore, the O–O bond energy in FOOF (95.4 kcal/mol) appears to be considerably *reduced* over that of O_2 (120.2).

Boron Fluorides. BF_3 was chosen as a calibrating molecule for the BF bond since its geometry and enthalpy of formation are well established. The theoretical atomization energy computed for BF, 185.2 kcal/mol, dependent only upon the the BF_3 rescaling energy, agrees well with the experimental 181.4. With an *estimated* structure for BF_2, we computed an atomization energy of 319.5 kcal/mol, a value more consistent with the enthalpy of formation of BF_2, −130 ± 6 kcal/mol, determined by Margrave[10] from appearance potentials than with the more recent photoionization result (−120.2 kcal/mol) of Dibeler and Liston.[11] Unfortunately it was the bond distances, on which energies depend more strongly, that had to be estimated in our calculations.

Durig, Thompson, Witt, and Odom,[12] on the basis of the Raman spectra of B_2F_4, propose that the symmetry of the gaseous molecule, like that in the solid, is D_{2h} rather than D_{2d}.[8] For planar and staggered structures with both bond lengths proposed for R(BB), 1.67 and 1.75 Å, we found HATT values differing little from 668 kcal/mol, considerably lower than the experimental 696.

The experimental value comes from a study by Gunn and Green[13] of the heat of reaction of B_2F_4 with Cl_2, these authors calculating a B–B bond energy of 72.4 kcal/mol. Combination of Gunn and Green's enthalpy of formation of B_2F_4 (−342.1 kcal/mol) with that of Margrave[10] for BF_2 (−130 kcal/mol) gives 82 kcal/mol for the bond dissociation process $B_2F_4 \rightarrow 2BF_2$. More recently Dibeler and Liston[11] have proposed a B–B dissociation energy of 103 kcal/mol. Our calculations indicated an initially surprising result that the rescaled E_{BB} in B_2F_4 is only 40–41 kcal/mol.

The cause of this unusual and erroneous prediction is that for our calibrating molecule, B_2, the ground-state CNDO configuration is $2\sigma_g^2 1\pi_u^3 2\sigma_u$ ($^3\Pi_g$), with a rough bond order of 2, as opposed to the experimental single bonded molecule of configuration $2\sigma_g^2 2\sigma_u^2 1\pi_u^2$ ($^3\Sigma_g^-$). Accordingly, we have considered two crude methods of estimating the B–B bond energy from our results. First, we ignore the computed E_{BB} and assume on the basis of agreement between calculated and experimental atomization energies for BF and BF_2 that the rescaled energy of the BF bonds in B_2F_4 is reliable (626 kcal/mol). The difference between this and the experimental HATX (696) reflects the BB bond energy, 70 kcal/mol. Secondly, since CNDO based energies for B_2 are describing a bond order of about 2, we half them before determining the energy equivalent. This doubles E_{BB} values in Tables II and III and increases the B–B bond energy to 82 kcal/mol and the predicted atomization energy to 708.4 kcal/mol (experimental 695.9). These corrective measures, although admittedly desperate, appear to support the lower values for the B–B bond energy in B_2F_4. Studies on inorganic chlorides, now in progress, may clarify this question.

References and Notes

(1) A. L. Companion, *Theor. Chim. Acta*, **25**, 268 (1972).
(2) A. L. Companion and Y. P. Hsia, *J. Mol. Struct.*, **14**, 117 (1972).
(3) J. A. Pople and D. L. Beveridge, "Approximate Molecular Orbital Theory," McGraw-Hill, New York, N. Y., 1970.
(4) P. Dobosh, "CNINDO: CNDO and INDO Molecular Orbital Program," Number 141, Quantum Chemistry Program Exchange, Indiana University, Bloomington, Ind.
(5) K. Wiberg, *J. Amer. Chem. Soc.*, **90**, 59 (1968).
(6) H. Fischer and H. Kollmar, *Theor. Chim. Acta*, **16**, 163 (1970).
(7) P. A. G. O'Hare and A. C. Wahl, *J. Chem. Phys.*, **53**, 2469 (1970).
(8) "JANAF Thermochemical Tables," 2nd ed, *Nat. Stand. Ref. Data Ser., Nat. Bur. Stand.*, **No. 37**, June (1971).
(9) P. A. G. O'Hare, Argonne National Laboratory Report No. ANL-7315, July 1968.
(10) J. L. Margrave, *J. Phys. Chem.*, **66**, 1209 (1962).
(11) V. H. Dibeler and S. K. Liston, *Inorg. Chem.*, **7**, 1742 (1968).
(12) J. R. Durig, J. W. Thompson, J. D. Witt, and J. D. Odom, *J. Chem. Phys.*, **58**, 5339 (1973).
(13) S. R. Gunn and L. G. Green, *J. Phys. Chem.*, **65**, 178 (1961).

A Conductance Study of 1-1 Electrolytes in Propylene Carbonate

Murray L. Jansen and Howard L. Yeager*

Department of Chemistry, The University of Calgary, Calgary, Alberta, Canada *(Received July 26, 1973*

Publication costs assisted by the National Research Council of Canada

Precise conductance measurements are reported for alkali metal and tetraalkylammonium halides and perchlorates in propylene carbonate. Analysis of the data by an extended form of the Fuoss-Onsager conductance theory indicates negligible ion pairing. Single ion conductivities were derived using the reference electrolyte $(i\text{-Am})_4\text{N}(i\text{-Am})_4\text{B}$. Ion mobilities are discussed in terms of the Boyd-Zwanzig equation and the solvent properties of propylene carbonate.

Introduction

Propylene carbonate (PC) is an interesting dipolar aprotic solvent in several respects. It has a wide liquid range (mp −49.2°; bp 241.7°), high dielectric constant (64.92 at 25°),[1] and is inert toward reducing materials such as lithium metal. PC appears to be a relatively unstructured liquid[1,2] as evidenced by a Trouton constant of 23 and a Kirkwood correlation factor of unity (g = 1.01 at 25°).[1]

Several studies of ionic solvation thermodynamics in this solvent have been reported.[3-7] The results indicate that PC has moderate Lewis base and weak Lewis acid properties, and it has served as a useful reference for comparison of ionic solvation parameters among solvents.[3,4,7]

Electrolytic conductance measurements are also important in order to characterize ionic solvation processes, but few studies have been reported in PC.[3a,8-11] Of these, only Mukherjee and coworkers[10,11] have studied a relatively wide variety of salts with high precision methods. However, lack of internal consistency among several salts suggests large systematic errors. For example, the Kohlrausch difference between the perchlorate and the chloride salts of lithium is +1.42, but the corresponding difference for the tetraethylammonium salts is −0.42. This represents possible errors of over 5% in reported limiting equivalent conductances.

We have, therefore, repeated some of this work and have measured the conductances of several additional alkali metal and tetraalkylammonium salts in PC. Single ion conductivities have been derived using the reference electrolyte tetraisoamylammonium tetraisoamylboride. The results are interpreted in terms of the cation and anion solvating ability of PC and comparison is made with results obtained in other dipolar aprotic solvents.

Experimental Section

Reagents. Propylene carbonate (Jefferson Chemical Co.) was stirred over molecular sieves (J. T. Baker Type 5A) for 48 hr and then distilled using a 1.5-m vacuum-jacketed column packed with nichrome helices (Podbielniak, Inc.). The column was operated at a reflux ratio of 10:1, with a stillhead temperature of 80° at 1-mm pressure. Only the middle 60% of the distillate was used. Water content of the purified product by Karl Fischer titration was $<4 \times 10^{-4}$ M. Gas chromatographic analysis was performed using a Porapak Q column with N_2 carrier gas and flame ionization detector. Detectable impurities were 1,2-propylene glycol, 10 ppm; allyl alcohol, <2 ppm; and propylene oxide, <1 ppm. The purified product had a specific conductivity of $<3 \times 10^{-8}$ ohm^{-1} cm^{-1}, a density of 1.1993 g cm^{-3}, and a viscosity of 2.513 cP.

Highly purified, fused lithium perchlorate (MCB Polaroquality, sealed under argon) was used without further purification. Sodium perchlorate (Fisher Certified) was recrystallized from a 1:5 water-acetone mixture and then precipitated in turn from ethyl acetate and acetone with dioxane. Potassium perchlorate (Fisher Certified) was recrystallized twice from water. Rubidium perchlorate (K & K Laboratories, Inc.) was recrystallized four times from a 1:1 methanol-water mixture. Cesium perchlorate (K & K Laboratories, Inc.) was recrystallized once from water and then twice from a 1:3 methanol-water mixture. These purified salts were powdered and dried under vacuum at 200° for 50 hr.

Tetramethylammonium, tetraethylammonium, and tetra-n-butylammonium perchlorates (G. F. Smith Chemical Co., Polarographic Grade) were powdered and dried under vacuum at 60° for 24 hr. Tetrapropylammonium perchlorate (Eastman) was recrystallized twice from acetone and dried under vacuum at 90° for 40 hr. Tetra-n-butylammonium bromide and iodide (G. F. Smith Chemical Co., Polarographic Grade) were used as received.

Potassium chloride (J. T. Baker, Ultrex) and sodium and potassium iodides (Research Organic/Inorganic Chemical Corp., 99.99%) were used as received. Potassium thiocyanate (Fisher Certified) was powdered and dried under vacuum at 60° for 15 hr.

Tetraisoamylammonium tetraisoamylboride was prepared by the method of Coetzee and Cunningham.[12] The salt was then precipitated six times from acetone with water and dried under vacuum at 50° for 12 hr. (*Anal.* Calcd for C, 80.88; H, 14.94; N, 2.36. Found: C, 80.76; H, 15.14; N, 2.27.) Tetraisoamylammonium iodide (Pfaltz and Bauer, Inc.) was recrystallized from a 1:8 acetone-water mixture and dried under vacuum at 60° for 12 hr. Analysis by silver nitrate titration: 100.0%. This material was also used in the preparation of $(i\text{-Am})_4\text{N}(i\text{-Am})_4\text{B}$.

Apparatus and Procedure. A 1-l. Kraus type conductance cell with lightly platinized electrodes was used.[13,14] A salt cup dispenser[15] was used to deliver weighed amounts of salt to the cell. Salt dissolution was hastened with a Teflon-coated magnetic stirring bar. With the exception of a few nonhygroscopic salts, all salt transfers were performed in a glovebox under N_2 atmosphere. A calibrated platinum resistance thermometer was used to

TABLE I: Conductance Parameters for 1-1 Electrolytes in PC at 25°

Salt	Λ_0	K_A	J_2	$\sigma\Lambda$
$LiClO_4$	27.34 ± 0.005	−1.5	130.6	0.003
	27.32 ± 0.003	−1.0	78.2	0.002
$NaClO_4$	27.89 ± 0.01	−1.1	99.5	0.006
	27.89 ± 0.002	−1.3	104.4	0.001
$KClO_4$	29.64 ± 0.002	0.6	97.0	0.001
	29.56 ± 0.003	0.5	98.1	0.002
	29.63 ± 0.008	0.7	73.9	0.005
$RbClO_4$	30.33 ± 0.004	0.9	169.7	0.002
	30.35 ± 0.004	1.4	88.5	0.003
$CsClO_4$	31.10 ± 0.006	2.7	−26.4	0.005
	31.10 ± 0.003	2.1	79.0	0.002
NaI	27.81 ± 0.004	−0.7	46.4	0.002
	27.80 ± 0.002	−0.4	1.4	0.002
KI	29.41 ± 0.005	−0.7	107.6	0.003
	29.56 ± 0.004	−0.1	10.1	0.003
KSCN	33.31 ± 0.001	3.1	53.6	0.001
	33.26 ± 0.01	3.2	26.8	0.008
Me_4NClO_4	32.60 ± 0.002	2.5	271.5	0.001
	32.61 ± 0.002	2.7	236.6	0.001
Et_4NClO_4	31.64 ± 0.03	1.2	519.0	0.02
	31.61 ± 0.01	1.0	437.0	0.006
Pr_4NClO_4	28.92 ± 0.002	1.8	271.8	0.001
	28.88 ± 0.008	1.6	319.8	0.004
Bu_4NClO_4	27.41 ± 0.003	2.2	228.6	0.001
	27.44 ± 0.002	2.3	223.1	0.001
Bu_4NBr	27.89 ± 0.007	2.6	210.2	0.004
	27.89 ± 0.002	2.4	241.2	0.001
Bu_4NI	27.32 ± 0.005	2.6	263.9	0.003
	27.33 ± 0.005	2.3	300.2	0.002
$(i\text{-}Am)_4NI$	26.52 ± 0.004	2.8	291.1	0.004
	26.52 ± 0.001	2.8	290.8	0.001
$(i\text{-}Am)_4N(i\text{-}Am)_4B$	16.33 ± 0.008	4.6	354.1	0.005
	16.36 ± 0.01	5.4	291.9	0.007

set the temperature of a 25-gal oil bath, which was maintained at 25.000 ± 0.002° during all experiments. Resistance measurements were made with a Leeds and Northrup conductance bridge in conjunction with a General Radio oscillator and tuned amplifier null detector.

A small residual frequency dependence of measured resistances was corrected by extrapolation of values measured at several frequencies to infinite frequency. The cell constant was determined frequently using potassium chloride solutions; results were analyzed by the averaged conductance equation of Lind, Zwolenik, and Fuoss.[16] The cell constant value changed by only 0.02% over a concentration range of $0.5\text{–}5 \times 10^{-3}$ M.

Molar concentrations were determined using solution densities calculated from the equation $d = d_0 + Am$, where m is the moles of salt per kilogram of solution. Density measurements were made on solutions remaining after conductance runs using a 30-ml capillary pycnometer similar to those described by Coetzee and Cunningham.[17]

Viscosity B coefficients in the Jones and Dole equation[18] were determined by measuring solution viscosities with a Cannon-Ubbelhode dilution viscometer. Solution manipulations were performed under an argon atmosphere. Efflux times were reproducible to ±0.1 sec.

Results

The measured equivalent conductances and corresponding electrolyte concentrations together with solution density and salt viscosity coefficients appear in the microfilm version of this volume of the journal.[19] Conductance data were analyzed by a modified form of the Fuoss-Onsager conductance theory[20] in which the term in $c^{3/2}$ is retained[21,22]

$$\Lambda = \Lambda_0 - S(c\gamma)^{1/2} + Ec\gamma \log c\gamma + (J_1 - B\Lambda_0)c\gamma - J_2(c\gamma)^{3/2} - K_A c\gamma\Lambda f_\pm^2 \quad (1)$$

where the ion pair association constant is given by

$$K_A = (1 - \gamma)/\gamma^2 c f_\pm^2 \quad (2)$$

In the calculation of J_1 and $f_\pm$, the ion size parameter was set equal to the sum of the ionic crystallographic radii for alkali metal salts, and to the sum of estimated ionic radii for the tetraalkylammonium salts.[23] A computer least-squares program was used to evaluate the adjustable parameters Λ_0, K_A, and J_2. These values are listed in Table I along with the standard deviations of fit, $\sigma\Lambda$. Results of duplicate runs are reported for each salt.

Small negative values of J_2 and K_A were obtained for some alkali metal salts. This is an indication of the difficulty in obtaining a separation between the J_2 and K_A terms and of approximations in the theory which these terms must absorb.[24]

Attempts to obtain transference numbers in PC by the autogenic moving boundary method were unsuccessful due to solvent decomposition. Approximate single ion conductivities were obtained by assuming that the cation and anion mobilities of tetraisoamylammonium tetraisoamylboride were equal;[17] these values are listed in Table II. It has been determined by precise transference number measurements that $(i\text{-}Am)_4N^+$ is 1.2% less mobile than $(i\text{-}Am)_4B^-$ in acetonitrile.[25] This appears to be the limit of accuracy of this approach for deriving single ion conductivities.

TABLE II: Single Ion Conductivities of Univalent Ions in PC at 25°

Ion	λ_0[a]	Ion	λ_0[a]
Li^+	8.89	Bu_4N^+	8.98
Na^+	9.45	$(i\text{-}Am)_4N^+$	8.17
K^+	11.17	$(i\text{-}Am)_4B^-$	8.17
Rb^+	11.90	ClO_4^-	18.44
Cs^+	12.66	I^-	18.35
Me_4N^+	14.16	Br^-	18.91
Et_4N^+	13.18	SCN^-	22.12
Pr_4N^+	10.46		

[a] Values based on reference electrolyte $(i\text{-}Am)_4N(i\text{-}Am)_4B$.

Discussion

Kohlraush differences calculated from average Λ_0 values of Table I agree within 0.05 conductance units in all cases. A comparison of our limiting equivalent conductances with those of Mukherjee and coworkers[10,11] shows large differences, from −1.25 for lithium perchlorate to +1.25 for potassium iodide. They report a solvent viscosity which is 1.3% lower than our value, which accounts in part for their generally higher Λ_0 values. In order to estimate the precision of these earlier data they were reanalyzed by eq 1 using our least-squares program. Standard deviations of fit were found to be larger than those reported in this work, as great as 0.5 cm^2 ohm^{-1} $equiv^{-1}$ in the case of lithium percholate. Differences between Λ_0 values obtained by their graphical methods and our

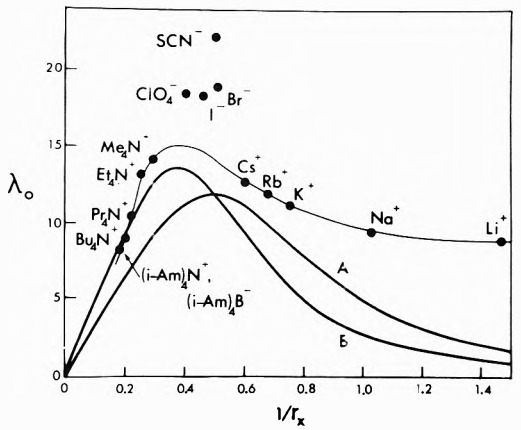

Figure 1. Single ion conductivities in PC *vs.* the reciprocal of estimated crystallographic radii: smooth curve drawn through cation points; (A), eq 3 assuming ion-solvent sticking; (B), eq 3 assuming ion-solvent slipping.

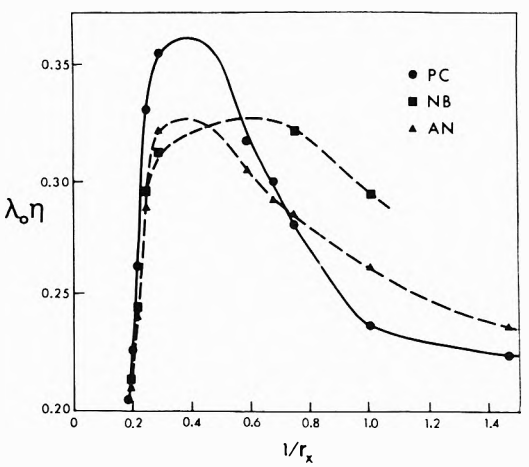

Figure 2. Single ion conductivity-viscosity products *vs.* the reciprocal of estimated crystallographic radii for tetraalkylammonium and alkali metal ions: PC, propylene carbonate; NB, nitrobenzene; AN, acetonitrile.

reanalysis are not sufficient to explain the discrepancies between the two sets of data. In view of the large standard deviations of fit and the lack of internal consistency in their results, we believe our values to be more reliable.

The calculated association constants in Table I show all salts to be essentially unassociated, with the possible exception of potassium thiocyanate. Presumably this salt indicates slight ion pairing due to the small size of the anion, for potassium iodide and perchlorate are unassociated. Potassium thiocyanate was found to be the most associated of these salts in acetonitrile as well.[26]

Following a suggestion by Justice, the data were reanalyzed by eq 1 after setting the ion size term in J_1 equal to the Bjerrum distance, q.[27] Small positive values of K_A resulted. Reanalysis of the data by a form of the Fuoss-Onsager theory which neglects the $c^{3/2}$ term[20,28] yielded slightly more negative K_A values than those listed in Table I. We conclude here that any ion pairing of these salts in PC must be at most very slight.

The single ion conductivities in Table II are plotted *vs.* the reciprocal of estimated crystallographic radii in Figure 1. As observed in other solvents, large cations show a normal size-mobility dependence, but alkali metal ions produce a reverse trend, with the lithium ion having the smallest mobility. Anions have much higher mobilities than cations relative to their crystallographic size, indicating relatively poor solvation by PC. A molecular orbital calculation of electron density in the PC molecule suggests this to be true.[29] Positive centers of charge are shown to be on the three ring carbons, and by steric considerations it is difficult to see how extensive anion-dipole interactions can take place. However, the three oxygen atoms all show significant negative charge and are accessible for cation interactions.

Boyd[30] and Zwanzig[31] have derived an equation which correctly predicts the occurrence of a maximum in the mobility-size dependence of ions by including the effects of a dielectric frictional force.

$$\lambda_i^0 = ze\mathfrak{F}/\left[A_V \pi r_i \eta + A_D \frac{(ze)^2}{r_i^3} \frac{(\epsilon_0 - \epsilon_\infty)\tau}{\epsilon_0(2\epsilon_0 + 1)}\right] \quad (3)$$

The equation contains two constants, A_V and A_D, whose values depend on whether it is assumed the solvent sticks to or slips by the ion at its surface. This equation has been plotted in Figure 1 for both cases. Although reasonable agreement is found for larger cations, discrepancies become large as the cation size decreases. Similar differences were seen in a variety of protic and aprotic solvents.[32] It was suggested that neglect of a dielectric saturation effect in the vicinity of the ion was a probable cause for at least part of these differences,[32] but a recent evaluation of this effect shows that this is not the case.[33] Another factor may be strong solvation of these smaller ions, which would produce larger kinetic entities and less dielectric friction than predicted by eq 3.[32,33]

The single ion conductivity-viscosity products in PC exhibit interesting differences from those of other representative dipolar aprotic solvents. In Figure 2 Walden products of tetraalkylammonium and alkali metal ions in acetonitrile[25] and nitrobenzene[17] have been plotted with those of PC. The higher Walden products of tetraalkylammonium ions in PC may be due to its higher dielectric constant, as predicted by eq 3. However, the PC curve decreases sharply with decreasing cation size, crossing the other Walden product plots. This cannot be explained by the parameters in eq 3. Kay and coworkers[15] observed a similar crossover effect of Walden products in ethanol and methanol when compared to those of acetonitrile. The greater Walden products of large cations in the alcohols was attributed to their smaller dipole moments, while the crossover effect was explained in terms of the greater Lewis basicities of the alcohols.

This approach does not explain the crossover seen in Figure 2, however. PC and acetonitrile have approximately the same Lewis base character, as estimated by Gutmann's donor number concept.[34] In addition, PC has a larger dipole moment than acetonitrile, 4.94 *vs.* 3.37 D.[35] Nitrobenzene does have a large dipole moment (4.0)[35] but poor donor ability.[34] Therefore, both donor properties and dipole moments must be considered to explain this crossover effect. In addition, the large size of the PC molecule may play a part in producing small Walden products for the smaller metal ions.

It appears that these solvent parameters in addition to those used in eq 3 may play a significant role in explaining ion mobilities in solvents, in that they could be factors in a model which considers the dynamics of solvation.

Acknowledgments. The authors wish to thank Professor J.-C. Justice for analyzing initial conductance runs with

his computer program. Financial support by the National Research Council of Canada and the University of Calgary is gratefully acknowledged.

Supplementary Material Available. The measured equivalent conductances and corresponding electrolyte concentrations together with solution density and salt viscosity coefficients will appear following these pages in the microfilm edition of this volume of the journal. Photocopies of the supplementary material from this paper only or microfiche (105 × 148 mm, 20× reduction, negatives) containing all of the supplementary material for the papers in this issue may be obtained from the Journals Department, American Chemical Society, 1155 16th St., N.W., Washington, D. C. 20036. Remit check or money order for $3.00 for photocopy or $2.00 for microfiche, referring to code number JPC-73-3089.

References and Notes

(1) R. Payne and I. E. Theodorou, *J. Phys. Chem.*, **76**, 2892 (1972).
(2) L. Simeral and R. L. Amey, *J. Phys. Chem.*, **74**, 1443 (1970).
(3) (a) Y. C. Wu and H. L. Friedman, *J. Phys. Chem.*, **70**, 501 (1966); (b) *ibid.*, **70**, 2020 (1966); (c) H. L. Friedman, *ibid.*, **71**, 1723 (1967); (d) C. V. Krishnan and H. L. Friedman, *ibid.*, **73**, 3934 (1969).
(4) G. Choux and R. L. Benoit, *J. Amer. Chem. Soc.*, **91**, 6221 (1969).
(5) M. Salomon, *J. Phys. Chem.*, **73**, 3229 (1969).
(6) M. Salomon, *J. Phys. Chem.*, **74**, 2519 (1970).
(7) B. G. Cox and A. J. Parker, *J. Amer. Chem. Soc.*, **95**, 402 (1973).
(8) R. M. Fuoss and E. Hirsch, *J. Amer. Chem. Soc.*, **82**, 1013 (1960).
(9) J. Courtot-Coupez and M. L'Her, *C. R. Acad. Sci., Ser. C*, **271**, 357 (1970).
(10) L. M. Mukherjee and D. P. Boden, *J. Phys. Chem.*, **73**, 3965 (1969).
(11) L. M. Mukherjee, D. P. Boden, and R. Lindauer, *J. Phys. Chem.*, **74**, 1942 (1970).
(12) J. F. Coetzee and G. P. Cunningham, *J. Amer. Chem. Soc.*, **86**, 3403 (1964).
(13) H. M. Daggett, E. J. Bair, and C. A. Kraus, *J. Amer. Chem. Soc.*, **73**, 799 (1951).
(14) B. Kratochvil and H. L. Yeager in "Topics in Current Chemistry," Vol. 27, Springer-Verlag, New York, N. Y., 1972.
(15) R. L. Kay, B. J. Hales, and G. P. Cunningham, *J. Phys. Chem.*, **71**, 3925 (1967).
(16) J. E. Lind, J. J. Zwolenik, and R. M. Fuoss *J. Amer. Chem. Soc.*, **81**, 1552 (1959).
(17) J. F. Coetzee amd G. P. Cunningham, *J. Amer. Chem. Soc.*, **87**, 2529 (1965).
(18) G. Jones and M. Dole, *J. Amer. Chem. Soc.*, **51**, 2950 (1929).
(19) See paragraph at end of paper regarding supplementary material.
(20) R. M. Fuoss and F. Accascina, "Electrolytic Conductance," Interscience, New York, N. Y., 1959.
(21) R. M. Fuoss and K.-L. Hsia, *Proc. Nat. Acad. Sci. U. S.*, **59**, 1550 (1967).
(22) R. Fernandez-Prini, *Trans. Faraday Soc.*, **65**, 3311 (1969).
(23) R. A. Robinson and R. H. Stokes, "Electrolyte Solutions," 2nd ed, Butterworths, London, 1968, p 124.
(24) R. Fernandez-Prini, *Trans. Faraday Soc.*, **64**, 2146 (1968).
(25) C. H. Springer, J. F. Coetzee, and R. L. Kay, *J. Phys. Chem.*, **73**, 471 (1969).
(26) H. L. Yeager and B. Kratochvil, *J. Phys. Chem.*, **74**, 963 (1970).
(27) J. C. Justice, *Electrochim. Acta*, **16**, 701 (1971).
(28) R. L. Kay, *J. Amer. Chem. Soc.*, **82**, 2099 (1960).
(29) H. L. Yeager, J. D. Fedyk, and R. J. Parker, *J. Phys. Chem.*, **77**, 2407 (1973).
(30) (a) R. H. Boyd, *J. Chem. Phys.*, **35**, 1281 (1961); (b) *ibid.*, **39**, 2376 (1963).
(31) (a) R. Zwanzig, *J. Chem. Phys.*, **38**, 1603 (1963); (b) *ibid.*, **52**, 3625 (1970).
(32) R. Fernandez-Prini and G. Atkinson, *J. Phys. Chem.*, **75**, 239 (1971).
(33) R. Fernandez-Prini, *J. Phys. Chem.*, **77**, 1314 (1973).
(34) V. Gutmann, *Rec. Chem. Progr.*, **30**, 169 (1969).
(35) A. L. McClellan, "Tables of Experimental Dipole Moments," W. H. Freeman Co., San Francisco, Calif., 1963.

Anomalous Properties of Supercooled Water. Heat Capacity, Expansivity, and Proton Magnetic Resonance Chemical Shift from 0 to −38°

C. A. Angell,* J. Shuppert, and J. C. Tucker

Department of Chemistry, Purdue University, West Lafayette, Indiana 47907 *(Received March 21, 1973)*

Publication costs assisted by the Department of the Interior, Office of Water Resources Research

Expectations of a rapidly increasing heat capacity for water at low temperatures are confirmed by differential scanning calorimetry. C_p is found to rise very rapidly from 18 to 29 cal mol^{-1} deg^{-1} between −10° and the homogeneous nucleation temperature, −40°. Proton magnetic resonance chemical shift measurements suggest this behavior is associated with a cooperative acceleration in hydrogen bond strength or formation rate at low temperatures. It is shown that in light of these results the existence of vitreous waters which soften and crystallize near 150 K is paradoxical. To resolve the paradox the existence below the homogeneous nucleation temperature of a λ-type transition similar to that encountered in liquid sulfur is postulated. Its origin is tentatively accounted for in terms of the cooperative bond lattice model. It is apparent that the positive volume change associated with hydrogen bond formation plays a dominant role in determining the observed constant pressure behavior on cooling, the positive volume change itself being a consequence of the geometry of formation of the four coordinate random network.

In a recent discussion of thermodynamic and transport properties of water based on a simple statistical treatment of the defect hydrogen bond quasi-lattice ("bond lattice model"),[1] it was concluded that a knowledge of properties of water well below the normal melting point would prove of great importance in testing theoretical models of this un-

usual liquid. Unfortunately, even such significant thermodynamic properties of water as the heat capacity have never been reported for temperatures below −10°.

It is well known that the smaller the sample of liquid chosen for study, the smaller is the chance that it will contain a "mote" or foreign particle on which crystallization can commence at small undercooling. Thus water samples in fine capillaries (diameter ~10 μ) commonly do not crystallize before −35°, and have been used to study density[2,3] and dilute solution conductivity[2] by Schufle[2] and Zheleznyi.[3] Subdivision by droplet formation achieves the same ends, and very useful emulsification techniques have been developed by Rasmussen and MacKenzie[4,5] which allow water as a fairly stable 1–5 μ diameter droplet dispersion, to be supercooled almost to its homogeneous nucleation temperature, T_H (−40 to −41°),[6] in volume fractions as large as 50%. It is not expected that subdivision will have a major effect on the properties of water, since one calculates that only 0.6% of the molecules in a 1-μ droplet are present in a surface layer taken to be 10 Å (~4 molecules) thick. On the other hand, minor effects of small sample size seem to have been present in some capillary experiments.[2b]

With interests in confirming the expectation[1] of very large heat capacities at low temperatures, and in exploring the possibility that such behavior could be linked with a bond cooperativity-based acceleration in the hydrogen bond reformation process, we have used the above supercooling techniques to measure both the heat capacity and the proton magnetic resonance chemical shift. The results amply confirm the expectation of uniquely anomalous behavior in this low-temperature region.

Experimental Section

Heat capacities have been measured on water emulsified in heptane according to Rasmussen's procedure,[4,5] using differential scanning calorimetry to minimize the time of experimentation. This is important at the low-temperature extreme where behavior is most interesting but homogeneous nucleation of ice is most probable. With several emulsions we were able to reach −39°. Data were obtained using a 10 K min^{-1} scan speed on both the Perkin-Elmer DSC-1B calorimeter and the much improved DSC-2 instrument. One set of data on the latter instrument was obtained on an upscan to eliminate the possibility that the results from downscans were influenced by small but exponentially increasing contributions from droplet crystallization with increasing supercooling. The uniqueness of the behavior of water and D_2O was further confirmed by comparisons with behavior of emulsions of concentrated aqueous salt solutions and of the water-like solvent hydrazine, which showed no anomalies as T_H was approached.

The difference in heat capacity of ice and water, ΔC_p, was calculated at 5-deg temperature intervals from comparison of scans in which the water fraction was present in supercooled liquid and frozen conditions, respectively. The known heat capacity change of water at 0° was set equal to the DSC amplitude difference between the supercooled and frozen water emulsions. Measurements were also successfully performed on a clean bulk water sample down to −20° using the DSC-1B. To check on data reliability, the heat of crystallization at −38° was calculated, ignoring temperature rise, from

$$\Delta H_T = \Delta H_{273} - \int_T^{273} \Delta C_p dT$$

and found equal to the experimental value of 1005 cal mol^{-1} to within ±2%. For this measurement, the mass of water in the emulsified sample was determined from the heat absorbed on fusion of a completely crystallized emulsion at 0°.

Proton chemical shifts were measured using a standard Varian A-60 high-resolution spectrometer, introducing the sample in a standard 5-mm nmr tube either as an emulsion or as a bundle of 6 cm long Pyrex glass capillaries pulled from standard 1-mm i.d. 6-mm o.d. Pyrex capillary tubing. The internal diameters of the capillaries were varied in order to ascertain the magnitude of the effects of capillary size on the chemical shift and its temperature dependence.

Shifts were measured relative to various external references the choice of which depended on the amounts of water and of reference material which could be placed within the nmr tube. A 7-atm pressure methane reference, in a container capillary of the dimensions used by Hindman,[7] was used to demonstrate our ability to reproduce the latter author's bulk water measurements. For the water in capillary measurements the size of the reference capillary had to be reduced or sufficient water to give an acceptable signal could not be introduced. The amount of methane present then proved inadequate unless the pressure was increased. An estimated 37 atm of pressure was found satisfactory. The 37-atm reference also led to better signal-to-noise ratios in the case of the emulsion samples.

It is appropriate to note in this section that bulk water shifts referenced to methane at 7 atm agreed with those of Hindman to ±0.02 ppm. Differences between 37- and 7-atm references were assessed by comparison of bulk water shifts with respect to each, and all results were corrected to the 7-atm reference before any corrections for solution susceptibility effects were attempted.

Results

Results for our various heat capacity measurements and chemical shift determinations are tabulated at 5-K intervals in Table I. Data for water are plotted together with literature data above 273 K in Figure 1a. The difference between the heat capacity of ice and that of water, ΔC_p, which is the experimentally determined quantity, is plotted in Figure 1b. We include in Figure 1b some data currently being reported by Rasmussen and MacKenzie,[5] obtained by conventional drift calorimetry on emulsified water. Agreement with Rasmussen and MacKenzie's measurements is fairly good but the uncertainty in their data, particularly at their lowest temperature of −34°, is somewhat in excess of ours. It is important to note that our emulsion data superimpose within experimental error on the bulk water data which extend to −20°. This shows that the state of subdivision of the water does not strongly affect the measurement; hence it is very improbable that the exponential increase in ΔC_p with decreasing temperature is an artifact of the experiment. Certainly this large increase is not observed in the behavior of emulsions of NaCl solutions when the NaCl concentration is sufficient (>7 m) to break up the water structure.

The findings are in any case very compatible with the equally dramatic increase in negative expansivity assessed from Zheleznyi's density measurements on water in a 10-μ capillary.[3] For comparison, the latter data and the current emulsion data of Rasmussen and MacKenzie,[5] together with bulk water data calculated to −20° by Kell[8] using a curve-fitting function obtained from measurements above 0°K, are displayed in Figure 1c.

TABLE I: Heat Capacities of H_2O and D_2O

		H_2O					D_2O
		C_p (H_2O), cal mol^{-1} deg^{-1}				C_V, cal mol^{-1} deg^{-1}, (H_2O)	C_p, cal mol^{-1} deg^{-1}, (D_2O)
T, °C	T K	Av DSC-1B	DSC-2	Av	Bulk	Av	Av DSC-2
4	277					18.1	20.3
0	373	18.3	18.3	18.3	18.4		
−3	270	18.2	18.0	18.1	18.3	18.0	20.1
−8	265	18.1	18.0	18.0	18.2	17.9	20.5
−13	260	18.1	18.2	18.1	19.0	17.9	21.2
−18	255	18.3	19.0	18.6	18.9	18.0	22.0
−23	250	18.8	20.1	19.5		17.9	24.2
−28	245	19.3	22.5	20.9		17.8	26.3
−33	240	22.1	25.1	23.6		17.7	30.9
−38	235	~27	28.9	28.0		17.8	

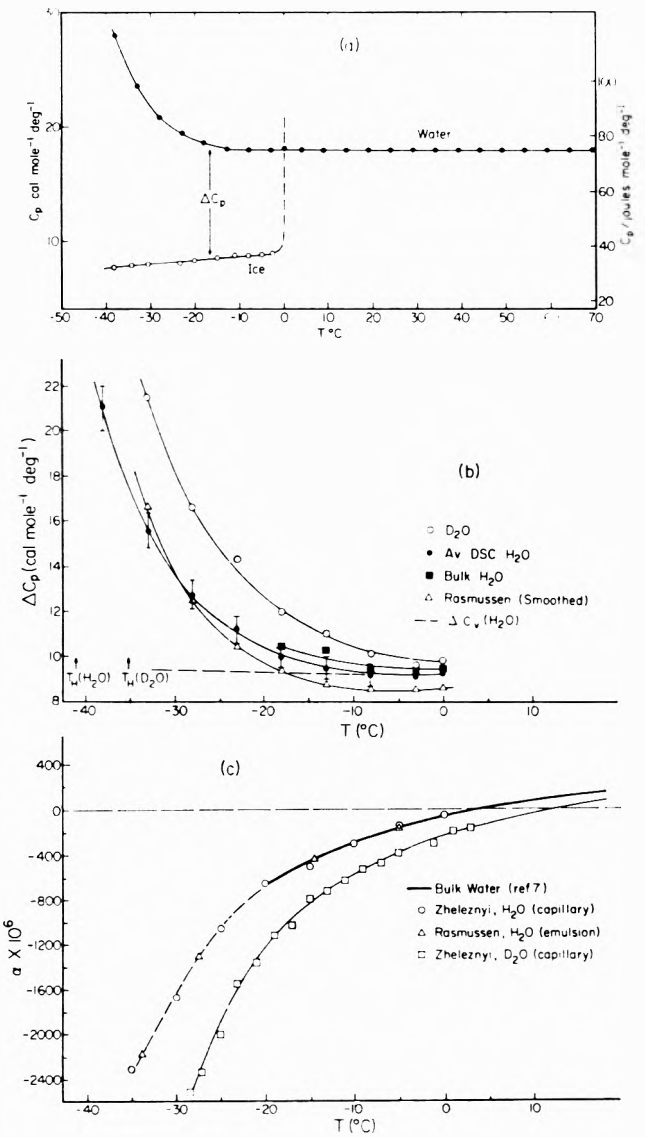

Figure 1. (a) Heat capacity of H_2O between 70 and −38°. (b) Difference in heat capacity between supercooled water and ice and supercooled D_2O and D_2O ice, as a function of temperature. (c) Total expansion coefficients of water and D_2O between 10 and −35°.

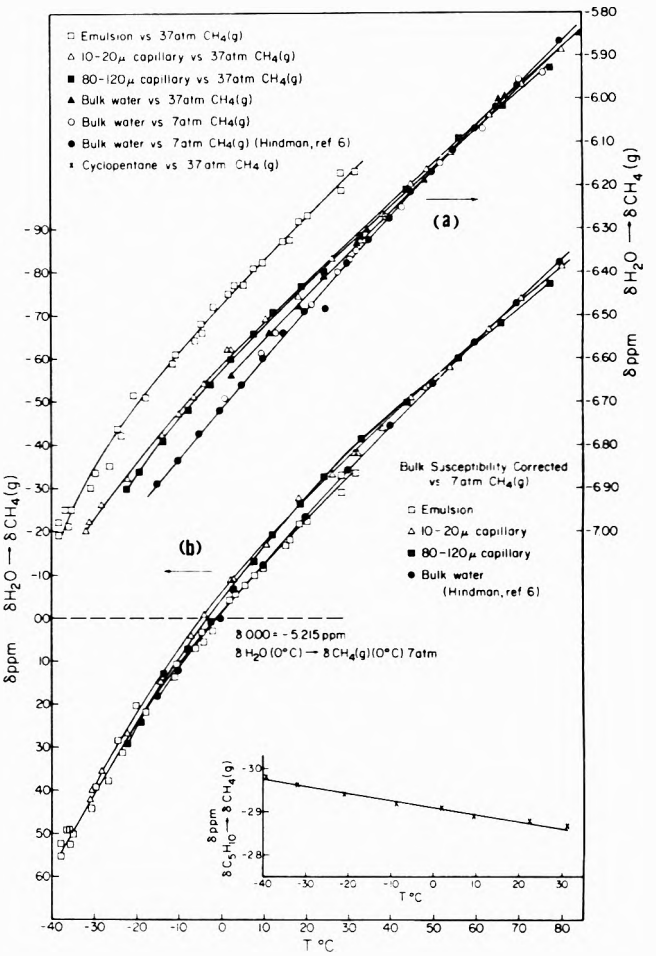

Figure 2. (a) Uncorrected proton chemical shifts for bulk water, water in fine capillaries, and in emulsion form, in the temperature range −38 to 80° relative to the reference proton resonances indicated in legend (right-hand ordinate scale). (b) Corrected shift values all referred to the resonance frequency for bulk water at 0° (left-hand ordinate scale). Inset: shift of methane reference against pentane over temperature range of the present measurements.

In Figure 2a the pmr chemical shifts, δ, are presented as raw data referenced as indicated in the legend. Because the susceptibility corrections for capillary and emulsion experiments are different, the different data sets do not superimpose.

In Figure 2b we show the data after susceptibility corrections have been introduced, all data being reduced first to shifts relative to methane at 7 atm and then finally plotted as shifts relative to that of bulk water at 0°. The susceptibility of the emulsion was taken to be a volume

fraction weighted average of heptane and water. Since capillary data and bulk water data coincide at high temperatures, it was assumed that the bulk water susceptibility correction was applicable to both. The susceptibility correction for water was made using an extrapolation of Auer's susceptibility data[9] and Zheleznyi's density data.[3]

Susceptibility corrections are all a little uncertain, especially at low temperatures, because the susceptibility of water is sensitive to the extent of hydrogen bonding which is evidently changing particularly rapidly at low temperatures. It is clear, however, that the susceptibility corrections must render even more pronounced the curvature in the δ *vs.* T plot already present in the raw data. Since this curvature is of prime interest we demonstrate, in Figure 2b inset, that the curvature cannot be associated with the high-pressure methane reference by showing that $\delta(CH_4, 37 \text{ atm}) - \delta(\text{cyclopentane})$ varies quite linearly with temperature.

We find Figure 2b, which summarizes data gathered in many individual runs over the temperature range, quite pleasing. The emulsion data in particular are found in very good accord with the data on bulk water from +40° (at which the emulsion breaks down) to −15°, the lowest temperature accessible with bulk samples.[7] There appear to be some real differences between results for bulk water and for water in capillaries, though the departures from the bulk water plot are similar for capillaries differing by about an order of magnitude in internal diameter. The discrepancies may therefore originate in the corrections rather than in the actual water structure. Because the emulsion data, which extend to lower temperatures, proved quite satisfactory we chose not to pursue the capillary problem.

The accelerating nonlinear downfield chemical shift temperature dependence is common to both measurement sets and is therefore unambiguously established by these measurements. It is notable that it occurs in the same temperature region in which the great increases in heat capacity and (negative) expansivity magnitudes occur.[9a]

Discussion

First it must be noted that there is probably nothing about the remarkable behavior of C_p seen in Figure 1a which cannot be "explained" by the equally remarkable behavior of α shown in Figure 1c. If the expansion with decreasing temperature were forcibly prevented, allowing pressure to increase, then the heat capacity (now C_v) would evidently remain approximately constant at 18.0 cal/mol. This can be shown using the familiar relation

$$C_v = C_p - TV\frac{\alpha^2}{\beta} \tag{1}$$

where β is the isothermal compressibility, tabulated to −20° by Kell.[8] Calculated values of C_v are given in Table I and include values obtained using a further but unreliable extrapolation of β to −40°.

Restriction of volume to some constant value, however, only serves to prevent, or at least to restrict, just that factor which makes water so interesting, *viz.* the increasing connectedness at lower temperatures of the hydrogen bond network. Furthermore, the entropy problem for supercooling water[10,11] which with the new data now becomes much more urgent, can only be posed for a constant-pressure system. Thus, we will restrict our attention to constant-pressure behavior and, in later consideration of models, will treat the work done against internal pressure during any volume-changing excitation as an integral part of the energy of that excitation. It should be noted, however, that in a constant volume experiment the factors responsible for the constant-pressure heat capacity anomaly will give rise to a pressure-temperature anomaly. Such an anomaly should be found, for instance, in an extension to lower temperatures of the interesting molecular dynamics calculations of Rahman and Stillinger.[12] Its presence or otherwise should provide an important test of the adequacy of the Ben-Naim–Stillinger potential[13] to represent water–water interactions. Although such calculations become more time consuming (and ultimately impractical) at lower temperatures where structural equilibration times are longer, they do have the great advantage that the "experiment" will not be terminated by an unwanted crystallization.

Considering further the constant pressure behavior we ask first the significant question, "What is in store for liquid water at lower temperatures if we extract its thermal energy at a rate sufficiently high that nuclei of ice are unable to form and grow?". The practical possibility of achieving such conditions depends on the molecular mobility at the homogeneous nucleation temperature which, in water, has evidently become quite small. These conditions are reached quite commonly in the quenching of viscous liquids and the result is that glassy solids are produced at temperatures not too far below T_H.[14] Since vitreous or at least X-ray amorphous water can be obtained by vapor deposition procedures[15] and by splat-quenching of liquid water,[16] we are led to ask whether the glass formation event can be predicted from now-available data on water, and if so, at what temperature it would occur. Arguing both from mass transport data and from our own thermodynamic data we shall show that the answers are at first sight paradoxical.

Mass transport data on supercooled water are now available both from viscosity (to −25°),[17] self-diffusion (to −31°),[18] and proton spin relaxation studies (to −16°)[19] studies. All processes show strongly non-Arrhenius temperature dependences (which are also apparent in data obtained above 0°). While the departures from Arrhenius behavior are themselves not of special interest (being common to most classes of liquids in this viscosity range), the quantitative aspects of the observed departures are, since they normally provide a means of estimating the temperature at which the viscosity would rise (or the diffusivity fall) to values characteristic of the glassy state. For most moderately viscous liquids, departures from Arrhenius behavior are well accounted for by a modified Arrhenius equation, (the so-called VTF equation) for the transport property W

$$W(T) = A_w \exp[-B_w/(T - T_0)] \tag{2}$$

where A_w, B_w, and T_0 are constants. T_0, according to various authors[20-22] sets the theoretical low-temperature limit on the possibility of particle diffusion or change of liquid structure, and usually falls 20–30 K below the temperature T_g at which the glassy state is reached on cooling.[23]

We have analyzed the water transport data using eq 2 and, significantly, find the fit rather poor. In Table II we show the nature of the deviations by giving the least-squares best fit value of the key parameter T_0, according to the temperature range of data fitted, for viscous flow (η),[17] self-diffusion (D/T),[18] and dielectric relaxation (τ_D), and spin-lattice relaxation (T_1)[19] processes.

TABLE II

T range, °K	$T_0(\eta)$, °K	$T_0(D/T)$, °K	$T_0(\tau_D)$, °K	$T_0(\tau_S)$, °K
0 to 70	143[a]	145[b]	145[c]	138
0 to −24	179	161		165[d]
−19 to −31	...	217		

[a] Data from L. Korson, W. Drost-Hansen, and F. J. Millero, *J. Phys. Chem.*, **73**, 34 (1969). [b] Data cover temperature range 1–45°. [c] Data from C. H. Collie, J. B. Hasted, and D. M. Riston, *Proc. Roy. Soc., Ser. A*, **60**, 145 (1948). [d] Data cover temperature range 0 to −16° (ref 19).

The progressive increase in T_0 of eq 2 with decreasing mean temperature of data fitted, Table II, shows that the rate of decrease of the water molecule mobility at low temperatures is even more rapid than predicted by the VTF equation. The parameters imply that the vitreous state would be reached[23] at or above 217°K which is not far below the homogeneous nucleation temperature of −41°. This behavior proves to be consistent with the rate at which, according to our thermodynamic data, the cooling liquid is losing entropy over this same temperature range, and indeed would be predicted by the Adam–Gibbs interpretation of eq 2.[19]

We show the consistency using Figure 3a where the total heat capacities of supercooled water and ice are plotted against log T so that the area under the heat capacity curve for a given phase corresponds to an entropy generated in (or lost from) that phase over any chosen temperature interval. Permissible extensions to lower temperature of the water heat capacity are governed by the third-law requirement, discussed in more detail elsewhere,[10] that the area between the supercooled liquid and crystalline solid C_p between 273 and 0°K amount to no more than that representing the entropy of fusion, ΔS_F (since the total entropy of a disordered phase at 0°K can never underlie that of the stable crystal).

From Figure 3a we find that if the heat capacity of water supercooled below −38°[24] continues to increase at the rate observed between −30 and −38° then all the excess entropy gained on fusion (*i.e.*, ΔS_F, shown as an area in Figure 3a) would be lost by 205–210 K (~ −65°). This is shown more clearly by Figure 3b in which the calculated entropy difference between water and ice, which is ΔS_F at 273°K, is plotted as a function of decreasing temperature. The difference tends to zero as $T \to -65°$. At ~ −65°, then, assuming the residual entropy of ice due to proton disorder would also be present in glassy water, a precipitous decrease in the water heat capacity to that of ice would have to occur to avoid thermodynamic embarassment. The state of the substance at this temperature could be described as an "ideal glass"[10,25] in which structural change, hence viscous flow, is proscribed.

This result, although consistent with the observed transport behavior, is paradoxical because experimentally it is found that vitreous water passes through the glass transition (*i.e.*, exhibits a heat capacity increase[15b,c] and a relaxation time of the order of seconds which permits crystallization[15,16]) at a temperature of about −130°.

The observations are not reconciled by supposing, unrealistically, that at −40° C_p reaches its maximum value and remains constant thereafter until the entropy of fusion is exhausted at −79° (curve 2, Figure 3a).

In order to resolve the paradox it is necessary to suppose that not far below −40° supercooling water passes through a λ-type heat capacity anomaly not unlike that due to a ring-chain equilibrium exhibited by liquid sulfur at 159°.[26,27] This alternative was illustrated by curve 3 of Figure 3a. A qualitative theory for such behavior based on the cooperative bond lattice model is given below. We will consider in a later paper the possible appropriateness of a branched-chain $\rightleftharpoons$ connected-ring equilibrium treatment suggested by Gibbs' polymer approach to the water problem,[28] and by the empirical similarities of liquid sulfur and supercooled water properties in their anomalous temperature ranges.

Because viscous liquid transport property temperature dependences generally follow changes in configurational entropy or enthalpy contents,[22] the λ transition would presumably be accompanied by a sharp drop in viscosity and diffusivity temperature dependences which would postpone the temperature at which the glass transition occurs[20] to the experimental value.

It is, of course, possible that the paradox prompting the above discussion is only an illusion. Uhlmann's splat-quenched material could conceivably have been microcrystalline rather than glassy, and the vapor-deposited vitreous form of water could have a quite different structure from that toward which supercooling water tends, in which case its glass transition temperature would be irrelevant. However, we and others[29] believe that this is not the case. Our position is supported by the finding that the vitreous water density, 0.93 g cm^{-3} at 84°K,[30] which is close to the density of ice (0.94 g cm^{-3}), is the density which supercooled water would reach at ~−60° according to Zheleznyi's extrapolation[3] of his data in the negative expansion range. Curve 1 of Figure 3a shows that an entropy extrapolation based on data in the anomalous expansion range would also lead one to conclude that the terminal, fully bonded glass state should be reached by ~ −60°.

It is to be noted in this connection that the vitreous form of SiO_2, which is also produced from a supercooled liquid of negative expansion coefficient[31] (though α is small), has a density which is only 5% less than that of the crystalline form, crystobalite. The detailed relationship between the ice and SiO_2 polymorphic structures is well known. Metastable cubic ice, which is formed when vitreous water crystallizes, has the crystobalite structure while the more stable hexagonal form of ice has the tridymite structure. In view of these analogies, and of the fact that the vitreous silicas formed by vapor deposition and liquid cooling procedures are indistinguishable, it would be surprising indeed if the vitreous form of water, however produced, were not also of network character. The extent to which such networks should be regarded as random is, however, currently under vigorous review.[32]

We note that an alternative explanation of the heat capacity anomaly is provided by Rasmussen and Mackenzie[5] in terms of heterophase fluctuation theory. This approach interprets the increased specific heat in terms of a progressive release of the enthalpy of fusion by increasing concentration and sizes of embryo ice crystals. The paradox we have discussed is avoided in this approach by the requirement that either the nuclei grow to macroscopic sizes under nonequilibrium conditions (first-order transition) or that the liquid ultimately becomes 100% embryo ice at ~−63°. This, like the ideal glass, would evidently be a state of zero excess entropy but considerable excess enthalpy presumably resident in the embryo surface

layers. The nature and significance of the vitreous waters and their ability to crystallize at −130° are not interpreted in their treatment.

Cooperative Bonding? It is of interest to consider whether it is reasonable or not to view the expansivity and heat capacity anomalies as manifestations of the often-mentioned cooperative character of the hydrogen bond which, as in other order–disorder processes, only becomes manifest in the properties when a considerable degree of (short-range) order has already been developed.

For this purpose the proton chemical shift data presented in Figure 2b are informative. It has been shown by Hindman[7] that δ, which measures the magnetic shielding effectiveness of the average proton electronic environment, can serve as an index of the strength, extent, or linearity of hydrogen bonding in water. Figure 2b shows that this bonding index, which varies almost linearly with temperature above 25°, becomes markedly curvilinear in the lower temperature region. Thus it seems probable from Figure 2b that the thermodynamic and mass transport anomalies can be associated with bonding anomalies. Evidently, either the number of bonds formed per degree of temperature decrease, or the strength or linearity of each bond formed, increases below 25° and increases rapidly between −20 and −40°.[33] Like the heat capacity anomaly this bond-forming anomaly would probably vanish in a constant volume experiment.

We find here some support for the "bond lattice" approach[1] to the description of water and its properties.[34] A one-dimensional representation of the "bond lattice" with nearest neighbor interactions included was compared with the Ising model for cooperative processes in a previous publication.[1] Formally, the "bond lattice" model is equivalent to the Ising model for a system of spins in a large and constant external magnetic field; the work of inverting an atomic spin against the external field is the equivalent of the bond-breaking energy, while the spin–spin interaction of the Ising model corresponds to the bond–bond interaction of the bond lattice model.

One important point of distinction is that in the bond lattice a large volume change is intrinsic to the elementary excitation. In this case the problem under consideration is changed or at least complicated, if one compares model predictions with the experimental constant volume properties of the system as is usually considered appropriate. At constant volume the excitations can only occur by "borrowing" volume from the lattice, in effect by imposing an elastic tension or compression on it (depending on the sign of the volume change on excitation). In fact, under true constant *configurational* volume conditions the excitations would be completely repressed. This effect is seen in the great reduction under constant volume conditions of the magnitude of the λ-type heat capacity anomaly in well-studied cases such as NH_4Cl.[35] Such constant volume quelching of the anomaly will be more effective the larger the volume of excitation; hence the effective disappearance of the anomaly in the case of water under constant volume conditions (Figure 1b) is not surprising. We feel that to remain in contact with the problem of interest in such cases, one must focus attention on the constant-pressure heat capacity of the system at zero external pressure. This is probably particularly true in the case of water where the presence of the cooperative effect may depend on, if not originate in, the geometrical aspects of progressive buildup of the expanded tetrahedral network with decreasing temperature.

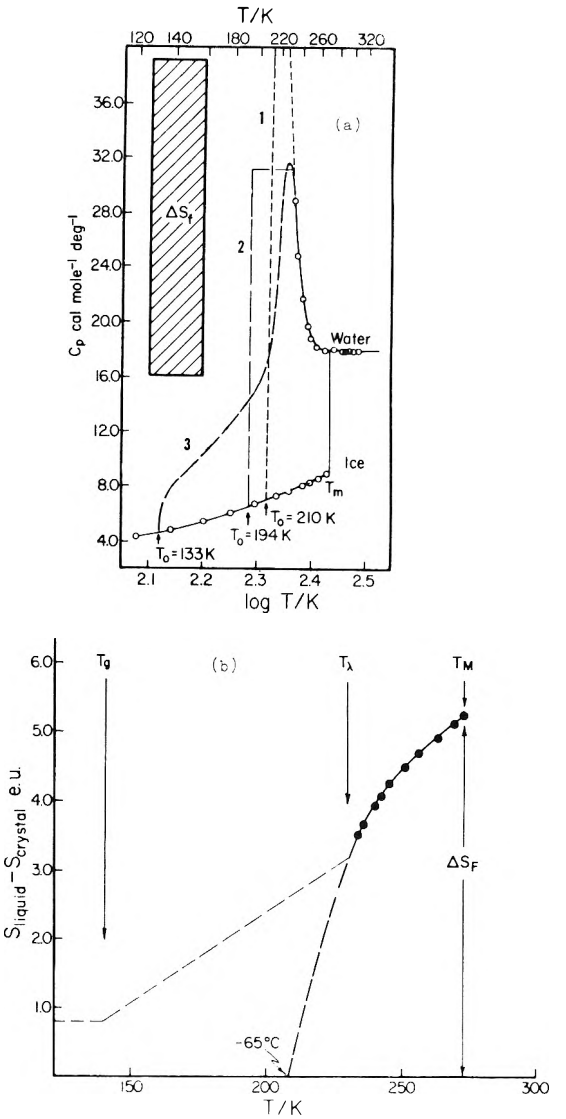

Figure 3. (a) Heat capacities of water and ice as a function of log T, showing relation between entropy of fusion (5.213 cal mol^{-1} deg^{-1}) and thermodynamically admissable extensions to lower temperature of liquid water heat capacity. (b) Difference in total entropies of water and ice as a function of temperature below the equilibrium melting point.

The case of disordering processes accompanied by large volume changes has been treated in a rather general way by the "Compressible Ising Model" of Garland and Renard,[36] in which the changes in volume are related directly to the changes in Ising configurational energy. This model, which has successfully described the constant pressure behavior of NH_4Cl in its anomalous region, predicts instability very close to T_c but otherwise leaves the form of the heat capacity anomaly (though of course not its magnitude) intact.

The extreme cases for the constant-volume heat capacity–temperature relation for the three-dimensional Ising model are known, and are illustrated in Figure 4. Curve 1, which is a Shottky-type heat capacity, is obtained when the external field opposing spin inversion is very large compared with the spin–spin interaction term. In this case, there is no cooperative phenomenon. It corresponds to the noncooperative (zeroth order) case of the constant-pressure bond lattice model but is not of great interest in ferromagnet statistical mechanics. If the spin–spin inter-

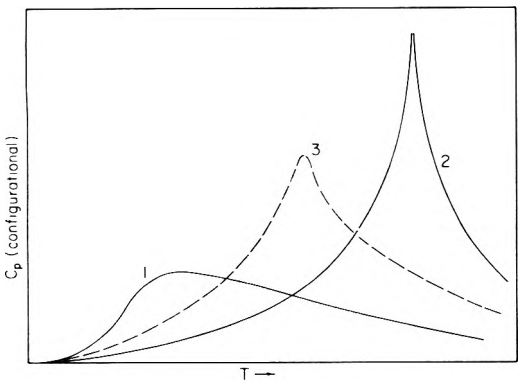

Figure 4. Representation of heat capacity *vs.* temperature relations for cooperative bond lattice model for three cases of relations between bond energy and bond-bond interaction energy magnitudes: (1) Shottky type anomaly for bond energy dominant; (2) physically unmeaningful case in which interaction energy is dominant (analogous to ferromagnet in zero external field); (3) intermediate case suggested as representative of interactions in water (*cf.* Figure 3a, curve 3).

action term which further opposes the spin inversion against the field is made large compared with the same external field term, the heat capacity-temperature relation for the system will convert to the λ form with the "spike" at a higher temperature, as shown in curve 2, Figure 4. This extreme has no physical meaning in the bond lattice context. An intermediate case can be envisaged in which a moderate spin-spin interaction helps oppose the inversion against an external field, or, in the water case, a moderate cooperative terms adds strength to the "on" or intact bond hence opposes its rupture. For this case, the heat capacity behavior should be intermediate in character, and is represented by curve 3 in Figure 4. Curve 3, which is an intuitively reasonable but not theoretically calculated form, has much in common with the configurational heat capacity of water approximated by (C_p (liquid) − C_p(ice)) which we found necessary to resolve the entropy paradox (Figure 3a).

The cooperative bond lattice therefore appears to provide one model framework within which the description of the total liquid water anomaly can be approached. We note that the ordering which is occurring as the λ point is approached is an ordering of "on" and "off" bonds. Thus in this model clustering of hydrogen bonds follows naturally from the assumed nature of the water-water interactions. This seems preferable to the previous introduction by fiat of water molecule clusters as a first step in the development of theories for water properties.[37] The present results suggest that the clustering tendency consequent on cooperative interactions only leads to important departures from random statistics at temperatures near and below the melting point.

Finally, we will make brief further comments on the sulfur analogy, a matter which will be taken up in more detail in a future paper in which the effects of structure breaking components on the behavior of each liquid will be examined. If we ask what structural form the clustering of bonds might take, we conclude that a conspicuous and thermodynamically significant feature would be the presence of closed rings of hydrogen bonds, the linking of which would become more extensive the lower the temperature. However, as Gibbs, *et al.*,[28] point out in their attempt to interpret the existence of a crystal ⇄ liquid phase transition for water, closed rings are entropy-poor structures. Thus with increasing temperature such rings, which would characterise the structure of vitreous as well as crystalline ice, will degrade to chain structures. A more specifically structural approach to the water anomaly might therefore be taken through an extension of the quantitatively successful Eisenberg-Tobolsky ring ⇄ chain polymerization theory for the liquid sulfur anomaly.[27] It is worth noting that the Eisenberg-Tobolsky theory leads to λ-like transition only if ΔH_3 is positive,[27b] *i.e.*, if a ring S-S bond is stronger than a chain S-S bond. This is the equivalent of the del Bene-Pople result for water molecule clusters which showed an energetic advantage for cyclic structures.[38,39] In the sulfur case, however, the expansivity anomaly is relatively weak, and $C_v \approx C_p$. This contrasts with the water phenomenon in which structural factors, specifically the "tetrahedrality," would appear dominant. Supercooled liquid germanium may, for this reason, behave analogously.

Concluding Remarks

Although water is generally considered remarkable in its behavior in the stable liquid region, it becomes much more unusual at lower temperatures. Our heat capacity measurements and deductions based thereon suggest, however, that its most surprising aspect—a liquid state damped λ transition—remains to be observed, being hidden at the moment behind a screen imposed by the homogeneous crystal nucleation phenomenon. Direct observation of this previously unsuspected transition will require the development of micro- or nanosecond calorimetry techniques currently not available. In the meantime, it is at least very important that the splat-quenching experiment by which the glassy state of water can evidently be reached from the liquid[14] be repeated and refined, and that other methods of bypassing crystallization during liquid cooling be developed.

It is hoped in the near future to use emulsion techniques to obtain accurate sound velocity and attenuation measurements on supercooled water from which compressibility and viscosity temperature dependences will be estimable. Ir spectral studies to −38° of overtone bands in the 1-1.5-μ region have also been shown feasible.

Acknowledgments. We are indebted to the Office of Water Resources Research, U. S. Department of the Interior, for support of this work under Water Resources Research Act 1964, Project No. B-051-IND. (Agreement No. 14-31-0001-3883).

References and Notes

(1) C. A. Angell, *J. Phys. Chem.*, **75**, 3698 (1971).
(2) (a) J. A. Schufle and M. Venugopalan, *J. Geophys. Res.*, **72**, 3271 (1967); (b) N. Muller and J. A. Schufle, *ibid.*, **73**, 3345 (1968); (c) J. A. Schufle and Nai Teng Yu, *J. Colloid Interface Sci.*, **46**, 395 (1968).
(3) B. V. Zheleznyi, *Russ. J. Phys. Chem.*, **43**, 1311 (1969); **42**, 950 (1968).
(4) D. H. Rasmussen and A. P. MacKenzie, "Water Structure at the Water-Polymer Interface," H. H. G. Jellinek Ed., Plenum Publishing Corp., New York, N. Y., p 126. We are very grateful to Dr. Rasmussen for advice and cooperation concerning the preparation of these emulsions. He and MacKenzie have in press an article (ref 5) describing volume and enthalpy measurements on emulsions which yield results essentially similar to those described herein. Their interpretation of results, however, differs from ours in important aspects.
(5) D. H. Rasmussen and A. P. MacKenzie, *J. Chem., Phys.*, in press.
(6) B. J. Mason, *Advan. Phys.*, **7**, 221 (1958).
(7) J. C. Hindman, *J. Chem. Phys.*, **44**, 4582 (1966).
(8) G. S. Kell, *J. Chem. Eng. Data*, **12**, 66 (1967).
(9) H. Auer, *Ann. Phys.*, **18**, 593 (1933).
(9a) Note Added in Proof. We have recently repeated the emulsion chem-

ical shift measurements using a spherical TMS reference to eliminate the necessity for susceptibility corrections (J. Shuppert and C. A. Angell, to be submitted for publication). The emulsion chemical shift in these experiments proves identical with that of bulk water measured in the same sample–reference assembly over a common temperature interval from 0 to 35°, thus establishing that our earlier correction procedures quoted in this paper were adequate. These correction-free results also confirm the emulsion data seen in Figure 2b in the temperature range from 0 to −37°.
(10) C. A. Angell, *J. Chem. Educ.*, **47**, 583 (1970).
(11) C. A. Angell and E. J. Sare, *J. Chem. Phys.*, **52**, 1058 (1970).
(12) A. Rahman and F. H. Stillinger, *J. Chem. Phys.*, **55**, 3336 (1971); **57**, 1281 (1972).
(13) A. Ben-Naim and F. H. Stillinger in "Water and Aqueous Solutions; Structure, Thermodynamics, and Transport Processes," R. A. Horne, Ed., Wiley, New York, N. Y., 1972.
(14) See, *e.g.*, ref 4, which shows these relations for some aqueous solutions (Figure 18 p 169).
(15) (a) J. A. Ghormley, *J. Amer. Chem. Soc.*, **79**, 1862 (1957); (b) J. A. McMillan and S. C. Los, *J. Chem. Phys.*, **42**, 829 (1965); (c) M. Sugisaki, H. Suga and S. Seki, *Bull. Chem. Soc. Jap.*, **41**, 2591 (1968); (d) C. A. Angell and E. J. Sare, *Science*, **168**, 280 (1970).
(16) D. R. Uhlmann, unpublished results privately communicated. This X-ray amorphous product crystallized at ~150°K on warming, as do the vapor-deposited glasses. It should be noted many previous attempts to vitrefy liquid water by fast quenching techniques have failed.
(17) J. Hallet, *Proc. Phys. Soc.*, **82**, 1046 (1963).
(18) K. T. Gillen, D. C. Douglass, and M. J. R. Hoch, *J. Chem. Phys.*, **57**, 5117 (1972). These data appear to be more reliable than those of H. R. Prupacher, *ibid.*, **56**, 101 (1972), which extend to −25°. The most reliable cata above 0° seem tc be those reported recently by R. Mills, *J. Phys. Chem.*, **77**, 685 (1973), in the range 1–45°K.
(19) J. C. Hindman, A. Svirmickas, and M. Wood, *J. Chem. Phys.*, **59**, 1517 (1973).
(20) M. H. Cohen and D. Turnbull, *J. Chem. Phys.*, **31**, 1164 (1959).
(21) F. Bueche, *J. Chem. Phys.*, **30**, 748 (1959).
(22) G. Adam and J. H. Gibbs, *J. Chem. Phys.*, **43**, 139 (1965).
(23) The experimental glass transition temperature, T_g, is defined as some point (different authors vary) in the narrow temperature range over which the liquid falls out of internal equilibrium during cooling. The loss of equilibrium is a direct consequence of the increase of the liquic structural relaxation time to values corresponding to the time scale of the experiment by which the state of equilibrium is measured (usually a heat capacity or expansion measurement). Since for molecular liquids the structural relaxation time usually changes by orders of magnitude over a few degrees near the glass temperature, T_g is usually quite well defined experimentally even though intrinsically rate-dependent. For time scales of the order of seconds, T_g occurs at a viscosity around 10^{11} P.
(24) The heat capacity in question is now that which would be measured in some as-yet-unperformed experiment for which the time scale is "fast" with respect to the crystal nucleation and growth rate but "slow" with respect to the liquid structural relaxation time.
(25) D. Turnbull, "Physics of Non-Crystalline Solids," J. A. Prins, Ed., North-Holland Publishing Co., Amsterdam, 1965, p 41.
(26) E. D. West, *J. Amer. Chem. Soc.*, **81**, 29 (1959).
(27) (a) A. V. Tobolsky and A. Eisenberg, *J. Amer. Chem. Soc.*, **81**, 2302 (1959); (b) A. Eisenberg and A. V. Tobolsky, *J. Colloid Sci.*, **17**, 49 (1962).
(28) J. H. Gibbs, C. Cohen, P. D. Fleming, and H. Porosoff, *J. Solution Chem.* **2**, 277 (1973).
(29) S. Olander and S. A. Rice, *Proc. Nat. Acad. Sci. U. S.*, **G9**, 98 (1972).
(30) J. A. Ghormley, *Science*, **171**, 62 (1971). On the other hand, it is to be noted that B. A. Seiber, B. E. Wood, A. M. Smith, and P. R. Muller, *ibid.*, **170**, 652 (1970), using a less direct technique obtained a considerably lower density of 0.81 ± 0.02 g cm^{-3}.
(31) R. Bruckner, *J. Non-Cryst. Solids*, **5**, 123 (1970).
(32) We note the recent suggestion, based on refined X-ray studies (J. H. Konnert and J. Karle, *Science*, **179**, 177 (1972)) that the short-range order in the SiO_2 glass (out to 20 Å) is tridymite-like: details of the RDF at longer ranges (~20 Å) indicate some crystobalite-like character. A. H. Narten, on the other hand, concluded that a model for the glass based on a quartz-like short range order gave the best combination of RDF and censity predictions (*J. Chem. Phys.*, **56**, 1905 (1972)).
(33) Extrapolation to −63° suggests that δ for the fully bonded state, which should be close to the to-date-undetermined value for ice, should be about 1.0 ppm downfield from that of water at 0°.
(34) Lattice models have been deemed inappropriate to the discussion of liquid water (A. T. Hagler, H. A. Scheraga, and G. Nemethy, *J. Phys. Chem.*, **76**, 3229 (1972)) because of the lack of order in the liquid and of the cooperative character attributed the hydrogen bonding. However, there seems to be little justification for this objection since it is well known that lattice models provide an adequate basis for the statistical treatment (Ising models of the cooperative gas–liquid and liquid–liquid critical phenomena. Rice, on the other hand, views the model favorably among "simple" models while noting problems of structural underdefinition and inadequate consideration of coupling between vibrational and configurational degrees of freedom (O. Weres and S. A. Rice, *J. Amer. Chem. Soc.*, **94**, 8983 (1972)).
(35) A. W. Lawson, *Phys. Rev.*, **57**, 417 (1940).
(36) (a) C. W. Garland and R. Renard, *J. Chem. Phys.*, **44**, 1120 (1966); (b) C. W. Garland and R. Renard, *ibid.*, **44**, 1125 (1966).
(37) (a) G. Nemethy and H. A. Scheraga, *J. Chem. Phys.*, **36**, 3382 (1962); (b) A. T. Hagler, H. A. Scheraga, and G. Nemethy, *J. Phys. Chem.*, **76**, 3229 (1972).
(38) J. del Bene and J. A. Pople, *J. Chem. Phys.*, **52**, 4858 (1970). It should be noted that these results are contradicted by the recent calculations of B. R. Lentz and H. A. Scheraga, *J. Chem. Phys.*, **58**, 5296, (1973), but supported by the work of P. Barnes (Contribution to conference entitled "The Liquid State: van der Waals Centenery," held at University of Canterbury, Kent, England, Apr 16–18 (1973).
(39) For a polymer approach to the water problem to be plausible a configurational–vibrational degree of freedom separability assumption must be justifiable. For hot water such an assumption is hardly reasonable, but by −40° a difference in vibrational and structural relaxation times of some three orders of magnitude has opened up. For such time scale differences a weak coupling assumption is acceptable; thus structural approaches to the thermodynamic behavior are feasible and worth developing.

Equilibrium Studies by Electron Spin Resonance. VI. The Benzoquinone Free Ion–Ion Pair Equilibrium

Gerald R. Stevenson* and Antonio E. Alegria

Department of Chemistry, University of Puerto Rico, Rio Piedras, Puerto Rico 00931 *(Received August 16, 1973)*

Publication costs assisted by the University of Puerto Rico

The reduction of *p*-benzoquinone by alkali metal in hexamethylphosphoramide (HMPA) leads to the formation of the "free" anion radical only. However, the addition of an alkali metal iodide or chlorate salt leads to the formation of ion pairs, which can be seen simultaneously with the "free" ion by esr. The thermodynamic parameters controlling the ion pair dissociation were determined, and the negative values for the entropy and enthalpy are compared with those for similar ions in other solvents. For the potassium salt at high temperatures three ions can be observed simultaneously in solution: the "free" ion, the contact ion pair, and the solvent-separated ion pair. At very high concentrations of added salt, a rapid cation exchange is observed between the ion pair and the solvent.

Esr spectroscopy has proven itself to be the most powerful tool for investigating the nature of ion pairs in solution and has been used by several workers to investigate the thermodynamics of dissociation of these ion pairs. There have been two basic esr techniques used to obtain these parameters. When the rate of ion pair formation and dissociation is fast on the esr time scale, the esr coupling constants observed are those of a time-averaged species. If the coupling constant for the contact ion pair and that for the solvent-separated ion pair (or free ion) can be accurately estimated, time-averaging equations can be applied, and the equilibrium constant for the ion pair dissociation to form free ion (eq 1) or to form the solvent-separated ion pair (eq 2) can be determined. This type of investigation into ion pairing thermodynamics has been employed by Hirota in his work with naphthalenide and anthracenide ions.[1] The fact that this technique has some inherent errors has been pointed out by Szwarc, *et al.*[2] The use of time-averaging equations has not yet been employed for the ion pair dissociation to form the free ion. However, they have been used to study hydrogen-bonded anion radical dissociation to form the free ion.[3]

$$\pi^{\cdot-}M^+ \rightleftharpoons \pi^{\cdot-} + M^+ \quad (1)$$

$$\pi^{\cdot-}M^+ \rightleftharpoons \pi^{\cdot-}\,|\,M^+ \quad (2)$$

The second technique is based upon the simultaneous observation of the ion pair and the free ion. For this situation, the esr signal for the two species are observed together, and by simply utilizing the fact that the esr signal intensity is proportional to the respective spin concentration, one can obtain thermodynamic parameters for the ion pair dissociation. This technique has recently been utilized for studying ion pair dissociation of the salts generated from durosemiquinone,[4] nitrobenzene,[5] and substituted nitrobenzenes.[6] For the thermodynamic parameters determined in this manner ΔH° can be determined with greater accuracy than ΔG° or ΔS°. This is due to the fact that either the alkali metal cation concentration or the total spin concentration must be determined. This latter term can be determined with the use of a spin concentration standard.[4] Even with the errors involved in the determination of the total spin concentration (about 50%), this technique appears to be superior to the use of time-averaging equations.

Hexamethylphosphoramide (HMPA) is one of the most powerful solvents for alkali metal cations known.[7] However, in a recent review by Normant, it has been revealed that anion radicals are practically unsolvated in this solvent due to steric hindrance around the phosphorus center.[8] These facts make HMPA particularly useful in the study of ion pair dissociation, since the heat of solution of the "free" ion plus the cation consists essentially of the heat of solution of the cation only. This makes the thermodynamic parameters of ion pair dissociation a function of the solvation of the ion pair and cation only.

HMPA is also particularly suited to the experimental determination of ion pair dissociation thermodynamics, since rates of electron transfer[2,9] and of ion pair formation and dissociation[10] are slower in this solvent than in the ethereal solvents. The slow kinetics of electron transfer and of ion pairing is most probably related to the high viscosity of HMPA.

Here we wish to describe the application of the method of simultaneous observation in HMPA coupled with a more accurate estimate of the cation concentration to probe the nature of ion pairing in the *p*-benzoquinone anion radical systems.

Experimental Section

The esr spectrometer system, the method of reduction of the neutral molecule to form the anion radical, and the method of purification of the HMPA have been previously described.[10]

The double integrations of the esr lines were accomplished by digitizing the spectra coupled with a numerical integration carried out by computer.

The equilibrium constants reported are the result of an average and standard deviation taken from at least eight different samples with different concentrations of added salt, alkali metal, and benzoquinone. The enthalpies were taken from the slopes of modified van't Hoff plots. The error in the slope of a single plot is smaller than the error obtained by comparing the individual plots to each other. Therefore, the errors reported represent the standard de-

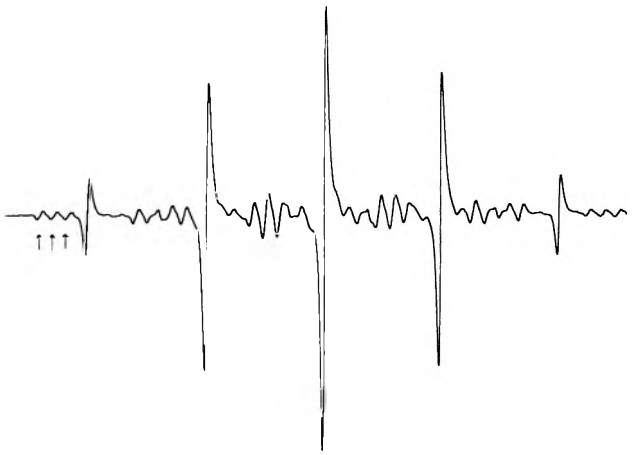

Figure 1. Esr spectrum of *p*-benzoquinone reduced by K in HMPA at room temperature. The two radicals are shown superimposed. The arrows indicate the first three lines of the ion pair.

TABLE I: Thermodynamic Parameters Controlling the Solvent-Separated Ion Pair Dissociation of the *p*-Benzoquinone Anion Salt with the Cations

Cation	$\Delta G°$, kcal/mol	$\Delta H°$, kcal/mol	$\Delta S°$, eu	$K_{eq} \times 10^2$
Na^+	1.1 ± 0.2	−1.05 ± 0.08	−7.3	15 ± 6
K^+	2.0 ± 0.1	−3.68 ± 0.09	−19	3.6 ± 0.7

viation in the enthalpy from the different plots. A single plot was taken for each sample.

Results and Discussion

Solutions (10^{-2} to 10^{-4} *M*) of *p*-benzoquinone in HMPA will dissolve small amounts of alkali metal to form the free anion radical, which exhibits a five-line esr spectrum resulting from four equivalent protons (a_H = 2.42 G).

For the potassium reductions, an addition of a small amount of potassium iodide or potassium chlorate (0.001–0.04 *M*) to the HMPA semiquinone solution results in the appearance of a second radical characterized by a triplet of 1.74 G due to two equivalent protons, a triplet of 2.30 G due to two equivalent protons, and a quartet of 0.30 G due to the splitting from a ^{39}K nucleus, Figure 1. The new radical is an ion pair of the semiquinone and has been previously characterized.[11] Based upon the relatively small a_K and the evidence developed below, the ion pair will be assigned to be a solvent-separated ion pair. This solvent-separated ion pair can dissociate to form the free ion as shown in eq 3, where $SQ\cdot^-$ represents the semiquinone.

$$K^+||SQ\cdot^- \rightleftharpoons SQ\cdot^- + K^+ \quad (3)$$

and

$$K_{eq} = [SQ\cdot^-][K^+]/[K^+||SQ\cdot^-] \quad (4)$$

Since the first three lines of the ion pair and the first line of the "free" ion are essentially uncomplicated K_{eq} can be expressed by eq 5, where $I(SQ\cdot^-)$ and

$$K_{eq} = I(SQ\cdot^-)[K^+]/4I(K^+||SQ\cdot^-) \quad (5)$$

$I(K^+||SQ\cdot^-)$ represent the intensities of the first line of the free ion and the first line of the ion pair, respectively. The factor 4 in the denominator appears because each line of the ion pair only represents one fourth of the spin concentration that is represented by an esr line of the free ion. To utilize eq 5, the K^+ concentration was taken to be equal to the concentration of added salt. This assumption is valid since for each sample the concentration of added KI or $KClO_3$ was much larger than the total spin concentration. It has been recently observed that salts of this type are fully dissociated in HMPA, thus the possibility of ion pairing between the cation and anion of the added salt was overlooked.

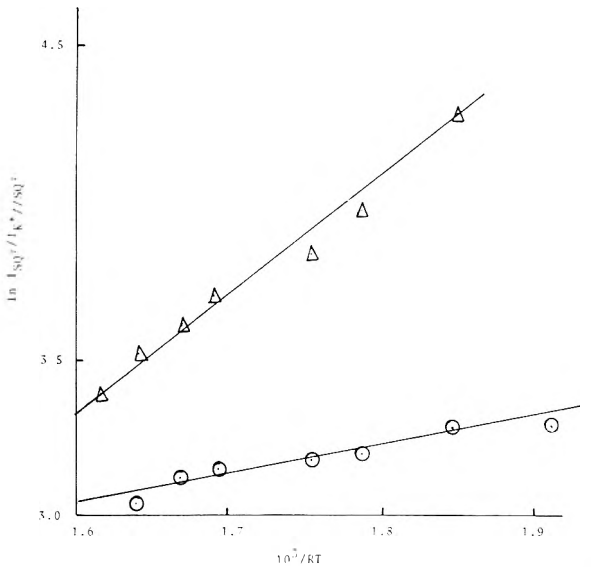

Figure 2. Modified van't Hoff plot for the system *p*-benzoquinone–HMPA–K with added KI, Δ, and *p*-benzoquinone–HMPA–Na, O.

Assuming a Lorentzian line shape for the esr line the intensities can be taken from the line height times the square of the extrema to extrema line width ($h\Delta w^2$). Values for K_{eq} calculated in this manner are larger by 40% than those calculated from the double integration. This is due to the fact that the first four lines of the ion pair are close together, and the wings of these lines are cut off by the neighboring esr lines. This results in a low value for the calculated intensities of the lines due to the ion pair and thus a value for K_{eq} that is too large. For this reason, the values reported in Table I were calculated from the use of $I = h\Delta w^2$.

Since $[K^+] \gg [SQ\cdot^-]$, $\Delta H°$ was taken from a modified van't Hoff plot of $\ln I(SQ\cdot^-)/I(K^+||SQ\cdot^-)$ *vs.* $1/RT$. These plots are linear (Figure 2), and the resulting thermodynamic parameters are given in Table I. The thermodynamic parameters did not vary with the choice of the added potassium or sodium salt.

The same experimental procedure was carried out for the sodium reductions. The added salts were NaI and $NaClO_3$. Again the experimental results were independent of the choice of added salt. The coupling constants for the sodium ion pair are 1.74 (two protons), 3.68 (two protons), and 0.29 G (sodium-23 nucleus).

The ion pair dissociation is expected to be controlled by more negative entropy and enthalpy terms in solvents that have more affinity for the cation that is formed. However, the entropy and enthalpy of dissociation of the durosemiquinone ion pair with sodium and potassium in dimethoxyethane are more negative than those reported here in HMPA.[4] This is due to the fact that the thermodynamic parameters reported here are those for the disso-

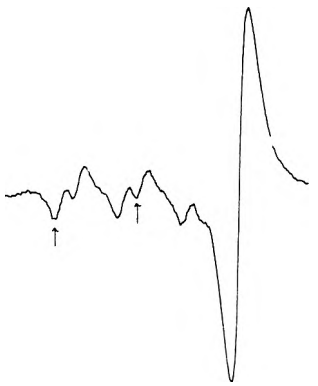

Figure 3. Esr spectrum of the system *p*-benzoquinone–HMPA–K with added KI at 45°. Only the first few lines of the ion pairs and the first line of the free ion are shown. The arrows indicate the first two lines of the tight ion pair.

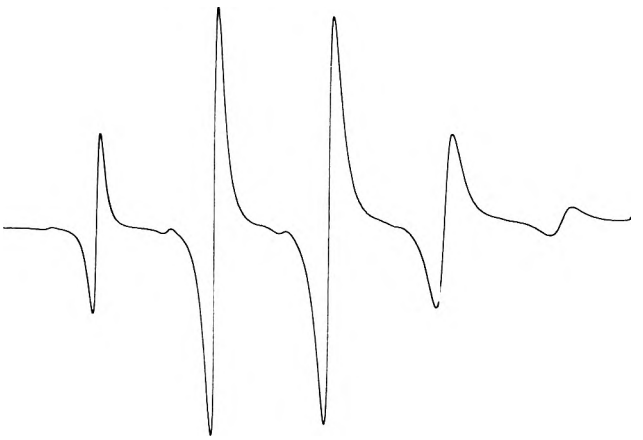

Figure 4. Esr spectrum of the system *p*-benzoquinone–HMPA–K in a saturated solution of KI.

ciation of a solvent-separated ion pair, and the HMPA is involved in considerable solvation of this ion pair.

At low temperatures the esr pattern for the potassium reduction is basically the same as that for the sodium reduction. However, above 45° a second ion pair appears for the potassium systems, Figure 3. This new ion pair yields a metal splitting of 0.45 G, in comparison to the 0.30 G for the solvent-separated ion pair. The fact that the metal splitting for the new ion pair is larger than that for the ion pair observed at lower temperatures indicates that it is a tight ion pair ($K^+SQ\cdot^-$). Further, since the concentration of the tight ion pair increases with increasing temperature, the enthalpy for its dissociation into the solvent-separated ion pair is negative. Equation 6 accounts for the results.

$$K^+SQ\cdot^- \rightleftarrows K^+||SQ\cdot^- \rightleftarrows K^+ + SQ\cdot^- \qquad (6)$$

This represents the first report of the simultaneous observation of two different ion pairs both exhibiting metal splitting. However, three species, two ion pairs and a free ion, have been simultaneously observed for some nitrosamine anion radicals in tetrahydrofuran.[12] In all other reports of two different ion pairs in equilibrium, only the time-averaged spectrum could be observed.

When *p*-benzoquinone is reduced in a saturated HMPA solution of KI, a solution results that exhibits only five esr lines, but the pattern is unsymmetric with respect to the line widths. The line widths increase with increasing magnetic field, Figure 4. This spectrum is obviously due to two different anion radicals in solution with slightly different coupling constants and *g* values. If the radical with the smaller *g* value also possess the smaller coupling constant, then the differences in the positions of the esr lines for the two radicals will decrease with the magnetic field. A similar effect was observed for the nitrosamine anion radicals in etheral solvents.[13] The two radicals observed in the saturated solution are the free ion and ion pair. The ion pair, of course, has the lower *g* value and coupling constant. The fact that the ion pair does not exhibit metal splitting and all of the four protons are equivalent is probably due to the fact that there is a rapid exchange of the cation between the ion pair and the saturated solvent, eq 7.

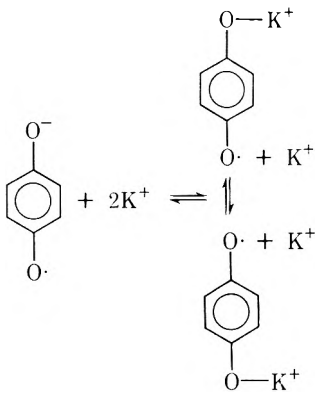

(7)

Acknowledgments. The authors are grateful to the Research Corporation and the National Institute of Health for support of this work. The NIH support was from Grant No. RR-8102 from the Minority Schools Biomedical Support Program of the Division of Research Resources.

References and Notes

(1) N. Hirota, *J. Phys. Chem.*, **71**, 127 (1967).
(2) K. Hofelmann, J. Jagur-Grodzinski, and M. Szwarc, *J. Amer. Chem. Soc.*, **91**, 4645 (1969).
(3) G. R. Stevenson and H. Hidalgo, *J. Phys. Chem.*, **77**, 1027 (1973).
(4) R. D. Allendoerfer and R. J. Papez, *J. Phys. Chem.*, **76**, 1012 (1972).
(5) G. R. Stevenson, L. Echegoyen, and L. R. Lizardi, *J. Phys. Chem.*, **76**, 2058 (1972).
(6) G. R. Stevenson and L. Echegoyen, *J. Phys. Chem.*, **77**, 2339 (1973).
(7) G. Levin, J. Jaugar-Grodzinski, and M. Szwarc, *J. Amer. Chem. Soc.*, **92**, 2268 (1970).
(8) H. Normant, *Angew. Chem., Int. Ed. Engl.*, **6**(12), 1046 (1967).
(9) G. R. Stevenson and J. G. Concepción, *J. Phys. Chem.*, **76**, 2176 (1972).
(10) G. R. Stevenson, L. Echegoyen, and L. R. Lizardi, *J. Phys. Chem.*, **76**, 1439 (1972).
(11) B. S. Prabhananda, M. P. Khakhar, and M. R. Das, *J. Amer. Chem. Soc.*, **90**, 5980 (1968).
(12) G. R. Stevenson and J. G. Concepción, *J. Phys. Chem.*, **77**, 611 (1973).
(13) G. R. Stevenson and C. Colón, *J. Phys. Chem.*, **75**, 2704 (1971).

Effects of the Intramolecular Hydrogen Bond on Intermolecular Hydrogen Bonding in Hydroxybenzene–Ether Systems

J. N. Spencer,* R. A. Heckman, R. S. Harner, S. L. Shoop, and K. S. Robertson

Department of Chemistry, Lebanon Valley College, Annville, Pennsylvania 17003 *(Received August 13, 1973)*

Publication costs assisted by Lebanon Valley College

The hydrogen bonding of phenol, catechol, guaiacol, and pyrogallol in diethyl ether–carbon tetrachloride solutions was studied over the temperature range 20–50° by monitoring the hydroxyl stretching frequency at about 3 μ. The intramolecular hydrogen bond in guaiacol was not disrupted by association with diethyl ether. Equilibrium constants and enthalpy and entropy changes for the other systems were calculated. The intramolecular bond in catechol and pyrogallol is disrupted and both compounds form complexes containing one and two ether molecules. The frequency shift, enthalpy change, and equilibrium constant for the formation of the monoether complex with catechol and pyrogallol are larger than the corresponding properties for the phenol complex and reflect the influence of the intramolecular hydrogen bond on intermolecular hydrogen bonding.

Introduction

The study of the influence of the intramolecular hydrogen bond on hydrogen bonded properties has been largely limited to effects on ionization constants. Various investigators[1,2] have reported abnormally large first ionization constants and abnormally small second ionization constants for dibasic acids which have intramolecular hydrogen bonding capability. If the intramolecular bond in such compounds as catechol and pyrogallol acts to increase the first ionization constant, the increased acidity of the hydrogen of the free hydroxyl group should be reflected in the thermodynamics of the intermolecular association of this hydroxyl with diethyl ether. A comparison of the thermodynamics of the phenol–ether complex with those of the catechol and pyrogallol ether complexes will thus allow a determination of the extent of the influence of the intramolecular bond on intermolecular hydrogen bonding.

Three studies of the hydrogen bonding between phenol and diethyl ether in carbon tetrachloride solvent have been reported. Gramstad[3] determined the equilibrium constant for the phenol–diethyl ether complex to be 9.6 at 20° and 4.5 at 50°. The enthalpy change was found to be -4.75 kcal mol^{-1}. Powell and West[4] found the equilibrium constant for this system to be 8.83 at 25° and found ΔH to be -5.41 kcal mol^{-1}. Bellamy, *et al.*,[5] report the phenol–diethyl ether equilibrium constant as 6.0 at 29°. No studies of the bonding of catechol (o-hydroxyphenol), guaiacol (o-methoxyphenol), or pyrogallol (1,2,3-trihydroxybenzene) to diethyl ether have been reported. Because these compounds have intramolecular hydrogen bonding capabilities, a study of their complex formation with diethyl ether may provide a determination of the influence of the intramolecular bond on intermolecular hydrogen bonding.

Experimental Section

Baker analyzed spectrophotometric quality carbon tetrachloride was fractionally distilled under a dry nitrogen atmosphere through a 3-ft column packed with glass helices. Refractive index and boiling point were used as purity criteria. Baker analyzed reagent grade phenol and Baker practical grade guaiacol were fractionally distilled in a 3-ft spinning band column under reduced pressure. The middle cuts of the distillate were taken. Baker reagent grade catechol and Baker analyzed reagent grade pyrogallol were both purified by sublimation under reduced pressure. Baker analyzed reagent grade anhydrous diethyl ether was used without further purification. All reagents were stored in a dry nitrogen atmosphere. Solutions were prepared under anhydrous conditions.

Spectra were recorded by the Beckman DK-2A recording spectrophotometer using 1-cm Teflon stoppered cells.

A mixture of diethyl ether and carbon tetrachloride was used in the reference beam. Concentrations were about 0.002 M for phenol and catechol, 0.0005 M for pyrogallol, and 0.004 M for guaiacol. The ether concentration was 0.1 M for the phenol, catechol, and guaiacol systems. If ether concentrations in excess of 0.04 M were used for the pyrogallol system, the absorbance of the free hydroxyl was too low for accurate measurements due primarily to the limited solubility of pyrogallol. Thus the ether concentrations ranged from 0.03 to 0.04 M for pyrogallol studies. A Beckman temperature regulator in combination with a water bath was used to control the temperature to within ±0.5°. Corrections for the change in concentration with temperature were made by using the pycnometrically determined densities of ether–carbon tetrachloride mixtures over the temperature range of this work.

The molar absorptivities of phenol, catechol, and guaiacol in carbon tetrachloride were determined as a function of temperature and are in excellent agreement with those previously reported.[6] The molar absorptivity of pyrogallol as a function of temperature is given in Table I.

The concentration of free phenol in the phenol–ether equilibrium mixture was found by use of Beer's law and the molar absorptivity at the temperature of interest. The complex concentration was found by subtracting the free phenol concentration from the initial phenol concentration. The methods of calculation for the catechol and pyrogallol systems are more complicated and are dealt with in a later section. A small correction due to overlap of the intramolecular bonded absorbance band with the free hydroxyl absorbance band was made for the catechol and pyrogallol systems by resolving the bands by symmet-

TABLE I: Temperature Dependence of the Molar Absorptivity of Pyrogallol

T, °C	ϵ_f[a]	ϵ_b[b]
20	205	412
30	196	410
40	194	407
50	187	405

[a] Molar absorptivity of the free hydroxyl group at 3611 cm^{-1}. [b] Molar absorptivity of the bonded hydroxyl groups at 3569 cm^{-1}.

ric reflection about their centers. The equilibrium constants reported in Table II for pyrogallol and catechol are the average of a minimum of six determinations at each temperature.

Ternary systems such as those used in this investigation may offer experimental difficulties when an automatically operated slit is used.[7] In order to compensate for the diethyl ether present in the ternary solutions, the slit may open to a greater extent than when no ether is present. This opening leads to a decrease in the absorbance maximum and thus, since the molar absorptivities were determined in the absence of diethyl ether, may lead to errors in the determination of the concentration of the nonhydrogen bonded species in the equilibrium mixture. In this work it was found that at the diethyl ether concentrations used, the slit width was not seriously affected. Spectral studies of guaiacol showed that the intramolecular bond was not disrupted by association with diethyl ether. The molar absorptivity of guaiacol was found to be the same at all temperatures in the presence and in the absence of the base, verifying that no serious change in slit width occurred due to the presence of the ether. In addition, the excellent agreement found for the phenol–diethyl ether complex properties with those previously reported[3-5] indicates that no difficulties with changing slit width were encountered.

Results and Discussion

The thermodynamic properties and frequency shifts for the complexes formed with the various phenols and diethyl ether are given in Table II and Table III, respectively. The standard enthalpy change was found from a plot of log K *vs.* T^{-1} and the entropy change was calculated from $\Delta G° = \Delta H° - T\Delta S°$.

Spectra of solutions of catechol in carbon tetrachloride show two absorbance peaks, the higher frequency peak at 3611 cm^{-1} corresponds to absorption by the free hydroxyl group and the lower frequency peak at 3565 cm^{-1} is due to absorption by the intramolecularly hydrogen bonded hydroxyl. That catechol undergoes no cis–trans equilibrium similar to that observed in the *o*-halophenols is evident from the behavior of the molar absorptivities with temperature.[6] In the presence of 0.1 M ether the absorbance of both peaks decreases and a third absorbance maximum at 3266 cm^{-1} is found. The decrease of the absorbance maximum at 3565 cm^{-1} implies that the intramolecularly bonded hydroxyl in catechol participates in the complex formation. The complex formation between catechol and ether was thus considered to occur in stepwise fashion according to eq 1 and 2

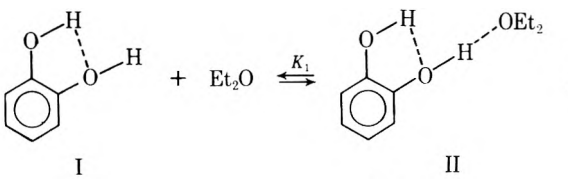

(1)

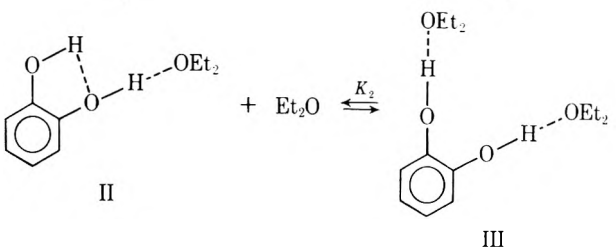

(2)

The absorbance at the higher frequency peak due to the free hydroxyl is

$$A_f = \epsilon_f C_I \tag{3}$$

where ϵ_f is the molar absorptivity of the free hydroxyl and C_I is the free catechol concentration in the equilibrium mixture. The absorbance at the bonded frequency (3565 cm^{-1}) A_b is given by

$$A_b = \epsilon_b C_I + \epsilon_b C_{II} \tag{4}$$

where ϵ_b is the molar absorptivity of the intramolecular bond, assumed to be the same for catechol and the catechol–ether complex, and C_{II} is the concentration of the catechol–ether complex of eq 1. Equations 3 and 4 may be

TABLE II: Thermodynamic Functions for the Hydrogen Bonding of Phenols to Diethyl Ether

	T, °C	K_1	K_2	K_{12}	$\Delta H°$,[a] kcal mol^{-1}	$\Delta S°$, cal deg^{-1} mol^{-1}	ν, cm^{-1}
Phenol	20	9.6					
	30	7.3			$\Delta H = -5.3 \pm 0.2$	$\Delta S = -14$	3610
	40	5.2					
	50	4.3					
Catechol	20	12.0	7.6	85			
	30	7.9	9.5	70	$\Delta H_1 = -8.0 \pm 0.3$	$\Delta S_1 = -22$	
	40	5.1	13	61	$\Delta H_2 = +4.7 \pm 0.2$	$\Delta S_2 = +20$	3611
	50	3.3	16	47	$\Delta H_{12} = -3.3$	$\Delta S_{12} = -2$	(3565)[b]
Pyrogallol	20	27	25	6.8×10^2			
	30	16	29	4.6×10^2	$\Delta H_1 = -7.1 \pm 0.8$	$\Delta S_1 = -18$	
	40	11	38	4.2×10^2	$\Delta H_2 = +3.1 \pm 0.5$	$\Delta S_2 = +17$	3611
	50	8.6	40	3.4×10^2	$\Delta H_{12} = -4.0$	$\Delta S_{12} = -1$	(3569)[b]
Guaiacol							(3567)[b]

[a] The precision reported was obtained from the error in the least-squares slope of a plot of log K *vs.* T^{-1}. [b] Absorption frequency of the intramolecular bond.

TABLE III: Frequency Shifts for the Hydroxybenzene–Ether Complexes Compared to pK_{a_1}

	$\Delta\nu$,[a] cm^{-1}	pK_{a_1}
Hydroquinone	254	9.91[b]
Phenol	276	9.952,[c] 9.90[d]
Resorcinol	285	9.15[b]
Phloroglucinol	269	8.45[b]
Catechol	345	9.13[b]
Pyrogallol	340	9.02[b]

[a] The frequency shift is the difference between the free hydroxyl absorbance and that of the complex in CCl_4 solution. [b] G. Kortum, W. Vogel, and K. Andrussow, "Dissociation Constants of Organic Acids in Aqueous Solution," Butterworths, London, 1961. $T = 30°$. [c] D. T. Y. Chen and K. J. Laidler, *Trans. Faraday Soc.*, **58**, 480 (1962). $T = 30°$. [d] E. H. Binns, *Trans. Faraday Soc.*, **55**, 1900 (1959). $T = 30°$.

solved for C_I and C_{II}. The concentration of the diether complex may then be found by subtracting the sum of $C_I + C_{II}$ from the initial catechol concentration.

The first stepwise formation constant, K_1, is slightly larger than the equilibrium constant for the phenol–ether complex and the frequency shift and enthalpy change are considerably larger. These differences may be correlated with the difference between the first ionization constant of catechol (7.5×10^{-10}) and that of phenol (1.2×10^{-10}). These ionization constants, as well as others reported in this work, were determined from measurements on aqueous solutions and thus may be misleading when applied to situations where a nonaqueous environment exists.

In order to determine if the increase in acidity produced by nonintramolecularly hydrogen bonded hydroxyl groups would be sufficient to account for the observed differences between the catechol and phenol ether complexes, frequency shifts for resorcinol and hydroquinone complexes with ether were determined in carbon tetrachloride and are recorded in Table III. The frequency shifts for these complexes are close to that found for the phenol–ether complex and imply that the hydrogen bond enthalpies for these systems are similar. The differences in frequency shift and hydrogen bond enthalpy for the phenol–ether and catechol–ether complexes may be attributed only in a small part to a second hydroxyl group and largely to the intramolecular hydrogen bond. The smaller differences in equilibrium constants are due to the relatively large entropy change for the catechol complex with ether.

The second stepwise formation constant, K_2, for the catechol–ether complex is smaller than K_1 and increases with temperature corresponding to an endothermic process. A positive enthalpy change of the magnitude found for step 2 is unusual although Fishman and Chen[8] and Busfield, Ennis, and McEwen[9] have reported small positive enthalpies for the formation of the intramolecular bond in butanediols. The energy required to disrupt the intramolecular bond in catechol must be partially responsible for the endothermic character of the reaction given by eq 2. A positive ΔS is also found for this reaction which indicates that the catechol–ether complex must be loosely bound and that considerable disruption of the solvent structure must occur.

The overall equilibrium constant, K_{12}, is the product of K_1 and K_2 and corresponds to the reaction given by the sum of eq 1 and 2; ΔH_{12} and ΔS_{12} reported in Table II are similarily defined.

The molar absorptivities for pyrogallol are given in Table I and show the relative effects of temperature on the free and bonded hydroxyl absorptivities. It has commonly been assumed that the molar absorptivities of free and intramolecularly bonded hydroxyl groups are the same.[9,10] While this may be a reasonable assumption over a small temperature interval, the assumption becomes less acceptable as the temperature interval is increased due to the difference in the temperature dependence of the molar absorptivities of the free and bonded hydroxyls. Finch and Lippincott[11] have interpreted the temperature dependence of the molar absorptivity as being due to a change in the hydrogen bonded distance with temperature. According to this interpretation, the smaller temperature dependence of the intramolecular molar absorptivity would result from the rigid geometry of the intramolecular bond which allows relatively little bond length change with temperature.

The molar absorptivities of the free and bonded hydroxyls of catechol show similar trends with temperature[6] to those for pyrogallol and the change in molar absorptivity of guaiacol with temperature[6] parallels the trends found for the intramolecular bonds of catechol and pyrogallol. A comparison of the molar absorptivities of the free and bonded peaks of pyrogallol and catechol[6] indicates that the ratio of bonded to free hydroxyl groups in pyrogallol is twice as great as in catechol. The temperature dependence of the free hydroxyl molar absorptivity of pyrogallol so closely parallels that of phenol and catechol and the temperature dependence of the molar absorptivity of the bonded peak so closely parallels that of catechol and guaiacol, that no cis–trans equilibrium seems likely. Thus pyrogallol in carbon tetrachloride solution exists in the conformation of species IV of eq 5.

The molar absorptivity of the intramolecularly bonded peak of pyrogallol was found to decrease to about two-thirds its value in carbon tetrachloride solution in the presence of 0.04 *M* diethyl ether indicating that the intramolecular bond was disrupted by association with the ether. The bonding of diethyl ether to pyrogallol was also considered in stepwise fashion.

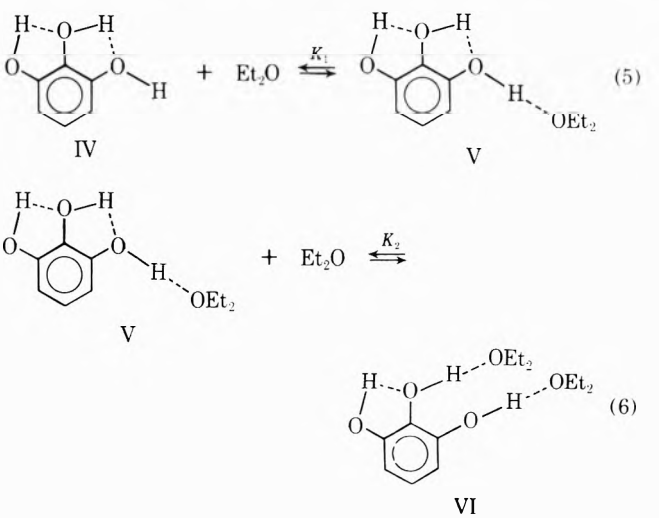

The overall equilibrium constant is defined as K_{12}, and refers to the reaction given by the sum of eq 5 and 6. A complex species containing three ether molecules per pyrogallol molecule was considered negligible at the ether concentrations used.

For the equilibrium species given by eq 5 and 6 the absorbance, A_f, at the free hydroxyl peak is

$$A_f = \epsilon_f C_{IV} \quad (7)$$

where ϵ_f is the molar absorptivity of the free hydroxyl of pyrogallol and C_{IV} is the free pyrogallol concentration. The absorbance, A_b, at the intramolecularly bonded peak is

$$A_b = \epsilon_b C_{IV} + \epsilon_b C_V + \tfrac{1}{2}\epsilon_b C_{VI} \quad (8)$$

where ϵ_b is the molar absorptivity given in Table I and C_V and C_{VI} are the equilibrium concentrations of the species so labeled in eq 6. It has been assumed that the molar absorptivity of the single intramolecular bond in species VI is one-half that given in Table I. The assumption is reasonable because the molar absorptivities for the intramolecular bond of catechol and guaiacol have been shown to be nearly the same[6] and are approximately equal to one-half the value of the molar absorptivity of the two intramolecular bonds in pyrogallol.

Rearrangement of (8) together with the condition $C = C_{IV} + C_V + C_{VI}$, where C is the initial pyrogallol concentration gives

$$A_b = \epsilon_b(C - C_{VI}) + \tfrac{1}{2}\epsilon_b C_{IV} \quad (9)$$

Thus C_{VI} is calculated directly from the absorbance at the intramolecularly bonded peak, the initial concentration, and the molar absorptivities given in Table I. Equation 7 gives C_{IV} directly from the absorbance at the free peak and the molar absorptivity, and C_V is found by difference.

The first stepwise formation constant, K_1, for the pyrogallol–ether complex is about twice as large as that for the catechol–ether complex at all temperatures and nearly three times as large as that for the phenol–ether complex. The frequency shifts for the catechol and pyrogallol systems are about the same and within experimental error the enthalpy changes are comparable. The frequency shift and ΔH_1 are considerably larger for the pyrogallol complex than for the phenol complex. A comparison of the frequency shifts given in Table III shows that catechol and pyrogallol complexes have much larger frequency shifts than the complexes formed with those compounds in which no intramolecular hydrogen bond exists. The frequency shift found for phloroglucinol (1,3,5-trihydroxybenzene) in 1 M diethyl ether is 269 cm^{-1} as compared to 340 cm^{-1} for pyrogallol. The increase in frequency shift and ΔH_1 for pyrogallol over that of phenol must be attributed to the influence of intramolecular hydrogen bonding.

The second stepwise formation constant, K_2, for the pyrogallol–ether complex is about equal to K_1 at 20° and increases with increasing temperature. Thus the process corresponding to eq 6 is endothermic, similar to the equivalent process for the addition of a second ether molecule to catechol. The entropy change for this step is also positive, probably for the same reasons advanced for the corresponding step for catechol. The quantities ΔH_{12} and ΔS_{12} are defined analogously to those for the catechol system. If the assumption is made that a fourth pyrogallol species containing three ether molecules is formed, K_1 must be larger than those given in Table II if the experimental data are to be satisfied. The relationship between K_1 and K_2 is such that the maximum value for K_1 at 20° is 38 if K_2 is to be greater than zero. K_2 decreases rapidly with increasing K_1 and if the relationship between K_1 and K_2 for the pyrogallol complex is approximately the same as that between K_1 and K_2 for the catchol complex, a value much greater than 30 for K_1 does not seem likely. It thus appears that neglect of this pyrogallol complex will not seriously affect the conclusions of this work.

A single absorption peak at 3567 cm^{-1} was found for solutions of guaiacol in carbon tetrachloride indicating that the cis form of this phenol is preferred in this solvent. Likewise only a single absorption peak is observed in 0.1 M ether solution. No change in the molar absorptivity except that due to the temperature dependence was found in the presence of 0.1 M diethyl ether. Ether concentrations in excess of 0.2 M likewise did not cause disruption of the intramolecular bond. Tetrahydrofuran, a stronger proton acceptor than diethyl ether, was also found not to cause disruption of the intra bond. On the basis of the entropy and enthalpy changes found for the reactions of eq 2 and 6, both ΔH and ΔS would be expected to be positive for the formation of a guaiacol–ether complex. The positive entropy change would favor the formation of the complex while the enthalpy change, probably positive due to the energy required to break the intramolecular bond, is unfavorable. Because no complex formation between guaiacol and ether is observed the enthalpy change must overshadow the entropy change to such an extent that the equilibrium constant is too small to allow observation of the complex by spectroscopic methods.

Acknowledgment. Support for this work was provided by Research Corporation through the Cottrell College Science Grants program.

References and Notes

(1) D. H. McDaniel and H. C. Brown, *Science*, **118**, 370 (1953).
(2) G. C. Pimentel and A. L. McClellan, "The Hydrogen Bond," W. H. Freeman, San Francisco, Calif., 1960, pp 181–183.
(3) T. Gramstad, *Spectrochim. Acta*, **19**, 497 (1963).
(4) D. L. Powell and R. West, *Spectrochim. Acta* **20**, 983 (1964).
(5) L. J. Bellamy, G. Eglinton, and J. F. Morman, *J. Chem. Soc.*, 4762 (1961).
(6) E. A. Robinson, H. D. Schreiber, and J. N. Spencer, *J. Phys. Chem.*, **75**, 2219 (1971).
(7) D. Bloser, J. Murphy, and J. N. Spencer, *Can. J. Chem.*, **49**, 3913 (1971).
(8) E. Fishman and Tun Li Chen, *Spectrochim. Acta*, **25**, 1231 (1969).
(9) W. K. Busfield, M. P. Ennis, and I. J. McEwen, *Spectrochim. Acta*, **29**, 1259 (1973).
(10) L. Kuhn and R. E. Bowman, *Spectrochim. Acta*, **17**, 650 (1961).
(11) J. Finch and E. Lippincott, *J. Phys. Chem.*, **61**, 894 (1957).

Effect of Chain Length on Heats of Mixing in Tri-*n*-alkylamine–Benzene Systems[1a]

A. S. Kertes*[1b] and F. Grauer

Institute of Chemistry, The Hebrew University, Jerusalem, Israel *(Received July 12, 1973)*

Excess enthalpies of mixing normal triethyl-, tributyl-, trioctyl-, and tridodecylamine with benzene at 303.15°K are compared. The data for the first system were taken from the literature, the others measured in this laboratory, the last one having been reported earlier. All heats of mixing are endothermic, increasingly so with increasing chain length of the amine. The effect of chain length is explained as being due to an increased shielding of the lone-pair nitrogen electrons, decreasing thus its availability for bonding with the π electrons of benzene. The results were analyzed in terms of a model involving the lattice theory of mixtures and group and molecular interchange enthalpies of interacting surfaces. The calculated parameters support the above hypothesis.

The systems under considerations are representative of noninteracting nonelectrolytes in which specific interactions should not be expected. Nevertheless, a possible n–π interaction between the nonassociated triethylamine and benzene has been suggested in recent years.[2-5] That conclusion was based on the comparison of heats of mixing of triethylamine with *n*-heptane and benzene. The former binary system is nearly ideal with H_{max}^E of about 84 J mol^{-1} (at an equimolar composition) at 25°, as compared to about 330 J mol^{-1} in the latter system under similar conditions.[2,4] More recent heats of mixing data from this laboratory[6] suggest that if such an interaction involving triethylamine exists, its extent must be seriously diminished in similar mixtures of the equally nonassociated tridodecylamine. The corresponding maximum excess enthalpies of mixing at 30° were found to be ~64 and ~1350 J mol^{-1} in tridodecylamine–*n*-octane and -benzene systems, respectively. It has been suggested[6] that the effect is due to an effective screening of the lone-pair nitrogen electrons by the three long aliphatic chains, decreasing thus the extent of possible n–π interactions.

In the above comparison, the difference in the heat effects due to the molar volume between *n*-heptane (triethylamine system) and *n*-octane (tridodecylamine system) is negligibly small[2,7,3] and can be neglected. Accordingly, the differences in H_{max}^E between amine–alkane and amine–benzene systems, which is a factor of 4 in the case of triethylamine, but becomes a factor of 20 in the case of tridodecylamine, merits further consideration.

We now report the heats of mixing of a number of long-chain normal and symmetrical tertiary amines with benzene at 30° as determined calorimetrically. The enthalpies of mixing in these binary systems were found to be increasingly asymmetric and endothermic as the number of carbon atoms per chain increases from two to twelve.

Experimental Section

Tri-*n*-butylamine (BDH) and tri-*n*-octylamine (Fluka), of the highest purity commercially available, were purified by fractional distillation under reduced pressure. The fractions collected gave a single peak when gas chromatographed on a 1.5-m long column of S.E.30(15%) at 150° for tributyl-, and 300° for trioctylamine. The estimated purity was 99.8 and 99.9%, respectively. The boiling point of tributylamine was found to be 91.2° at 9 mm, as compared to 91° given in the literature.[9] The densities of the purified products were as follows: tributylamine 0.7784 g/ml at 20° as compared to 0.7782 in the literature;[9] trioctylamine 0.8086 at 25°, 0.8088 in the literature.[10] Benzene (Mallinckrodt) was dryed over sodium for several days prior to distillation, and after it. The purity, checked by gas chromatography using a 2-m long column of Apiezon L 10% at 150°, was better than 99.85%. The density was 0.8687 at 30°, as compared to 0.8685 given in the literature.[11] The water content of the amines and benzene was determined by Karl Fischer titration and found that the purified compounds contained less than 0.01% of water. It is essential that the components be anhydrous in view of the fact[12] that even small concentrations of water in either of the components could have significant effect on the relatively small heat effects recorded in this study.

Heats of mixing were determined at 30.000 ± 0.001° using a Tronac Model 1000A continuous automatic titration calorimeter. The calorimeter, experimental method, and calculation procedures were identical with those described earlier.[6,13]

Results

The experimental excess enthalpies of mixing for benzene with tri-*n*-butylamine and tri-*n*-octylamine are compiled in Table I. The smoothed values at 0.1 mole fraction intervals for all four trialkylamine–benzene systems considered here are given in Table II. Those for tridodecylamine have been taken from our earlier report,[6] and those of triethylamine are taken from the literature.[4] The latter system has been reported in three publications[3,4] by two different teams. A comparison reveals that over most of the composition range there are significant differences among the three sets of heat of mixing data. Letcher and Bayles' data at 25 and 45° refer to a much wider composition range, and have been adopted here for comparison with our own results. The enthalpies of mixing listed in Table II at 30° were calculated by Kirchhoff's equation assuming that the molar heat capacity is constant within the temperature range studied.

Discussion

Chemical Interaction. Let us first discuss in qualitative chemical terms the increasingly positive enthalpies of mixing with increasing number of carbon atoms in the

TABLE I: Excess Enthalpies of Mixing of Tri-*n*-butylamine and Tri-*n*-octylamine with Benzene at 303.15°K[a]

$(C_4H_9)_3N$		$(C_8H_{17})_3N$	
x_2	H^E	x_2	H^E
0.1330	255.6	0.1942	351.7
0.2399	461.5	0.2872	538.1
0.3277	592.3	0.3610	667.3
0.4005	689.6	0.4553	812.8
0.4623	744.5	0.5252	918.3
0.5153	781.1	0.6160	1023
0.5611	802.4	0.7025	1062
0.6010	813.2	0.7621	1062
0.6359	819.5	0.8053	1023
0.6687	814.1	0.8383	965.8
0.6965	800.9	0.8720	882.9
0.7208	785.9	0.9029	780.2
0.7425	762.9		
0.7798	716.5		
0.7958	689.7		
0.8104	663.2		
0.8239	636.1		

[a] x_2 = mole fraction of benzene; H^E, joules per mole.

alkyl chains of the amine. By a quasichemical interaction approach one may assume that the observed heats are resultant of two thermal effects of opposite signs: (i) the endothermic effect of disrupting the π–π bounds of the associated benzene, and (ii) the exothermic effect of newly formed bonds between the lone-pair electrons of nitrogen and the π electrons of benzene. In the triethylamine–benzene mixtures, effect ii compensates for a sizeable fraction of effect i, and the net resulting enthalpies of mixing are relatively small. They are only four times that of the $H_{max}{}^E$ in the triethylamine–alkane system,[4] where obviously neither of the interactions is operative, and the endothermic heats of mixing are essentially due to nonspecific interactions. While with increasing chain length of the amine (increasing aliphaticity of the molecule), effect i becomes of course more pronounced, the main reason for increased endothermic enthalpies of mixing is still the markedly lower compensation by effect ii. The physical meaning of the decreased compensation by effect ii is that of screening of the lone-pair nitrogen electrons from the sight of benzene's π electrons, and fewer exothermic n–π bonds formed as a consequence.

Similar are the trends in heats of mixing observed in *n*-alcohol–benzene[14] and in the homologous series of symmetrical di-*n*-alkyl ether–benzene[15] systems. In the ether systems, the excess enthalpies of mixing of equimolar mixtures have the values of ~0, ~185, and ~310 J mol^{-1} for diethyl, dipropyl and dibutyl ethers, respectively. This effect of chain length on the variation of H^E is however significantly smaller than in the tertiary amine–benzene systems under consideration. The more pronounced influence of the chain length in our systems is most probably due to a more effective screening of the functional donor group by three alkyl chains in the amines, as compared to only two alkyl chains of the dialkyl ethers. From diethyl to dibutyl ether there is a difference in the corresponding H^E values of only 310 J mol^{-1}, as compared to ~500 J mol^{-1} between triethyl- and tributylamine. In the *n*-alcohol–benzene systems the difference in H^E (equimolar mixtures) between ethanol–benzene and butanol–benzene systems in only 270 J mol^{-1} in the same direction. These systems, however, may not be strictly comparable to the previous ones since alcohols are hydrogen-bonded associated liquids, where the extent of association is affected by the chain length.

TABLE II: Smoothed Values of Excess Enthalpies of Mixing of Tri-*n*-alkylamines with Benzene at 303.15°K[a,b]

x_2	$(C_2H_5)_3N$[4]	$(C_4H_9)_3N$	$(C_8H_{17})_3N$	$(C_{12}H_{25})_3N$[5]
0.1	116.6	202.2	212.4	258.2
0.2	209.6	380.4	380.9	546.4
0.3	276.9	550.4	550.2	788.7
0.4	319.7	683.7	709.0	972.3
0.5	339.5	775.1	880.0	1120
0.6	328.1	818.0	1025	1251
0.7	293.0	796.3	1093	1342
0.8	226.4	683.1	1013	1314
0.9	129.2	437.4	686.2	975.3

[a] Smoothing equations: $(C_4H_9)_3N$–benzene, 303.15°K, $H^E = x_1x_2[3100 - 1384(x_1 - x_2) + 707(x_1 - x_2)^2 - 389(x_1 - x_2)^3]$ $(C_8H_{17})_3N$–benzene, 303.15°K, $H^E = x_1x_2[3520 - 3290(x_1 - x_2) + 2300(x_1 - x_2)^2]$, $(C_{12}H_{25})_3N$–benzene, 303.15°K, $H^E = x_1x_2[4480 - 2704(x_1 - x_2) + 3695(x_1 - x_2)^2 - 3525(x_1 - x_2)^3]$. [b] x_2 = mol fraction of benzene, H^E, joules per mole.

We offer this argument of comparisons in support of the hypothesis that it is the diminishing compensation by effect ii (screening efficiency) rather than the increased extent of effect i which governs the trend of endothermicity in the homologous series discussed.

In somewhat different terms, but still to the same point, the electronegativity of the nitrogen atom should decrease with increasing chain length of tertiary alkylamines.[16] The effect, of course, is expected to be more pronounced with the lower members of the homologous series. A decreasing electronegativity means increasing electron-donating property, which in turn means enhanced basicity of the amine. However, the basicity of a series of normal tertiary amines, including those discussed here, in organic solvents, among them benzene, indicates that the influence of the chain length on the pK values derived from spectral measurements[17] is very small. It is again the shielding effect of the alkyl chains on the electron-donor nitrogen atom which compensates for the increased basicity of the amines, acting as a kind of steric hindrance.[16]

Due primarily to the large differences in the molar volumes of the components, but also to the changing partial compensation of the effects discussed above, the shape of the H^E *vs.* x_2 curves becomes increasingly asymmetric as the molecular weight of the amine increases. Figure 1 gives the experimental H^E points for the three amines studied in this laboratory, and the smoothed H^E values at 0.1 mole fraction intervals for the triethylamine–benzene system as taken from the literature (Table II). At low benzene mole fractions, a large proportion of the benzene molecules will be interacting with the amine so that the expected positive contribution due to the rupture of the benzene–benzene bonds is not fully realized. At the other end, in the benzene-rich region, the exothermic compensation by n–π bonds becomes increasingly smaller with the higher members of the homologous series.

Statistical Thermodynamic Model. Turning now to the quantitative interpretation of the enthalpy data, it is apparent that the binary systems reported here can provide a good test for the generalized lattice theory of Barker, since they refer to a homologous series of nonassociated molecules containing identical groups. The ratio of nitro-

gen atom to the number of methylene groups is sufficiently different, in the series ranging from 1/3 in triethylamine to 1/33 in tridodecylamine, to lead to significant differences in the excess enthalpies of mixing with the same solvent. To satisfy this requirement, however, benzene (or other aromatic solvents[6]) had to be chosen rather than an alkane, because the heat effects with the latter solvent are small, amounting to a difference in $H_{max}{}^{E}$ of only about 30 J mol^{-1} between triethyl- and tridodecylamine,[4,6] as compared to over 1000 J mol^{-1} when benzene is used as the second component.

Thus the experimental results can be treated by a combination[15,18] of the group interaction model[19-21] and the zeroth approximation form of the lattice theory of mixtures[22,23] for molecules of different sizes at a completely random arrangement.

It is supposed that each molecule, i, consists of m_i segments, each occupying one site on a lattice of coordination number z. The number of contact points for each type of molecule i is thus given by

$$s_i = m_i(z - 2) + 2 \quad (1)$$

Each segment on the surface of the molecule has a characteristic capability of interaction which is proportional to the "group cross section" s^u, s^v, s^t ... of u, v, t .... type surfaces of molecule i. The "molecular group sections" are thus defined by

$$s_i = \Sigma m_i{}^u s^u \quad (2)$$

representing the sum of the appropriate group cross sections of molecule i. Following Kehiaian,[15] the corresponding "molecular coverages" are defined by the ratio

$$\alpha_{is} = m_i{}^u s^u / s_i \quad (3)$$

For the binary systems under consideration, according to the model of characteristic group interactions, we take that the surface of amine molecules is composed of aliphatic (CH_3 and CH_2) and amine-nitrogen elements, and that of the homogeneous benzene molecule, of one aromatic element. Thus, in terms of the theory, the three interacting surfaces are (u) aliphatic, (v) aromatic, and (t) amine nitrogen assuming that the methyl and methylene surfaces are of the same kind.[15]

The experimentally determined excess enthalpy of mixing per mole of mixture is defined[16] as

$$H^E = s_1 s_2 \frac{x_1 x_2}{s_1 x_1 + s_2 x_2} A_{12} \quad (4)$$

(x = mole fraction) through the "molecular interaction parameter" A_{12}, given for our binary systems with a total of three characteristic surfaces u, v, and t, by the relationship

$$A_{12} = -[k^{uv}(\alpha_1{}^u - \alpha_2{}^u)(\alpha_1{}^v - \alpha_2{}^v) + k^{ut}(\alpha_1{}^u - \alpha_2{}^u)(\alpha_1{}^t - \alpha_2{}^t) + k^{vt}(\alpha_1{}^v - \alpha_2{}^v)(\alpha_1{}^t - \alpha_2{}^t)] \quad (5)$$

where k^{uv}, k^{ut}, and k^{vt} are the "molar interchange enthalpies" per conventional unit area of the interacting surfaces indicated by the superscripts, and the sum of all molar coverages for any given molecule is equal to unity

$$\alpha_1{}^u + \alpha_1{}^v + \alpha_1{}^t = \alpha_2{}^u + \alpha_2{}^v + \alpha_2{}^t = 1 \quad (6)$$

Group and Molecular Parameters. The group and molecular cross sections and the corresponding derivatives of molar coverages were estimated by adopting a lattice coordination number of $z = 8$, thus an area of 0.125 for each bond.[15] Accordingly, in the tertiary amine molecules, each methyl, methylene, and nitrogen group constitute one section which would have a value of unity in the isolated state, but

$$s^{CH_3} = 0.875 \text{ (one bond per group)}$$
$$s^{CH_2} = 0.750 \text{ (two bonds)}$$
$$s^{N} = 0.625 \text{ (three bonds)}$$

when chemically bound.

For the benzene molecule, Kehiaian[15] has derived the value of $s^{C_6H_6} = s_2 = 3.800$, which has been adopted for the present calculations.

From these values of group sections, the molecular cross sections, the four s_1 values corresponding to the four different amines, were calculated by simple addition, and the values obtained are

$$s_{(C_2H_5)_3N} = 5.500$$
$$s_{(C_4H_9)_3N} = 10.000$$
$$s_{(C_8H_{17})_3N} = 19.000$$
$$s_{(C_{12}H_{25})_3N} = 28.000$$

The corresponding molecular coverages of interest for the binary systems under consideration are only those of the amine coverages

$$\alpha_{(C_nH_{2n+1})_3N} = s^N / s_{(C_nH_{2n+1})_3N} \quad (7)$$

with the values

$$\alpha_{(C_2H_5)_3N} = 0.1135$$
$$\alpha_{(C_4H_9)_3N} = 0.0625$$
$$\alpha_{(C_8H_{17})_3N} = 0.0329$$
$$\alpha_{(C_{12}H_{25})_3N} = 0.0223$$

Molar Interchange Enthalpies. The molar interchange enthalpies k^{uv}, k^{ut}, and k^{vt}, account for the thermal effect of interactions of the various groups occurring in randomness of the molecules in the solution. The aliphatic (u)-aromatic (v) interchange enthalpy, k^{uv}, has been determined previously[15] from heat of mixing data for a large number of benzene-*n*-alkane mixtures using eq 4 and 5, when $\alpha_1{}^v$, $\alpha_2{}^u$, and $\alpha_i{}^t$ are equal to zero and $\alpha_1{}^u = \alpha_2{}^v = 1$ (subscript 1 = *n*-alkane; 2, benzene), thus

$$A_{12} = k^{uv} \quad (8)$$

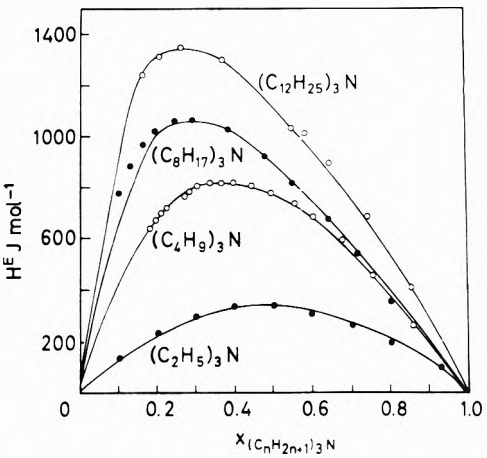

Figure 1. Comparison of theory with experiment for the excess enthalpies of mixing of tri-*n*-alkylamines with benzene at 303.15°K. Points show experimental results, except for $(C_2H_5)_3N$ for which the points were those from Table II. Full lines show values predicted by the theory (see text).

While, of course, the molar interchange enthalpies should be temperature dependent, a recalculation of the experimental data at 20 and 25° of the sources quoted by Kehiaian,[15] and new[24] data for the benzene-*n*-octane system at 30°, have shown that the temperature coefficient of k^{uv} in the 20–30° temperature range is such as to increase the uncertainty by an additional 2.4%, to a total of 3.6%. Thus, a more conservative value of k^{uv} should be 830 ± 30 J mol^{-1}, rather than 830 ± 10 J mol^{-1} given by Kehiaian.[15]

For the estimation of the aliphatic (u)–amine (t) interchange enthalpy, k^{ut}, when α_1^u, α_2^t, and α_i^v are equal to zero, and α_2^u is unity (subscript 1 = amine; 2, *n*-alkane), eq 5 becomes

$$A_{12} = k^{ut}(\alpha_1^t)^2 \qquad (9)$$

The k^{ut} values derived from the two systems available for estimation, those of triethylamine-*n*-heptane[4] and tri-*n*-dodecylamine-*n*-octane,[6] while internally consistent, were much at variance with no possibility for a sensible estimate of an average value. We have thus adjusted both k^{ut} and k^{vt} values by a least-squares computer program to fit the experimental data for all four trialkylamine–benzene systems under consideration. For the calculation of the latter interchange enthalpy, k^{vt}, eq 5 was used in the form

$$A_{12} = (1 - \alpha_1^t)k^{uv} + \alpha_1^t(1 - \alpha_1^t)k^{ut} + \alpha_1^t k^{vt} \qquad (10)$$

since in the interchange between benzene (v) and amine (t), the values of α_1^v, α_2^u, and α_2^t are equal to zero, α_2^v = 1 and $\alpha_1^u = 1 - \alpha_1^t$ (subscript 1 = amine; 2, benzene).

k^{ut} and k^{vt} thus adjusted have the values of 15,000 ± 700 and 9500 ± 500 J mol^{-1}, respectively. The fit of the calculated H^E values is shown in Figure 1 along with the experimentally determined points. The agreement found should be considered satisfactory. As additional and reliable heat of mixing data gradually become available on tertiary amine–*n*-alkane systems, it will be possible to calculate the two interchange enthalpies separately, which then will eliminate the need for the least-squares adjustment employed here.

References and Notes

(1) (a) Presented in part at the 3rd International Conference on Chemical Thermodynamics, Vienna-Baden, Sept 1973. (b) Present address, Department of Chemistry, McGill University, Montreal, Canada.
(2) H. Kehiaian, *Bull. Acad. Polon. Sci., Ser. Sci. Chim.*, **14**, 703 (1966).
(3) (a) H.-J. Bittrich, Ch. Kupsch, R. Gotter, and G. Bock, *Proc. Int. Conf. Calor. Therm., First. Warsaw* (1969); (b) R. Siedler, L. Grote, E. Kauer, U. Werner, and J.-H. Bittrich, *Z. Phys. Chem.*, **241**, 203 (1969).
(4) T. M. Letcher and J. W. Bayles, *J. Chem. Eng. Data*, **16**, 266 (1971).
(5) T. M. Letcher and J. W. Bayles, *J. S. Afr. Chem. Inst.*, **25**, 53 (1972).
(6) F. Grauer and A. S. Kertes, *J. Chem. Eng. Data*, **18**, 405 (1973).
(7) R. Siedler and H.-J. Bittrich, *J. Prakt. Chem.*, **311**, 721 (1969).
(8) J. H. van der Waals and J. J. Hermans, *Recl. Trav. Chim. Pays-Bas*, **69**, 971 (1950).
(9) "Dictionary of Organic Compounds," Vol. 5, Oxford University Press, New York, N. Y., 1965, p 3108.
(10) R. R. Dreisbach, *Advan. Chem. Ser.*, **No. 29**, 384 (1961).
(11) J. A. Riddick and W. B. Bunger, "Organic Solvents," 3rd ed, Wiley-Interscience, New York, N. Y., 1970.
(12) P. R. Garrett, J. M. Polock, and K. W. Morcom, *J. Chem. Thermodyn.*, **3**, 135 (1971).
(13) A. S. Kertes and E. F. Kassierer, *Inorg. Chem.*, **11**, 2108 (1972).
(14) I. Brown, W. Fock, and F. Smith, *J. Chem. Thermodyn.*, **1**, 273 (1969).
(15) H. V. Kehiaian, K. Sosnkowska-Kehiaian, and R. Hryniewicz, *J. Chim. Phys.*, **68**, 922 (1971).
(16) M. Tamres, S. Searles, E. M. Leighly, and D. W. Mohrman, *J. Amer. Chem. Soc.*, **76**, 3983 (1954).
(17) A. Rieux, M. Rumeau, and B. Tremillon, *Bull. Soc. Chim. Fr.*, 1053 (1964).
(18) H. V. Kehiaian, *J. Chim. Phys.*, **68**, 935 (1971).
(19) H. Tompa, *Trans. Faraday Soc.*, **45**, 101 (1949).
(20) O. Redlich, E. L. Derr, and G. J. Pierotti, *J. Amer. Chem. Soc.*, **81**, 2283 (1958).
(21) M. N. Papadopoulos and E. L. Derr, *J. Amer. Chem. Soc.*, **81**, 2285 (1958).
(22) E. A. Guggenheim, "Mixtures," Clarendon Press, London, 1952.
(23) R. W. Kershaw and G. N. Malcolm, *Trans. Faraday Soc.*, **64**, 323 (1968).
(24) F. Grauer, Ph.D. Thesis, The Hebrew University, Jerusalem, 1973.

Mass Spectra of Rare Earth Triiodides

C. Hirayama* and P. M. Castle

Westinghouse Research Laboratories, Pittsburgh, Pennsylvania 15235

(Received July 23, 1973)

Publication costs assisted by the Westinghouse Research and Development Center

The mass spectra of vapors over the stable lanthanide triiodides have been measured. Enthalpies of sublimation of the triiodides and enthalpies of formation and dissociation of the positive ions have been estimated. The electron impact fragmentation pattern of these iodides is discussed.

1. Introduction

Except for samarium, europium, ytterbium, and lutetium, the trivalent salt is the normally stable state for the lanthanides. The divalent salt is the normally stable state for the four exceptions. In these stable valence states the halides of the lanthanides are believed to vaporize as the monomeric molecule in the region of low pressures. Mass spectrometric evidences for the congruent evaporation of the monomer have been obtained for a number of stable trifluorides[1] and trichlorides,[2] and also of some stable di-

chlorides,[3] dibromides,[4] and diiodides.[5] There has been no report of the mass spectra of stable lanthanide triiodides other than NdI_3.[6]

We earlier reported on the mass spectra of vapors over NdI_3 and SmI_3,[6] as well as the vapor pressures over NdI_3 and PrI_3.[7] Although the vapor pressures over most of the lanthanide fluorides and chlorides have been measured, this has not been the case with the iodides. Feber[8] had earlier estimated the enthalpies of sublimation of all of the lanthanide iodides, and his estimates have generally been in excellent agreement with the small number of measured values. We have measured the vapor pressures of a number of lanthanide iodides, and have determined the mass spectra of vapors over these iodides. We here report on the mass spectra of the vapors over the stable triiodides. A number of thermodynamic quantities have been obtained, and the fragmentation pattern of these iodides on electron impact is also summarized.

2. Experimental Section

2.1. Materials Preparation. The triiodides were prepared by the direct reaction of the metal with iodine vapor. The metal (99.9% purity in all cases) was contained in a crucible of tungsten, molybdenum, or tantalum which was placed in a fused silica tube. After resublimed iodine was admitted into a side arm of the silica tube, the system was evacuated at least to 10^{-4} Torr and sealed. The crucible section of the silica tube was placed in a furnace while the iodine pressure was controlled by the temperature of the side arm. The reaction temperature was maintained slightly above the melting point of the iodide. The iodides were subsequently purified by sublimation. Analysis of the products all showed at least 99.99% purity of the triiodides.

2.2. Measurements. The mass spectra were measured on a Bendix time-of-flight mass spectrometer, Model 12-101, with a Knudsen cell attachment supplied by Bendix. The spectrometer and Knudsen cell system have been described by White, *et al.*[9] The tantalum Knudsen cell was heated by radiation in all of the measurements. The cell was constructed of a cylindrical, machined cup of 0.5 in. i.d. × 0.5 in. depth, over which was slip-fitted a cap with an orifice of approximately 0.25 in. The cap was machined internally with a ledge so that it seated firmly onto the bottom cup. A tantalum foil of 2 mil thickness, with an orifice of 0.030 in. in the center, was placed between the cup and the cap. A Pt–Pt—10% Rh thermocouple was placed in a recess in the bottom of the cell for temperature measurements.

Approximately 0.3–0.5 g of sample was loaded into the cell for each run. In the loading operation, the sample vial was first placed in a polyethylene glove bag (Instruments for Research and Industry), which was connected to argon and vacuum lines. The bag was then hermetically sealed above the flange attachment of the Knudsen cell chamber to the mass spectrometer. The bag was flushed with argon, and this atmosphere was maintained while the Knudsen cell chamber was released from the spectrometer, loaded with the sample, and reattached. The Knudsen cell was then evacuated at approximately 10^{-6} Torr for a few hours while keeping the cell at about 250°. The cell was then heated and the spectrum scanned rapidly, generally at 28 V. As soon as species were detected above the background, the temperature was stabilized to within ±3°, and the spectrum was scanned at the appropriate gain and recorded on a Hewlett-Packard Model 7100B recorder. The spectrum was recorded at several temperatures to obtain the relative intensities of the different species. The shuttering effect on each species was also recorded at at least one temperature. The relative multiplier gains were obtained by measuring the intensity of a given peak, usually a peak of high intensity, at different gain settings.

The ionization efficiency curves were determined by the usual method for this instrument using a Keithley digital multimeter of ±0.05-V accuracy for the electron energy measurements. The ionization efficiency curves of nitrogen and of oxygen were determined as internal standards for the determination of appearance potentials (AP). The AP were determined by linear extrapolation with measurements generally at 0.5-V intervals.

3. Results

The lanthanide triiodides all sublime congruently as the monomolecular MI_3, where M is the lanthanide. This is verified, in part, by the parallel plots of the usual log IT *vs.* $1/T$, where I is the ion intensity, T the absolute temperature, and IT is proportional to the partial pressure, for all of the lanthanide-containing species for any given triiodide. Although most of the spectra were determined at an electron-accelerating energy of 28 eV, the spectra for CeI_3 and NdI_3 were obtained also at 44 eV. At the latter accelerating energy, doubly charged ions were also observed. For example, CeI^{2+}, Ce^{2+}, and CeI_2^{2-} were observed in decreasing abundance in the order shown. At 28 eV the doubly charged ions were generally not detected because of the high appearance potentials, >25 eV, of these ions. The measurements of the singly charged ions at 28 eV were based on the observation that the ionization efficiency curves for these species leveled off above 20 eV.

The mass spectra of the triiodes all showed strong intensities from I_2^+ and I^+. The former ion showed practically no shuttering effect whereas the I^+ shuttered to the extent of approximately 20%. The lanthanide-containing species, on the other hand, showed complete shuttering. The appearance potential of the I_2^+ (~10.0 eV) and I^+ (~13.5 eV), and the lack of shuttering of these ions show that I_2 is the parent. The iodine arises predominantly from the desorption from the ionization chamber and to a certain extent from the Knudsen cell chamber walls. Gupta[10] has observed similar strong I_2^+ and I^+ peaks arising from wall desorption in the mass spectrometric measurement of tungsten iodide. However, the fact that the I^+ intensity showed some shuttering effect suggests that some I(g) may be effusing out of the Knudsen cell. Some indication of this gaseous species was suggested by a relatively long tail on the low-energy side of the efficiency curve. Presently, we cannot conjecture the reaction source from which this species originates. It does not appear to be from the decomposition of the triiodides since these compounds all evaporate congruently. Furthermore, these salts evaporate completely without any residue at the measurement temperatures; if the iodine originated from the decomposition of the triiodide the other product would be a low vapor-pressure, lower iodide or the metal.

Table I summarizes the relative intensities of all of the stable lanthanide triiodides measured in this work. The most intense ion peak in these iodides is that of the MI_2^+ ion. In the first group of the rare earths, Ce, Pr, and Nd, the relative intensities decrease in the order $MI_2^+ > M^+$

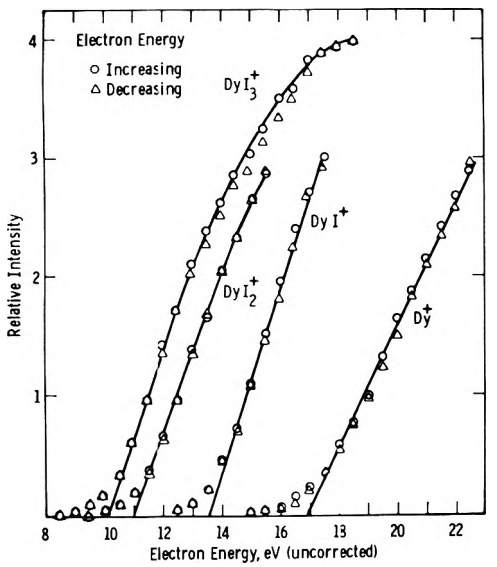

Figure 1. Ionization efficiency curves for ions from DyI_3.

> MI^+ > MI_3^+. The intensity of the MI_3^+ is also only 0.1–0.2 of that for the MI_2^+ ion in this group. Similar relative intensities have been reported for ions from NdF_3, LaF_3,[1] and $LuCl_3$.[2] However, in the spectrum of GdI_3 the relative intensities vary as GdI_2^+ > GdI_3^+ > GdI^+ ~ Gd^+, and the GdI_3^+ intensity is 0.69 that of the GdI_2^+ ion. There does not appear to be any definite trend in the relative intensities of the ions in the second group of rare earth triiodides after GdI_3, but the MI_3^+ relative intensity is 0.4 to 0.6 of that for the MI_2^+ ion.

Figure 1 shows the ionization efficiency curves for ions from DyI_3 taken at decreasing and at increasing electron energies at 0.5-eV intervals. The efficiency curves for the other iodides were similar to those in this example. However, the measurements for CeI_3 and NdI_3 were made at 1.0-eV intervals. The estimated error in the AP from curves similar to those in Figure 2 was ±0.2 eV, while the estimated error for the AP for ions from CeI_3 and NdI_3 were ±0.5 eV. Table II summarizes the AP's of the single-valent positive ions, as well as the calculated AP's for the M^+ ions, based on the ionization potentials of the lanthanide metals[11] and the enthalpies of atomization of the gaseous triiodides.[8] The AP's of the lanthanide iodide positive ions are generally lower than those reported for the lanthanide chlorides and fluorides, with the AP's decreasing in the order fluorides > chlorides > iodides. The magnitudes of the AP's of the iodides in Table II are in agreement with those expected for the processes.

$$MI_3 + e \longrightarrow MI_3^+ + 2e$$

$$MI_3 + e \longrightarrow MI_2^+ + I + 2e$$

$$MI_3 + e \longrightarrow MI^+ + 2I + 2e$$

$$MI_3 + e \longrightarrow M^+ + 3I + 2e$$

Hariharan and Eick[5] recently reported on the mass spectra of EuI_2. The AP's of the ions obtained for the positive ions from this normally stable diiodide are 8.8, 9.9, and 12.4 eV for EuI_2^+, EuI^+, and Eu^+, respectively. We have obtained similar values of the AP's of ions from SmI_2,[12] *i.e.*, 8.7, 9.2, and 12.5 eV for the ions SmI_2^+, SmI^+, and Sm^+, respectively.

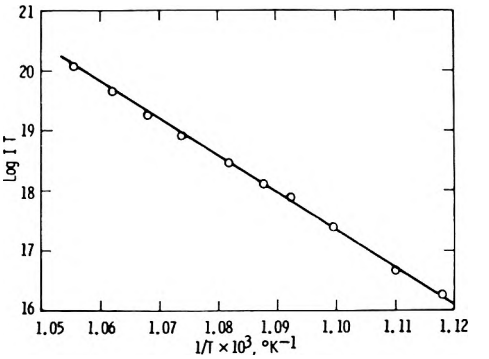

Figure 2. Log IT *vs.* $1/T$ for the DyI_2^+ ion.

TABLE I: Mass Spectra of Rare Earth Triiodides

	Rel intensity at 23 eV			
	MI_3^+	MI_2^+	MI^+	M^+
CeI_3	14	100	29	76
PrI_3	17	100	34	58
NdI_3	11	100	28	69
GdI_3	69	100	66	47
TbI_3	37	100	41	38
DyI_3	50	100	32	32
HoI_3	51	100	39	70
ErI_3	58	100	43	69

Heats of sublimation of the lanthanide triiodides were obtained from the slopes of the log IT *vs.* $1/T$ plots of the MI_2^+ ions. This ion was chosen because of its highest intensity in the spectra. Figure 2, for the DyI_2^+ ion, shows a typical plot of the data for the triiodes. Table III summarizes the mass spectrometric heat of sublimation. The mass spectrometric heat of sublimation for PrI_3 and NdI_3 at measurement temperatures around 900°K are not included because of the low values of 52 and 54 kcal/mol, respectively. The reason for this discrepancy is not known at present. The enthalpies of sublimation were extrapolated to 298°K by assuming $\Delta Cp = -14$ cal/mol deg. Table III also summarizes the $\Delta H_s°_{298}$ for all of the triiodides measured. The $\Delta H_s°_{298}$ for PrI_3 and NdI_3 are values obtained earlier from vapor pressure measurements.[7] The mass spectrometric $\Delta H_s°_{298}$ for CeI_3 and DyI_3, 79.0 ± 5 and 69.4 ± 1.6 kcal/mol, respectively, are in excellent agreement with the values obtained from vapor pressure measurements.[13] The latter values of $\Delta H_s°_{298}$ for CeI_3 and DyI_3 are 77.0 ± 1.0 and 68.1 ± 0.6 kcal/mol, respectively. Earlier, Feber[8] had summarized the enthalpies of sublimation of all of the lanthanide halides, only few of which were experimental values. Table III shows that Feber's values agree excellently with those obtained in our laboratory.

We have utilized Feber's $\Delta H_f°_{298}$ of the solid triiodides, the experimental enthalpies of sublimation, the enthalpy of formation of I(g),[14] and the appearance potentials of Table II to calculate the enthalpies of formation of the positive iodide ions. These enthalpies of formation are summarized in Table IV. It was also of interest to estimate the enthalpies of dissociation of the positive ions for the processes $MI_n^+ \rightarrow MI_{n-1}^+ + I$ in order to determine the relative strength of the $I\text{-}MI_{n-1}^+$ bond of the ions. Table IV also summarizes this bond dissociation energy of the ions. It is seen that the dissociation energies of the

TABLE II: Appearance Potentials of Positive Ions

	AP, eV										
	MI_3^+		MI_2^+		MI^+		M^+		MI^{2+}		M^+, calcd
CeI_3	9.6	±0.5	9.7	±0.5	13.6	±0.5	17.7	±0.5	28	±1	>16.7
PrI_3	9.2	±0.2	10.0	±0.2	12.9	±0.2	17.0	±0.2			16.0
NdI_3	9.2	±0.5	9.3	±0.5	13.6	±0.5	15.9	±0.2			15.7
GdI_3	9.2	±0.2	10.1	±0.2	13.5	±0.2	17.0	±0.2			16.4
TbI_3	9.5	±0.2	10.5	±0.2	13.7	±0.2	17.6	±0.2			16.2
DyI_3	9.6	±0.2	10.5	±0.2	13.1	±0.2	16.4	±0.2			15.2
HoI_3	9.2	±0.2	10.4	±0.2	13.2	±0.2	16.7	±0.2			15.7
ErI_3	9.0	±0.2	10.2	±0.2	13.3	±0.2	16.2	±0.2			15.9

TABLE III: Heats of Sublimation, kcal/mol

	ΔH_T	T, °K	$\Delta H_s°_{298}$	$\Delta H_s°_{298}$ (Feber)
CeI_3	69.7	933	79 ± 5	77
PrI_3			78.9 ± 1.5	76.0
NdI_3			77.8 ± 0.6	74.9
GdI_3	61.1	943	70.5 ± 0.5	70
TbI_3	58.8	931	68.0 ± 0.5	69.5
DyI_3	60.4	916	69.4 ± 1.6	68.5
HoI_3	64.0	880	72.5 ± 1.8	68
ErI_3	60.7	895	69.4 ± 3.8	67

MI_3^+ ions are significantly lower than those of the MI_2^+ and MI^+ ions.

4. Discussion

Hastie and Margrave[15,16] have extensively discussed the mass spectra of metal halides. They have obtained correlations between the ionization potentials of some mono- and dihalides with the bond type. They have also shown, from available mass spectroscopic data, that the fragmentation pattern of halides with open electron shell type shows predominantly the parent ion. In contrast, the halides of closed electron shell type show the parent ion in least abundance, while the most abundant species in the mass spectrum is that with one less halogen than the parent. They also indicate that the more covalently bonded species, such as the iodide, are less likely to fragment than ionic bonded species. These generalizations are not so simply applied to the rare earth halides with unfilled f orbitals, but the rules derived by Hastie and Margrave are helpful.

The stable lanthanide triiodides studied here behave similarly to the closed shell metal halides, in spite of the incomplete f shells on the lanthanide ion. This is attributed[16] to the large coulombic interaction between the charged metallic nucleus and the f electrons. The low abundance of the parent ion in the first group lanthanide triiodides, compared with that in the second group starting from GdI_3^+, may be related to the interaction of the nucleus with the f electrons in association with the lanthanide contraction.

A more clear understanding of the mass spectra of these lanthanide iodides may be obtained by reference to the $I\text{-}MI_{n-1}^+$ dissociation energies of Table IV. The dissociation energy $D(I\text{-}MI_2^+) \lesssim 1$ eV is significantly lower than $D(I\text{-}MI^+)$, so that the MI_2^+ species is expected to dominate the lanthanide triiodide mass spectra. The increasing abundance of the parent ion, MI_3^+, from GdI_3^+ to ErI_3^+ is a reflection of the higher $D(I\text{-}MI_2^+)$ in this group as compared to that in the first group.

TABLE IV: Heats of Formation and Dissociation Energy of Positive Ions[a]

	ΔH_f (ion), eV				$D(I\text{-}MI_{n-1}^+)$, eV		
	MI_3^+	MI_2^+	MI^+	M^+	MI_3^+	MI_2^+	MI^+
CeI_3	6.1	5.1	7.9	10.4	0.1	3.9	3.6
PrI_3	5.8	5.5	7.3	9.4	0.8	2.9	3.2
NdI_3	6.0	5.0	8.2	8.9	0.1	4.3	1.8
GdI_3	5.9	5.7	8.0	9.9	0.9	3.4	3.0
TbI_3	6.3	6.2	8.2	8.8	1.0	3.1	2.7
DyI_3	6.5	6.2	7.7	8.9	1.0	2.6	2.2
HoI_3	6.3	6.2	8.2	9.3	1.0	3.1	2.2
ErI_3	6.0	6.1	8.1	9.5	1.2	3.1	2.5

[a] ±0.5 eV.

It is interesting to compare some of the derived quantities of the lanthanide iodides with those of the fluorides,[1] since the latter have been exhaustively studied by Margrave and coworkers. The appearance potentials of the M^+, MF^+, and MF_2^+ from the fluorides are by approximately 10.0, 6.5, and 3.5 eV, respectively, greater than those from the corresponding iodide positive ions. The abundance of the MF_3^+ parent ion is extremely low in the fluorides. The bond dissociation energy of the MF^+ ion is approximately 5.5 eV, as compared with 2-3.5 eV in the MI^+ ions. These large differences in the comparisons all arise from the stronger bond energy between the metal and fluorine in the more ionic fluorides, as compared with the more covalent metal–iodine bond.

5. Conclusions

The electron impact fragmentation pattern of the stable lanthanide triiodides are characterized by a strong MI_2^+ peak. Depending on whether the metal is in the first or second group of the lanthanide series, the parent ion peak is either the weakest or the second strongest in the spectrum. The relationship of the MI_2^+/MI_3^+ relative intensity is best explained by their relative bond dissociation energies.

The appearance potentials and enthalpies of sublimation of the triiodides are all very similar. These triiodides all sublime congruently.

References and Notes

(1) K. F. Zmbov and J. L. Margrave, *Adv. Chem. Ser.*, **No. 72**, 267 (1968).
(2) J. W. Hastie, P. Ficalora, and J. L. Margrave, *J. Less-Common Metals*, **14**, 83 (1968).

(3) A. V. Hariharan and H. A. Eick, *High Temp. Sci.*, **4**, 91 (1972).
(4) J. M. Haschke and H. A. Eick, *J. Phys. Chem.*, **74**, 1806 (1970).
(5) A. V. Hariharan and H. A. Eick, *High Temp. Sci.*, **4**, 379 (1972).
(6) C. Hirayama and P. M. Castle, presented at 4th Central Regional Meeting of the American Chemical Society, Pittsburgh, Pa., May 3–5, 1972.
(7) C. Hirayama and F. E. Camp, *J. Chem. Eng. Data*, **17**, 415 (1972).
(8) R. C. Feber, "Heats of Dissociation of Gaseous Halides," LA-3164, Los Alamos Scientific Laboratory, 40th ed. 1965.
(9) D. White, A. Sommer, P. N. Walsh, and H. W. Goldstein, "Advances in Mass Spectrometry," Vol. 2, R. M. Elliott, Ed., Macmillan, New York, N. Y., 1963, pp 110–127.
(10) S. K. Gupta, *J. Phys. Chem.*, **73**, 4086 (1969).
(11) J. L. Franklin, J. G. Dillard, H. M. Rosenstock, J. X. Herron, K. Draxl, and F. H. Field, *Nat. Stand. Ref. Data Ser., Nat. Bur. Stand.*, **No. 26** (1969).
(12) C. Hirayama and P. M. Castle, unpublished work.
(13) C. Hirayama and F. E. Camp, unpublished work.
(14) D. R. Stull and G. C. Sinke, *Advan. Chem. Ser.*, **No. 18** (1956).
(15) J. W. Hastie and J. L. Margrave, *Rev. Fluorine Chem.*, **2**, 77 (1968).
(16) J. W. Hastie and J. L. Margrave, *High Temp. Sci.*, **1**, 481 (1969).

Serial Statistics: Is Radioactive Decay Random?

John Lynde Anderson and George Wesley Spangler*

The Department of Physics and Astronomy, The University of Tennessee at Chattanooga, Chattanooga, Tennessee 37401
(Received November 21, 1972; Revised version received September 13, 1973)

Publication costs assisted by The University of Tennessee at Chattanooga

Based on more than 10^8 counts obtained from γ emissions arising from cobalt-60 and cesium-137 nuclei, *serial* statistical tests—the sum of squares of 0,1 standardized slopes of linear regressions and the sum of squares of the closely related 0,1 standardized correlation coefficients—exhibit significant deviations from the theoretic (random) expectation as a function of differences in the source environment. On the other hand, more conventional, *nonserial* statistical tests—the χ-square goodness-of-fit and index of dispersion tests—derived from the same data are indistinguishable from those expected for random events. These serial discrepancies raise a substantial question as to the randomness of the detected emissions and, insofar as emissions and decay events are appropriately interrelated, the independence of the events themselves.

Introduction

Recently, Anderson, employing nonserial index of dispersion tests, reported that, under certain conditions, β radiation emitted by carbon-14-labeled organic submonolayers is not properly described by the Poisson distribution.[1] In contrast to generally accepted nuclear theory, the implication of this work is that the events themselves are thus not independent under those particular conditions.

Since it is unlikely that the causal factor for such anomalous statistical behavior is the formation of interactions *only* under those specific monolayer conditions cited, the possibility exists that such interactions, as shown by detected emissions being other than random, would generally be present also in nonmonolayer configurations. In order to test this possibility, a large number of sequential count totals arising from detected γ emissions of cobalt-60 and cesium-137 sources held under several different environmental conditions have been examined using a variety of statistical tests.

Historically, *nonserial* statistical methods have been employed to test experimental observations of radioactive emissions and thereby the adequacy of the thesis of independence of radioactive decay events. Primarily these have been the *chi-square* (χ^2) test which permits testing of the hypothesis that an observed frequency distribution is of the same population as a theoretic one and the *index of dispersion* (s^2/m) which is the ratio of the observed variance to the best estimate of σ^2, *i.e.*, the mean for Poisson distributions. Each test measures only specific parameters of the observed distributions and, in general, these parameters are not identical for the different tests.

Applied to radioactive counting, conformance of observed distributions with the expectation using a single statistical test has, in the literature, generally been taken as proof that the underlying assumption of independence has been verified. All that can reasonably be concluded, however, from conforming results of a single test, (*e.g.*, P's of >0.05 or 0.01) is that the results are not inconsistent with the thesis of randomness and, insofar as emissions are directly related, of the independency of the events themselves.

If a series of numbers (such as radioactive counts) are, in fact, random, then each statistical test which measures at least one property of randomness must consistently show conforming results with an appropriately high frequency; the population of the counts must be, within accepted probability limits, of the same population as theory would predict and as would result from randomly generated numbers themselves. In the absence of artifact, consistently nonconforming results as shown by even one valid test are thus sufficient to raise serious questions as to the validity of the thesis of randomness of what is actually measured and to render the generality of this thesis untenable.

The earlier published evidence shows that the observed distributions, primarily of α emissions, were not differen-

tiated from the expectation, *i.e.*, the Poisson.[2] At least one exception has already been noted.[3] Berkson has more recently reevaluated some of the earlier work using the s^2/m test; this evidence does not now appear as compelling as was originally thought.[4] Further, in studying times-between-α-emissions arising from ^{241}Am, Berkson, employing nonserial tests primarily, did not observe significant differences between the observed and expected distributions, although he noted what seemed to be a high correlation among consecutive times in one case. He concluded: "... *can we consider this examination a fairly definitive establishment of the randomness of such emissions? I do not think so ... I had the impression that a quite extreme departure from randomness might be operative without its being detected by these statistical tests* ..." (italics added).

Statistically, radioactive counts obtained as a sequential series of count totals (counts per unit time) may be considered as a set of *nonserial* totals for purposes of calculating the χ^2 goodness-of-fit test or the index of dispersion.

Such sequential counts may also be considered as *serial* values with respect to time, permitting the derivation of statistical indices such as, for example, the linear correlation coefficients or the slopes of linear regressions. In such series, each correlation coefficient is a measure of the linear correlation that exists within the set between counts and time while the slope statistic is a measure of the change in "mean" within each set also with respect to time. Since the population mean does not sensibly change due to radioactive decay for isotopes of such long half-lived species as ^{60}Co and ^{137}Cs during counting periods of less than 15 min as are described herein, the theoretic distribution of the slope is the distribution of the *apparent* slopes observed for finite samples and is a function of the mean and of the number of counting periods in each data set. The statistics, derived from the linear regression analysis, may thus be compared as is reported herein with well defined theoretic distributions in order to obtain probabilities that the observed distributions are of the same population as are those expected theoretically.

Other serial statistical tests may also be employed to test the adequacy of the thesis of randomness. Thus autocorrelation coefficients for the same data sets as have been examined herein have been calculated and have been compared to approximate theoretic distributions, distributions which are considerably less rigorously derived than are those of the linear regression cited. Largely confirming the linear regression statistics, the analyses based on the autocorrelation coefficients are summarized in the supplemental notes [5]

Experimental Section

Detection and Counting Equipment. Counts for the various statistical analyses were all produced by detection of γ emissions from small sources (*i.e.*, less than 5 μCi per source of ^{60}Co or ^{137}Cs) positioned more than 3 cm from the detector using in sequence a sodium iodide crystal detector and photomultiplier tube, preamplifier, amplifier, single channel analyzer, and a multichannel analyzer operated in the multiscale mode thereby permitting automatic accumulation of data sets of 1024 separate and precisely timed consecutive count totals (0.4 sec/channel for all ^{60}Co series and 0.8 sec/channel for all ^{137}Cs runs). The multichannel analyzer analog-to-digital converter was bypassed in the arrangement with the result that the equipment resolution time loss was insignificant at the relatively low levels of count rate involved (in excess of 1500 counts/sec in only 5 of the 262 series and less than 2600 cps in all runs).

The detector–PMT assembly, whose case was electrically grounded, was surrounded by lead bricks on top and on the sides, all positioned inside a styrofoam box to decrease to a minimum any possible counting fluctuations due to ambient temperature variations within each 409.6- or 819.2-sec period as well as to reduce the effect of background. Experimentally the variations of the ambient were observed to be less than 0.1 °C/15-min period during several tests with the result that the variations within the enclosure must have been even less. Except for loss of power due to line interruptions which occurred two or three times over the 10 months of the project, both the high voltage and the main power were kept "on" over the period of the project. Further to ensure maximum stability of the detector–PMT output, a highly stabilized high-voltage supply was employed.[6]

The basic multichannel analyzer was made by Nuclear Data and the auxiliary equipment by Canberra Industries.[7] The equipment was demonstrated on several occasions (prior to the start of the tests, approximately midway during the 10-month period of the tests, and following completion of the tests) to record "standard" counts properly in each channel using similar "window" limits for the particular input signal and bypassing only the detector–PMT system. When these "standard" tests were run using pulses based ultimately on a crystal oscillator, the input/output counts per channel did not vary at all over the 1024 channel sequences. At similar count rates to those employed during the radioactive counting, no drift whatsoever was observed under this test condition. These checks demonstrate a high likelihood that this portion of the equipment (preamplifier, amplifier, SCA, and multichannel analyzer portions) made no random or nonrandom contribution to the recorded counts.

The output of the PMT was also examined repeatedly during the course of the work using a visual oscilloscope presentation. No apparent variation in the form of the output was observed during these tests (*cf.* note 8).

For ^{137}Cs, the SCA baseline was set in the valley below the photopeak and the window was set at a point above the peak so that no sensible loss of signal occurred but also so that substantially only photopeak signals were counted. In the case of ^{60}Co, both photopeaks were similarly included within the baseline–window setting but the sum peak was excluded. Both baseline and window settings were verified frequently; no significant long term drift was noted.[8]

The memory-retained counts were typed out by teletypewriter and simultaneously punched into paper tape (ASR-33 terminal). The paper tapes were subsequently converted into series of punched cards using a computer program that automatically flagged those numbers which did not conform to the standard pattern of six digits (*e.g.*, 000544). The few errors thus defined were corrected by comparison with the teletyped record and new cards were punched. In only two cases, zero values were observed both in the paper tape and in the teletyped records; these two particular sets of 1024 counts each were discarded and are not included in the statistical summaries.

Following preparation of the punched cards, the data were analyzed using an IBM 360/30 computer and Fortran IV programs (double precision where indicated) that were

prepared specifically for the purpose. Each punched card was individually verified to be in sequence prior to analysis of the serial statistics.

No human-error-producing step was thus encountered between the actual decay events and the derivation of statistical properties, as shown by the several tests. The average count total per unit time (*i.e.*, channel) was approximately 400 with very few data sets having more than 600 or less than 200 counts per unit time.

Radioactive Sources. All radioactive sources used in the work reported herein were prepared by evaporative deposition (aided by a heat lamp above) of mildly acid chloride solutions (generally of 10 μl or less) onto 3003 aluminum foil or onto clear adhesively surfaced plastic film substrates (acetate of 0.13-mm thickness) followed by covering of the crystalline residues with another small section of adhesively surfaced plastic. In one source, two self-adhesive films were used to encapsulate an aqueous solution of ^{137}CsCl (*ca.* 20 μl). Prior to counting, the source substrates were trimmed to *ca.* 3 × 3 cm size with the actual radioactive portion centered in the sandwich.

Prior to deposition of the radioactive solutions, the aluminum foil was freed of prior adsorbents by heating at 320° in the laboratory atmosphere for a period of at least 20 min as has been described elsewhere.[1]

Following preparation, sources which had been deliberately subjected to an environment other than ambient were never used a second time at ambient nor were they used other than in sequential series at other than ambient.

Environmental Conditions during Source Counting. (*1*) *Nongrounded Aluminum Substrates.* (*a*) ^{60}*Co.* Forty series (8 sources) were counted under "steady state" conditions in which the aluminum backing was insulated from electrical ground by wedging the source between two nested styrofoam cups (in turn rigidly positioned with respect to the detector crystal), the inner one having a small *ca.* 1-cm hole cut out on the lower side, the hole being positioned adjacent to the aluminum on the other side of which was the site of the radioactive salt. Thirty-three series (10 sources) were counted while the source, positioned as described above, was cooled with liquid nitrogen by keeping the nitrogen level in the inner cup well above the exposed aluminum backing. Another 16 series (4 sources) were counted with the source taped to a polyethylene sleeve in turn immersed in liquid nitrogen in a Pyrex Dewar. (No apparent change in the statistical behavior was noted in the two types of −196° cooling.) When the styrofoam cups were used they were, in turn, immersed to approximately 1 cm from the top of the outer cup in *ca.* 1 l. of water to prevent changes in count due to adventitious condensation of moisture. While cooled, counts were recorded immediately after the nitrogen had become quiescent and each half-hour thereafter but in no event maintaining the cooling for longer than four consecutive counting sequences (<2 hr per source). Twenty-two series (5 sources) were recorded during warmup from the −196° condition, in each case within 105 min of disappearance of coolent.

(*b*) ^{137}*Cs.* Fifty-four series (7 sources) were counted under "steady-state" conditions; 4 series (2 of the same sources) were recorded during the first 40 min of cooling to −196° while 4 more (the same 2 sources) were obtained during the first 40 min following disappearance of the liquid nitrogen from the styrofoam cups as in (1a) above.

(*2*) *Grounded Aluminum Substrates.* ^{137}*Cs.* Forty-one series (4 sources) were counted while the aluminum substrates were deliberately electrically grounded, in each case the source being maintained at ambient; 8 series (1 source) were counted while the source was held at −196° during 320 min.

(*3*) *Plastic Encapsulated Sources.* ^{137}*Cs.* Seventeen series (4 sources) were counted at ambient while 10 series (2 of the 4 sources) were counted during cooling to −196° in a Dewar during 135 min in each case; 13 series (1 source) were counted using the aqueous solution of CsCl.

Statistical Tests

The nonserial tests listed herein involved comparisons of observed distributions with the theoretic expectation using (1) the χ^2 goodness-of-fit test of frequencies of observed counts per unit time with frequencies of actual Poisson generated counts and (2) the index of dispersion (s^2/m) employing each group of 1024 sequential count totals as an independent set of data. In addition, the linear correlation coefficient and the regression slope (and, as recorded in the supplemental notes, the autocorrelation coefficients using lags of 1 through 320 in each set of data) have been calculated for each set of 1024 automatically time-sequenced counting series.[9]

No attempt was made directly to derive statistics from among the several sets (such as common means or cross correlations) since the starting points (in time) of each set were always initiated manually and somewhat arbitrarily. Once derived, statistical indices have been combined with others calculated similarly (as the sum of the squares) in order to examine overall probabilities for many sets of data observed under the homogeneous conditions listed above.

To facilitate analysis, linear correlation coefficients were converted to values (that would have an approximate 0,1 normal distribution if they were derived from random data) by means of the "z" transformation, *i.e.*, by calculating the hyperbolic arc tangent of each ($= 0.5 \ln \{(1 + r)/(1 - r)\}$), by subtracting the approximate theoretic mean ($= 0$), and by dividing by the approximate theoretic standard deviation ($= 1/(n - 3)^{1/2} = 0.031296$).[10] The sum of the squares—and the mean square (called $s^2/\hat{\sigma}^2$ in the tables)—was then calculated, separately, for the standardized hyperbolic arc tangents of the correlation coefficients. Each sum of squared standardized values is distributed (approximately) as χ^2 with the degrees of freedom equal to the number of independent data sets.

Since the regression slopes are theoretically normally distributed, they were 0,1 standardized merely by subtracting the theoretic mean ($= 0$) and by dividing by the best estimate of the theoretic standard deviation ($= \{m/\Sigma(t_i - t)^2\}^{1/2}$).[11] Since m is itself a variable, derived from a Poisson distribution, the resulting 0,1 standardized distribution is not, strictly speaking, normally distributed. However when the slope variance for each data set is accumulated by summation of the squared 0,1 standardized slopes, the summation within each homogeneous grouping is almost identical with the similar measure of the overall variance obtained by substituting the value $\{m(n - 1)\}$ for $\{\Sigma(a_i - m)^2\}$ followed by calculating the individual values by means of the "z" transformation, thus indicating that the deviation from the 0,1 distribution is relatively insignificant at least for the variance analysis employed herein.

Since independently (as well be seen in Table I) the index of dispersion (s^2/m) has been found to approximate

TABLE I: Non-serial Tests and Probabilities

Source (data sets)[a]	χ^2 Test (Poisson) χ^2/DF (D.F.)	P^b	Index of dispersion s^2/m (D.F.)	P^b
(1a) ^{60}Co: Steady State (40)	0.993 (3188)		0.997 (40920)	
: Low Temp (49)	0.982 (3610)		1.001 (50127)	
: Warmup (22)	0.990 (1226)		1.006 (22506)	
Combined (111)	0.988 (8024)	*0.217*	1.001 (113553)	*0.553*
(1b) ^{137}Cs: Steady State (54)	0.991 (4322)		0.996 (55242)	
: Low Temp (4)	1.120 (226)		1.011 (4092)	
: Warmup (4)	0.987 (222)		1.021 (4092)	
Combined (62)	0.997 (4770)	*0.443*	0.999 (63426)	*0.401*
(2) ^{137}Cs: Steady State (41)	0.980 (3477)		0.995 (41943)	
: Low Temp (8)	0.973 (575)		0.998 (8184)	
Combined (49)	0.979 (4052)	*0.173*	0.996 (50127)	*0.238*
(3) ^{137}Cs: Aq. Solution (13)	1.008 (1191)		0.986 (13299)	
: Crys. SS (17)	1.030 (1106)		0.996 (17391)	
: Crys. LT (10)	1.006 (589)		0.975 (10230)	
Combined (40)	1.023 (2866)	*0.731*	0.988 (40920)	*0.036*
Randomly generated (90)	0.985 (7870)	*0.174*	0.997 (92070)	*0.260*

[a] Groups 1a and 1b or nongrounded Al; group 2 on grounded Al; group 3 in plastic (acetate) encapsulation. [b] Probability (P) is expressed as the likelihood that a value of the statistic (of the same or lesser size) would be observed in a random distribution.

TABLE II: Serial Tests and Probabilities

Source[a]	Linear correlation coefficient (r), $s^2/\hat{\sigma}^2$	Degrees of freedom	Linear slope (b)[c] $s^2/\hat{\sigma}^2$	Probability, P^b
(1a) ^{60}Co: SS	2.013	40	1.971	*d*
: LT	1.244	49	1.232	
: WU	0.840	22	0.849	
Combined	1.441	111	1.422	*0.998*
(1b) ^{137}Cs: SS	2.890	54	2.843	*d*
: LT	1.966	4	1.973	
: WU	1.007	4	1.026	
Combined	2.709	62	2.670	*>0.9999*
(2) ^{137}Cs: SS	0.682	41	0.683	*d*
: LT	0.461	8	0.451	
Combined	0.646	49	0.645	*0.025*
(3) ^{137}Cs: AS	0.256	13	0.256	*d*
: SS	0.656	17	0.633	
: LT	0.629	10	0.613	
Combined	0.519	40	0.506	*0.004*
Random generated	1.011	1024	1.008	*0.577*

[a,b] Same as in Table I. [c] Values of $s^2/\hat{\sigma}^2$ (combined) based on randomly rearranged data are 1a: 1.016; 1b: 1.036; 2: 0.866; and 3: 0.984. [d] P's are 1a-(SS): 0.9998; 1b(SS): >0.9999; 2(SS): 0.061; 3(SS + AS): 0.006.

unity in each group of data sets, the mean square of the standardized slopes within each such group would be expected to be (and is—Table II) almost identical with that of the 0,1 standardized correlation coefficients.

A large number of data sets of random deviates fit to a Gaussian distribution and truncated to integers—a very close approximation to the Poisson for the mean involved (*ca.* 529)—were generated using the IBM RANDU subroutine and employing continually changing starting values. These sets of random deviates were then analyzed using the same computer programs as were used with the detected emissions sets.

To test further for the existence of serial relationships in the data sets based on radioactive emissions, each set of count totals was shuffled randomly with respect to order (using a RANDU type subroutine) prior to recalculating each regression slope and the variance of 0,1 standardized statistics based on each randomized order.

Results

The results of the analyses are given in Tables I and II. These tables list summaries of all the runs made and known to the authors which meet the aforesaid counting conditions during the period Dec 10, 1971 through Oct 31, 1972. No runs have been omitted from the analyses other than the two previously noted which had at least one zero total in each.

Based on the 262 data sets derived from the radioactive γ emissions as well as on those from the computer generated random deviates, the nonserial χ^2 tests and the index of dispersion comparisons are, with one marginal exception, well within the 0.05 probability limit: the nonserial tests do not differentiate the distributions of randomly generated numbers or those of the radioactive counting sequences from the theoretic (random) expectation. With the exception of ref 1 and 3 as noted, this con-

clusion is entirely consistent with the recorded literature known to the authors.

On the other hand, using the same 262 data sets derived from the radioactive emissions, the tests of the linear correlation coefficients (r) and of the slopes of the linear regressions (b) show marked deviations from the expectation: all probabilities, when grouped as shown in Table II, lie outside $0.05P$ and three fourths are well outside $0.01P$.[12] However when the order within each set is randomized, the sets cannot be differentiated from the expectation with respect to these same statistical tests (Table II, footnote c). Similar tests of the sets based on the randomly generated numbers also cannot be differentiated from the expectation.

Table II, footnote *d*, also lists the probabilities associated with the variances of the regression slopes when only "steady state" counting environments are considered. Again, three of the four groups have probabilities which lie outside $0.01P$. While the value of $0.06P$ for group 2 is within the $0.05P$ limit, when these 41 sets of 1024 were subdivided into 82 half-sets (41 × 1-512 and 41 × 513-1024), the mean square ($s^2/\hat{\sigma}^2$) of standardized half-to-half slopes was 0.553—the probability associated with this value is $0.0003P$.

The serial tests also indicate a rather pronounced effect due to lowering the source temperature and subsequent raising of the source temperature to ambient. In all four groups the effect of lowering the temperature was to lower the variance of the correlation coefficients and the slopes. However only in group 1a were sufficient runs carried out to draw this conclusion with any reasonable degree of an assurance of repeatability. Whether the effect is, in fact, an effect of temperature, *per se*, or of changing the electronic environment (by contact of the metal substrate with the liquid nitrogen in groups 1a and 1b) has not been determined.

Discussion

In experimental testing of the hypothesis of randomness by measuring emissions of radioactive decay events, the conformance of the data distributions as shown by nonserial statistical tests with the theoretic (random) expectation must be considered necessary but insufficient *proof* that the data are, in fact, random. Thus the nonconforming serial statistical tests such as are illustrated in Table II raise substantial questions relative to the general applicability of the thesis of randomness.

The existence of both significantly *high* and *low* serial tests does not in itself suggest that the nonserial tests are faulty—but it does imply that such tests fail to measure the nonrandom characteristics shown by the serial ones.

Even though the present work was originally undertaken to explore the possibility that additional examples of low or restricted values of the index of dispersion might be observed, the marked similarity of the variance tests of the 0.1 standardardized slopes of the regressions with those of the correlation coefficients as well as the agreement with theoretical expectation of the index of dispersion values indicates that variance *per se* does not contribute significantly to the observed anomalies reported herein.

Possible artifactual errors which might contribute to the nonconformance of serial statistics can be classified as faults in the experimental design or as equipment-based shortcomings such as drift.

Adventitious movement of the source with respect to the detector (during the 13.7 min of counting ^{137}Cs or 6.9 min of counting the ^{60}Co series) would cause an artifactual increase both in the nonserial and serial tests used in this paper. Also any time-phased change in detected emissions during cooling (by adventitious condensation of moisture in the path of the emissions, for example) must also result in an increase of the several statistics. Neither can cause a *decrease* in the variance of the slopes of the regressions however. Thus since the high values of the variances of the slopes (and of the correlation coefficients) have been observed during "steady state" counting of nongrounded sources only, the authors have concluded that such artifactual effects have not occurred to any significant degree.

A discussion of the effect of small angle detectors was included in ref 1 (supplemental note 1). To determine statistical properties of radioactive emissions, the use of such detectors (assuming independent decay events and random emissions) can be considered as noncasual for statistical abnormalities insofar as the detected emissions are concerned with the single exception (b) discussed below. Since all the statistics discussed in this paper depend only on detected emissions, such a conclusion also applies here.

If emissions (between decay events and detection) are pushed into or out of the solid angle detection zone deliberately or adventitiously one of two effects result.

(a) If the *number* of detected emissions is *consistently* increased (or decreased), the net effect is to enlarge (or make smaller) the solid angle detection zone. From the standpoint of the detector it is as if the source were larger (or smaller) than it actually is. This situation has, in itself, no adverse effect on any of the statistical analyses employed in this paper.

(b) If the number of detected emissions is *inconsistently* increased or decreased or both within the overall elapsed time of each 1024 data set, the observed counts would vary more than would be expected on the basis of random emissions. Such an effect would overall be manifested by an *increase* both in the index of dispersion (s^2/m) and in the $s^2/\hat{\sigma}^2$ of the regression slopes. Since the $s^2/\hat{\sigma}^2$ statistic is *less* than is expected in groups 2 and 3, the likelihood that such an artifact would be causal of the overall phenomenon is very low.

Within the subject of potential equipment-based artifacts, only the inherent drift of the detector-PMT appears to be of such a magnitude as to influence the slope variances (or those of the correlation coefficients) to any extent at all. The rest of the equipment (preamplifier to printout) was independently shown to be artifact-free—at least during the course of the specific equipment checks cited; further, the method of temperature stabilization of the detector-PMT and the use of the highly stabilized high-voltage supply appears to preclude any possible artifact from such causes.

For purposes of discussion this inherent drift capability can be separated into two components: long-term drift and short-term drift in which the term short term drift refers to shift of the PMT output within the time of accumulation of an individual data set. In each case the effect of drift is to change the count rate and the number of counts within the data set artifactually.

According to the manufacturer (*cf.* note 8), the short-term drift is rarely if ever greater in magnitude than the long-term drift, and thus the showing below that the long-term drift (as shown by mean shift) is of a very low order

TABLE III: Compressed data for 23 Data Sets[a]

Group	Run	Mean + (deviations from mean)[b]	Intercept and slope[c] + (deviations from linear trend)[b]
1a	Z20	519.5 + (−3.1, −2.5, −2.5, −0.8, +2.0, +2.7, +1.4, +2.8)	515.2 + 0.94*n* + (+0.2, −0.2, −1.1, −0.3, +1.5, +1.3, −1.0, −0.5)
	Z97	486.5 + (+2.2, −0.3, +1.3, −0.5, +1.2, −0.9, −0.7, −2.3)	488.6 − 0.45*n* + (+0.6, −1.4, +0.6, −0.7, +1.4, −0.2, +0.4, −0.7)
	X01	714.3 + (−1.8, −1.8, +0.7, −0.4, +0.3, +0.7, +2.6, −0.2)	712.5 + 0.41*n* + (−0.4, −0.8, +1.4, −0.2, +0.1, +0.1, +1.6, −1.6)
	V04	328.5 + (−0.4, −2.4, −1.1, −0.3, +1.3, +0.9, +1.0, +1.0)	326.7 + 0.40*n* + (+1.0, −1.4, −0.5, −0.1, +1.1, +0.3, +0.0, −0.5)
1b	Q01	305.5 + (+2.5, +0.9, +1.9, −1.1, −0.9, −1.1, −0.0, −2.1)	308.0 − 0.55 *n* + (+0.6, −0.5, +1.0, −1.4, −0.6, −0.2, +1.3, −0.2)
	Q11	371.8 + (−1.9, −1.8, −1.7, +1.3, +0.7, +1.7, +0.8, +0.7)	369.6 + 0.49*n* + (−0.2, −0.6, −1.0, +1.6, +0.5, +1.0, −0.4, −1.0)
	Q18	408.0 + (−3.9, −2.2, −0.8, +1.5, +0.9, +0.6, +1.1, +2.8)	404.4 + 0.80*n* + (−1.1, −0.2, +0.4, +1.9, +0.5, −0.6, −0.9, +0.0)
	Q19	360.0 + (+3.0, +0.8, +0.0, −0.8, −0.6, −0.7, −1.5, −0.3)	362.0 − 0.44*n* + (+1.5, −0.3, −0.6, −1.0, −0.4, −0.0, −0.4, +1.2)
	VCB	384.7 + (+1.4, +2.5, +1.9, +1.7, −0.4, −2.0, −2.3, −2.8)	388.3 − 0.80*n* + (−1.4, +0.5, +0.7, +1.3, +0.0, −0.8, −0.3, −0.0)
	QQ3	542.2 + (+3.3, −0.3, +1.0, +0.0, −1.6, −0.9, −1.1, −0.4)	544.2 − 0.44*n* + (+1.7, −1.4, +0.4, −0.2, −1.4, −0.2, +0.0, +1.1)
3AS	Q61	550.4 + (+0.1, −0.9, +0.1, −0.8, +1.1, −0.2, +0.0, +0.5)	550.0 + 0.10*n* + (+0.5, −0.6, +0.2, −0.8, +1.1, −0.4, −0.2, +0.2)
	Q62	551.2 + (−0.0, −1.3, +0.8, +1.8, +0.6, −0.2, +0.6, −2.2)	551.8 − 0.12*n* + (−0.5, −1.6, +0.6, +1.7, +0.7, −0.0, +0.9, −1.8)
	Q63	551.0 + (−0.7, +0.2, +1.9, −0.2, −1.0, −0.3, +0.4, −0.3)	551.2 − 0.04*n* + (−0.8, +0.1, +1.8, −0.2, −1.0, −0.2, +0.5, −0.2)
	Q64	551.2 + (+0.6, −1.5, −0.4, +0.4, +1.0, −1.5, +1.1, +0.3)	550.7 + 0.10*n* + (+0.9, −1.3, −0.2, +0.4, +1.0, −1.6, +0.9, −0.1)
	Q65	550.6 + (−0.2, +0.2, −1.3, +2.1, −0.9, −0.4, +0.1, +0.4)	550.4 + 0.04*n* + (−0.1, +0.3, −1.2, +2.2, −0.9, −0.5, −0.0, +0.2)
	Q66	549.2 + (−1.2, +0.7, +0.1, +0.3, +0.3, −0.1, −0.3, +0.3)	548.9 + 0.06*n* + (−0.9, +0.8, +0.1, +0.3, +0.3, −0.2, −0.5, +0.1)
	Q67	550.3 + (+0.9, −0.4, +0.3, −0.7, −0.6, +0.3, +0.4, −0.1)	550.5 − 0.04*n* + (+0.8, −0.5, +0.2, −0.7, −0.6, +0.3, +0.5, −0.0)
	Q68	549.9 + (+0.5, −0.4, −1.5, −0.6, +0.1, +0.5, +1.3, +0.0)	549.3 + 0.14*n* + (+1.0, −0.0, −1.3, −0.6, +0.1, +0.3, +1.0, −0.4)
	Q69	550.1 + (−0.0, +1.2, −0.8, −1.0, +0.5, +0.2, −0.4, +0.4)	550.1 − 0.01*n* + (−0.0, +1.2, −0.8, −1.0, +0.5, +0.2, −0.4, +0.4)
	Q70	549.8 + (+0.6, +0.2, −1.0, +0.8, −0.0, −0.3, −0.3, −0.0)	550.1 − 0.07*n* + (+0.3, +0.1, −1.1, +0.8, +0.0, −0.2, −0.2, +0.2)
	Q71	549.5 + (−0.7, +0.2, +1.1, −1.6, −0.5, +0.6, +1.5, −0.5)	549.1 + 0.08*n* + (−0.4, +0.4, +1.2, −1.6, −0.5, +0.4, +1.3, −0.8)
	Q72	549.6 + (+1.3, −1.5, −0.4, −0.4, +0.3, +0.7, +0.8, −0.8)	549.5 + 0.01*n* + (+1.3, −1.5, −0.4, −0.4, +0.3, +0.6, +0.3, −0.8)
	Q73	549.9 + (+0.5, −0.1, +0.6, −0.6, −0.6, +0.5, −1.0, +0.6)	550.1 − 0.06*n* + (+0.3, −0.2, +0.6, −0.6, −0.6, +0.6, −0.8, +0.8)

[a] Compressed data calculated as $2\sqrt{\text{sum of 128 count totals}}$. [b] The entries in the line for Q01, for example, correspond to observed $2\sqrt{\text{count}}$ values of 305.5 + 2.5 = 308.0, 305.5 + 0.9 = 306.4, 305 5 + 1.9 = 307.4 (and so on) on the left and to 308.0 − 1(0.55) + 0.6 = 308.0, 308.0 − 2(0.55) − 0.5 = 306.4, 308.0 − 3(0.55) + 1.0 = 307.4 (and so on) on the right. (Occasional discrepancies of ±0.1 or ±0.2 in other lines are due to rounding. [c] Since $\Sigma(n - \bar{n})^2 = 42$, the rms coefficient of *n* for Poisson randomness should be about 0.15.

is presumptive evidence that the short-term drift is also of a low order.

Long term drift is often stated in terms of drift per day or drift per 8 hr. Although the authors have drawn, in this paper, no detailed statistical conclusions based on mean shifts over long periods (*e.g.*, 8 hr), such shifts have indeed been examined. Thus when six series encompassing 70 data sets (35 sets in daily sequences of 10, 12, and 13 series based on grounded aluminum substrates—group 2—and a similar 35 sets based on nongrounded substrates —group 1b) were examined, the largest apparent 8-hr shift amounted to only *ca.* 0.6% or, if linear over this 8-hr period, only *ca.* 0.02% per 13.7 min counting period. In these same six series, essentially no overall mean shift was observed in three of them. The largest set-to-set shift within each of these six series was under 0.5%—just in excess of a not too unexpected 3σ, assuming the Poisson applies. For a mean of 400 counts, the *maximal* long term mean shift, if linear, thus amounts to only ±0.1 count over each 1024 count set, a change which is, overall, insignificant with respect to increased slope variance.

In these considerations it is necessary to differentiate mean shift from drift of the PMT since (as mentioned in the Experimental Section) drift is not linearly related to mean shift (the drift affects photopeak *position* within the particular SCA window settings employed). The observed

long-term mean shift (and even the short-term ones) may also be due to factors other than PMT drift *per se*, such as small, nonrecorded adjustments in the source-detector geometry, excessive (but not expected) temperature changes in the ambient, and/or even a randomness type factor in decay itself. (Note: The authors recognize that this argument relative to mean shift based on radioactive counting is open to some question since the results of this paper raise substantial questions relative to randomness of detected emissions. However, no better evidence of PMT behavior is available since the γ's required to pulse the detector-PMT cannot readily be generated in any other way.)

The potential effect of short-term drift on the output of the detector-PMT (and the resultant effect on the detected counts) was also discussed in the Experimental Section. The *maximal* expected drift was shown to be of only small moment ($< 0.5\sigma$) under the conditions cited, a finding which is entirely consistent with the observations of mean shift cited.

Certainly for high variance values of the regression slopes, the small (but not negligible) potential drift of the detector-PMT might be responsible for a minor portion of the observed variances but in no manner can it be causative in the two groups exhibiting *low* slope variances. Actually, if such drift is indeed a factor in any appreciable degree in the high variance examples (groups 1a and 1b), the low variances of groups 2 and 3 are likely to be *understated* (*i.e.*, the listed results are likely to be higher than they would have been in the absence of drift).

In the two cases of nongrounded substrates (groups 1a and 1b), there existed ten data sets (out of the 173 listed ones) in which the values of the standardized slopes of the linear regressions were above 2.56 (*i.e.*, the 1% level of significance) whereas only two are expected. These ten contribute greatly to the excessively high levels of the variances since the variance is proportional to the sum of squares of such standardized values. Of these ten, none was individually unusual in the nonserial tests; the overall index of dispersion for these ten was 0.994 which is indistinguishable from the overall value of all 173 runs.

One of the referees suggested that it might be instructive to list the values of these ten series in compressed form as $2\sqrt{\text{sum of 128 counts}}$ since, for Poisson distributions, $2\sqrt{\text{sum}}$ − mean has very nearly unit variance. Thus the sizes of changes from the expectation on the approximately minute-to-minute time scale can be appreciated. Table III lists the deviations of such double-square-roots-from-run-means for each of these ten series and the deviations from the linear trend in each case as well. (In the table note that run Q11 may be a step change.) Also included in Table III for comparison purposes are similar analyses of the 13 data sets that comprise the aqueous solution runs of group 3; these latter represent a series in which the variances of the slopes are extremely low.

It is of interest that excessive mean shifts have previously been reported during counting of β-emissions from thin layers of carbon-14 containing material when the source holder was nongrounded; the authors apparently did not question the statistics of counting, however.[13] A significant statistical effect associated with nongrounded substrates was, however, observed during counting of the carbon-14 submonolayers previously cited.[1]

While the meaning of high (or low) variance of the regression slopes can be interpreted as higher than expected (or lower than expected) shift of the mean, a similar analysis of the high and more particularly of the low variances of the linear correlation coefficient does not appear to have such a straightforward physical explanation. At this time all the authors wish to conclude with respect to these serial tests is that they show that the time-related order of the data is not consistent with random expectation. Other serial tests might also have been used, permitting increased (or decreased) definition of the nonrandom phenomenon herein described.

Conclusion

γ Emissions detected following radioactive decay of cobalt-60 and cesium-137 nuclei deviate significantly from the theoretic (random) expectation as shown by tests of serial statistics even though nonserial tests fail to differentiate the same data distributions from the (random) expectation. Insofar as emissions and decay events are appropriately interrelated, the evidence is inconsistent with the thesis of decay independence.

Acknowledgments. The authors thank Mr. T. E. Adkins, Professor Eric T. Lane, without whose help the computer and statistical programming could not have been accomplished, and the other members and students of the Department of Physics (UTC) who have willingly given of their time and thoughts. We also thank Professor L. D. Davis and his staff of the Computer Center (UTC) and Mr. B. M. O'Bryant, Mrs. Sandra Emond, and Mrs. N. B. Anderson of the Tennessee Valley Authority. Mr. F. L. Miller of the Department of Statistics (ORNL) gave valuable advice and aid. While the help of so many is gratefully acknowledged, the conclusions are those of the authors alone. The authors wish also to express their appreciation to the University of Chattanooga Foundation for the award of a grant (to GWS) during a portion of the work. The authors express their sincere appreciation to the two referees selected by the Editor and in particular to Professor J. W. Tukey who kindly examined many of the data series in more statistical detail than has been presented herein; as noted, one of his suggestions has been incorporated in the discussion section.

Supplementary Material Available. Supplemental notes and material will appear following these pages in the microfilm edition of this volume of the journal. Photocopies of the supplementary material from this paper only or microfiche (105 × 148 mm, 20× reduction, negatives) containing all of the supplementary material for the papers in this issue may be obtained from the Journals Department, American Chemical Society, 1155 16th St., N.W., Washington, D. C. 20036. Remit check or money order for $3.00 for photocopy or $2.00 for microfiche, referring to code number JPC-73-3114.

References and Notes

(1) J. L. Anderson, *J. Phys. Chem.*, **76**, 3603 (1972).
(2) *Cf.* E. Rutherford and H. Geiger, *Phil. Mag.*, **20**, 698 (1910); L. F. Curtiss, *J. Res. Nat. Bur. Stand. A*, **8**, 339 (1932). See also, A. P. Kovarik, *Phys. Rev.*, **13**, 272 (1919), which describes β emissions.
(3) The "exception": W. Kutzner, *Z. Phys.*, **21**, 281 (1924); **44**, 655 (1927); L. F. Curtiss, *J. Res. Nat. Bur. Stand. A*, **4**, 595 (1930).
(4) J. Berkson, "Examination of Randomness of Alpha Particle Emissions," in "Research Papers in Statistics," F. N. David, Ed., Wiley, New York, N. Y., 1966, pp 37–54.
(5) See paragraph at end of paper regarding supplementary material.
(6) Canberra Industries, Inc., Model 3015 High-Voltage Power Supply. This unit is designed to have less than 0.05% voltage variation over an 8-hr period with a 3° temperature variation and less than 0.01% output voltage change for a 10% change in nominal line voltage. Experimental checks of the power supply unit did not indicate any adverse deviation from the design specifications.

(7) Model numbers were: multichannel analyzer, ND Model 2200; detector–PMT, CI Model 802-1; preamplifier, CI Model 805; amplifier, CI Model 1417B; and timing SCA, CI Model 1437.

(8) As shown by actual data on which the window used for counting the plastic encapsulated CsCl in aqueous solution was established, these settings were determined by observing the counts per channel (averaged over at least 10 channels) at a series of baseline (0 to 10.0) settings with the window (also 0 to 10.0) set at 0.10 and with the amplifier coarse gain held at 8 and fine gain at 0. The values shown are baseline settings followed by the counts in parentheses: 3.6(16); 3.7(11); 3.8(10); 3.9(8); 4.0(12); 4.1(22); 4.2(71); 4.3(190); 4.4(352); 4.5(448); 4.6(367); 4.7(221); 4.8(84); 4.9(22); 5.0(5); 5.1(1); and 5.2(1). In this case a baseline of 3.9 was selected with the window at 1.30. Note: The summation of counts for the baseline of 3.9 and a window of 1.3 (assuming linearity of window) is 1803. The actual 13 × 1024 series (hereinafter detailed) had a mean of slightly less than 600 since the source-to-detector subtended solid angle was smaller during the actual counting series cited. Any adventitious variation in detector–PMT output (which causes a shift primarily in the *position* of the photopeak) is thus seen to be unlikely to cause a significant shift in counts per channel. While the manufacturer (CI) has stated in a personal communication that as much as a 1% shift in the PMT output over a 1-hr period is relatively rare and unexpected, even a 1.0% net overall shift in 13.7 min (the duration of ^{137}Cs counting sequences) would have caused a maximal shift of ca. 1 count (for the means of 600). As is discussed later in this paper, such an unusual and artifactual shift is relatively insignificant ($<0.5\sigma$) for the serial tests used.

(9) The equations used to calculate these statistics are listed below where the symbols are defined as: a_i denotes the counts per unit time, m denotes the mean of the data set ($= (1/n)\Sigma a_i$), t_i denotes the time expressed as a digit (1 to 1024) at which the a_i count total was observed, $\bar{t}$ denotes the mean of the times ($= 512.5$), and n denotes the value 1024. For the nonserial χ^2 tests, o_i are the observed frequencies and f the theoretic frequencies with a minimum of at least 5 components in each theoretic cell, p being the number of such cells.

χ^2

$$\chi^2 = \sum_{i=1}^{p}(o_i - f)^2/f$$

Index of dispersion

$$s^2/m = [1/(n-1)]\sum_{i=1}^{n}(a_i - m)^2/m$$

Linear correlation coefficient (r)

$$r = \left\{\sum_{i=1}^{n}(t_i - \bar{t})(a_i - m)\right\} / \left\{\sum_{i=1}^{n}(t - \bar{t})^2 \cdot \sum_{i=1}^{n}(a_i - m)^2\right\}^{1/2}$$

Slope of the regression (b)

$$b = \sum_{i=1}^{n}(a_i - m)(t_i - \bar{t}) / \sum_{i=1}^{n}(t_i - \bar{t})^2$$

The relationship of r to b may be expressed

$$r = b\left\{\sum(t_i - \bar{t})^2/(n-1)s^2\right\}^{1/2} = \text{constant} \cdot (b/m^{1/2})/(s^2/m)^{1/2}$$

(10) J. S. Bendat and A. G. Pierson in "Random Data; Analysis and Measurement Procedures," Wiley, New York, N. Y., 1971, pp 126–128.

(11) N. R. Draper and H. Smith in "Applied Regression Analysis," Wiley, New York, N. Y., 1966, p 18. Since for Poisson distributions (and that is, essentially, the hypothesis being tested) the sample mean (m) is the best estimate of the population variance, the expression for the standard deviation of the theoretic slope reduces to the form shown.

(12) It may be worthy of note that when one of the data sets of the 111 group 1a series (*i.e.*, Z20—see Table III) is removed, the $s^2/\bar{\sigma}^2$ falls to ca. 1.10 and the whole remaining group cannot be differentiated from the (random) expectation. However there is no reason known to the authors to suspect that any artifactual factor caused the excessively high value in Z20 particularly since the run made 30 min earlier appeared completely normal with respect to the tests employed. The significant deviation from the expectation of the autocorrelation coefficients of this group of data sets (supplemental notes) is *not* appreciably affected by the removal of Z20. Further, no such similar removal of a single run has any particular effect in group 1b.

(13) H. J. Perkins and M. D. MacDonald, *Science*, **138**, 1259 (1962).

COMMUNICATIONS TO THE EDITOR

Periodicity in the Rate of Heat Evolution during the Temporal Oscillation in the 2,4-Pentanedione–Bromate–Catalyst System

Sir: Recently Bowers, Caldwell, and Prendergast[1] claimed that during the oxidation of 2,4-pentanedione with bromate in the presence of manganese(II) as a catalyst temporal chemical oscillation occurred which could be followed spectrophotometrically.

In the course of our studies on the Belousov–Zhabotinsky type oscillating chemical reaction[2,3] we started to investigate the heat changes accompanying the temporal concentration oscillations.[4] (Earlier observations in this field have been reported by Franck and Geiseler,[5] and by Busse.[6]) We have found that the rate of heat evolution is periodic in character; the high rate of heat evolution is synchronized with an abrupt increase in the redox potential and a sudden decrease in the bromide concentration.

We regarded it of interest to find out what heat changes accompany the oscillating reaction described by Bowers, *et al.*,[1] and to compare these findings with those obtained with the malonic acid–bromate–catalyst systems. In both cases manganese(II) and cerium(III) were used as catalysts.

The calorimetric measurements were performed as described previously.[4] The redox potential was recorded against a smooth platinum electrode, and a double junction calomel reference electrode was used with a 10% potassium nitrate solution making contact with the reaction mixture. Unfortunately in the case of 2,4-pentanedione the bromide concentration could not be recorded with a bromide selective solid-state electrode which we had found to be the most suitable[7] and which was used throughout our studies on the Belousov–Zhabotinsky reaction.[2,3] Namely, 2,4-pentanedione attacked the plastic body of the electrode making the function of it unreliable. Also an Ag|AgBr electrode could not be applied since its proper function was handicapped by the high sulfuric acid concentration (1 *M*) and the oxidizing nature of the oscillating system. The solutions were stirred.

The heat and potential *vs.* time curves for the four systems are shown in Figures 1–4.

The malonic acid–bromate–catalyst systems exhibit very similar curves (Figures 1 and 2) only the heat evolution and the potential change in a single step is greater with manganese as a catalyst; this means that the amount of reactants transformed in one period is greater.

The 2,4-pentanedione–bromate–catalyst systems, however, differ considerably both from the other system and also from each other, *i.e.*, the curves are considerably different when manganese is replaced by cerium.

Figure 3 shows the manganese-catalyzed system. After mixing the reagents the temporal chemical oscillation starts immediately. In the early period of the reaction the heat output during one oscillation is large and it decreases considerably in time; the reaction proceeds with a strongly damped character. The chemical oscillation is observable also by color change of the solution, as it has been reported by Bowers, *et al.*;[1] the colorless solution at the sudden potential and temperature jumps turns yellow. The potential change of this system shows over- and under-shoots. This probably involves manganese(IV) formation. After a certain period of time especially above 30°

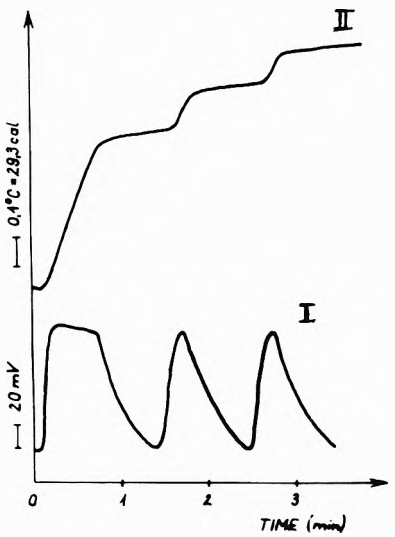

Figure 1. Typical potential (I) and temperature (II) against time curves for the chemical system containing malonic acid (0.4 *M*), $KBrO_3$ (0.1 *M*), $MnSO_4$ (0.0046 *M*), and H_2SO_4 (0.5 *M*) at 25°.

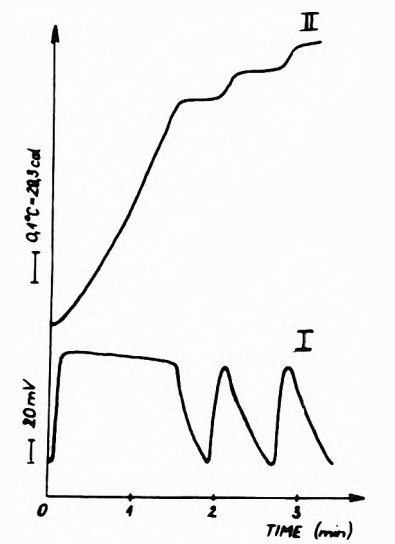

Figure 2. Typical potential (I) and temperature (II) against time curves for the chemical system containing malonic acid (0.3 *M*), $KBrO_3$ (0.1 *M*), $Ce(NO_3)_3$ (0.0046 *M*), and H_2SO_4 (0.5 *M*) at 25°.

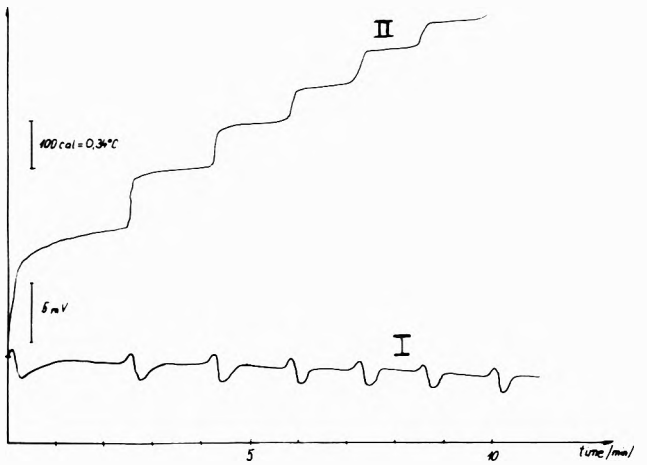

Figure 3. Typical potential (I) and temperature (II) against time curves for the chemical system containing 2,4-pentanedione (0.05 *M*), $KBrO_3$ (0.07 *M*), $MnSO_4$ (0.045 *M*), and H_2SO_4 (1 *M*) at 25°.

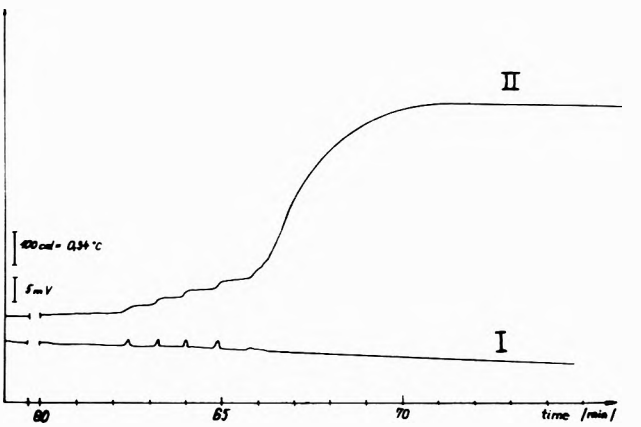

Figure 4. Typical potential (I) and temperature (II) against time curves for the chemical system containing 2,4-pentanedione (0.05 *M*), $KBrO_3$ (0.07 *M*), $Ce(NO_3)_3$ (0.046 *M*), and H_2SO_4 (1 *M*) at 25°.

a dark brown precipitate (hydrated manganese(IV) oxide) separated.

The behavior of the cerium-catalyzed system is given in Figure 4. After an induction period of 1 hr, only a few (three-four) oscillations were observable. Small temperature jumps and small potential changes indicated the oscillating period of the reaction. This was followed by a great heat output; further heat evolution and potential oscillations, however, did not occur. The large heat output is not associated with a change in the redox potential; thus it can be assumed that a direct reaction occurs between the brominated dione and bromate.

Comparing the 2,4-pentanedione–bromate–catalyst and the malonic acid–bromate–catalyst oscillating systems it can be established that there should be considerable difference in the mechanism of the reactions. In the malonic acid system the reaction between bromomalonic acid (which has formed in the course of the reaction) and the oxidized form of the catalyst generated the bromide ions, which later play an important role in switching on and off an autocatalytic reaction and thus controlling the steady-state concentration of $HBrO_2$ (for details see ref 3). The role of bromide ions can not be excluded even in the case of the 2,4-pentanedione–bromate–catalyst system; the mechanisms, however, are more involved owing to the separation of a precipitate in a later period of the reaction. Especially the peculiar behavior of the cerium-catalyzed system needs extensive investigations.

References and Notes

(1) P. G. Bowers, K. E. Caldwell, and D. F. Prendergast, *J. Phys. Chem.*, **76**, 2185 (1972).
(2) R. M. Noyes, R. J. Field, and E. Koros, *J. Amer. Chem. Soc.*, **94**, 1395 (1972).
(3) R. J. Field, E. Koros, and R. M. Noyes, *J. Amer. Chem. Soc.*, **94**, 8649 (1972).
(4) E. Koros, M. Orbán, and Zs. Nagy, *Nature (London), Phys. Sci.*, **242**, 30 (1972).
(5) U. Franck and W. Geiseler, *Naturwissenschaften*, **58**, 52 (1970).
(6) H. G. Busse, *Nature (London), Phys. Sci.*, **233**, 137 (1971).
(7) E. Koros and M. Burger, *Magy. Kém. Foly.*, **79**, 184 (1973); "Ion Selective Electrodes," Akadémiai Kiadó, Budapest, 1973, p 191.

Institute of Inorganic and Analytical Chemistry
L. Eötvös University
1088 Budapest, Hungary

E. Koros*
M. Orbán
Zs. Nagy

Received May 4, 1973

ADDITIONS AND CORRECTIONS

1970, Volume 74

Sang Hyung Kim, Terrell N. Andersen, and Henry Eyring: Structure of Electrical Double Layer between Mercury and Dimethyl Sulfoxide in the Presence of Chloride Ions.

Page 4557. Equation 2 should read

$$-d\xi^{-} = -E^{-}dq + \Gamma_{+}d\mu \qquad (2)$$

Page 4558. Equation 4 should read

$$\Phi = \tfrac{1}{2}\left(\xi_0^{+} - \xi_{+} + \int_{-\infty}^{\mu} \frac{q - z^{2-}}{F} d\mu\right) \qquad (4)$$

Page 4559. Equation 9b should read

$$\ln\left(\frac{a_{\pm}}{\Gamma_s}\right) - \frac{\Delta G}{kT} = \ln\left(\frac{\Gamma}{\Gamma_s - \Gamma}\right) + A\frac{\Gamma}{\Gamma_s} \qquad (9b)$$

Page 4562. Left hand column, the second line: "... or 1^{45} $\mu C/cm^2$" should read "... or -1^{45} $\mu C/cm^2$."—Sang Hyung Kim.

1973, Volume 77

Russell Y. Yanagida, Allen A. Amaro, and Karl Seff: A Redetermination of the Crystal Structure of Dehydrated Zeolite 4A.

Page 805. The captions to Supplementary Tables I and II, which appear in the microfilm edition only, should both read $10F_o$ and $10F_c$ instead of F_o and F_c.—Karl Seff.

Sang Hyung Kim and B. T. Rubin: Theoretical Free Energy of Activation for Dehydration of Hydrated Ions in Solution.

Page 1248. Right-hand column at bottom of page: "$\Delta G_{sea}^{\circ} > 0$ for Cl^{-}..." should read "$\Delta G_{sea}^{\circ} < 0$ for Cl^{-}...."

Page 1249. Left-hand column, line 9 below Table III: "$Cl^{-} < Br^{-} < I^{-}$" should read "$Cl^{-} > Br^{-} > I^{-}$." Also, line 12 below Table III: "$I^{-} < Br^{-} < Cl^{-}$" should read "$I^{-} > Br^{-} > Cl^{-}$."—Sang Hyung Kim.

K. Klier, J. H. Shen, and A. C. Zettlemoyer: Water on Silica and Silicate Surfaces. I. Partially Hydrophobic Silicas.

Page 1459. In Table I, line 1, column 3 should read 58 instead of 87. Line 1, column 4 should read 23 instead of 34.

Page 1460. In Figure 2, the symbols accompanying the legend inside the picture should be replaced by the symbols given in the caption below the picture.—K. Klier.

AUTHOR INDEX to Volume 77, 1973

Note: In this Author Index, titles of papers are listed after the name of each author of the paper. Multiple authorship is not indicated. Complete authorship may be ascertained by consulting the original paper.

KEYWORD INDEX to Volume 77, 1973

There's nothing theoretical about the value of I&EC Process Design and Development

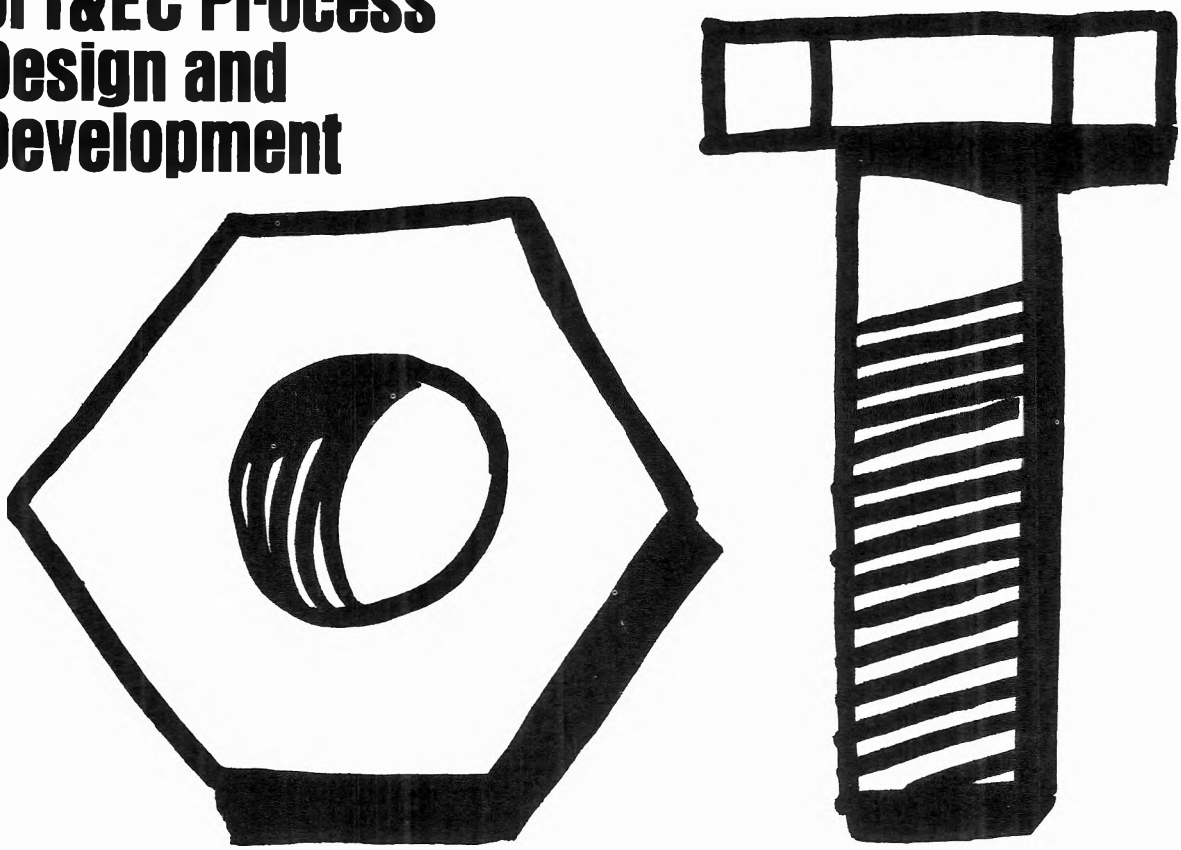

The original papers contained in this quarterly present theoretical and experimental results relating to the development of processes and process equipment—and the value of our publication is a known quantity to our constant readers. Subjects covered include:

- Empirical or Semi-theoretical correlations of data
- Experimental determinations of design parameters
- Methods of integrating systems analysis and process control into process design and development
- Scale-up procedures
- Many other experimental process development techniques.

Put us to the test. Complete and return the order form below today.

. . . *another ACS service*

I&EC Process Design and Development
American Chemical Society
1155 Sixteenth Street, N.W.
Washington, D.C. 20036

Yes, I would like to receive I&EC PROCESS DESIGN AND DEVELOPMENT at the one-year rate checked below:

	U.S.	*Canada*	*Latin America*	*Other Nations*
ACS Member Personal-Use One-Year Rate	☐ $ 7.00	☐ $10.00	☐ $10.00	☐ $10.50
Nonmember	☐ $21.00	☐ $24.00	☐ $24.00	☐ $24.50

Bill me ☐ Bill company ☐ Payment enclosed ☐

Name

Street Home ☐ Business ☐

City State *Zip*

O-73

AMERICAN CHEMICAL SOCIETY PUBLICATIONS IN MICROFORM

- Well over a million pages of chemistry's premier publications
- Back volumes and current subscriptions available in 35- or 16-mm microfilm and various cartridges
- Unlimited copying privileges built into microfilm subscriptions
- Current availability of nonprint materials in microfiche
- For full details of the ACS microform program, write or call:

Mr. Kenneth Phillips
Special Issues Sales
American Chemical Society
1155 16th St., N.W.
Washington, D. C. 20036
Tel: (202) 872-4364

and ask for your free copy of the informative booklet on the "Information Implosion!"